Pressure Screening Studies with Wood Pulp

A thesis submitted for the
requirements for the degree of

Doctor of Philosophy

at

The University of Waikato

by

Zuben Weeds

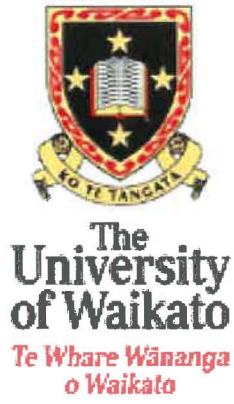

The University of Waikato

2006

ABSTRACT

Pressure screening is used in paper making to separate components of a wood pulp slurry (water, wood fibre and solid contaminant material) and to concentrate the wood fibre. The complex solid-liquid and solid-solid mechanisms involved in pressure screening are still poorly understood. This thesis reviews the literature on pressure screening mechanisms and highlights the problems in the models used to describe pressure screening.

Two models, based on well-mixed tanks in series, are developed to describe reject thickening behaviour of long and short screens. The first model uses a single one row of tanks to model steady flow from feed to accept and from feed to reject streams of a screen. A back-flow model, which had two rows of well-mixed tanks, one for the feed-side and another for the accept-side of the screen, was also developed. The passage ratio for back-flow of fibre P_B was estimated numerically by deducing the passage ratio for forward-flow of fibre P_F. The model showed that P_B can decrease more quickly than P_F when feed consistency increases, even when overall passage ratio Pp remains constant.

A small industrial pressure screen (diameter 203 mm, length 220 mm) was used to investigate the effect of screen length L_s and feed consistency C_f on pressure screening performance. The effects of pulp type (eucalypt for short fibre and pine kraft pulp for short fibre), feed consistency (from 0.005% to 2% compared to approximately 1% in industrial plants), screen length and placement along the length of the screen, rotor type (bump or step), and screen hole shape (round holes or slots) were investigated. Measurements of pulp consistency in the feed, reject and accept streams under different processing conditions were used to assess the screen models developed. Screening behaviour of screens less than 220 mm was studied extensively for the first time.

The tanks-in-series model showed that the effect of screen length on reject thickening could be described as well-mixed tanks in series with plug flow behaviour when the screen was modelled as 100 tanks. The reject thickening factor T decreased semi-logarithmically when number of tanks was decreased but increased slightly when the number of tanks was increased. Reject thickening factor decreases when a screen with 1-mm hole is shortened from 220 mm to 27 mm. This reduction can be attributed mainly to the flow regime changing from plug to mixed flow.

The maximum volumetric accept flow rate Q_{max} decreased by approximately 30 % when a 55-mm screen section was moved from the feed end to the reject end. This decrease in Q_{max} was consistent with an axial decrease in relative speed (difference between rotor tip and pulp suspension in the feed annulus), along with an estimated 33% reduction in the negative pressure pulse P_{NP} along the screen. Overall fibre passage ratio P_p also decreased when the screen section was moved to the reject end, or when pulp was accelerated in a feed chamber upstream of the feed annulus.

The three distinct regions and two critical feed consistencies observed when C_f increased from 0.005% to 2% are postulated to indicate when fibre accumulation on the feed and accept sides of the screen produces screen plugging. The critical C_f for the accept side is about ten times greater than that for the feed side due mainly to the fact that the conical holes have a larger diameter on the accept side so more fibre must accumulate before backflow is hindered. In Region 1 (crowding number < 1), reject thickening is independent of feed consistency and remains constant regardless of rotor type (bump or step) and screen type (smooth holes or contoured slots). In Region 2 (1< crowding number < 60), reject thickening decreases with feed consistency. In Region 3 (crowding number > 60), reject thickening either decreases with feed consistency or remains constant depending on the ratio of forward to back-flushing flow exhibited by the rotor and as predicted by the two-tanks in series model. For the step rotor with a flow ratio of 2:1 reject thickening is constant with feed consistency regardless of screen type. For the bump rotor with a flow ratio of 5:1 reject thickening decreases with feed consistency regardless of the screen type.

Fibre-length fractionation index Φ increased with increasing C_f to a maximum at about C_f=0.7% when using a 1-mm smooth-holed screen with a bump rotor or at C_f=2% for a 2.4-mm smooth-holed screen. Fractionation index then decreased with increasing C_f.

It is recommended that the back-flow model be further developed so that the volumetric flow ratio (ratio of forward flow to back flow) can be calculated from a residence time distribution. It is also recommended that fibre-length fractionation be attempted at various positions along the screen for medium consistency pulp (C_f of 8 to 12%) using unconventionally large holes (3-5 mm).

ACKNOWLEDGEMENTS

I wish to acknowledge and thank the following people and organisations:

- My supervisor, Dr Michael Walmsley, for his supervision.
- My co-supervisor, Associate Professor Janis Swan, for her supervision and showing me how to finish my PhD.
- The University of Waikato for the financial support.
- The Weeds family and Athena for their love and support.
- Martin Atkins for his encouragement and help.
- Brian Clark and Chris Sistern for their encouragement and help with setting up equipment.
- Tasman Pulp and Paper for supplying the pine and eucalypt pulps.

TABLE OF CONTENTS

LIST OF FIGURES

LIST OF TABLES

NOTATION

A_s Screen cylinder aspect ratio

A_z Open area of feed annulus

C_a Pulp consistency of the accept stream

C_{crit} Critical (minimum) pulp consistency for flocculation

C_f Pulp consistency of the feed stream

$C_{F(L)}$ Concentration of long fibre in the feed stream

$C_{F(S)}$ Concentration of short fibre in the feed stream

C_m Pulp consistency

C_r Pulp consistency of the reject stream

$C_{R(L)}$ Concentration of long fibre in the reject stream

$C_{R(S)}$ Concentration of short fibre in the reject stream

C_s Consistency of pulp flowing through the apertures of a screen

C_{sed} Pulp fibre sedimentation consistency

$C_{sed(3)}$ Pulp sedimentation consistency at which a fibre is in contact with 3 other fibres

$C_{sed(4)}$ Pulp sedimentation consistency at which a fibre is in contact with 4 other fibres

C_u Consistency of pulp flowing upstream of the apertures of a screen

$C_{(y)}$ Fibre point consistency

C_z Pulp consistency in the feed annulus

D_f Weighted mean fibre diameter

D_s Screen cylinder diameter

$e_{l(L)}$ Fibre removal function for the long fibre fraction

$e_{l(S)}$ Fibre removal function for the short fibre fraction

E Modulus of elasticity or removal efficiency

F_A Normalised local volumetric accept flow rate

F_F Mean fibre flexibility of pulp fibre

F_m Longitudinal fibre flexibility

h Distance between screen surface and rotor body

H Exit layer height

I Moment of inertia

K_H Pressure loss coefficient

L_f Length weighted mean fibre length

L_F Fibre length

L_L Weighted mean fibre length

L_N Numerical mean fibre length

L_s Screen cylinder length

M Mass

M_d Oven-dry mass of pulp

M_w Wet mass of pulp

N Fibre crowding number

N_T Number of tanks

O_A Open screen area

P_B Fibre passage ratio for back-flow

P_c Passage ratio for solid contaminants

P_F Fibre passage ratio for forward flow

P_p Overall fibre passage ratio

$P_{p(L)}$ Passage ratio for the long fibre fraction

$P_{p(S)}$ Passage ratio for the short fibre fraction

$p_{(y)}$ Probability of passage function

P_z Local passage ratio

Q Screening quotient (Q index

Q_a Accept volumetric flow rate

Q_f Feed volumetric flow rate

Q_r Reject volumetric flow rate

Q_s Local volumetric accept flow rate

Q_x Q index for fraction of interest

Q_z Local axial volumetric flow rate through the feed annulus

r_f Weighted mean fibre radius

r_L Weighted mean fibre length

R_m Mass reject ratio

R_v Volumetric reject ratio

R_z Local volumetric reject ratio

S Slip factor

S_w Fibre stiffness

T Reject thickening factor

t_B Time period for back-flow

T_{BF} Time period ratio

t_F Time period for forward flow

T_p Total number of fibre trajectories passing through a slot

T_t Total number of fibre trajectories from an initial starting point upstream of an aperture

T_z Local reject thickening factor

V_{ax} Tangential velocity of fibre or fluid

V_n Normalized slot velocity (ratio of V_s to V_u)

V_s Aperture velocity calculated from screen open area and volumetric accept flow rate

V_{tan} Tangential velocity of fibre or fluid

V_{tip} Rotor tip velocity

V_u Fluid velocity upstream of an aperture, calculated from open area of feed annulus and volumetric feed rate

W Slot width

W_f Weighted mean fibre wall thickness

X_a Fraction of interest in accept stream

x_o Position of fibre upstream of an aperture

X_r Fraction of interest in reject stream

y Distance (height) above screen in feed annulus

Z_N Normalised axial position

α Separation ratio

Φ Fractionation index

λ Coefficient for relating fibre length to passage ratio

θ_o Angle of a fibre approaching an aperture

μ static coefficient of friction

ρ density

σ Weighted mean fibre coarseness

τ_w Shear stress

1. INTRODUCTION

Producers of pulp and paper are under pressure from a need to cover costs and make returns to their investors. Therefore, they must lower costs and improve product quality to survive in a competitive industry that is capital intensive and suffering excess supply. There is insufficient information about operation parameters of the complex machines used to produce pulp and paper, which makes it difficult for producers to reduce costs or improve quality.

Paper is produced from wood pulp. Modern paper machines are 10 meters wide and produce paper at 30-40 meters per second. Although these modern machines increase the economics of making paper, producers have not obtained the economic benefits because these new machines have contributed to excess supply. Therefore, production costs need to be decreased by other means. One way to achieve this is to reduce the number of stages in pulp production by using the unit stages in a smart way.

Pulp production is a stage-wise process. The number and configuration of stages vary considerably, but most processes have a pulping stage, a refining stage, a pressure screening stage and a washing stage. The pressure screening stage is usually essential; this stage has the potential to improve pulp quality considerably. Smart use of these machines can also eliminate unnecessary stages, resulting in large capital and energy savings. However, insufficient is known about pressure screens operation boundaries for this potential to be realised. The aim of this thesis is to elucidate the mechanisms controlling behaviour of these machines. The machines can then be used in a way that could ultimately lower costs and improve pulp quality.

Chapter 2 is a critical review of the literature on screen design and operation directly relevant to the work carried out in Chapters 4 and 5. A description of experimental equipment and methods are presented in Chapter 3, along with a description of the main screening trials conducted during these investigations. Two variables that affect pressure screen performance are screen length and consistency of the pulp feed stream. Chapters 4 5 and 6 examine how these two variables affect pressure screen operation. Conclusions drawn from this work and recommendations for future work are presented in Chapter 7.

2. LITERATURE REVIEW

2.1 Introduction

This review examines literature pertaining to the properties and flow behaviour of wood fibre suspensions. It also examines pressure screening, including the history of development, applications of this technology, screening mechanisms, modelling and reject thickening studies. A critical review of the literature is conducted mainly where the information relates directly to the work presented in following chapters. For example, pressure screen modelling is reviewed critically (and in more detail) because modelling a screen is an important facet of work conducted in this thesis.

2.1.1 Overview of Pulping - The Prelude to Making Paper

Pulp production produces the fibrous material for making paper using predominantly wood as the raw material. A stage-wise pulp production process is depicted in Figure 2.1. Wood (in chip form) is pulped using chemicals and heat (chemical pulping) in high-yield and medium yield digesters. The resulting wood pulp is then pumped from the blow tanks to the refiners and then onto the pressure screens. The final stage in this example of pulp production is washing, but the washing stage often occurs immediately after pulping to remove and recover pulping chemicals.

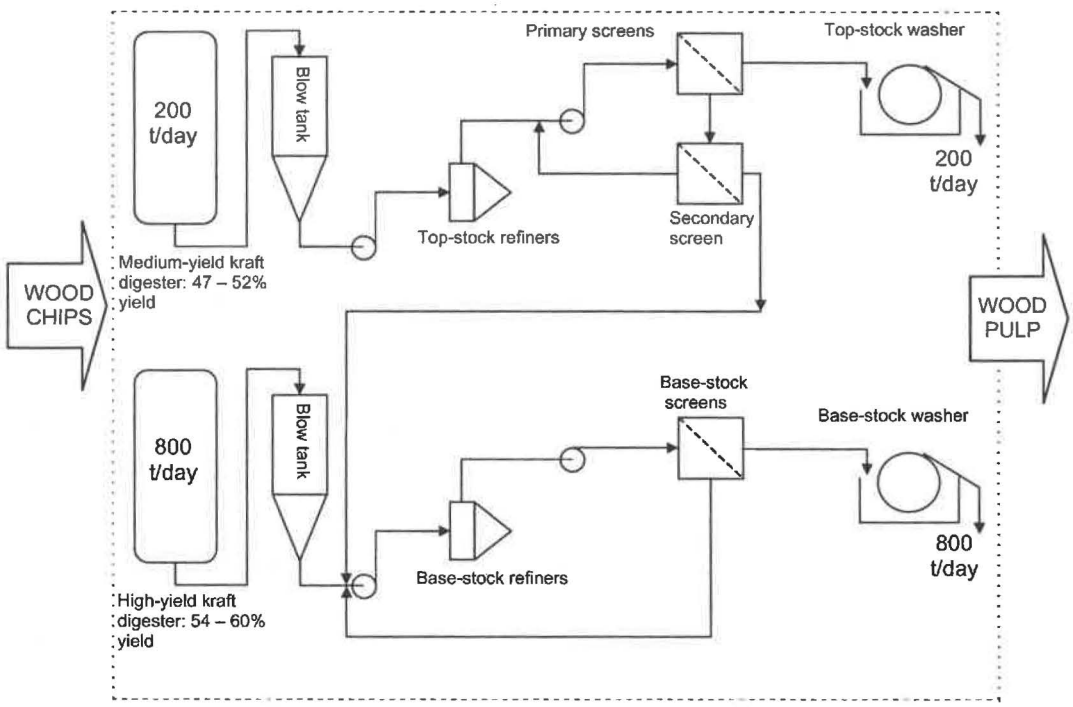

Figure 2.1 Pulp production process with high- and medium-yield digesters (drawn from [1]).

2.2 Wood Pulp Fibre Suspensions

Wood pulp produced by the pulping process is a mixture of mainly fibrous wood material (solid) suspended in liquid pulping chemicals. The fibrous wood material is usually referred to as wood fibre because of the fibre-like characteristics of the wood fibres. Wood fibres (of length L_f) are long hollow tubes (high aspect ratios) and the mass of wood fibre relative to the mass of slurry (solid + liquid) is an important pulp property commonly called pulp consistency.

2.2.1 Pulp/Fibre Consistency

The term pulp consistency indicates the amount of dry mass (wood fibre, shives, inorganic filler such as calcium carbonate and titanium dioxide, sand and dirt, etc) in a pulp slurry. Fibre consistency defines the amount of wood fibre in a suspension of pulped fibres. As wood fibre is the predominate material in pulp, pulp and fibre consistency are usually similar. At room temperature, pulp consistency is approximately equal to the mass concentration of fibre C_m (Equation 2.1), where M_d is the oven dry mass of fibre, and M_w is the wet mass of pulp. In this thesis, because the work is carried out at ambient temperature, consistency is synonymous with mass concentration of fibre.

$$C_m(\%) = \frac{M_d}{M_w} 100 \qquad (2.1)$$

There are four consistency ranges in pulp and paper production (Table 2.1). Usually pressure screens are used to concentrate low consistency pulps, pulp refining is used for medium consistency pulps, and pulp bleaching is used for high consistency pulps. The ultra-high consistency range only occurs in the paper making machine after the suspension has been dewatered, formed and pressed.

Table 2.1 Processes used at different pulp consistencies (from [2]).

Low consistency	Medium consistency	High consistency	Ultra-high consistency
0%	8%	20%	40%
PRESSURE SCREENING ↓	Pulp refining ↓	Pulp bleaching ↓	Paper products ↓
8%	20%	40%	90%

It is more economic to process pulps at the highest consistency possible. Process volumes are reduced, operations can be simplified and equipment scaled down [3, 4]. However, consistency affects equipment selection and efficiency. For example, medium consistency pulps can be difficult to pump and mix, and thickened, medium consistency pulps can readily block pressure screens apertures.

2.2.2 Other Pulp Properties

- ***Fibre length*** L_f is considered the most important fibre property because it affects pulp flow through conduits and apertures [5] and fibres flocculation [6]. Mean fibre length also affects paper properties [7-10]. There is no general agreement on mean fibre length [11]. Three measures exist: numerical mean length L_N (Equation 2.2), the length weighted-mean length L_L (Equation 2.5), and the weight weighted-mean length L_W (Equation 2.6). L_f is the fibre length and n is the frequency.

$$L_N = \frac{\sum nL_f}{n} \tag{2.2}$$

$$L_L = \frac{\sum nL_f^{\,2}}{nL_f} \tag{2.3}$$

$$L_W = \frac{\sum nL_f^{\,3}}{nL_f^{\,2}} \tag{2.4}$$

Clark [11] reviews ways to measure fibre length. Manual measurements have the disadvantage of deciding whether to include fibre wall fragments, split fibres or very short fibres (fines). The electronic sequential fibre length analyser, which measures fibres optically, has the disadvantage of measuring all fibre-like particles and requiring the sample to be suitably dilute so fibres do not overlap in the measuring tube. If many fibres overlap, mean fibre length will be higher than it actually is.

Modern commercial fibre analysers such as the Fibre Quality Analyser (FQA), Kajaani Fibre Lab and the Kajaani FS200 allow for these difficulties. They typically report fibre length data either as a fibre frequency versus fibre length or mass.

- ***Fibre coarseness*** is the mass per unit length of fibre and has the units milligrams per 100 meters of fibre (decigrex). Different species and different parts of the same tree can produce pulps with markedly different coarseness values. There is a high positive correlation between fibre length and coarseness [12-14]. The term is often used

(inaccurately/erroneously) to indicate pulp flexibility and deformability (lumen collapse). Low coarseness pulps (decigrex of less than 10 mg/100 m) are considered to have thin walled fibres that are more prone to collapse and bend while high coarseness pulps (decigrex close to 30 mg/100 m) are considered to have thick-walled fibres with a low tendency to collapse and bend. However, Clark [11] noted that both fibre wall thickness and diameter affect fibre flexibility and deformability.

- ***Pulp freeness*** describes the ease that water drains from a pulp/fibre network. In the Canadian Standard Freeness tester, a 1000-mL pulp sample at 0.3% consistency is allowed to suddenly drain against a screen plate [15]. Water collects in a conical receiver below the plate, which has a narrow constriction at the bottom. Fast draining pulps will quickly fill the receiver so any overflow from a large outlet in the side of the receiver is collected in a container. High freeness pulps drain quickly and between 600-700 mL can be collected. Low freeness pulps drain slowly and only 75-250 mL may be collected. Although papermakers and pulp producers find freeness values useful for characterising their pulps, test reproducibility is often low [11].

Pulp freeness is often used to monitor the refining process because the increase in fibre flexibility due to wall delamination and increased fibrillation correlates with pulp drainage rate (CSF). However, freeness values are not always reproducible [16-19].

- ***Fibre flexibility*** can be estimated assuming fibres are flexible ideal hollow elastic beams. If longitudinal fibre flexibility F_m is the inverse of fibre stiffness S_w [20], then stiffness is the product of the modulus of elasticity E and the moment of inertia I in the plane of bending (Equation 2.5).

$$F_m = \frac{1}{S_w} = EI \tag{2.5}$$

For a circular hollow beam, the moment of inertia is a function of internal diameter d_i and the outside diameter d_o, both to the fourth power (Equation 2.6).

$$I_{cir} = \frac{\pi}{64}\left(d_o{}^4 - d_i{}^4\right) \tag{2.6}$$

For a hollow rectangular beam, the moment of inertia is a function of internal and outside fibre width (b_i and b_o respectively), and internal and outside height (h_o and h_i respectively) (Equation 2.7).

$$I_{rec} = \frac{b_o h_o^{\,3} - b_i h_i^{\,3}}{12} \qquad (2.7)$$

Fibres are rarely perfect cylinders or hollow rectangular tubes but information from bending theory is useful for comparing with flexibility measurements. Precise measurement, however, is difficult. For example, fibres may be crushed when being loaded into the apparatus. Tam Doo and Kerekes [20] described equipment that supports the fibres at both ends rather being clamping one end, which overcomes fibre compression/crushing. Loading was applied by fluid drag normal to fibre axis/length. Although this method had other advantages, the researchers noted that effective rather than absolute flexibility is measured. All methods, assume that the fibre is uniform. Kinks and fractures could be present from pulping or natural defects so fibre flexibility can vary along the length [21].

2.2.3 Fibre Length Fractions of Pulp

Most softwood chemical pulps can be separated into long and short fibre fractions. The specification of long and short fibre varies, especially when using different length measuring devices and fibre classifiers. Olson *et al.* [22] defines the short fibre fraction as all fibre between 0 and 2 mm (including the fines fraction) and the long fibre fraction as all fibres greater than 2 mm but less than or equal to 4 mm. Fibres longer than 4 mm are ignored because this is usually a very small fraction.

Because fibre length and coarseness are directly correlated, properties of pulp and paper made from different fractions are appreciably different. Pulp with unrefined short fibre fraction, including fines, has a lower freeness [7, 23-25] and produces a more uniform [26, 27], smoother [7, 25], denser paper [7, 25, 28]. This short fibre fraction is suited to surface layer(s) of stratified (layered) paper sheet where smoothness is important.

Fibre conformability is a function of fibre collapse and fibre flexibility [29] and increases when hollow fibres collapse and flexible fibres bend. Both conformability and flexibility depend on fibre cross-sectional dimensions [29-31]. Because shorter fibres typically have smaller diameters [32], thinner cell walls [33, 34] and less mass per unit length [12-14, 35, 36], they more readily collapse and bend, producing a dense, smooth paper sheet. Conversely, paper made from the unrefined long fibre fraction is less dense [37], rougher [37], and sometimes has lower burst and tensile strengths [24]. Refining the long fibre fraction produces paper with increased density, and burst and tensile strength [25, 38].

2.2.4 Fibre Flocculation

- ***Floc and Fibre Network Formation***

Wood fibres readily entangle to form flocs (also called agglomerations, aggregates or mass concentrations), and flocs entangle to form fibre networks. Flocs give pulps a non-uniform, mottled appearance and fibre network can be a continuous, self-supporting structure occupying the entire container/vessel. Both flocs and fibre networks restrict fibre mobility, and both fibre structures have measurable mechanical strength.

The process of floc formation has been described [2, 39-42]. Smaller, weaker flocs can form at very low consistencies but will not form below a critical (minimum) consistency (C_{crit}). Floc size and cohesiveness increase with increasing consistency [43, 44] and increasing fibre length [6, 45]. Stable coherent flocs form if consistency is high enough and flow characteristics favour flocculation rather than dispersion (i.e. floc disintegration). When exposed to shear, fibres bend, rotate and collide with one another. Collisions with other bent fibres, prevents fibres from straightening. Forces are generated normal to contact points, which generates friction that imparts fibre cohesion. Duffy [46] points out that it is forces of repulsion rather than forces of attraction that are responsible for holding fibres together. Three forces other than elastic fibre bending also contribute to floc and network cohesion. Kerekes *et al.* [2] discusses colloidal forces, mechanical surface linkages, and surface tension forces due to the presence of air bubbles.

- *Colloidal Forces*: Electrostatic and electrokinetic forces exist between small particles. Their strength depends on intimacy of contact (which is difficult to achieve between the rough fibre surfaces), and chemical additives that modify the negative charge on fibre surfaces.
- *Mechanical Surface Linkage Forces*: This is a hooking force caused by mechanical entanglement of kinked or curled fibres, or from fibrillated surfaces. When a force is applied to separate fibres, the reaction force caused by hooking at contact points opposes relative movement. This type of cohesion depends on surface fibrillation, the degree the fibres are contoured, and fibre stiffness.
- *Surface Tension Forces*: Bubbles of gas (usually air) at fibre interstices produce cohesive forces as a result of surface tension.

- ***Minimum Consistency for Floc Formation***

At very low consistencies, below the critical consistency C_{crit}, pulp may flow as an un-flocculated fibre suspension where fibres are relatively free to move [40, 47, 48]. At C_{crit}, the fibre suspension may begin to form a flocculated fibre suspension when fibres collide

and contact other fibres, especially in rotational motion. However, this depends in the flow conditions. Mason [47] derived a mathematical expression (Equation 2.8) to estimate the critical consistency, L_L is the weighted-mean fibre length, D_L is the weighted-mean fibre diameter, and W_L is the weighted-mean fibre wall thickness.

$$C_{crit} = \frac{2}{3}\left(\frac{L_L \pi}{D_L W_L 2}\right)^2 \tag{2.8}$$

The calculation is based on the spherical volume (termed orbits) swept by fibres as they rotate about their centres. The mean orbit diameter equals the mean length of fibres in suspension. The C_{crit} indicates the order of magnitude when fibre contact will occur. A more precise estimate of C_{crit} incorporates a log-normal distribution of fibre lengths [49]. The predictive value of this equation is limited because flow conditions are not included.

- ***Minimum Consistency for Fibre Network Formation***

When pulp consistency increases to a second critical consistency, called the sedimentation consistency C_{sed}, fibre flocs mechanically entangle with other flocs to form a fibre network. The sedimentation consistencies $C_{sed(3)}$ and $C_{sed(4)}$ are the consistencies when a single fibre is in contact with at least three or four other fibres respectively. These two sedimentation consistencies can be predicted using Equations 2.9 and 2.10, where r_L is weighted-mean fibre radius and L_L is weighted-mean fibre length.

$$C_{sed(3)} \approx 339\left(\frac{r_L}{L_L}\right)^2 \tag{2.9}$$

$$C_{sed(4)} \approx 536\left(\frac{r_L}{L_L}\right)^2 \tag{2.10}$$

Values for C_{sed} can be determined by settling tests [50], which involves allowing a dilute fibre suspension, with an initial consistency $C_{o(i)}$, to settle in a column (Figure 2.2). The consistency of the sediment layer $C_{o(f)}$ at the bottom of the column can be calculated using Equation 2.11, where $h_{t(i)}$ is initial height of suspension before settling, and $h_{t(f)}$ is height of sediment layer after a certain settling time. The value of $C_{o(f)}$ tends towards a constant value approximately equivalent to C_{sed} [51]. Thalen and Wahren [50] used this method to determine sedimentation consistencies in early studies of fibre networks. Settling data have shown that C_{sed} is closer to $C_{sed(4)}$ [52].

$$C_{o(f)} = \frac{C_{o(i)} h_{t(i)}}{h_{t(f)}} \tag{2.11}$$

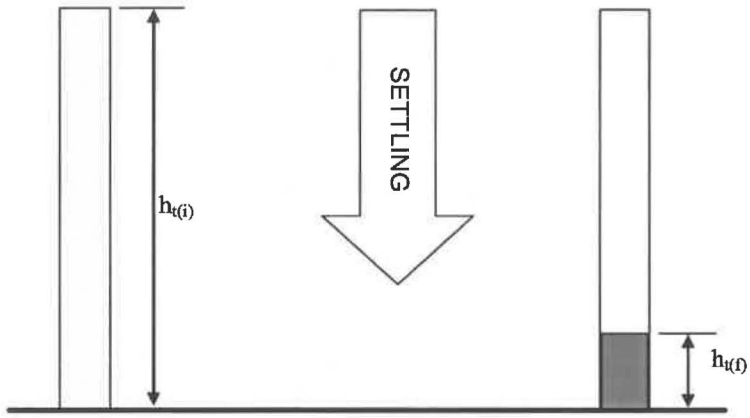

Figure 2.2 Obtaining sedimentation consistencies using the settling test.

- ***Crowding Number***

Kerekes and Schell [40] characterised fibre suspensions using a crowding number N (Equation 2.12) to indicate flocculation and network formation at the sedimentation consistency. This crowding number, which is based on earlier work of Mason [47], is calculated from mass consistency of pulp C_m, weighted-mean fibre length L_L, and weighted fibre coarseness σ_L of a pulp suspension.

$$N = \frac{5C_m L_L^{\,2}}{\sigma_L} \qquad (2.12)$$

Flocculation begins at a crowding number of 1 and fibre network formation begins at a crowding number of 60. Crowding numbers between 1 and 60 define three fibre suspension regimes including a dilute regime, semi-concentrated regime and concentrated regime where fibre contact differs (Table 2.2). Chance fibre collisions occur in the dilute regime, forced fibre collisions and collisions occur in the semi-concentrated regime, and forced fibre contact occurs in the concentrated regime.

Table 2.2 Types of fibre contact in the three pulp regimes (from [40]).

Regimes	Type of fibre contact	N value
Dilute	chance collision	N<1
Semi-concentrated	forced collisions/contact	1<N<60
Concentrated	continuous contact	N>60

2.2.5 Pulp Mixing, Floc Dispersion and Re-flocculation

Pulp mixing and floc dispersion liberate fibres from fibre networks and flocs. Initiating mixing and maintain motion within a pulp suspension involves applying forces greater than the network strength of the pulp suspension [53]. Network strength increases with pulp consistency, so greater force is required to disrupt more concentrated pulps [54]. Bennington [53] differentiates between macro- and fibre-scale mixing. Macro-scale mixing is bulk movement of suspension over long distances and could involve movement of flocs rather than individual fibres. Fibre-scale mixing involves movement of fibres over short distances proportional to fibre length and must be preceded by floc dispersion. Floc dispersion involves floc rupture and decay, which liberates entangled fibres.

Fibre network disruption and floc dispersion has been studied in straight pipes [55], rotational shear devices [53], elongational flows [56], the wake of grids [57] and constrictions [58, 59], and paper-machine head-boxes [60]. Most researchers agree that dispersion depends on the intensity and scale of turbulence [39, 61-63]. For effective, energy efficient dispersion, intense small-scale turbulence should be used because intense, large-scale turbulence is not energy efficient [3]. The mean size of turbulent eddies corresponds with mean floc size which in turn indicates the scale of turbulence. Wagle and Lee [62] observed that macro eddies decrease flocs rapidly but micro eddies cause complete dispersion.

Pulp mixing and pulp flow behaviour in a rotary shear device, made of a shear element rotating concentrically within an outer chamber at up to 5000 rpm, have been studied [53]. The shear element had lugs and the outer chamber was baffled, which created chaotic flow patterns and caused pulp mixing in the gap between the element and outer chamber. At a critical speed, intense pulp mixing occurred as radial, tangential and axial flows developed in the gap between the shear element and outer chamber. This critical speed for intense mixing increased with pulp consistency, so more power was required with increased pulp consistency. However, even with intense mixing and combined radial, tangential and axial flows, flocs and individual fibres were observed flowing in the shear device, which indicted that the pulp network had been disrupted to liberate flocs but complete floc dispersion had not occurred.

Elongation flows cause flocs to stretch under tension forces [56, 64, 65] but the flocs may not necessarily rupture and disperse. Elongation flows at sudden contractions are irrotational flows and may disperse flocs more readily than shear flows [66]. Mechanical

pulp flocs elongated and ruptured in a conical contraction but softwood Kraft pulp flocs, which have longer fibres, elongated without rupturing [64].

Kerekes [56] filmed softwood kraft pulp flowing into narrow, rounded contractions. Generally, flocs only ruptured if they elongate five times their original length, rupturing under tension forces instead of shear forces. Kerekes also showed that flocs elongated more when flowing into narrow, sharp-edged contractions that produced a *vena contracta* because of the greater restriction and higher velocity produced. Flocs were not affected by the stationary vortices at the *vena contracta* but intense vortices downstream ruptured flocs and mixed the pulp, which concentrated against the wall of the constriction.

Elongated and ruptured flocs will rapidly re-flocculate downstream of grids [39, 43, 57, 60] (Figure 2.3) and contractions [58, 59] as turbulence decays [63]. Re-flocculation is almost instantaneous and re-flocculation times (decay times) decrease with increasing consistency [63, 67, 68].

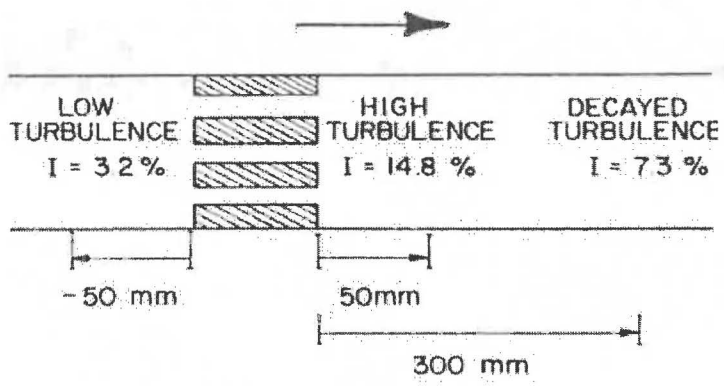

Figure 2.3 Regions of turbulence when a grid is inserted in a pipe (from [63]).

2.2.6 Wood Pulp Fibre Suspension Flow Behaviour

Flow behaviour of wood pulp fibre suspensions in large diameter pipes differs from flow of many other settling slurries and Newtonian and non-Newtonian fluids [46, 47, 55, 69-71]. The friction loss curve for a chemical pulp with 1% or greater consistency has three main regions: plug, transition, and turbulent flow (Figure 2.4). The plug flow (region A-C) occurs at low flow rates and friction loss is greater than water. Transition flow occurs at moderate flow rates (region A-B) and friction loss is lower than water. This difference in friction loss is termed drag reduction. Turbulent flow occurs at high flow rates (region beyond B) and friction loss is lower than water.

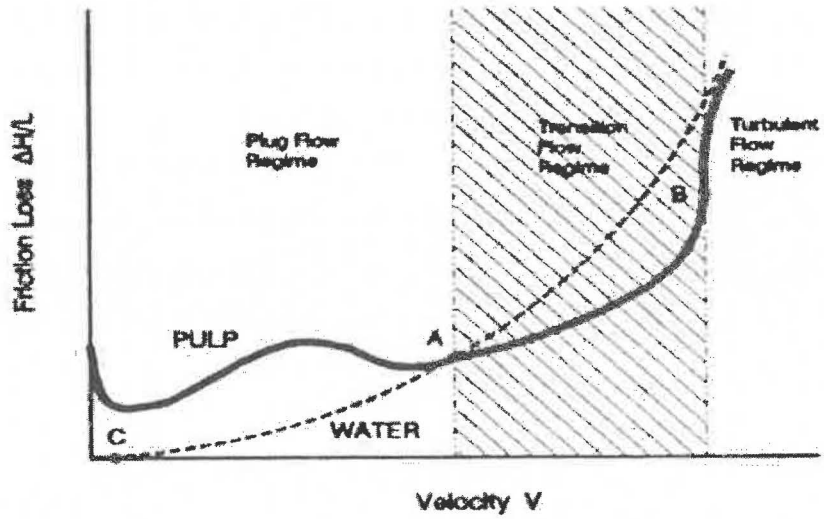

Figure 2.4 Friction loss curves for water and wood pulp suspensions (from [46]).

Structure of the pulp suspension differs in the three flow regimes. Robertson and Mason [55] observed pulp suspensions flowing in glass pipes. Pulp was a coherent plug in the plug flow region. When transition flow starts, flocs were dislodged from the edge of the plug and plug diameter progressively decreased and thickness of a fibre-water annulus increased with increasing flow rate. In turbulent flow, the plug completely disintegrates and pulp is a mixture of flocs, unstable fibre bundles (small flocs) and individual fibres.

Duffy *et al.* [70] described the mechanism of pulp flow in the various flow regions (Figure 2.5). In the plug flow region, A-C, wall interactions predominate and the pressure drop is relatively constant with velocity due to boundary friction between plug and wall of pipe. Over the region B-C, there is combined hydrodynamic shear and plug-wall interactions. Local interactions between the plug surface and pipe wall causes single flocs to break off and roll along pipe wall more slowly than the plug. Partial hydrodynamic shear arises from water pockets between flocs. At C, plug-wall interactions cease. In the region D-E there is plug flow with a thin water annulus in laminar shear. The change in flow mechanism is indicated the change in gradient of the friction curve. Flow stresses deform the fibre network and flocs and fibres protruding from the periphery of the plug are deflected. Thickness of water annulus increases with velocity. At E, turbulence begins in water annulus. In the region F-G, there the pulp is in plug flow and the water annulus has turbulent flow. Most of plug surface is still intact. At G-H, there drag reduction begins and there is permanent plug disruption. Friction in the pulp becomes greater than that of water. Most of the plug remains intact but flocs at the surface are removed by turbulent shear stresses. The H-I-J region is transition flow, with plug diameter decreasing with increasing flow rate. The turbulent fibre-water

annulus around the inner plug increases. At I (maximum drag), part of plug still exists. Flocs in the turbulent annulus are in dynamic equilibrium (dispersing and re-flocculating). The maximum drag reduction (turbulence suppression) is due to two competing mechanisms: large flocs are acting as solid links, enhancing momentum transfer, but small flocs and fibres dampen turbulence in the suspending phase, reducing momentum transfer. Fully-developed turbulence occurs in the J-K region. The plug is completely dispersed by turbulent shear stresses and drag reduction and turbulence decreases.

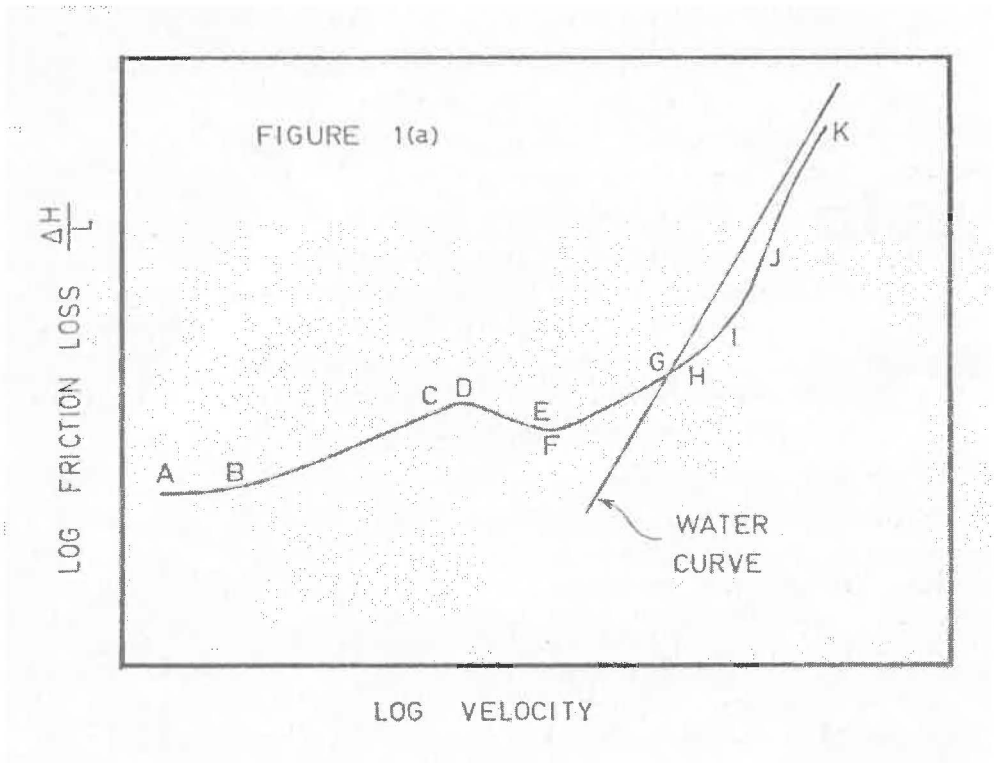

Figure 2.5 Typical friction loss curve for chemical pulp (from [86]).

Drag reduction (perhaps the most notable feature of pulp flow in large diameter pipes) begins when friction values for pulp and water are equal and indicates when fibres, flocs and floc fragments (unstable fibre bundles) are being dislodged from the surface of the plug. These solid particles undergo turbulent motion in the water annulus, modifying (an ultimately retarding) development of turbulence in fluid layers away from pipe wall.

In Newtonian fluids, momentum is transmitted by turbulent eddies. Fibres affect momentum transfer processes and suppress turbulent eddies (dampens turbulence), which affects velocity differences between fluid layers. However, fibres and fibre flocs enhance momentum transfer by providing solid, force-bearing links between neighbouring fluid regions/layers. In turbulent fibre suspensions, a significant part of momentum transfer

arises from moving flocs, similar to eddies in fluid flow. Thus, physical structure, especially floc size, of the fibre suspension affects momentum transfer. Robertson and Mason [55] reported that average floc size in a turbulent fibre suspension decreased as shear increased and proposed that average floc size occurs when floc formation and floc destruction (floc dispersion) are in equilibrium. Duffy and Lee [72] suggested that the destruction-reflocculation mechanisms were due to Reynolds shear stresses in the turbulent fibre-water annulus and proposed that these tend to break fibre flocs while simultaneously increasing movement between fibres. Reflocculation occurs more readily as frequency of fibre-fibre collisions increase. Because Reynolds stress is greatest in the turbulent zone next to the buffer zone, smaller flocs occur near the pipe wall. Reynolds stress decreases rapidly away from the wall, so larger flocs exist near the plug.

Drag reduction did not occur in small diameter pipes, probably due to spatial restriction of the flocs/fibre network [65]. 'Side-by-side' flow of unstressed flocs cannot occur if pipe diameter is smaller than mean floc size. Instead, single elongated flocs, stressed by contact with the pipe wall, flow through small diameter pipes [65]. A turbulent water annulus will not develop so drag reduction and momentum transfer cannot occur.

Bennington [53] and Gullichsen and Harkonen [4] studied flow behaviour in a rotary shear device without through flow (i.e. a closed vessel). Bennington described several flow regimes, detailing flow patterns in small and large annular gaps at different rotational speeds. The regimes for small annular gaps are described here because they are more relevant to pressure screening. A semi-bleached Kraft pulp has the following flow regimes (Figure 2.6):

a. Yield – void spaces appear behind rotor lugs

b. Formation of a shear plane – intense motion in the area influenced by rotor lugs – no motion in stagnant area shielded by baffles

c. Tangential-cavity flow – tangential flow fills annular chamber

d. Phase separation (flooding) – a smaller quantity of gas is present and flow pattern may cease at (b) or (c)

e. Inward radial flow

f. Post-transition flow – intense flow fills the annular chamber – the flow pattern is unknown although it is likely to have axial, radial and tangential flow patterns.

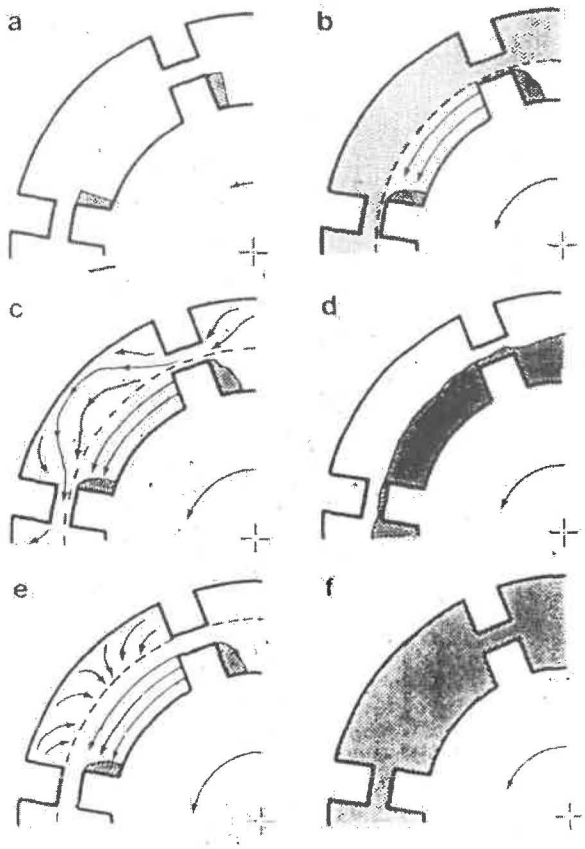

Figure 2.6 Pulp flow regimes in a rotary shear device as rotor speed increases (from [53]).

Both groups [4, 53] found that torque/rotational speed curves for pulp and water differed. At low speeds, values for pulp were much higher than for water; at a certain speed they were the same; and sometimes torque for pulp was much lower than for water. The reduction in torque cannot be attributed to drag reduction only [46, 53]. Bennington attributed the lower torque to phase separation and gas accumulating around the rotor, which reduced momentum transfer from the rotor to pulp suspension. In some cases, the rotor would be spinning in air and the pulp suspension would remain stationary.

Bennington [53] and Gullichsen and Harkonen [4] reported a sudden increase in torque when rotor speed was increased due to the flow pattern changing from predominantly tangential to radial flow. When the whole vessel became vigorously mixed and tangential, radial and axial flow patterns could be observed. Gullichsen and Harkonen[4] interpreted this as complete mixing (sometimes incorrectly called fluidization), fully developed turbulence or complete turbulence [46]). In this flow regime, fibres undergo relative motion and fibre-scale mixing occurs. Bennington observed flocs undergoing relative motion and claimed this could not be onset of fully developed turbulence.

Duffy [46] noted that Bennington [53] reported different sets of results for the two chamber geometries (wide annular gap and narrow annular gap) and claimed that torque and rotational speed data were geometry dependent. Therefore, disruptive shear stress in a pulp suspension did not correlate directly to the point where torque suddenly increases, which in turn is not the point where the friction curve for pulp (pulp flow through straight pipes) crosses that of water (Point A in Figure 2.4). Duffy then points out that care must be taken when transferring data from rotary shear devices to pipe flow systems. Rotary shear devices can be viewed as continuously stirred baffled tanks with secondary flow patterns (back-mixing) from the base and walls; a straight pipe can viewed as an infinitely tall tank where the base and pipe walls do not cause secondary flow patterns. The reverse must also be true. Data from pipe flow systems may not necessarily transfer to rotary shear devices such as pressure screens. For example, although a bulk/mean pipe velocity of 40-50 ms^{-1} is needed for fully developed turbulence in a 10% consistency pulp, this does not mean that a rotor tip speed of 40-50 ms^{-1} is required for fully developed turbulence in a pressure screen.

2.3 Pressure Screens

Pressure screens are rotary shear devices used predominantly to improve the quality of pulp. They are available in many designs and configurations [71, 73-92]. A typical centrifugal pressure screen (Figure 2.7) has three main components: a cylindrical housing; a stationary screen cylinder; and a rotating shear element.

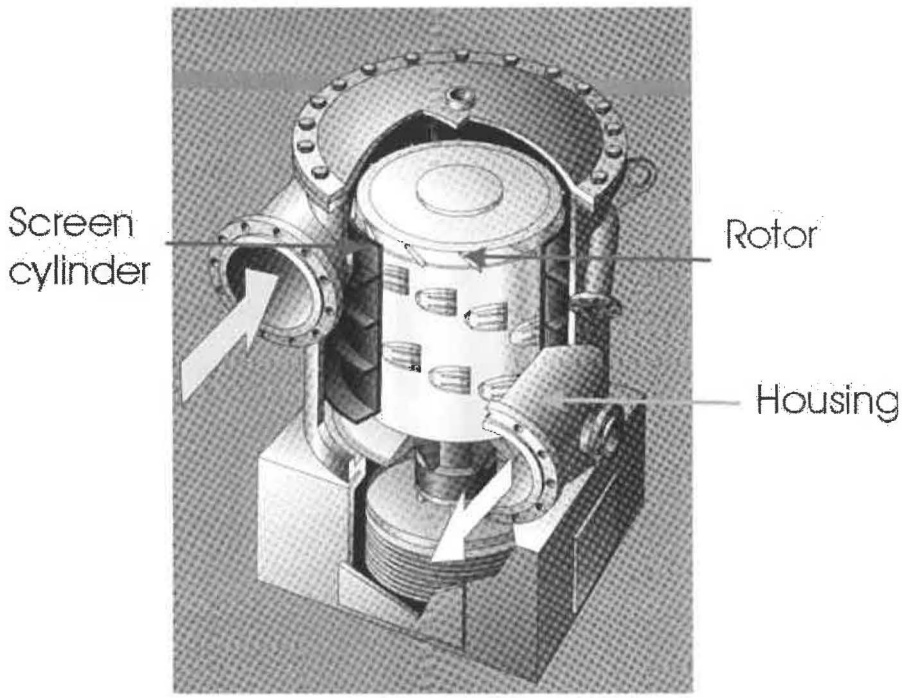

Figure 2.7 Typical centrifugal pressure screen showing housing, screen cylinder and rotor.

The cylindrical housing has an inlet port (feed stream) and two outlets, one for reject pulp and one for accept pulp. The screen cylinder is usually located concentrically within the housing. It has numerous apertures (either circular holes or narrow rectangular slots), a length of L_s and diameter D_s. The rotating shear element (called a rotor), is located concentrically within the screen cylinder and typically operates at peripheral tip speeds of 20-30 ms^{-1}. Pulp mixing occurs in a compartment between the rotor tip and screen cylinder called the feed annulus, and the macro mixing patterns in this compartment affect the performance of the pressure screen [93].

2.3.1 Applications of Pressure Screens

Smart use of pressure screens can alter the position of pressure screening stages in step-wise pulp production. Screening stages may arise immediately after pulping or just before the paper machine. Pressure screen knotters and coarse screens used immediately after pulping have relatively large apertures holes and have a primary function of preventing large pulping debris from entering the stock preparation stream. Guard screens are situated just before the paper machine with the primary function of preventing debris that will cause paper web breaks or objectionable visual defects from entering the paper machine. Fine screens and pressure screen fractionators are placed between the knotters and guard screens. The smart application of pressure screens can also result in cost savings and quality improvements in the final paper product.

- ***Contaminant Removal***

All pressure screens perform some separation function such as separating and removing undesirable solid contaminant particles such as shives, sand, dirt, ink specks [94-98] from chemical, mechanical and recycled pulp. These contaminants can interfere with running the paper machine and/or adversely affect paper quality. One of the most difficult contaminants in recycled pulp is the 'stickies' [99] because they can be small, sometimes deformable and pressure-sensitive particles that disintegrate in pressure screens [100], producing microscopic particles that pass through the narrowest/smallest screen apertures. Shives in chemical an mechanical pulps for instance can cause weak zones in the paper web and ultimately web breaks [101]. Up to 98.5% of web breaks may be attributed to weak zones caused by shives [102].

Separating contaminants from fibre is achieved by preventing contaminant passage through the screen and ultimately removing or concentrating them in the reject stream. Because contaminants level is usually very low, contaminant screens operate at the lowest

possibly reject rate to minimise loss of valuable fibre. However, contaminant removal efficiencies decrease with lower reject rates [103] so more contaminants can pass through. To overcome this, multiple screens are used to concentrate contaminants in the reject stream. A cascading system of three interconnected screens (a large primary screen with a relatively high reject rate, followed by smaller secondary and tertiary screens) is often used. There are many configurations so optimisation the three screens is complex [104-108]. For example, Friesen *et al.* [109] report that over 100 configurations are possible for a three-stage screening system. Steenberg [110] described configurations that produce high removal efficiencies and outlined coupling rules. Kanazawa [106] reported greater contaminant removal with cascade feed-back (Figure 2.8) than a cascade feed-forward configuration. Julien Saint Amand [73] noted that benefits from some configurations are debatable.

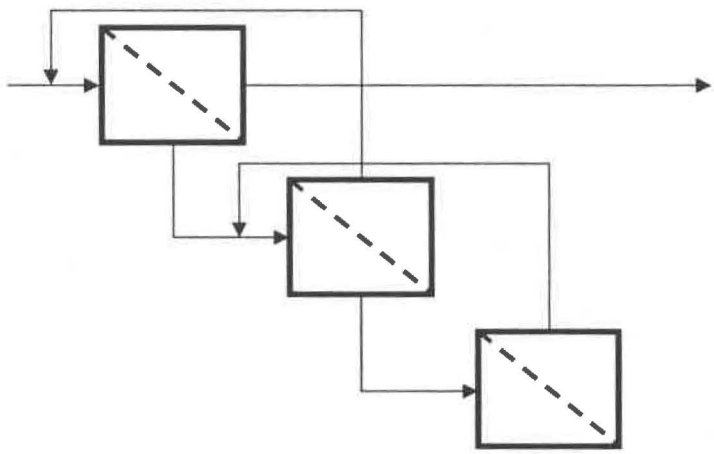

Figure 2.8 Cascade feed-back configuration of pressure screens (drawn from [106]).

- ***Reverse Screening, Filtrating on and Removal of Liquid Contaminants***

Removing liquid contaminants from pulp is an uncommon application of pressure screens and is often neglected in literature on pressure screening. Wax-laden water from pulped recycled wax containers can be removed in pressure screens [84]. The pressure screen acted as a pressurised filter and was the process was called reverse screening (because the contaminant is in the accept stream rather than the reject stream) and dynamic washing. Wax-laden water flowed through a filter screen cylinder and the valuable fibre was thickened and retained by the screen. A more recent report [111] describes fibre being retained on the feed side of a filter screen cylinder, which maximises the consistency change in the pressure screens. Consistency changes almost always occur with screening because most screens partially filter pulp so the accept consistency is lower than the feed consistency and the reject consistency is higher than the feed consistency. When reject consistency is higher than the feed, reject thickening is said to occur [93].

- ***Fibre Length Fractionation***

The objective in pressure screen fibre-length fractionation of wood pulp is to allow shorter (L_f<2 mm) fibres to pass through the screen apertures and thus separate (fractionate) them from longer fibres (L_f>2 mm) that cannot pass through the screen. The shorter fibres report to the accept stream and the longer fibres report to the reject stream (Figure 2.9).

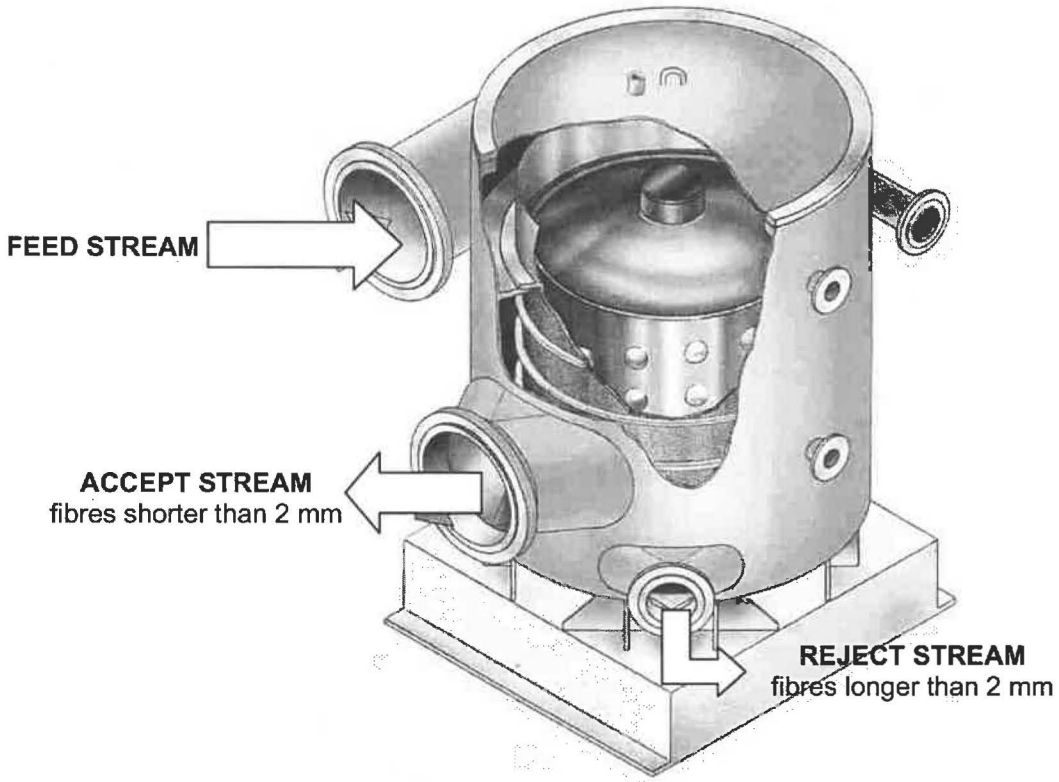

Figure 2.9 Pressure screen fibre-length fractionation.

Pressure screens can fractionate pulp into streams with differing coarseness (mass per unit fibre length) in a process termed coarseness fractionation, which is attributable to the relationship between fibre coarseness on fibre length. This process produces a rejects pulp with higher mean coarseness and an accept pulp with lower coarseness. However, other devices can produce better coarseness fractionation than pressure screens [30, 112-116]. Duffy [117] and Sloane [115] review coarseness fractionation devices.

2.3.2 Value from Smart Application of Pressure Screen Fractionation

Integrating pressure screen fractionation into step-wise pulp production offers the potential to lower costs and improve product quality [1, 38]. For example, the conventional linerboard process (Figure 2.1) can be simplified by incorporating pressure screen fractionation [1]. Simplification with either hot-stock fractionation (Figure 2.10)

or the brown stock fractionation (Figure 2.11) reduces the capital (less unit processes), energy, chemicals and wood to produce the same amount of fibre.

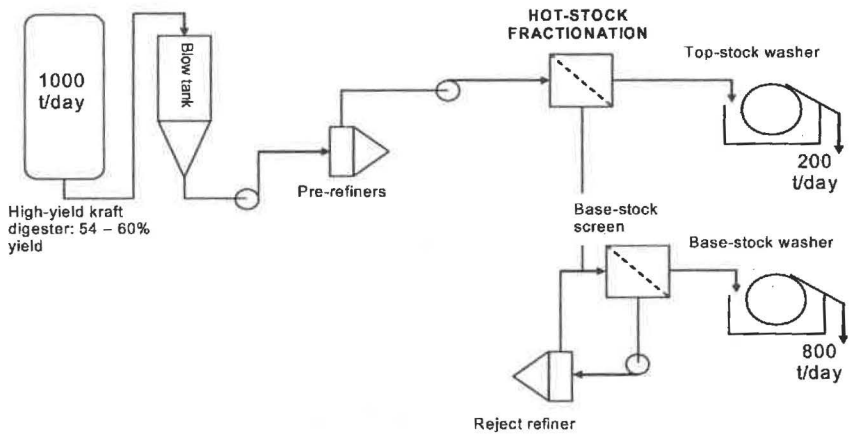

Figure 2.10 Simplified linerboard process featuring hot-stock fractionation (drawn from [1]).

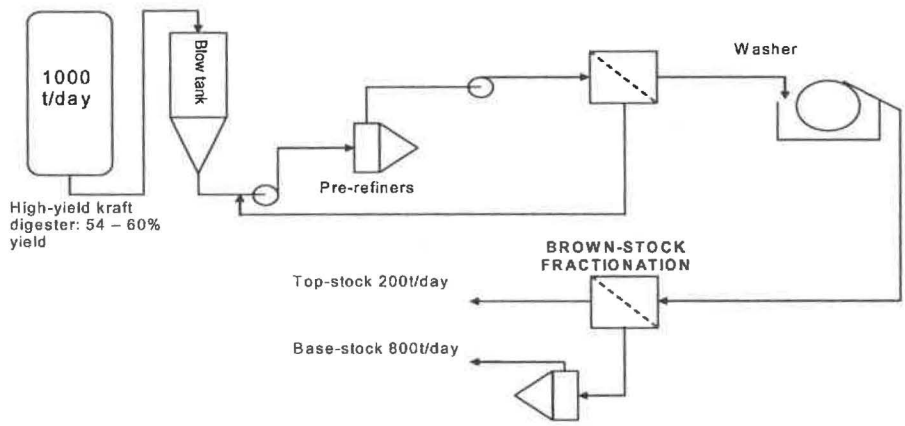

Figure 2.11 Simplified linerboard process featuring brown-stock fractionation (drawn from [1]).

Processes can be further simplified when the consistency of pulp feeding into a pressure screen C_f is increased, which would further increase capital and energy savings. For example, Fredricksson [118] described a simplified screening system by increasing feed consistency that required only two rather than three pressure screens. Eliminating a screen reduced piping, valves and controls. In addition, smaller, cheaper pipes were integrated into the system with lower volumetric flow-rates at higher feed consistencies. These modifications reduced capital cost by 50% and the energy by 50%. Gullichson *et al.* [71] reported that volumetric flow-rate through a pressure screening system was ten times lower when feed consistency increased from the low consistency range to the medium consistency range. Smaller pipes, pumps and pressure screens were required,

reducing lower capital and energy costs. Lower costs at higher feed consistencies may be negated, however, if mechanical entanglement due to flocculation increases and fractionation efficiencies are reduced.

Fractionation also offers the potential for product quality improvement. Multi-layered paper and paper products, using stratified forming technology, are manufactured to increase paper smoothness [119-121] and bending stiffness [119, 120, 122] at lower fibre cost by incorporating recycled fibre [119] or by using less fibre. Complete stratified forming deposits the fibre fractions, fillers, and additives using a single head-box and forming section instead of multiple head-boxes and forming sections. This gives better bonding between layers [119, 123] and less capital investment in head-boxes and forming sections [122]. Stratified forming technology [123-125] is used for manufacturing tissue paper and linerboard where problems of layer mixing and incomplete coverage of the middle layer are less critical.

2.3.3 History of Pressure Screen Technology

The first pressure screen was developed in 1939 [95] and had many features of a modern pressure screen. A wooden scraper rotated concentrically inside a screen cylinder at a peripheral speed (tip speed) of 3 ms^{-1}. The scraper contacted the screen physically, removing fibre accumulated at aperture openings. By the 1950s, the scraper had been replaced by a non-contacting rotating hydrofoil element and the screen was fully enclosed and operated above atmospheric pressures. The rotating element, now called an open type foil rotor, rotated at much higher speeds (10-20 ms^{-1}), which caused pressure fluctuations near the screen. Low pressure towards the trailing end of the foil was thought to cause temporary flow reversal (back-flow), which back-flushed the apertures allowing and continuous operation.

- ***Rotors***

Many rotors have now been developed. Bliss [95] describes the main types of rotors used today. The foil rotor is still widely used and called an open type rotor. Open rotors have a large gap between the rotor shaft (or central body of the rotor) and screen cylinder surface. The gap between the main rotor body and screen surface is much smaller in closed rotors (sometimes called solid-core rotors). The bump rotor is commonly-used closed type rotor.

Most researchers agree that the rotor induces temporary back-flow from the accept-side to the feed-side of the screen [87, 95, 126-138]. It is not known whether this back-flow is

water only or water and fibre. Nevertheless, back-flow flushes fibre and fibre flocs that have accumulated at aperture openings into the feed annulus [87] where fibre and flocs are subsequently mixed by the rotor, a process called back-mixing. Back-flow and back-mixing is thought to prevent the screen from blocking [137, 139], and without back-flow, continuous pressure screen operation seems impossible.

A typical pressure pulse of a step rotor (Figure 2.12) has positive and negative regions. The important features are the relationships of the peaks. The relative duration and size of the negative pulse affect the amount of back-flow from the accept-side of a screen to the feed annulus. It is thought that back-flow increases as pressure becomes more negative and as duration of the negative pulse increases.

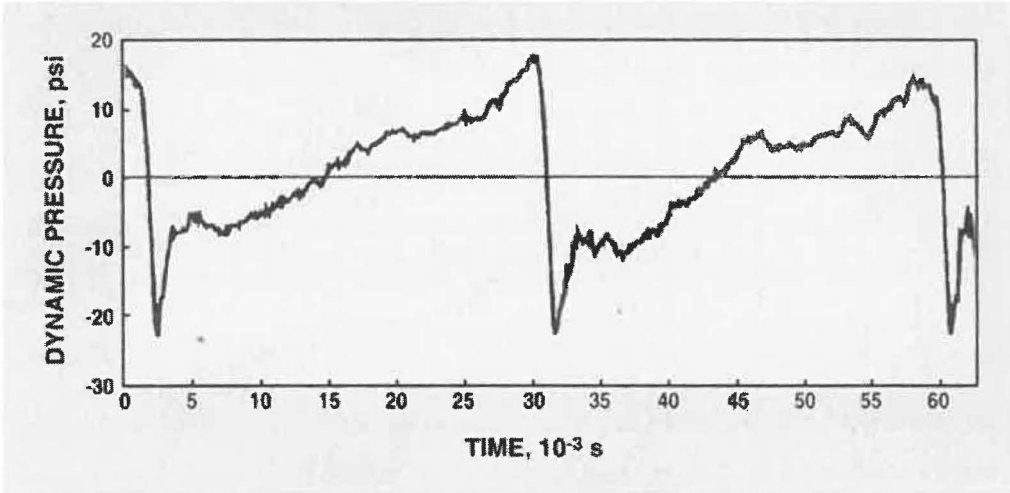

Figure 2.12 Pressure pulse of a step rotor (from [140]).

Back-flow has been measured ultrasonically [141]. Reported flow velocities support earlier speculation on flow being influenced by the pressure pulse signatures and that flow periodically reverses to back-flush the apertures. However, this research did not detail experimental methods, possibly because of commercial sensitivity, so flow data should be treated with caution. Interestingly, duration of back-flow in a step rotor is much longer than in a foil rotor but the back-flushing flow velocities are lower. As both effects can be interpreted from pressure pulse signatures, variables affecting back-flow can be interpreted from pressure pulse studies.

There are many reports on the pressure pulse [128, 130-132, 142, 143], which describe how rotor clearance, tip speed, rotor shape, and length of foil affect back-flow. Back-flow increases when the negative pulse lasts longer and the magnitude increases. The magnitude of the negative pulse increases with increasing rotor speed [133, 143],

decreasing clearance [133, 143] and decreasing consistency [130, 132]. However, Yu [131] reported that the pulses for water and pulp with 2% feed consistency were the same. The duration of the negative pulse increases with foil length [128] and step rotors have a longer negative pulses than foil rotors.

- ***Screen cylinders***

Early screens were punched or drilled holes. Drilled holes were conically drilled on the accept side to reduce pressure loss from a sudden expansion. Hole spacing is critical to avoid fibre stapling across the screen material between holes [94]. If the spacing is too close, longer fibre tends to staple across the material between holes. As the distance between holes increases, the open area decreases. The open area also decreases as hole size decreases. The smallest holes are typically 0.8-1 mm, which gives an open area of 10-14%. Large 5-mm holes are used for higher feed consistencies [71] and also for coarse screens and knotters. These screens have an open area of 20-40% [95].

A second type of screen now used widely in industry has slots (narrow rectangular axially-orientated gaps), which were originally cut with saw cutters. Having too many slots can compromise the screen's mechanical integrity so the early slotted screens had much lower open areas (3-7%) [95] than screens with holes.

Slotted screens are usually contoured to induce a favourable pulp flow field upstream of the contour (Figure 2.13). Microscopic studies of flows upstream of a contoured aperture [144] reveal that strategic positioning of contours increases passage of solid particles through an aperture [145]. Furthermore, additional small scale turbulence is produced as pulp flows past/over the contours. Floc dispersion and network disruption occurs at the sites of this extra turbulence, which is contour slotted screens can be operated at much higher feed consistencies [138]. Contouring affects flow at an aperture [144], and especially the position of a fluid recirculation zone (eddy). Fluid recirculation is upstream of a contoured aperture, effectively increasing the open area of the aperture. Having the recirculation zone upstream may prevent fibres and other solid debris accumulating at an aperture because any fibres that accumulate are transported away from the aperture and recirculated to the fluid in the feed annulus.

Holes are traditionally thought to be better for fractionating fibre length [146] and for high throughput. However, Wakelin [147] showed that slots give similar fractionation to holes, albeit at a much lower throughput. He also showed that slotted screens fractionate fibres on fibre cross-sectional dimensions better than screens with holes.

A

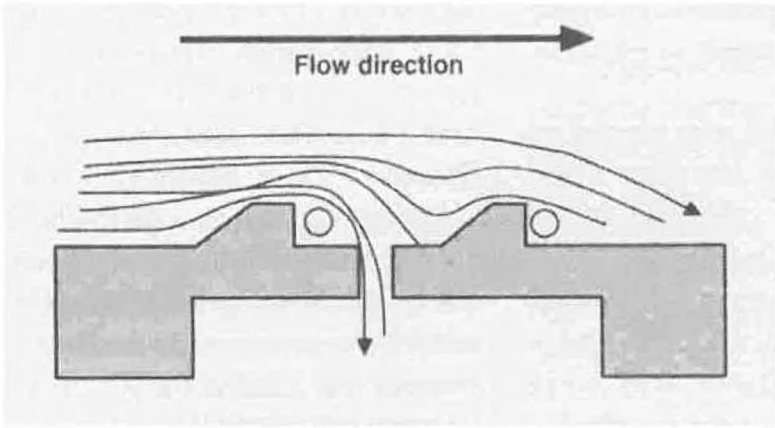

B

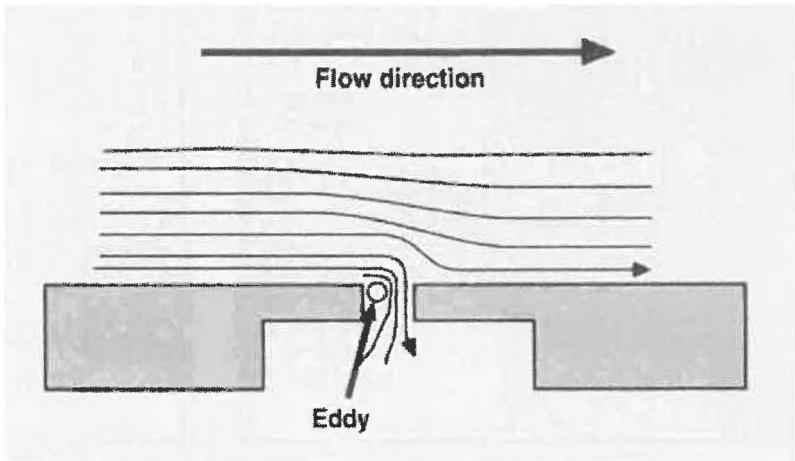

Figure 2.13 Fluid flow over a screen with (A) contoured and (B) flat apertures (from [144]).

A recent advance has wedge-wire screens, which are slotted screens made by welding bars parallel to one another. The spacing between the bars becomes to slot for fibre passage. This construction method doubles the open area of a slotted screens and a strong screen that resist buckling can be constructed relatively simply.

Julien Saint Amand [73] states that a goal for pressure screen manufacturers is to develop screens that can be operated with very fine slots at increased feed consistency, lower reject rates, and high separation efficiencies. Reducing fibre lost to the reject stream is also a goal because screening capacity decreases as more fibre is lost. Recently, screen cylinders have been shortened to reduce fibre loss (i.e screen cylinder length L_s reduced), but this decreases screen area, which reduces screening capacity. To overcome this, some new screens have multiple short screen sections that screen in parallel [89, 148] (Figure 2.14). Although these new screens may have higher capacities, they may not fractionate as effectively as conventional screens with longer screen cylinders. It is also uncertain if they exhibit the same macro mixing and flow behaviour because the length for pulp

mixing has been reduced. Consequently, existing screening models based on ideal flow configurations may not necessarily apply to the new screens.

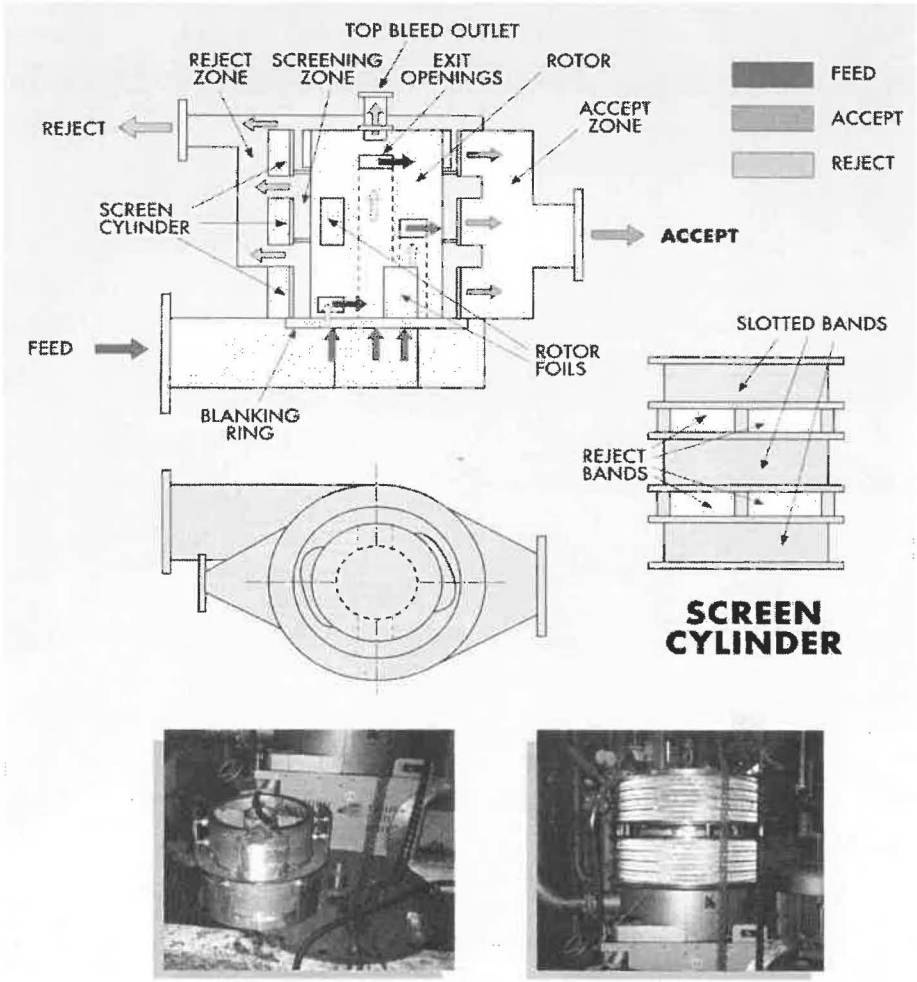

Figure 2.14 A pressure screen with multiple, short screen sections within a single housing (from [89]).

2.4 Mechanisms of Pulp Screening and Fractionation

Mechanisms of fibre-length fractionation are poorly understood. Two main mechanisms are often cited: the fibre mat mechanism based on fibre-fibre interactions, and the fibre alignment mechanism based on fibre alignment (mainly by fluid velocities) as a fibre approaches an aperture.

2.4.1 Fibre Mat Mechanism

A fibre mat forms temporarily on the screen apertures as flocs and fibre bundles consolidate. This temporary accumulation of fibre produces a separation mechanism during a cycle of the rotor, possibly on both sides of the screen. Separation of longer

fibres from the shorter fibres occurs when the longer fibres become mechanically entangled in the fibre mat, whilst shorter fibre remain relatively mobile and can flow through the screen apertures.

As early as 1938, Cowan proposed that fibres and sticks (shives) accumulated at the surface of the screen plate in a Cowan screen [149], which appears to be the first reference to a fibre mat screening mechanism. This fibre mat was used to explain the exaggerated increase in shive removal efficiency as hole size decreased. Because this increase could not be attributed to reduction in hole size, another factor was involved.

Beaulieu *et al.* [150] proposed that the fibre mat formed when TMP pulp is screened acts as a physical barrier to fibre and other particles, thus preventing shives passing the apertures. Reducing hole diameter from to 2.4 mm to 1.3 mm did not change shive removal efficiency. Wakelin *et al.* [151] also cited that Cowan [149] proposed a fibre mat to explain the exaggerated influence reducing hole size had on shive removal efficiency. They noted that Beaulieu *et al.* [150] and Cowan [149] proposed the existence of a fibre mat from "opposing observations". Wakelin *et al.* [151] and others [129, 152] argue that a fibre mat could form on both sides of the screen (feed side and accept side), but do not discuss the implications of this on fibre passage through screen apertures.

Yu and DeFoe [144] simulated mat formation on flat sections of a screen at the bottom of a transparent channel. High-speed video film of pulp flow and fibre accumulation showed that material accumulating at aperture openings on the screen surface was a collection of fibres, flocs, flakes and other solid debris. An important event before fibre accumulation and mat formation was immobilisation of fibres at the aperture openings by a stapling mechanism. Fibres and other solid debris collected and entangled around the immobilised fibres, forming piles. More fibre and other debris accumulated on these piles and consolidated. Adjacent piles joined and ultimately formed a continuous layer on the screen surface. A continuous, 2-3 mm thick fibre mat formed on the screen surface within milliseconds and then there was equilibrium between deposition and material moving into the main channel.

2.4.2 Fibre Alignment Mechanism(s)

Intensive studies on steady-state fluid and fibre flow through a single, rectangular slot at the bottom of a rectangle channel [5, 144, 153-162] have provided insights into possible mechanisms of fibre passage and fibre length fractionation in industrial pressure screens.

These findings are the basis of a Fibre Alignment Mechanism, where fibre alignment within an exit layer relative to the exit layer determines relative fibre passage and fibre fractionation. Fibre alignment is based on fibre interactions with the suspending fluid and fibre impacts with the screen but not on fibre-fibre interactions. Therefore, mechanisms identified in these fundamental studies probably only apply at very low pulp consistencies.

Data obtained by filming fluid and fibre flow at an aperture [144, 154, 163] together with fluid flow were modelled using Computation Fluid Dynamics (CFD) [5, 142, 158]. Thomas and Cornelius [164] reported a recirculation zone inside and on the upstream side of an aperture, which increased with increasing upstream fluid velocity V_u and decreased with increasing aperture velocity V_s. Yu and De Foe [144] filmed this phenomenon, which was also evident in CFD solutions [5, 142]. Because the size of the recirculation zone increases with decreasing aperture velocity and increasing upstream velocity, the effective open area of the aperture decreases. In addition, fibre passage decreases as the open area decreases with decreasing aperture velocity and increasing upstream velocity. However, although the decrease in open area accounts for the decreases in fibre passage, this mechanism does not explain how long and short fibres are fractionated.

Gooding [154] was one of the first researchers to systematically study fibre passage through a single slot and introduced the fibre passage ratio $P_{(x)}$ which quantified fibre passage through a single aperture. Passage ratio is synonymous with the probability of passage and was defined in terms of the concentration of fibres passing through the slot $C_{s(x)}$ and the concentration of fibre upstream of the slot $C_{u(x)}$ (Equation 2.13). He studied passage of fibres through a rectangular slot in a transparent rectangular test section, using dilute fibres suspensions (consistencies as low as 2000 fibres per litre) so individual fibres could be tracked, and to reduce blockage of the slots and fibre-fibre interactions. Factors investigated include: effects of slot velocity V_s, main channel velocity upstream of the slot V_u, fibre length L_F and fibre flexibility F_F. Passage ratio increased with shorter (1-mm) fibres, higher slot velocities, decreasing main channel velocities, and increasing fibre flexibility (particular for fibres longer than 3 mm).

$$P_x = \frac{C_{s(x)}}{C_{u(x)}} \tag{2.13}$$

Gooding observed that a fibre must be within the fluid exit layer (of height H in Figure 2.15), to have a chance of passing through an aperture. This observation was confirmed

in subsequent studies [5, 157, 158]. Gooding also observed stiff fibres (e.g. nylon fibres) colliding with the downstream edge when entering an aperture opening, rotating at the aperture edge and flowing back into the main channel. However, long flexible fibres could staple on the downstream edge of a slot. In addition, a phenomenon called a Wall Effect was observed, in which a fluid layer near the channel wall was depleted of fibre. Olson [5], using the same apparatus as Gooding, showed that the Wall Effect is the dominant factor determining fibre passage.

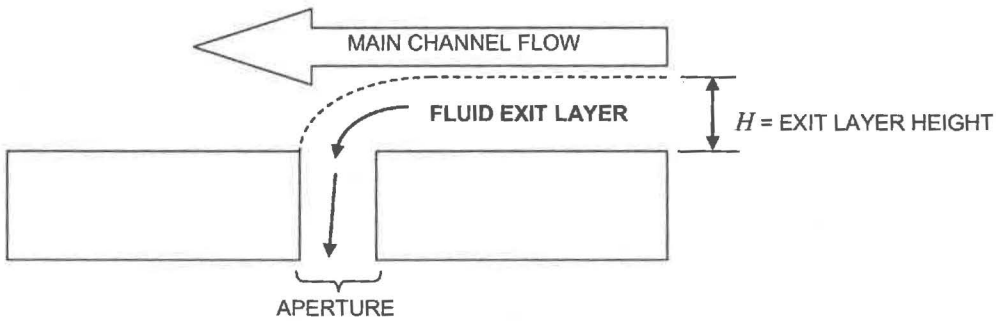

Figure 2.15 Exit layer of fluid flowing into an aperture at the bottom of a rectangular channel.

Kumar [157] examined the effect of fibre length L_f, slot width W, upstream slot velocity V_u and slot (aperture) velocity V_s on fibre passage through single slot type apertures and encompassed the effects of these variables in a dimensionless penetration parameter P_e (Equation 2.14), derived by considering a fluid mass balance at a slot entry and second analysis considering only velocity and time. The penetration parameter is an approximate physical representation of the degree fibre penetrates a slot/aperture or the size of main flow relative to a fibre length drawn into an aperture. His analysis does not include variation in pulp consistency within the exit layer or fibres having differing orientations. Although the penetration parameter was only linked in a general way to fibre passage, it was an important grouping of variables used in later analyses of fibre passage.

$$P_e = \frac{WV_s}{L_f V_u} \tag{2.14}$$

Characteristic curves can be produced for nylon fibres of various lengths by plotting passage ratio against normalised slot velocity V_n (the ratio of V_s to V_u). The characteristic curves for short fibres (fibre length is less than twice the slot width) were exponential, which Kumar [157] calls A curves. Characteristic curves for longer fibres (fibre length more than twice slot width) were a more complex S-shape, which Kumar termed B curves and are similar to cumulative probability distribution curves. Curves for

short fibres fit the penetration parameter well but curves for longer fibre do not. This may be because long and short fibre immobilised on the downstream edge of a slot behave differently, and there would be few long fibres near the screen in a short fibre pulp. Consequently, fibre stapling behaviour of sort and long fibre pulps will differ.

Olson [5] found that the layer of depleted fibre (Wall Effect) extends approximately 0.3 of a fibre length L_f above the channel surface. Thus, the depleted layer height is 0.3 mm for a 1-mm fibre and 1 mm for a 3- mm fibre. He also found that the fibre point consistency C(y) in the depleted layer above the channel wall, normalised by the main channel consistency C_u, was zero at the channel wall and increased linearly with distance from the channel wall (Figure 2.16).

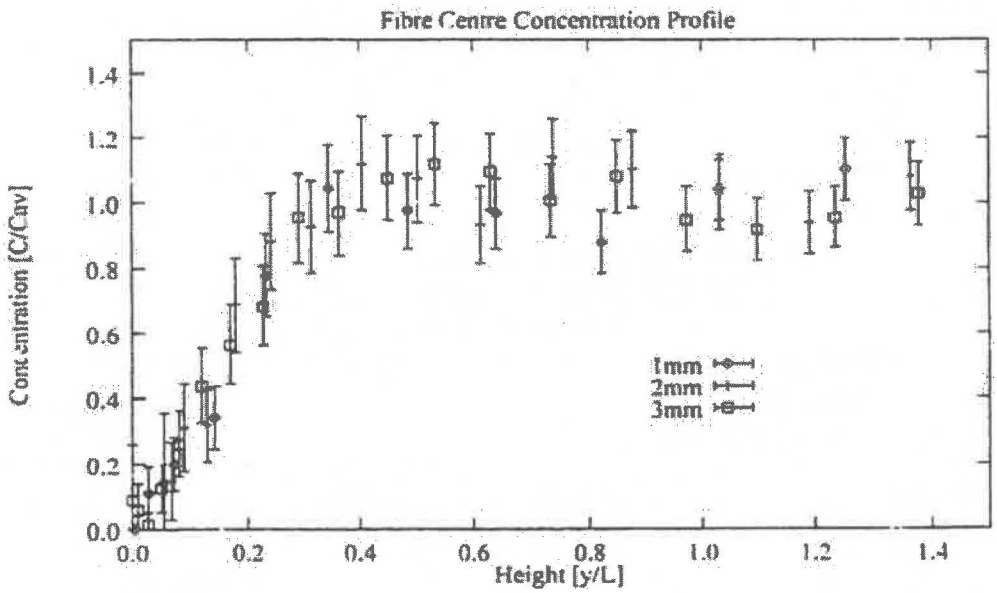

Figure 2.16 Effect of height from channel wall on fibre point concentration (from [5]).

Olson [5] also studied the effect of fibre orientation approaching a slot on fibre passage by modelling fibre trajectory. The motions of ridged, inertia-less fibres with infinitesimally small diameters in turbulent flow were modelled and equations of mean motion were integrated numerically through a turbulent bifurcating flow field given by a commercial κ-ϵ CFD software program. Olson [164] modelled fibre trajectory from an initial fibre position x_o upstream of a slot aperture as a function of distance y_o from the channel wall and initial angle of orientation θ_o (Figure 2.17). He found that fibres approaching a slot could (A) wedge in the slot, (B) pass into the slot, (C) continue down the channel, or (D) be horizontally stapled (Figure 2.18).

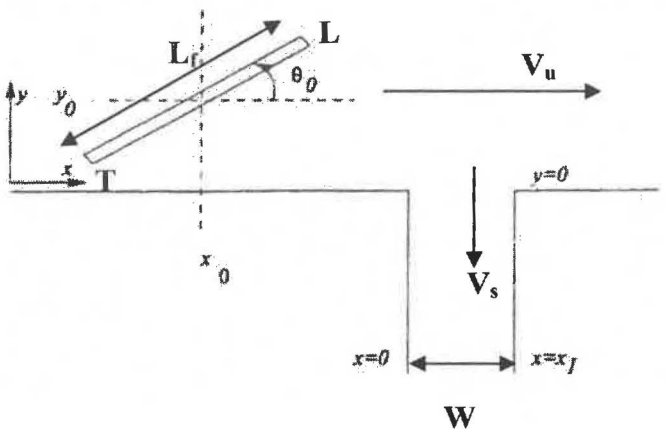

Figure 2.17 Fibre at initial position (x_0) and angle (θ_o) upstream of a rectangular slot (from [5]).

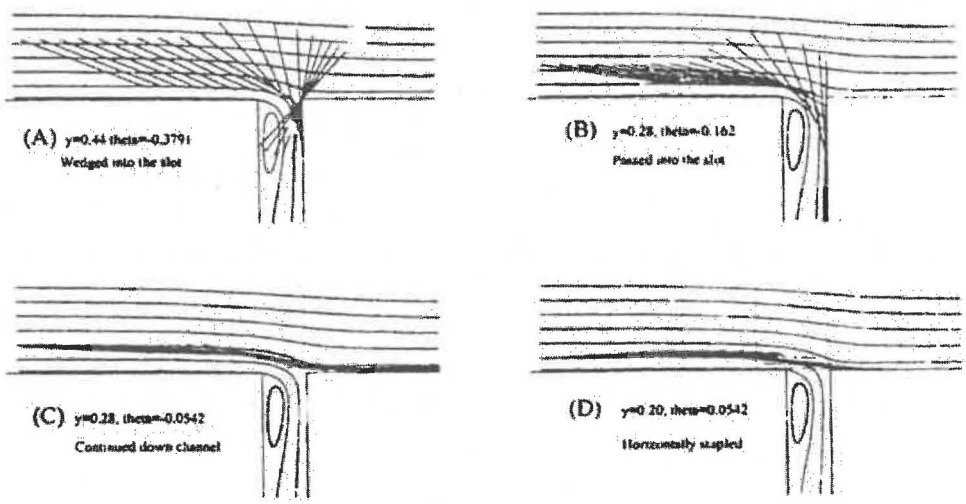

Figure 2.18 Fate of fibre determined from modelled fibre trajectories (from [5]).

Olson calculated the probability of passage function p(y) from the number of fibre trajectories passing through the aperture T_p divided by the total number of trajectories T_t (Equation 2.15) for all possible initial positions y_o and orientations θ_o upstream of the slot. The probability of passage function p(y) was approximately 1 when a fibre was within the exit layer of height H.

$$p(y) = \frac{T_p}{T_t} \tag{2.15}$$

Olson [5] derived a single expression for passage ratio (Equation 2.16), where H is exit layer height, L is fibre length, K is the Von Kármán constant (0.4), C is local fibre concentration, y is height above the channel wall, V_u is bulk fluid velocity upstream of an aperture, C_u is average fibre concentration upstream of an aperture, and B is equal to 5.5

assuming smooth channel walls. The value for v* is calculated from Equation 2.17, where ρ is density of water and τ_w is shear stress near the channel wall. Equation 2.16 can only be solved numerically.

$$P = \frac{1}{P_e} \int_0^{W/L} \frac{\left(\frac{v^*}{K} \ln\left(y\frac{v^*}{v}\right) + Bv^*\right)}{V_u} \frac{C\left(\frac{y}{L}\right)}{C_u} \frac{dy}{L} \tag{2.16}$$

$$v^* = \left(\frac{\tau_w}{\rho}\right)^{\frac{1}{2}} \tag{2.17}$$

Olson [5] compared theoretical values with experimental passage ratios obtained by Kumar [157] and found that the model could predict passage ratios of short fibres (Figure 2.19) but was less effective for longer fibres (Figure 2.20).

Olson and Wherrett [165] further developed the model for predicting fibre passage through apertures of a model screen (consisting of multiple apertures) using the main assumptions of Olson [5]. However, predicted ratios did not agree with observed passage ratios. They believed that the discrepancies could be due to the model not accounting for fibre flexibility effects, fibre impacts with the screen and fibre stapling. Nevertheless, the failure their model illustrates the complexity of the problem and pressure screening cannot be easily modelled.

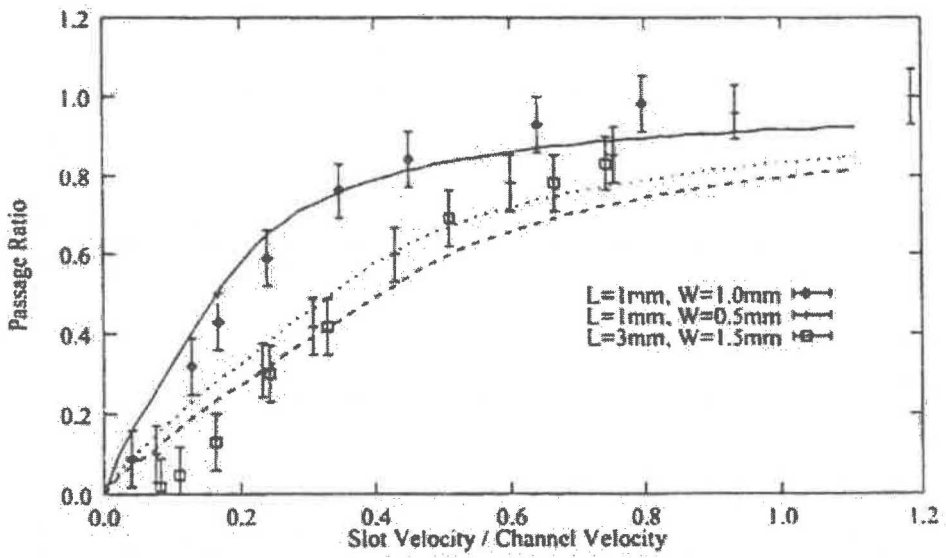

Figure 2.19 Modelled passage of short fibre through a single aperture (from [5]).

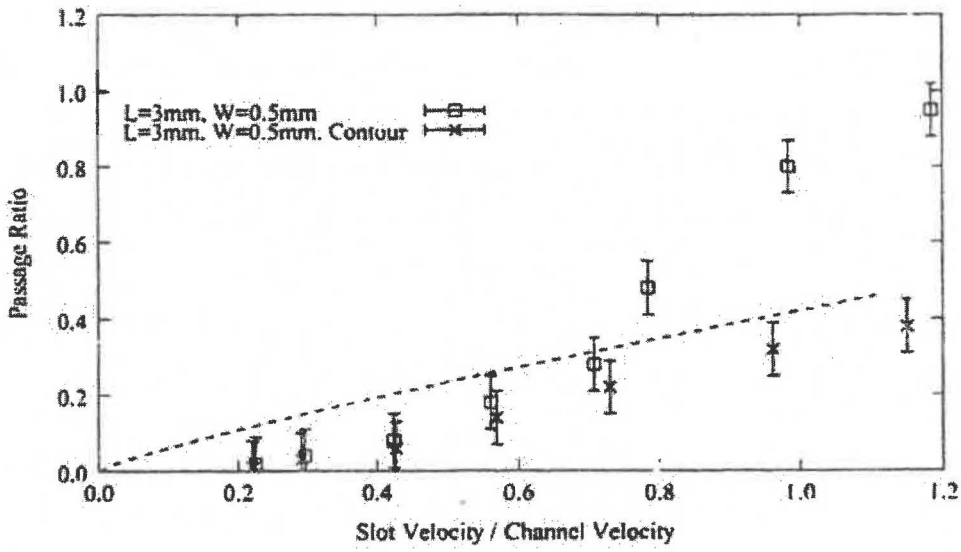

Figure 2.20 Modelled passage of long fibre through a single aperture (from [5]).

2.4.3 Criticisms of Fibre Alignment Mechanisms

Although velocities near an aperture are fundamental to alignment mechanisms for fibre passage, there is limited understanding of velocities in a real pressure screen as velocities have never been reported. Furthermore, it remains unclear whether fibre passage is controlled by velocities near an aperture, concentration of fibres in the exit layer, a fibre mat, or a combination of these factors. If it is a combination, the relative importance of each factor is not known.

Hooper [94] identified three main velocities inside a screen, excluding velocities associated with local turbulence: radial velocity V_{rad} (velocity through the screen); tangential velocity V_{tan} (circumferential velocity around screen); and axial velocity V_{ax} (velocity through the feed annulus in direction of the reject compartment). Radial velocity is assumed to be proportional to open area of the screen, tangential velocity is assumed proportional to rotor tip speed V_{tip}, and axial velocity is assumed proportional to open area of feed annulus A_z. Gooding [154] and others [151, 165, 166] used first principles to obtain values for these velocities. Radial velocity is approximately aperture velocity V_s and is sometimes called the superficial velocity, passing velocity or average aperture velocity. Aperture velocity is dynamic but a first approximation is to make it a function of open area A_o and volumetric accept flow-rate Q_a (Equation 2.18).

$$V_s = \frac{Q_a}{A_o} \tag{2.18}$$

Tangential velocity V_{tan} is proportional to rotor tip velocity V_{tip} and slip factor S (Equation 2.19). Gooding [154] estimated S assuming Newtonian flow and proposed that S = 0.85 approximated the decrease in fluid velocity from the rotor tip to the exit layer. However, this value is not definite, especially as pulp is not a Newtonian fluid [48].

$$V_{\tan} = (1 - S)V_{tip} \tag{2.19}$$

Axial velocity V_{ax} decreases linearly if accept flow-rate across the screen is uniform along a screen length z and can be calculated by Equation 2.20, where A_z is open area of the feed annulus, h is distance between screen surface and rotor body, Q_f is volumetric feed flow rate and Q_a is volumetric accept flow rate.

$$V_{ax} = \frac{1}{A_z}\left(Q_f - \frac{z}{h}Q_a\right) \tag{2.20}$$

The sum of V_{ax}^2 and V_{tan}^2 gives a squared velocity immediately upstream of an aperture opening V_u^2 (Equation 2.21). Because the axial velocity V_{ax} is usually much smaller than tangential velocity V_{tan}, it is often ignored.

$$V_{u(p)}^2 = V_{\tan}^2 + V_{ax}^2 \tag{2.21}$$

2.5 Modelling Pressure Screens

Modelling helps understand the behaviour and internal workings of a pressure screen. It has been used to predict contaminant removal efficiencies [167], consistency changes [93], and fibre length fractionation efficiency [22, 168]. Performance equations have been derived for mixed flow and for plug flow. Most modellers assume probability screening but Gooding and Kerekes [167] derived performance equations for combined probability and barrier screening that apply to shives removal by screens when a certain proportion of the shives are larger than the aperture in all dimensions.

Probability and barrier screening are modes of solid-solid separation where solid particles are separated from other solid particles. Probability screening occurs when particles of interest have at least one dimension smaller than the screen apertures. Depending on several factors, particles have a finite probability of either passing through the apertures (probability of passage) or being rejected by the screen (probability of rejection). Particle passage in probability screening in pressure screens is governed by complex interactions of hydrodynamic forces, particle orientation, particle-particle interactions and relative size of particles and apertures. Wood fibres with at least two dimensions smaller than the

screen hole will be screened by their probability of passage. Shives and contaminants, which can vary considerably in size, are screened by either probability or barrier screening. Barrier screening occurs when particles of interest are retained on the screen because all their dimensions are large than the aperture size. Relative particle size is the main factor in barrier screening, with hydrodynamic forces being less important.

Flow behaviour through a chemical reactor or separation vessel strongly affects product purities [169]. There are two ideal flow behaviours reported in the chemical engineering literature; flow through a continuous stirred tank reactor (CSTR), and flow through a plug flow tubular reactor (PFTR) [170-173]. In the pressure screening literature, these flow behaviours are called mixed flow (CSTR) and plug flow (PFTR) respectively.

Mixing is provided by mechanical agitation with mixed flow, and mixing time for a particle is vanishingly small compared to its mean residence time [173]. Fluid or slurry entering the vessel instantaneously and completely mixes with the contents of the vessel to give a uniform composition throughout, which equals composition of the outlet [170-173]. When modelling pressure screening as mixed flow, only the contents of the feed annulus are considered and it is assumed that the feed annulus consistency C_z is uniform (Figure 2.21) and equal to consistency of the reject stream C_r (Equation 2.22).

$$C_z = C_r \tag{2.22}$$

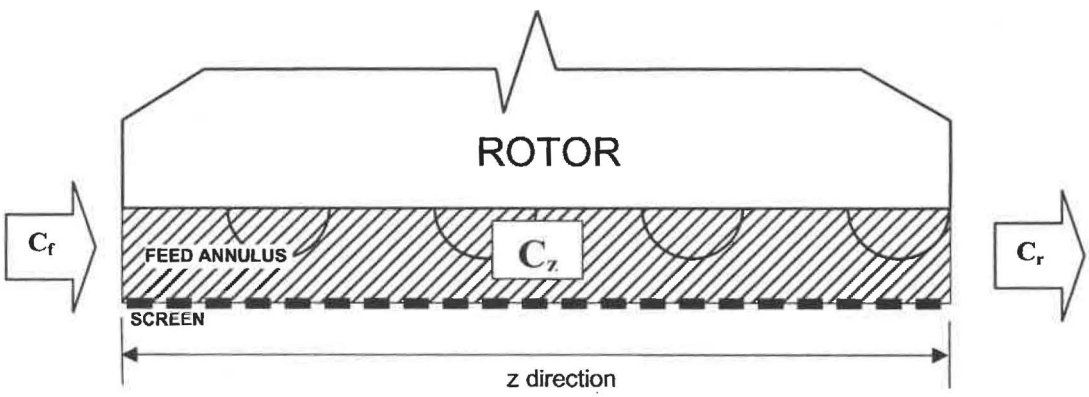

Figure 2.21 Mixed flow with uniform consistency in the feed annulus of a pressure screen.

In a plug flow separation device or reactor, flow rate and fluid/slurry properties are uniform over any cross-section normal to fluid motion. The radial velocity profile is flat and radial mixing is perfect. There is negligible axial mixing due to diffusion or convection and fluid elements flow through the vessel without mixing with adjacent fluid

elements. Liquid/slurry composition changes with axial position but at any given position are constant with time.

Plug flow modelling usually begins with a differential element within a separation device or reactor, with boundaries normal to fluid motion. As in mixed flow, the analysis only considers the contents of the feed annulus and begins with a material balance on volumetric flow and solids concentration around an annular element of thickness *dz* (Figure 2.22).

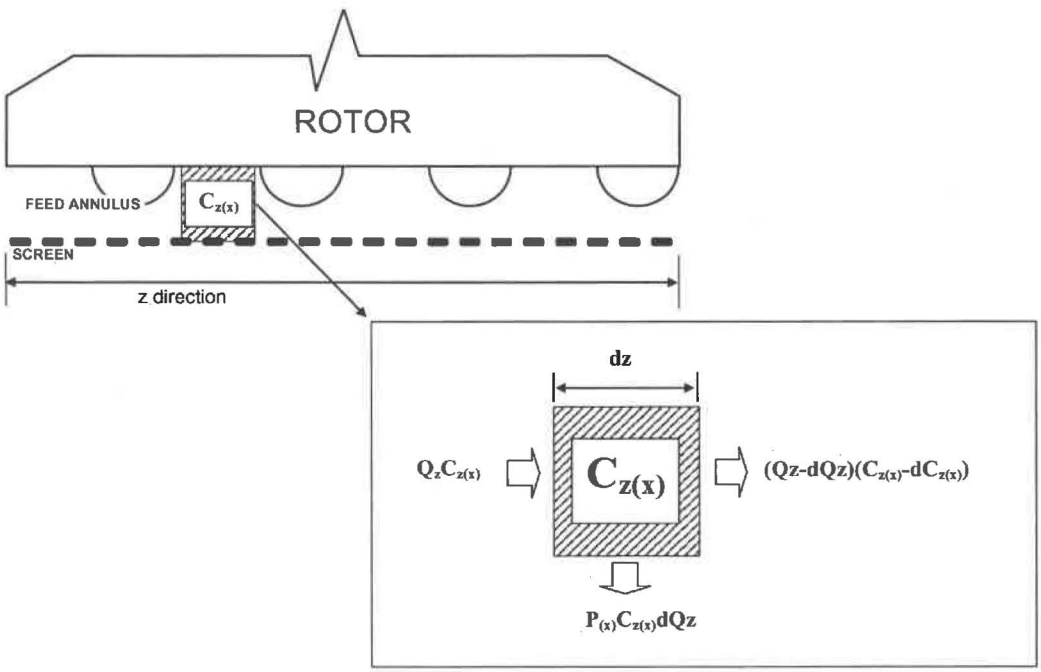

Figure 2.22 Mass balance around an infinitesimally small annular element (drawn from [93]).

2.5.1 Modelling Contaminant Removal

Kubat and Steenberg [174] were the first to model a screen. They assumed plug flow and probability screening and modelled the screen as a row of apertures. Screening occurs in series, which is why plug flow screening is sometimes called series screening. Although they did not give a full derivation in their paper, Gooding and Kerekes [167] extended their work and reported that contaminant removal efficiency E can be expressed as a function of the mass reject ratio R_m and an independent parameter B (Equation 2.23). Notably, E increases as B decreases.

$$E = R_m^{\ B} \tag{2.23}$$

Nelson [175] was the first to model a screen assuming mixed flow and probability screening. Efficiency was expressed as a function of mass reject ratio R_m and an independent parameter called the screening quotient Q (Equation 2.24). Efficiency increases as Q increases. This equation has found widespread use in pulp screening. However, Nelson also did not present a full derivation of his model but later Gooding and Kerekes [167] did.

$$E = \frac{R_m}{1 - Q + QR_m} \tag{2.24}$$

Gooding and Kerekes [167] based their model of contaminant removal E on the probability of passage at a single aperture, which is synonymous with the passage ratio for a particle of interest (Equation 2.15). Two passage ratios were defined, one for passage of pulp fibre P_p (fibre only), and another for passage of solid contaminant particles P_c. The passage ratio for pulp P_p is given by Equation 2.25 where $C_{s(p)}$ is pulp fibre concentration (fibre consistency) flowing through an aperture and $C_{u(p)}$ is pulp fibre concentration upstream of an aperture.

$$P_p = \frac{C_{s(p)}}{C_{u(p)}} \tag{2.25}$$

The passage ratio for contaminant particles P_c is given by Equation 2.26 where $C_{s(c)}$ is concentration of contaminant particles flowing through an aperture and $C_{u(c)}$ is concentration of contaminant particles flowing upstream of an aperture.

$$P_c = \frac{C_{s(c)}}{C_{u(c)}} \tag{2.26}$$

- **Mixed Flow**

In mixed flow, where apertures are screening in parallel (simultaneously), concentration of any particle of interest 'x' (x being either pulp fibre 'p' or contaminant particle 'c') flowing through an aperture $C_{s(x)}$ is equal to concentration in the accept stream $C_{a(x)}$ (Equation 2.27). Because composition in the feed annulus is uniform throughout, the concentration of any particle upstream of any aperture $C_{u(x)}$ is equal to concentration in the feed annulus $C_{z(x)}$ (Equation 2.28), which in turn is equal to concentration in the reject stream $C_{r(x)}$ (Equation 2.29).

$$C_{s(x)} = C_{a(x)} \tag{2.27}$$

$$C_{u(x)} = C_{z(x)} \tag{2.28}$$

$$C_{z(x)} = C_{r(x)} \tag{2.29}$$

The equations for passage ratio (Equations 2.25 and 2.26) can be rewritten by applying Equations 2.27, 2.28, and 2.29 to obtain Equations 2.30 and 2.31 in terms of concentrations in the accept and reject streams

$$P_c = \frac{C_{a(c)}}{C_{r(c)}} \tag{2.30}$$

$$P_p = \frac{C_{a(p)}}{C_{r(p)}} \tag{2.31}$$

A mass balance around a screen is used to derive equations for mass reject ratio R_m (fibre) and contaminant removal efficiency E. A feed mass flow M_f applied to a screen will separate into an accept mass flow M_a and a reject mass flow M_r (Figure 2.23). Mass (Equation 2.32) and volume (Equation 2.33) balances can be created for flow around a screen, where Q_f is volumetric flow rate of feed stream, Q_a is volumetric flow rate of the accept stream and Q_r is volumetric flow rate of the reject stream.

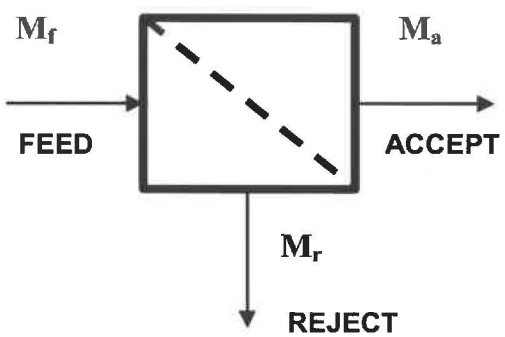

Figure 2.23 Mass balance around a pressure screen.

$$M_f = M_a + M_r \tag{2.32}$$

$$Q_f = Q_a + Q_r \tag{2.33}$$

The mass balance can be re-written in terms of the volumetric flow rates and solids concentration in the feed, $C_{f(x)}$, accept $C_{a(x)}$, and reject $C_{r(x)}$ streams (Equation 2.34).

$$Q_f C_{f(x)} = \left(Q_a C_{a(x)}\right) + \left(Q_r C_{r(x)}\right) \tag{2.34}$$

The mass reject ratio R_m (Equation 2.35) quantifies the mass fraction of fibre flowing to the reject stream.

$$R_m = \frac{Q_r C_{r(p)}}{Q_f C_{f(p)}} \tag{2.35}$$

The contaminant removal efficiency E (Equation 2.36) quantifies the mass fraction of contaminants flowing to the reject stream.

$$E = \frac{Q_r C_{r(c)}}{Q_f C_{f(c)}} \tag{2.36}$$

Dividing Equation 2.36 for contaminants (x=c) by the same equation for pulp fibre (x=p), and substituting the expressions for passage ratio of pulp (Equation 2.31) and contaminants (Equation 2.30) gives Equation 2.37.

$$\frac{P_c C_{r(c)} = (Q_f C_{f(c)}) - (Q_r C_{r(c)})}{P_p C_{r(p)} = (Q_f C_{f(p)}) - (Q_r C_{r(p)})} \tag{2.37}$$

Substituting in Equations 2.35 and 2.36 (for R_m and E respectively) and simplifying gives Equation 2.38.

$$\frac{P_c}{P_p} = \frac{\frac{1}{E} - 1}{\frac{1}{R_m} - 1} \tag{2.38}$$

Rearranging terms in Equation 2.38 gives an expression for efficiency in terms of passage ratio and mass reject ratio (Equation 2.39).

$$E = \frac{R_m}{R_m + \frac{P_c}{P_p} - \frac{P_c}{P_p} R_m} \tag{2.39}$$

Equations 2.39 and 2.24 (Nelsons equation [175]) are equivalent if Equation 2.40 is satisfied (where Q is Nelson's [175] screening quotient). Q is only meaningful if it is independent of the mass reject ratio but is not clear from literature whether this is true.

$$Q = 1 - \frac{P_c}{P_p} \tag{2.40}$$

- **Plug Flow**

A plug flow model assumes that apertures screen pulp in series and axial mixing in the feed annulus is incomplete. Radial mixing within infinitesimally narrow annular elements of width *dz* is instantaneous and complete (perfect mixing normal to the screen

surface). A model for contaminant removal efficiency can be obtained by mass balance for material flow across an annular element (Equation 2.41) where Q_z is axial flow-rate in the direction z, $C_{z(x)}$ is concentration at axial position z and $P_{(x)}$ is the passage ratio.

$$Q_z C_{z(x)} = dQ_z P_{(x)} C_{z(x)} - [(Q_z - dQ_z)(C_{z(x)} - dC_{z(x)})] \tag{2.41}$$

Equation 2.41 can be expanded, simplified, and rearranged into a differential mass balance (Equation 2.42).

$$\frac{dC_{z(x)}}{C_{z(x)}} = (P_{(x)} - 1)\frac{dQ_z}{Q_z} \tag{2.42}$$

Integrating Equation 2.42 in the *z* direction, between the following boundary conditions:

For z = 0, $C_{z(x)} = C_{f(x)}$ and $Q_z = Q_f$

For z = S, $C_{z(x)} = C_{r(x)}$ and $Q_z = Q_r$

where S = axial length of the feed annulus in the *z* direction

gives Equation 2.43:

$$\frac{C_{r(x)}}{C_{f(x)}} = \left(\frac{Q_r}{Q_f}\right)^{(P_{(x)}-1)} \tag{2.43}$$

Gooding and Kerekes [93] acknowledged that their plug flow model was valid only if passage ratio is constant along the length of a screen, i.e is independent of changes in $C_{z(x)}$ and Q_z. As an approximation, the rotor is assumed to dominate the flow field at an aperture and that changes in Q_z do not appreciably affect the flow field. The passage ratio could be independent of C_z if the rotor induces intense local turbulence, which will give complete disperse the flocs in the feed annulus, allowing fibres to act independently. However, flocs and unstable fibre bundles will persist even with intense mixing in rotary shear devices [53].

Equation 2.44 is for pulp fibre and Equation 2.45 is for contaminant particles.

$$\frac{C_{r(p)}}{C_{f(p)}} = \left(\frac{Q_r}{Q_f}\right)^{(P_p-1)} \tag{2.44}$$

$$\frac{C_{r(c)}}{C_{f(c)}} = \left(\frac{Q_r}{Q_f}\right)^{(P_c-1)} \tag{2.45}$$

Combining Equations 2.44 and 2.35 gives an expression for mass reject ratio R_m in terms of passage ratio and volumetric flow rates (Equation 2.46).

$$R_m = \left(\frac{Q_r}{Q_f} \right)^{P_p} \tag{2.46}$$

Likewise, combining Equations 2.45 and 2.36 gives an expression for contaminant removal efficiency based on passage ratio and volumetric flow rates (Equation 2.47).

$$E = \left(\frac{Q_r}{Q_f} \right)^{P_c} \tag{2.47}$$

Combining Equations 2.46 and 2.47 gives an expression for modelling contaminant removal efficiency in terms of mass reject ratio and passage ratios for pulp fibre and contaminants (Equation 2.48).

$$E = R_m^{\left(\frac{P_c}{P_p} \right)} \tag{2.48}$$

Equation 2.48 is equivalent to Equation 2.23 (Kubat and Steenberg [174]) if Equation 2.49 is satisfied, where B is the independent parameter in Equation 2.23.

$$B = \frac{P_c}{P_p} \tag{2.49}$$

The expressions for modelling contaminant removal assuming mixed flow and plug flow (Equations 2.41 and 2.50 respectively) apply to probability screening [167]. Gooding and Kerekes [167] also derived expressions based on combined probability and barrier screening (shive removal) by considering contaminant concentration in the feed stream to be the sum of two independent components - a probability contaminant concentration $C_{f(c.prob)}$ and a barrier contaminant concentration $C_{f(c.bar)}$ (Equation 2.50).

$$C_{f(c)} = C_{f(c.prob)} + C_{f(c.bar)} \tag{2.50}$$

Likewise, contaminant concentration in the reject stream is the sum of the two independent components (Equation 2.51).

$$C_{r(c)} = C_{r(c.prob)} + C_{r(c.bar)} \tag{2.51}$$

Substituting Equations 2.50 and 2.51 into Equation 2.36 (contaminant removal efficiency E) gives Equation 2.52.

$$E = \frac{Q_r}{Q_f}\left(\frac{C_{r(c.prob)}}{C_{f(c.prob)} + C_{f(c.bar)}}\right) + \left(\frac{Q_r}{Q_f}\frac{C_{r(c.bar)}}{C_{f(c.prob)} + C_{f(c.bar)}}\right) \quad (2.52)$$

Equation 2.55 defines contaminant removal efficiency for probability contaminants E_{prob}

$$E_{prob} = \frac{Q_r C_{r(c.prob)}}{Q_f C_{f(c.prob)}} \quad (2.53)$$

Equation 2.54 may be rewritten to give Equation 2.56 by applying Equation 2.55

$$E = E_{prob}\left(\frac{C_{f(c.prob)}}{C_{f(c.prob)} + C_{f(c.bar)}}\right) + \left(\frac{Q_r}{Q_f}\frac{C_{r(c.bar)}}{C_{f(c.prob)} + C_{f(c.bar)}}\right) \quad (2.54)$$

To satisfy barrier screening (zero probability of passage), mass flow of barrier contaminants entering the screen must equal mass flow leaving (Equation 2.57).

$$C_{f(c.bar)} = C_{r(c.bar)} \quad (2.55)$$

Equation 2.55 can be substituted into Equation 2.54 to give Equation 2.56.

$$E = E_{prob}\left(\frac{C_{f(c.prob)}}{C_{f(c.prob)} + C_{f(c.bar)}}\right) + \left(\frac{C_{f(c.bar)}}{C_{f(c.prob)} + C_{f(c.bar)}}\right) \quad (2.56)$$

For convenience, concentration of probability contaminants in the feed may be defined by Equation 2.57.

$$C_{f(c.prob)} = C_{f(c)} - C_{f(c.bar)} \quad (2.57)$$

Equations 2.39 (mixed flow) and 2.48 (plug flow) can then be substituted for E_{prob} to give overall efficiency for mixed flow (Equation 2.58) and plug flow (Equation 2.59).

$$E = \frac{R_m}{R_m + \frac{P_c}{P_p} - \frac{P_c}{P_p}R_m}\left(1 - \frac{C_{f(c.bar)}}{C_{f(c)}}\right) + \frac{C_{f(c.bar)}}{C_{f(c)}} \quad (2.58)$$

$$E = R_m\left(\frac{P_c}{P_p}\right)\left(1 - \frac{C_{f(c.bar)}}{C_{f(c)}}\right) + \frac{C_{f(c.bar)}}{C_{f(c)}} \quad (2.59)$$

2.5.2 Modelling Consistency Changes

The normalised consistency drop factor D (Equation 2.60) is used for the consistency change across the screen from feed to accept.

$$D = \frac{C_{f(p)} - C_{a(p)}}{C_{f(p)}} \tag{2.60}$$

The reject thickening factor T (Equation 2.61) quantifies consistency change from feed to reject.

$$T = \frac{C_{r(p)}}{C_{f(p)}} \tag{2.61}$$

The volumetric reject ratio R_v (Equation2.62), which represents the proportion of feed flow reporting to the reject stream, is a widely-used pressure screen operating variable because it is easier to measure than the mass reject ratio.

$$R_v = \frac{Q_r}{Q_f} \tag{2.62}$$

- **Mixed Flow**

Gooding and Kerekes [93] modelled consistency changes for mixed flow and plug flow pulp screening regimes. Modelling mixed flow began by combining and rearranging Equations 2.31, 2.34, 2.61 and 2.62 to obtain an expression for the accept consistency

$$C_{a(p)} = P_p C_{r(p)} \tag{2.63}$$

Equations 2.63, 2.33 (volumetric balance), and 2.34 (mass balance) were applied to the definition of D (Equation 2.60) to obtain expressions for D (Equation 2.64) and T (Equation 2.65) in terms of passage ratio and the volumetric reject ratio.

$$D = \frac{R_v - R_v P_p}{P_p - R_v P_p + R_v} \tag{2.64}$$

$$T = \frac{1}{P_p - R_v P_p + R_v} \tag{2.65}$$

- **Plug Flow**

Gooding and Kerekes [93] had already derived an expression to model consistency changes (fibre concentration changes) in an earlier paper. Their expression for the reject thickening factor (Equation 2.66) was obtained by applying Equations 2.61 and 2.62 to Equation 2.44.

$$T = R_v^{P_p - 1} \tag{2.66}$$

An expression for D (Equation 2.67) was obtained by combining Equation 2.44 with the overall mass (Equation 2.34) and volumetric balance Equation 2.33) balances.

$$D = \frac{R_v^{P_p} - R_v}{1 - R_v} \tag{2.67}$$

Data Gooding and Kerekes [93] obtained in pilot screening trials at various flow rates and range of screening equipment showed that the plug flow model predicted reject thickening better than the mixed flow model (Figure 2.24).

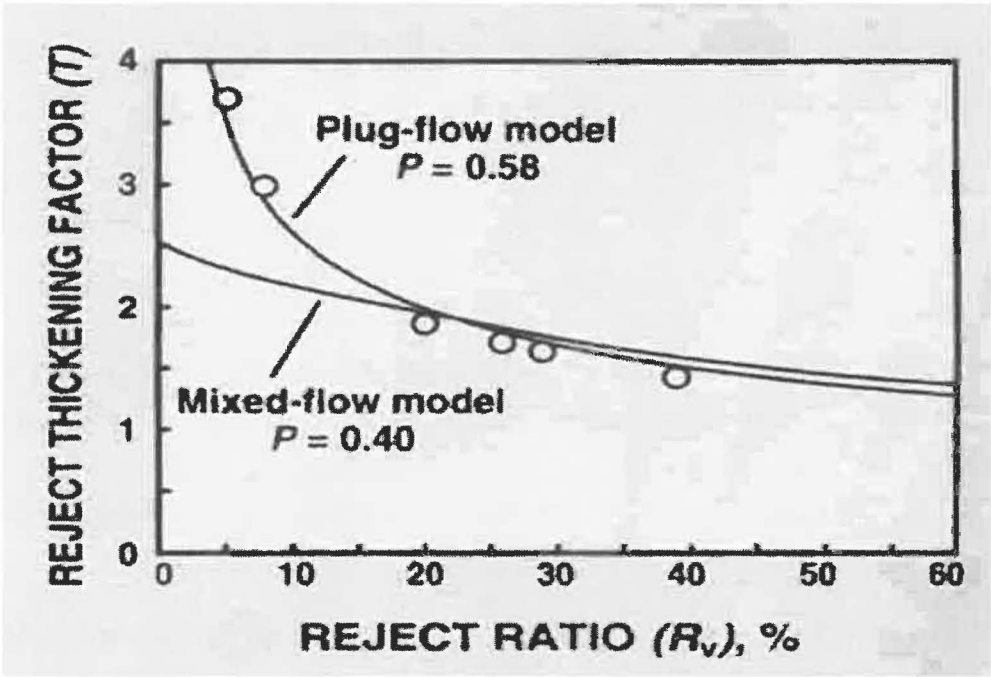

Figure 2.24 Comparison of models and data for reject thickening (from [93]).

2.5.3 Modelling fibre-length Fractionation

Olson and co-workers [22, 168, 176] introduced the fibre-length fractionation index ϕ (Equation 2.68), which sums the long fibre removal function $e_{l(L)}$ and the short fibre removal function $e_{l(S)}$. It is not known whether this index is widely used in industry.

$$\phi = e_{l(L)} - e_{l(S)} \tag{2.68}$$

The fibre removal function for a component/fraction of interest is defined by Equation 2.69 where $C_{f(f)}$ is fibre concentration in the feed stream and $C_{r(f)}$ is fibre concentration in the reject stream. These concentrations are slightly different to pulp fibre consistency described earlier ($C_{f(p)}$ and $C_{r(p)}$) because they are based on number of fibres per unit volume rather than mass of fibres per unit volume.

$$e_{l(x)} = \frac{C_{r(f)} Q_r}{C_{f(f)} Q_f} \tag{2.69}$$

Olson *et al.* [22] extended the work by Gooding and Kerekes [93, 167] to model fibre length fractionation, based on plug flow and passage ratios of short and long fibre fractions $P_{p(S)}$ and $P_{p(L)}$ respectively. They combined Equation 2.43 (Gooding and Kerekes [167]) with Equation 2.67 (letting x equal S or L for short and long fibre fractions) and applied Equation 2.64 (volumetric reject ratio) to obtain the fibre removal function for the long and short fibre fractions.

$$e_{l(S)} = R_v^{P_{f(S)}} \tag{2.70}$$

$$e_{l(L)} = R_v^{P_{f(L)}} \tag{2.71}$$

The fibre-length fractionation index is then expressed by Equation 2.72.

$$\phi = R_v^{P_{f(L)}} - R_v^{P_{f(S)}} \tag{2.72}$$

Olson and co-workers [22, 168, 176] obtained data from pilot screening trials for various flow rates and a range of screening equipment. They found that Equation 2.72 predicted changes in the fractionation index (Figure 2.25).

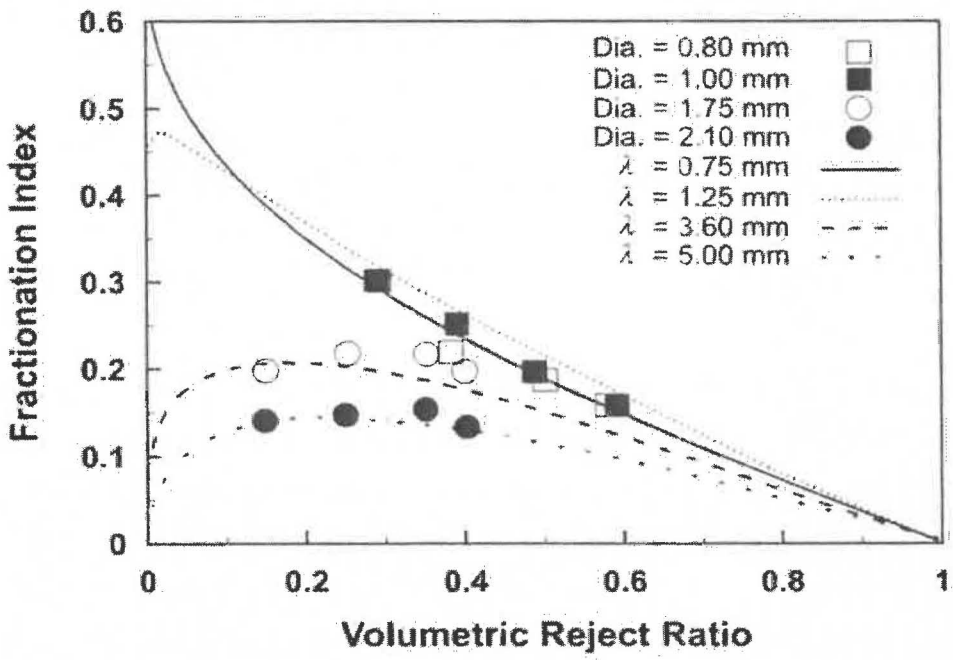

Figure 2.25 Effect of volumetric reject ratio and hole diameter on the fractionation index (from [22]).

2.6 Criticisms of Existing Screen Modelling

It is uncertain which model should be used to model screen performance because it is still unclear if screens behave like mixed flow or plug flow vessels. Contaminant removal data indicate that screens appear to behave like mixed flow reactors but consistency data indicate that screens behave like plug flow reactors [43, 93, 151, 168]. More data are needed to eliminate this uncertainty.

It is also uncertain whether existing screen models are suitable for some of the relatively new screens with unusual components and configurations [76, 89, 91]. For example, the new screens with relatively short screen sections screening in parallel or series are likely to perform differently to a conventional pressure screen with only one relatively long screen cylinder that exhibits plug flow.

Several research groups accept the plug flow model for predicting performance in terms of consistency changes caused by pressure screening [22, 36, 43, 73, 109, 147, 151, 166, 168, 176-181] but other groups [85, 86, 178, 182] challenge the model. For example, Ammala *et al.* [182] and Niinimaki *et al.* [85] question whether there is complete radial mixing in the feed annulus (perpendicular to screen surface), especially with open-type foil rotors but only Ammala *et al.* [182] present supporting data. Pulp consistency in the feed annulus C_z, measured by drawing samples through radially inserted small tubes, varied significantly in the radial axis in foil rotors (Figure 2.26). However, consistency data in Ammala *et al.* and Niinimaki should be treated cautiously because their sampling methods have not been verified and it is not known how representative pulp samples drawn through narrow tubes are. Also, tubes inserted into the screening zone may interfere with normal flow patterns and possibly cause new secondary flow patterns.

Predicted screen performance with plug flow and mixed flow is based on assumptions about internal flow mechanisms (macro mixing, flow distribution, fibre suspension structure) that have some physical realism so a pressure screen is not treated simply as a black box. However, the objective of any modelling should be to represent reality as close as possible but it is uncertain whether plug flow and mixed flow models represent the real mixing and flow distribution inside a screen. For example, uniform distribution of flow is one of the main assumptions in both the mixed flow and plug flow model, but this is questionable. Julien Saint Amand and Perrin [178] for instance did not believe flow is uniform along the length of the screen so they shortened their pressure screen cylinder to minimise axial variation in flow when studying screen performance.

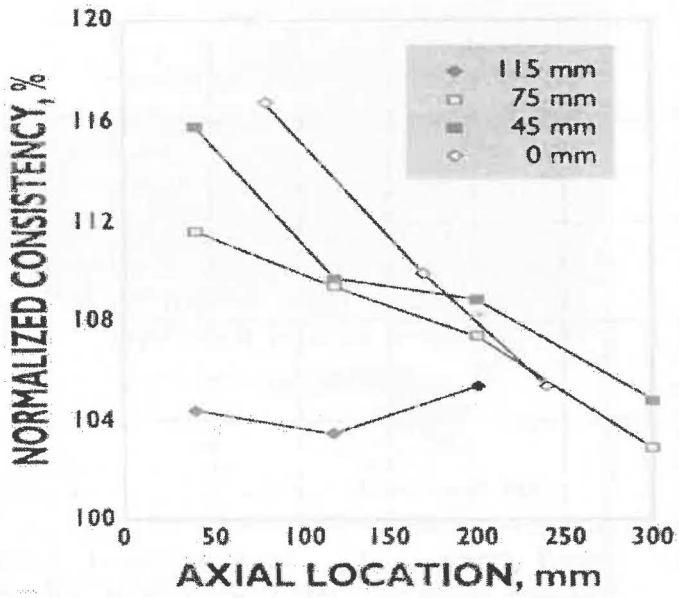

Figure 2.26 Axial and radial changes in fibre concentration in the feed annulus (from [182]).

Schweiss [183] used the finite volume method to show that volumetric flow can vary greatly in conventional screens that have a concentrically located screen within a housing and a conventional accept chamber (no taper). The local aperture volumetric flow rate was greater near the accept outlet, which was located at the top of the accept chamber towards the reject end. To overcome these flow disparities, the accept chamber was tapered and the screen was positioned eccentrically within the housing. The rigour of the modelling, however, cannot be assessed because a full description of modelling was not given. In addition, Schweiss did not experimentally validate his model and he probably assumed Newtonian flow but pulp flow is non-Newtonian [46, 48, 70].

Assumptions about passage ratio are also questionable. Passage ratio cannot remain constant along the length of the screen when conditions that affect passage ratio change. Reinecker [148] proposes that relative speed (speed difference between the rotor and pulp in the feed annulus) decreases along the length of a screen, and this affects turbulence intensity and pressure pulsation of the rotor. The pressure pulsation is stronger at the front and the rotor is more effective in keeping the apertures clear of fibre build-up. This suggests that fibre passage is higher at the feed end of the screen and lower at the reject end. However, this is uncertain because Reinecker [148] did not measure velocities inside a screen or pressure pulsation of the rotor. He did provide some evidence that conditions for fibre and contaminant passage change along the length of a relatively long (relative to diameter) screen. Contaminant removal efficiency was higher for the screen region at the feed end. If a section of the screen at the reject end was blanked off,

removal efficiency was greater than for a standard screen or a screen section at the reject end (section of screen towards front blanked). There were no data in the paper and it is uncertain how much of the screen was blanked. Furthermore, Reinecker does not describe the experimental conditions, but an axial variation in screening conditions is consistent with other reports [89, 91].

It is also not known whether fibres actually act independently inside a centrifugal pressure screen as there are few observations of macro and micro-scale mixing in the feed annulus. An observation of pulp mixing within the feed annulus of a centripetal pressure screen [87] report that pulps with feed consistencies of 2.2% and 2.9% were well dispersed in the feed annulus but did not describe flocs flowing in the main part of the feed annulus. However, hardwood pulp fibres accumulated at aperture openings, forming flocs that partially occluded aperture openings, and TMP pulp fibres formed flocs that completely blocked the screen apertures. Back-flow induced by the screen rotor flushed both hardwood pulp and TMP flocs from the apertures.

2.7 Reject Thickening and Fractionation Studies

2.7.1 Reject Thickening

Reject thickening is a pressure screening phenomenon where consistency of the reject stream is greater than consistency of the feed stream. Typically, feed pulp consistency doubles so a 2% pulp thickens to 4%. Severe reject thickening can sometimes thicken pulp by a factor of 4 (e.g. a 2% pulp thickens to 8%). Frictional resistance to flow increases and the reject line can block. Screen apertures can blind when screens are operated at high levels of reject thickening [151], which limits the feed concentration that can be used [147]. Feed consistency is usually diluted to a feed consistency between 1% (lower limit) or 2% (higher limit) with conventional screening and fractionation. If consistencies are less than 1%, greater power is needed for the high volumetric flow-rates required to maintain production. If consistencies are greater than 2%, high screen power is required to mix pulp and prevent the screen from blocking. However, operating at consistencies above 2% has been reported [1, 71, 77, 118, 138]. This is usually done with contour slotted screens because holes would need to be unconventionally large or slots very wide to process the high concentrations. Pressure screens with unusually large apertures has been used for 8-13% consistencies, usually in the primary screening position or as a knotter [71]. Shive removal efficiency with 5-mm holes and 2-mm wide slots was comparable to that of conventional screens with smaller holes and operating at lower consistencies. However, these screens were operated at low reject thickening.

The maximum tolerable reject thickening, for a given furnish, screen design and operating conditions has not been extensively studied. Wakelin *et al.* [151] recommend a maximum thickening factor of two for softwood furnishes and three for hardwood furnishes with lower network strengths. Excessive reject thickening can increase screen wear towards the reject end and increase the load on the screen motor. Also, downstream dewatering may be needed on the accept side of the screening process. However, fibre length fractionation efficiency increases with increasing reject thickening. Wakelin [147] first reported this effect after compiling data for fractionating chemical and mechanical pulps (Figure 2.27). Sloane [24] and then Olson [168] subsequently confirmed this finding. Thus, there is value in studying the variables that effect reject thickening. Understanding the mechanisms of reject thickening will help identify the mechanisms of fibre length fractionation.

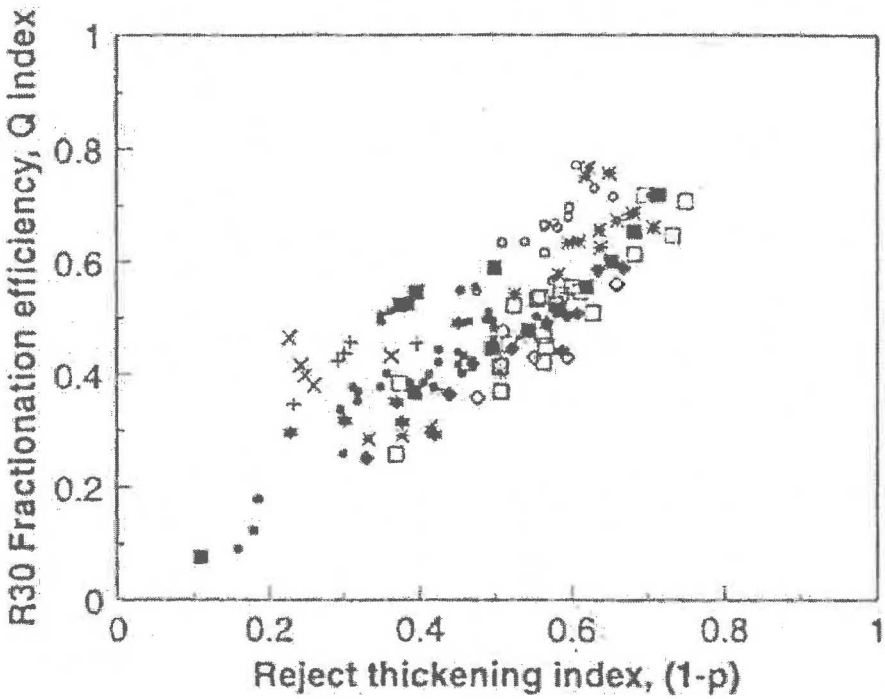

Figure 2.27 Effect of reject thickening on fractionation efficiency (from [147]).

Reject thickening has been studied relatively extensively [22, 24, 43, 93, 136, 147, 151, 166, 168, 177, 180]. Reject thickening increases when aperture size is decreased [22, 24, 25, 127, 151, 168], contour height is decreased [166], screen length is increased [89, 91], foils on the rotor are shortened [128], long fibre content increased, and viscosity of the suspending medium is decreased [43]. Increasing the viscosity of the suspending medium (water) from 1 cP to 40 cP resulted in the reject thickening factor decreasing from 4 to 1 (Figure 2.28) due mainly to having a more favourable flow field [43]. Fluid theory indicates that exit layer height increases at higher viscosities favouring fibre passage, but

increased fluid drag on fibres, CMC lubrication of fibres, and network effects could be secondary causes for the thickening factor decreasing at higher viscosities.

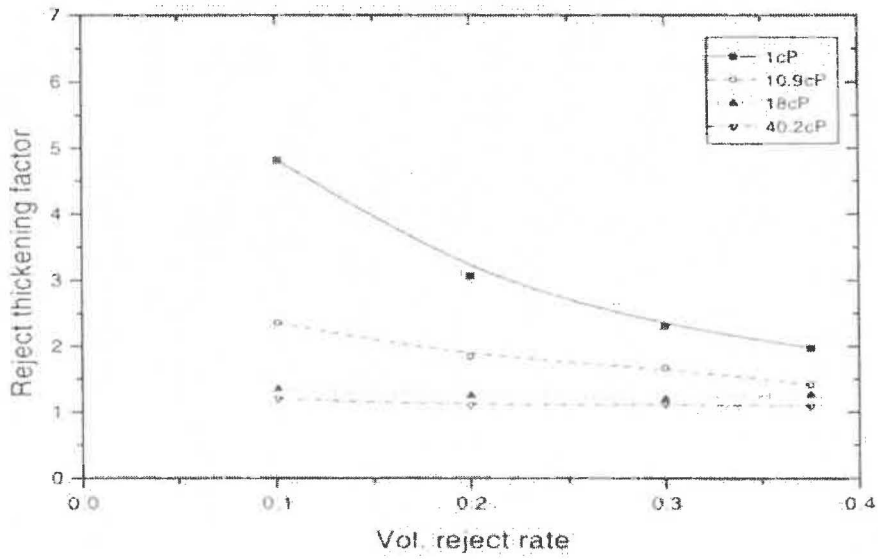

Figure 2.28 Effect of suspending medium viscosity on rejects thickening (from [43]).

The effect of feed consistency C_f on reject thickening is ambiguous because there are conflicting reports in the literature. Some workers [43, 128, 136, 178] reported that consistency did not affect reject thickening but others [93, 157, 181] reported that feed consistency and reject thickening were directly related.

Kumar [157] found that reject thickening increased with increasing consistency when screening with a foil rotor. Other research [43, 181] also show that feed consistency did not affect reject thickening when a foil rotor was used. For instance, Julien Saint Amand and Perrin [178], found that increasing the feed consistency from 1% to 3% had no affect.

Wakelin and Paul [136] found that increasing feed consistency from 0.72% and 2.5% had no effect for a LR rotor, but Gooding and Kerekes [93] report that reject thickening increased with consistency when screening with a bump rotor. Weeds [181] reported a similar effect when using a bump rotor, and from these reports, there is some suggestion the effect of feed consistency depends on the type of rotor (i.e. bump, foil, step, LR.). This has not been discussed in the literature and therefore has not yet been explained.
Different rotors induce different pressure pulse signatures, which probably cause different effects when consistency is varied. Yu [131] presented pressure pulse signatures for different rotors and proposed that the time period ratio effected reject thickening. The time period ratio t_{pn} was defined as the time of positive pressure t_p relative to the time for

negative pressure t_n (Equation 2.75); rotors with higher values produce more reject thickening. Yu reported that the nominal t_{pn} values for foil, cam and step rotors were 4.0, 1.9 and 1.1 respectively. Therefore, a step rotor was expected to produce less reject thickening at the same rotational speed but Yu did not present any data to support this. However, Julien Saint Amand and Perrin [128] validated Yu's work in a later study. The time period ratio of a foil rotor was decreased by increasing the length of the foils and reject thickening decreased appreciably. LeBlanc [184] also reported that reject thickening was eliminated using a step rotor with a low time period ratio. However, accept thickening occurred (accept consistency C_a greater than the feed C_f). Accept thickening is rare, and can only occur if appreciable amounts of dilute pulp flows from the accept side of the screen to the feed during the negative pulse.

$$t_{pn} = \frac{t_p}{t_n} \tag{2.75}$$

Some researchers claim that shortening a screen reduces reject thickening [89, 91], but this is uncertain with limited data and data that is difficult to interpret. For example, Serres and Rees [91] claim that shortening a screen cylinder decreases reject thickening but did not present any data. Pimley and Rees [89] report that blanking half a contoured-slotted screen at the reject end reduced the reject thickening factor from 1.57 to 1.34, but confusion arises because they report they maintained a constant throughput. It is unclear whether constant throughput meant maintaining a constant volumetric accept flow rate Q_a, constant mass flow rate M_a or a constant aperture velocity V_s. If a constant accept flow rate was maintained then the aperture velocity V_s would have doubled, and it is well known that reject thickening decreases with increasing aperture velocity when using a contour-slotted screen [93, 147, 151, 166, 168, 180].

Martin and McIntosh [185] reported that long fibre removal efficiencies were higher if Kraft pulp was screened at 110°C before the washer rather than being screened cold after the washer, probably because viscosity was lower at the higher temperatures. However, they did not examine whether black liquor (which would influence stock pH and also have a soaping effect that may affect fibre passage) in the hot stock affected screening performance. Wakelin and Paul [136] reported a slight decrease in reject thickening when screening PRMP softwood pulp if temperature was increased from 40°C to 90°C and attributed this decrease to increased fibre flexibility. Gooding [154] found that large changes in fibre flexibility did not affect passage ratio for 1-mm fibres, which would explain the small effect of temperature.

2.7.2 Fractionation

Many researchers have studied pressure screen fractionation. Comprehensive studies have been done by Wakelin and co-workers [24, 25, 30, 112, 127, 136, 147, 151, 186, 187] and Olson and co-workers [22, 37, 168, 176]. Most research indicates that fibre-length fractionation is better when the pressure screen is fitted with a bump rotor [38, 146, 188]. In addition, fibre length fractionation efficiency improves when aperture size and reject rate decrease [22, 24, 25, 37, 147, 151, 166, 168]. The effects of feed consistency, rotor tip speed, aperture velocity, screen length and stock temperature are less certain.

There are conflicting opinions on whether smooth-holes are better than contoured slots. Wakelin *et al.* [147] reported that a contour-slotted screen can fractionate as effectively as a screen with smooth holes, but at a lower production rate. Conversely, Olson [168] found that fractionation behaviour of smooth-holed screens and contour-slotted screens differed because the relationship between passage ratio P_p and fibre length L_f was different. In smooth-hole screens, the relationship between passage ratio and fibre length can be expressed using Equation 2.76, where e is 2.718 and λ is a coefficient independent of volumetric reject ratio R_v and aperture velocity V_s but proportional to hole size. The relationship between passage ratio and fibre length for slotted screens (Equation 2.77) is independent of volumetric reject ratio but proportional to aperture velocity and slot width.

$$P_p = e^{\frac{-L_F}{\lambda}} \tag{2.76}$$

$$P_p = e^{-\left(\frac{L_F}{\lambda}\right)^{0.5}} \tag{2.77}$$

Olson [168] used these relationships to show that the fractionation index ϕ was lower for slots than holes at equivalent reject thickening. Slotted screens accept longer fibres more readily but reject short fibres more readily (the slope of the curve using Equation 2.77 is flatter for long fibre and steeper for shorter fibre).

2.8 Summary

This literature review raised a number of important points in the areas of wood fibre suspensions, application of pressure screen fractionation, screen development, screening mechanisms, modelling and reject thickening.

- **Wood fibre**: kraft fibres (from kraft pulping) are longer and will form larger flocs. Where it is desirable, flocs can be eliminated by dilution (below critical consistency C_{crit}) or by dispersion, but with dispersion, reflocculation is almost instantaneous and reflocculation times decrease with increasing consistency.

- **Application of pressure screen fractionation**: integrating pressure screen fractionation into pulp production processes can reduce capital, energy, chemical and wood requirements; increasing feed consistency can result in further cost reductions.

- **Screen development:** rotors were developed that do not contact the screen. Instead of physically removing fibre accumulated at the screen surface (as with older contacting rotors), it is believed that fibre is removed from the screen when flow temporarily reverses during the negative pulse of the rotor. However, actual measurements of back-flow have only been reported once, and these measurements should be treated cautiously without a description of the measurement method.

- **Screening mechanisms**: The fibre alignment mechanism and the fibre mat mechanism are the two screening mechanisms most frequently cited in reports on screening. They are general in nature, and the relative importance of these mechanisms in determining fibre passage is unknown. Intuitively, the fibre mat mechanism (or some derivative of this mechanism) should have greater relevance when the feed consistency is increased to unconventionally high levels.

- **Screen modelling**: pressure screens have been modelled as a plug flow vessel and as a mixed flow vessel. Although both appear to have gained acceptance, it is still unclear which screen should be used to model screen behaviour. Furthermore, some assumptions about flow distribution and passage ratio are questionable.

- **Reject thickening:** separation of long and short fibre with pressure screens improves when reject thickening increases. Some evidence suggests that reject thickening increases with feed consistency; therefore, fractionation efficiency should increase with feed consistency. However, there is no evidence this happens, and the effect of feed consistency on reject thickening and fractionation efficiency is unknown.

3. EXPERIMENTAL

3.1 Equipment

3.1.1 Beloit Centrifugal Pressure Screen

A Beloit MR8 centrifugal pressure screen (Figure 3.1) was used to screen softwood and hardwood kraft pulps under controlled conditions. The screen has an unusual horizontal configuration, which makes pulp flow from the front (feed-end) to the back (reject-end) instead of from top to bottom that occurs in a normal vertical configuration. The horizontal configuration prevents any water that leaks from the screen and dripping onto bearings. It also reduces installation height, which can be an advantage in some commercial screening operations. Pulp flows through an 80-mm inlet fixed at a tangent into the MR8 feed chamber at the front of the screen (termed a tangential feed construction). Pulp flowing out of the screen either passes through a 50-mm reject port at the back through an 80-mm accept port at the top and in the centre of the screen

Figure 3.1 Beloit centrifugal pressure screen (model MR8).

The MR (Multi-Rotor) pressure screens were assembled with a step rotor to give "high" consistency screening. Because the 7.5-kW motor overheated when the step rotor was operated at tip speeds of 20 ms^{-1}, a 15-kW motor was installed. This motor, together with a variable speed drive, allowed continuous operation up to rotor tip speeds of 25 ms^{-1}.

3.1.2 Rotors

Two types of rotors were used in the trials - a bump rotor (termed a solid-core or closed-type rotor) and a step rotor (also referred to as a solid-core or closed-type rotor was used for some of the trials. The bump rotor had eight rows of bumps, with four bumps per row (Figure 3.2). Each bump was 160-mm in diameter and protruded 12-mm from the surface of the core/drum, giving a 9.25-mm gap between the tip of the bump and screen surface.

Figure 3.2 Bump rotor.

The step rotor had two 20-mm high steps (Figure 3.3), giving 12-mm gap between the tip of the step and screen cylinder.

Figure 3.3 Step rotor and screen cylinder.

3.1.3 Screen Cylinders

Two standard screen cylinders (Table 3.1) were used in the trial, each 203-mm in diameter and 220-mm long, giving a screening area of 0.11 m^2 and an aspect ratio of 1.1. The first standard screen, with 1-mm holes, was used for most of the study. It had a 3mm triangular pitch and the open area was 13.1% of the screen. At a volumetric accept flow rate of 640 L min^{-1}, the calculated aperture velocity is 0.6 ms^{-1}. The second standard screen was a conventional contour-slotted screen with machined slots and machined contours upstream of the slot. The slots were 0.15-mm wide and the contours were 0.8-mm high. The open area was 2.46% of the screen. At a volumetric accept flow rate of 160 L min^{-1}, the calculated aperture velocity is 0.6 ms^{-1}.

Table 3.1 Critical dimensions of the standard and RSC screens.

Attribute	Standard		RSC
Aperture	1-mm holes	0.15-mm contoured slots	2-mm holes
Open hole/slot area (%)	13.10	2.46	10.96
Pitch	3 mm triangular	-	4 mm triangular
Contour height	-	0.8 mm	-
Material	316S stainless	316S stainless	316S stainless

A 'rebuildable' screen cylinder (RSC) and 100-mm screen sections with 2.4-mm smooth holes were also manufactured from 4-mm 316S stainless steel by a machine shop and used for specific trials with softwood kraft pulp (Table 3.1). The RSC had two 100-mm screen sections. When the two screen sections were clamped together with a 20-mm dividing ring, they were equivalent to a full-length screen.

3.1.4 Flow Circuit

A flow circuit was constructed from stainless steel pipe and flexible hose so the pressure screen could be operated as a multiple pass system. This circuit contained a 3000-L pulp tank with top-entry mixer, a centrifugal pump, pressure screen and three main pulp streams (Figure 3.4). The three main pulp streams included a feed (80-mm diameter pipe), accept (80-mm diameter pipe) and reject (50-mm diameter pipe). Flow monitors and flow control equipment were put on the accept and reject streams.

The pulp tank was 1.3-m high and the bottom was 1-m above the ground. The top entry mixer had a marine impellor fixed at the end of a shaft, 0.4-m from the bottom of the tank. This mixer could mix a 2% softwood kraft pulp without the need for baffles.

Mixing speed was adjusted using an AC motor speed controller (PDL Electronics, Napier, New Zealand), which had a 16-bit micro-controller and 32 character alpha-numeric liquid-crystal-display.

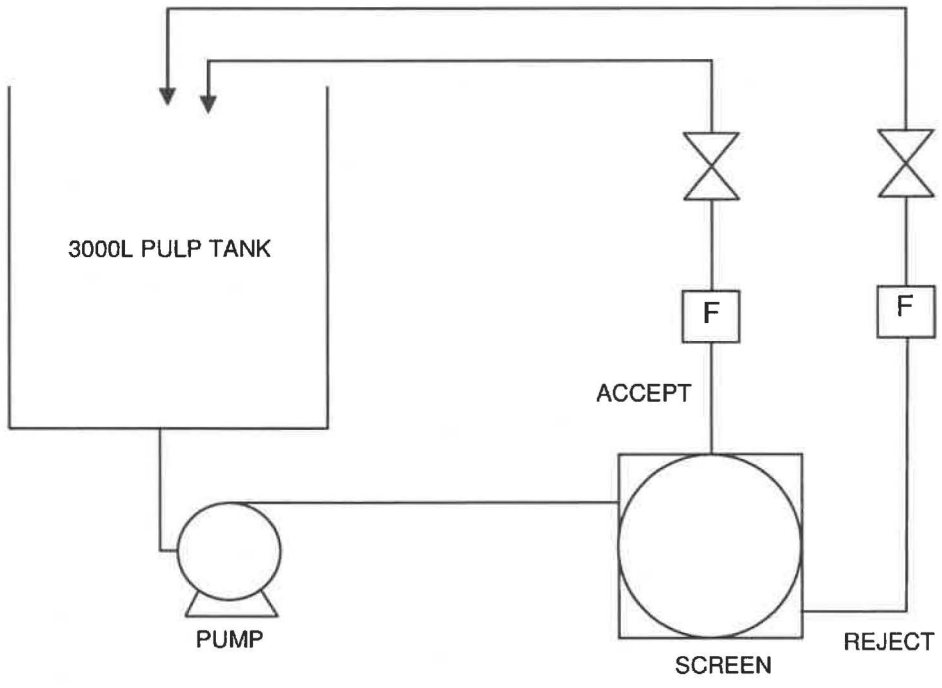

Figure 3.4 Schematic of the flow circuit.

Pulp was pumped through the flow circuit using a 200-mm open impellor centrifugal slurry pump. This pump was powered by a 20-kW AC motor with variable speed drive (PDL Electronics, Napier, New Zealand). Because the pump inlet and outlet were 100 mm in diameter, a concentric conical reduction was inserted into the feed line to reduce pipe diameter to 80 mm.

Neles-Jamesbury electromagnetic segment valves (model R21CA03CCJA/B6/NE7 of 80 mm and model R21CA02CCJA/B6/NE7 of 50 mm) were used to control flow in the accept and reject streams. These valves have a stainless steel v-port segment valve with a pneumatic double acting cylinder actuator and 4-20 mA electronic 'positioner'. Both the accept and reject electronic 'positioners' were controlled using set-point controllers mounted in a remote panel.

Flow through the accept and reject streams was monitored with Foxboro flow meters, which had a wafer body flow tube and side-mounted transmitters. Transmitters converted

the low level, high impedance signal from the two platinum electrodes in the flow tubes to a to a scaled 4-20 mA signal, which is proportional to flow rate.

3.1.5 Internal Sampling Systems

Sampling systems were periodically set up to sample pulp from the feed annulus and accept chamber to measure C_z and C_s. Two systems (called the axial and radial sampling systems) were used to get samples from the feed annulus and a different system was used to get pulp from the accept chamber.

- ***Axial Sampling System for Feed Annulus***

This was made from a 750-mm long, 8-mm diameter flexible tube with a ball valve on one end. The end of the tube, without the valve, was inserted through a port in the outer housing at the reject end of the screen (Figure 3.5). Wire bridges (at 15 mm spacing) held the axially-oriented tube against the screen cylinder. The tube could be pulled through the wire bridges to different axial positions.

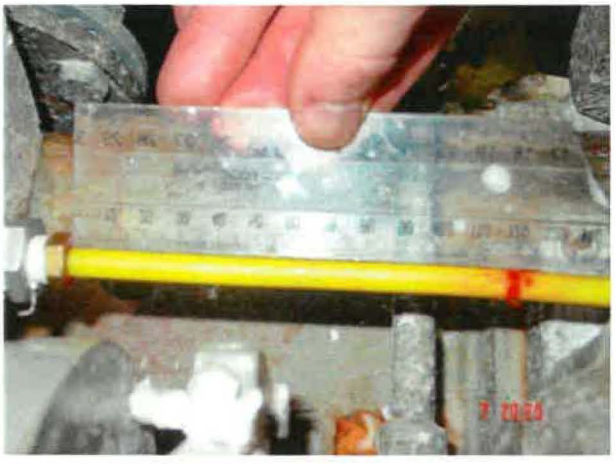

Figure 3.5 Axial sampling system for the feed annulus.

- ***Radial Sampling System for Feed Annulus***

Ten 300-mm long, 8-mm diameter flexible tubes with ball valves on one end were inserted radially through ports in the outer housing (Figure 3.6a) and connected to ten nipples along the axial direction of the screen. The nipples were threaded onto 1-mm diameter holes, drilled and tapped at 20-mm intervals along the screen (Figure 3.6a). The first hole was 20 mm from the feed edge and the tenth hole was 20 mm from the reject end. Tubes were flush with the feed surface of the screen cylinder to minimize disturbing flow in the feed annulus.

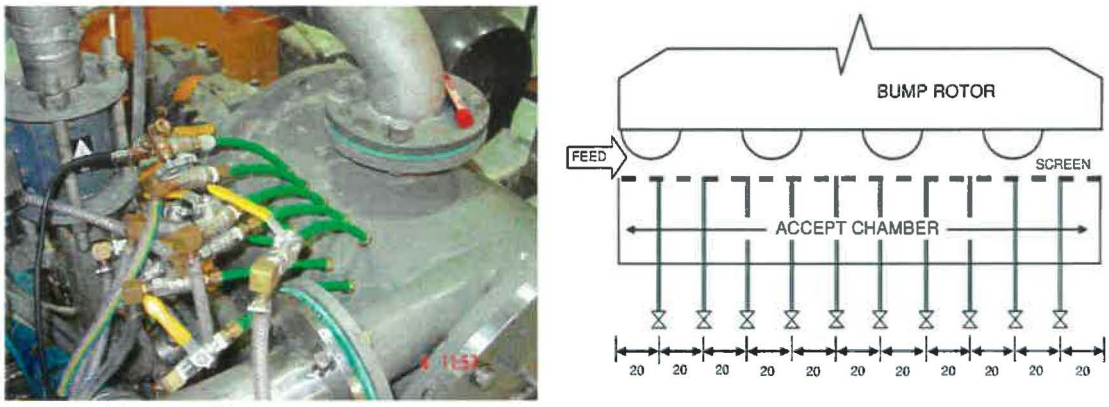

(a) (b)

Figure 3.6 Photograph (a) and schematic (b) of radial system for sampling pulp from the feed annulus.

- ***Radial Sampling System for Accept Chamber***

A bank of ten 8-mm diameter and 150-mm long copper tubes with a small ball valve at one end were set radial at 20-mm intervals to draw pulp from the accept chamber (Figure 3.6). The tubes were inserted through ports in the outer housing and collected samples 2 to 3 mm above the accept-side surface of the screen cylinder.

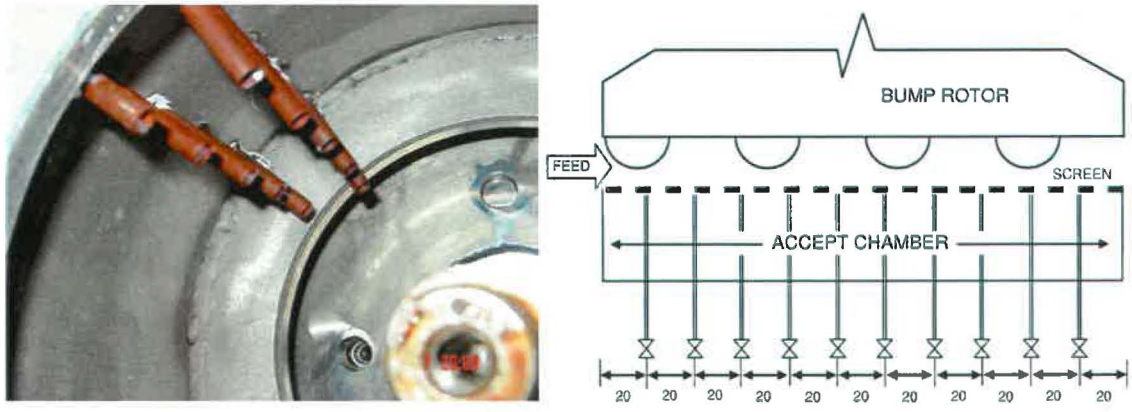

(a) (b)

Figure 3.7 Photograph (a) and schematic (b) of radial system for sampling pulp from the accept annulus.

3.1.6 Acceleration Chamber for Front of Pressure Screen

The front of the MR8 was reconfigured to accelerate pulp in a feed chamber upstream of the feed annulus (Figure 3.8). This involved fitting an acceleration chamber, 330 mm in the axial direction, to the front of the screen containing a concentrically positioned rotary shear element. The rotary shear element consisted of a plastic tube with six, 15-mm high paddles (Figure 3.9) fixed to the front of the rotor so it rotated at the same frequency.

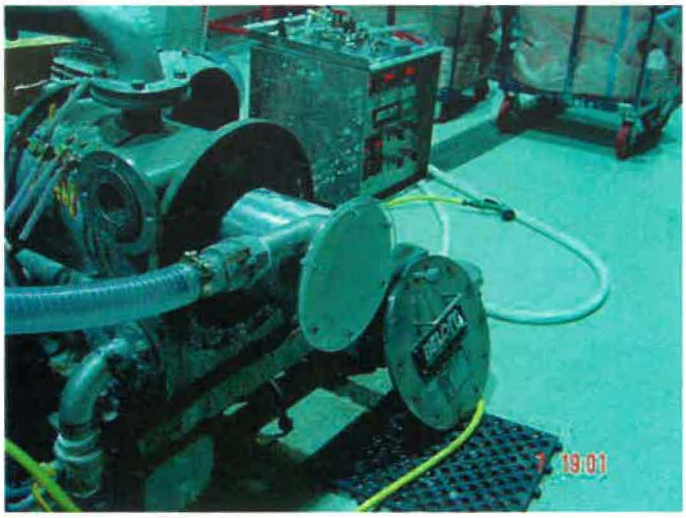

Figure 3.8 Screen reconfiguration to accelerate pulp upstream of the feed annulus.

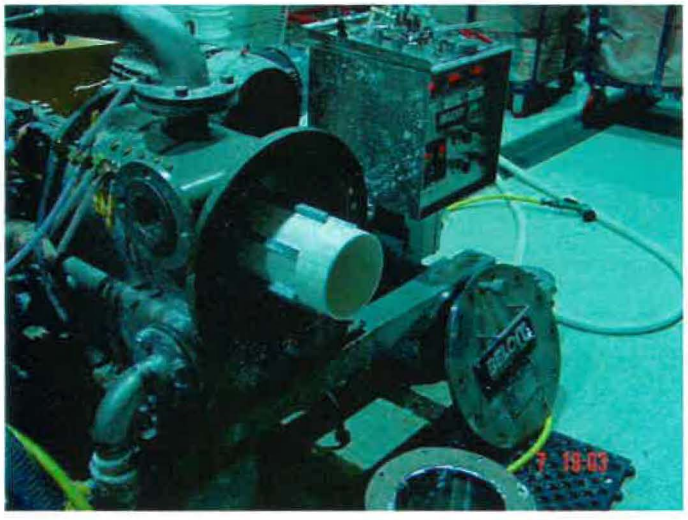

Figure 3.9 Photograph of rotary shear element fixed to the front of the rotor.

3.1.7 Fibre Analysis Equipment

Fibre length was measured with a Kajaani FS-200 fibre analyzer. A sample of approximately 5-mg (hardwood) or 15-g ((softwood) is placed in a 500-mL beaker/container. The analyser continuously mixes and dilutes the sample to a suitable range during testing. Once diluted, fibres are drawn into a 0.4-mm capillary tube and flow passed a laser. Fibre length is measured from the image projected onto a screen.

3.2 General Experimental Methods

3.2.1 Consistency Measurement

Samples for consistency of accept and reject returns were collected at the top of the pulp tank in tared 2-L jugs (consistencies above 0.01%) or in tared 5-L jugs (consistencies

below 0.1%). Jug contents were weighed and then filtered onto tared filter paper to remove excess water and then dried in a forced-draught oven for at least 24 hours. Oven dry pulp was weighed and consistency was reported as percentage of oven dry fibre in unit mass of wet pulp. The mean of three measured values were used for consistencies above 0.01% and the mean of five values was used for consistencies below 0.01%. Feed consistency was determined by mass balance.

3.2.2 Screen Operation

The tank stirrer was turned on. Valves in the flow circuit were then opened and then the pressure screen rotor was turned on. When feed consistencies were greater than 1%, the accept valve was kept closed. The rotor was run without any flow through the circuit (pump off) for at least 30 seconds to clear fibre that may have accumulated against the screen. The pump was then turned on and its speed adjusted to give the required flow rate. The desired flow rate was then set by adjusting the reject and accept valves, in combination with rotor and pump speed.

3.2.3 Setting Up Narrow Screen Sections (Ls < 220 mm)

The 1-mm hole screen cylinder was sectioned into eight 27.5-mm wide zones (called screen sections). Each section was 1/8th the total screen length and numbered from the feed (number 1) to the reject (number 8) end of the screen (Figure 3.8).

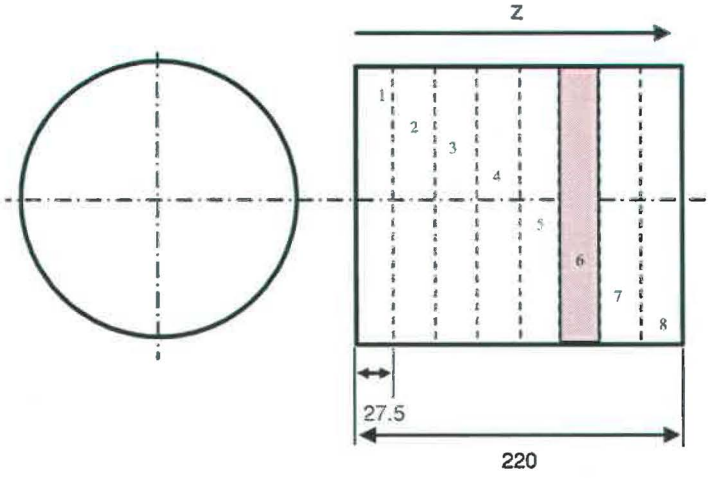

Figure 3.10 Schematic of sectioning the 1-mm hole screen cylinder.

Screen sections were created by blocking sections of the screen with duct tape around the accept side of the screen. The duct tape was reinforced with stainless steel support ring. An example (Figure 3.9) shows the 1-mm hole screen with duct tape covering half of the

screen at the reject end. Duct tape at the front 55-mm (one-quarter) of the screen is obscured by the stainless support ring used for reinforcing the seal. A narrow 55-mm section is exposed between the two blanked sections. The active screening section was changed by blanking different regions. For example, if the active screening section was located at position 6, positions 1-5 and 7-8 were blanked off.

Figure 3.11 Photograph showing blanked screen with active region at 3&4.

A schematic for the example above (Figure 3.12) shows the 55 mm section exposed at positions 3&4, a position which is 55 mm from the feed-end of the screen cylinder.

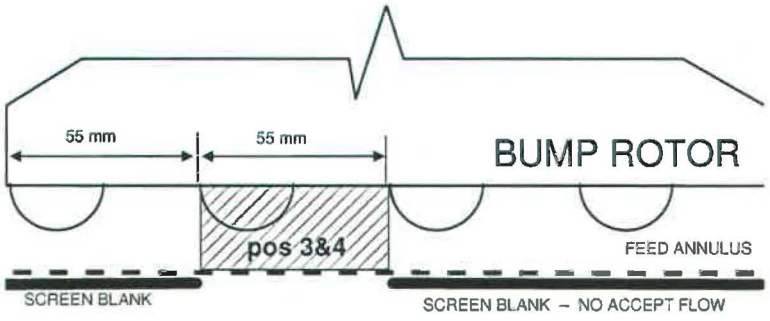

Figure 3.12 Schematic for 55-mm screen section located at positions 3&4.

3.2.4 Reject Thickening Data at Different Volumetric Reject Ratios

The screen was operated at a constant aperture velocity V_s (constant volumetric accept flow rate Q_a) by varying the volumetric reject ratio R_v. Data were initially obtained at a high volumetric reject ratio (usually greater than 0.5) then decreased to a minimum ratio, typically 0.1. If the reject line or screen plugged, further data collection was abandoned.

3.3 Kraft Pulps

Fibre characteristics of the dry sheets of bleached pine (*Pinus radiata*), unbleached pine, and a bleached eucalypt pulp used in the trials are summarized in Table 3.2.

Table 3.2 Characteristics of pulps used in the trials (from pulp manufacturer).

	Length weighted fibre length average, mm	Fibre coarseness, mg/g
Bleached pine	2.31	0.249
Bleached eucalypt	0.77	0.080
Unbleached pine	2.44	0.253

To prepare pulp for screening and fractionation, sheets were softened in water and then manually torn into approximately 50-mm x 50-mm pieces before being added to the continuous stirred tank (CST). Tank contents were pumped through the circuit for about 10 min to completely disintegrate the sheets. Sometimes pulp was reused, which involved draining the contents of the CST into large woven bags (Figure 3.7) to thicken pulp for storage.

Figure 3.13 Woven bags for dewatering the pulp.

3.4 Description of Trials

3.4.1 Effect of Screen Length L_s on Reject Thickening

The screen with 1-mm holes was used to investigate the effect of screen length on reject thickening using methods consistent with Serres and Rees [91]. Reject thickening data were initially obtained for a range of volumetric reject ratios for the standard, full-length

screen. Screen sections were then blanked from the reject end. Volumetric accept flow rate Q_a was decreased to maintain a constant aperture velocity V_s of 0.6 m s^{-1}. Rotor tip speed V_{tip} and feed consistency C_f were held constant. Bleached eucalypt furnish was screened using the bump rotor in a set of trials (Table 3.3) at fixed aperture velocity V_s, rotor tip speed V_{tip} and feed consistency C_f for various volumetric reject ratios R_v. The screen with 1-mm holes was eventually shortened to a 27-mm section at the front of the screen (position 1).

Table 3.3 Settings and codes for screen length trials, using a 1-mm aperture, bump rotor and eucalypt furnish

Screen (mm)	Position	V_s (m s^{-1})	V_{tip} (m s^{-1})	C_f (%)	Code
220	1-8	0.6	22	0.5	RTLB1
165	1-6	0.6	22	0.5	RTLB2
110	1-4	0.6	22	0.5	RTLB3
55	1&2	0.6	22	0.5	RTLB4
27	1	0.6	22	0.5	RTLB5

In another set of trials (Table 3.4), bleached eucalypt furnish was screened using the step rotor. Again, the screen was eventually shortened to a 27-mm section at the front of the screen (position 1).

Table 3.4 Settings and codes for screen length trials, using a 1-mm aperture, step rotor and eucalypt furnish.

Screen (mm)	Position	V_s (m s^{-1})	V_{tip} (m s^{-1})	C_f (%)	Code
220	1-8	0.6	22	0.5	RTLS1
165	1-6	0.6	22	0.5	RTLS2
110	1-4	0.6	22	0.5	RTLS3
55	1&2	0.6	22	0.5	RTLS4
27	1	0.6	22	0.5	RTLS5

3.4.2 Hydraulic Limit Q_{max}.

The hydraulic limits for 55-mm screen sections were determined using methods consistent with Martinez and Gooding [137]. The hydraulic limit was the maximum volumetric accept flow rate Q_{max} before screen plugging. It was determined by increasing volumetric accept flow rate Q_a for constant volumetric reject rate R_v, rotor tip speed V_{tip} and feed consistency C_f. Four trials (Table 3.5) were done screening bleached eucalypt pulp using the bump rotor and the screen with 1-mm holes. In each trial, the accept flow rate was increased while maintaining volumetric reject ratio R_v constant at 0.2.

Table 3.5 Settings and codes for the hydraulic limit (Q_{max}) trials, using a 1-mm aperture, bump rotor and eucalypt furnish.

Screen (mm)	Position	V_s (m s^{-1})	V_{tip} (m s^{-1})	C_f (%)	Code
55	1&2	0-max	22	0.2	HLB1
55	3&4	0-max	22	0.2	HLB2
55	5&6	0-max	22	0.2	HLB3
55	7&8	0-max	22	0.2	HLB4

3.4.3 Effect of Pulp Acceleration.

The effect of pulp acceleration was studied by comparing the reject thickening behaviour of a screen with and without acceleration. The screen with 1-mm holes and bump rotor were used to screen bleached eucalypt furnish at a feed consistency C_f of 0.5%. Initially, reject thickening behaviour of a 55-mm section located at the feed end of the screen was studied with (Trial ARTFB1) and without (Trial ARTFB2) acceleration (Table 3.6).

Table 3.6 Screen settings and codes for pulp acceleration trials, using a 1-mm aperture, bump rotor and eucalypt furnish.

Screen (mm)	Position	V_s (m s^{-1})	V_{tip} (m s^{-1})	C_f (%)	Code
55	1&2	0.6	22	0.5	ARTFB1&2

The reject thickening behaviour of a 55-mm section at the reject end was also studied with (Trial ARTRB1) and without (Trial ARTRB2) acceleration (Table 3.7).

Table 3.7 Screen settings and codes for pulp acceleration trials, using a 1-mm aperture, bump rotor and eucalypt furnish.

Screen (mm)	Position	V_s (m s^{-1})	V_{tip} (m s^{-1})	C_f (%)	Code
55 mm	1&2	0.6	22	0.5	ARTFB1&2

The standard screen with 1-mm holes was used to study the effect of pulp acceleration with (Trial ARTB1) and without (Trial ARTB2) acceleration (Table 3.8).

Table 3.8 Screen settings for pulp acceleration trials ARTB1-2, using a 1-mm aperture, bump rotor and eucalypt furnish.

Screen (mm)	Position	V_s (m s^{-1})	V_{tip} (m s^{-1})	C_f (%)	Code
220	1&2	0.6	22	0.5	ARTFB1&2

3.4.4 Effect of Feed Consistency C_f on Fibre Passage.

The screen was set initially to screen low consistency pulp. Volumetric accept flow rate Q_a, reject rate R_v, and rotor tip speed V_{tip} were held constant and samples of reject and accept pulp were collected as feed consistency C_f was increased to approximately 2%. If the reject line blocked, the trial was completed at the feed consistency prior to blocking.

Settings used in trials to investigate the effect of furnish type (pine or eucalypt), rotor type, and feed consistency with a 55-mm section located at positions 3&4 are in Table 3.9, settings used in trials to investigate furnish type, feed consistency and a different hole size are in Table 3.10, and settings used for trials to investigate rotor type, feed consistency and furnish type in a standard screen with 1-mm holes are in Table 3.11.

Table 3.9 Screen settings for consistency trials CF55-1-CF55-5 to investigate effect of furnish and rotor using a 1-mm aperture and 55-mm screen.

Rotor	Position	Furnish	V_s (m s^{-1})	V_{tip} (m s^{-1})	R_v	Code
Bump	3&4	Pine[B]	0.6	22	0.5	CF55-1
Step	3&4	Pine[U]	0.6	22	0.5	CF55-2
Bump	3&4	Euc	0.6	11	0.5	CF55-3
Step	3&4	Euc	0.6	11	0.5	CF55-4
Bump	3&4	Euc	0.6	22	0.5	CF55-5

[B] bleached; [U] unbleached

Table 3.10 Settings to investigate the effect of aperture size and rotor type on consistency of unbleached pine pulp.

Aperture (mm)	Screen (mm))	Position	Rotor	V_s (ms^{-1})	V_{tip} (ms^{-1})	R_v	Code
1.6	55	3&4	Step	0.6	22	0.5	CF55-7
1.6	55	3&4	Bump	0.6	22	0.5	CF55-8
2.4	55	3&4	Bump	0.6	22	0.5	CF55-9

Table 3.11 Settings to investigate the effect of furnish and rotor type using the 220-mm screen with a 1-mm aperture.

Position	Rotor	Furnish	V_s (m s^{-1})	V_{tip} (m s^{-1})	R_v	Code
1-8	Bump	Pine[U]	0.6	22	0.5	CF55-10
1-8	Step	Pine[U]	0.6	22	0.5	CF55-11
1-8	Bump	Euc	0.6	22	0.5	CF55-12
1-8	Step	Euc	0.6	22	0.5	CF55-13

[U] unbleached

3.4.5 Effect of Feed Consistency C_f on Fibre-length Fractionation

Fibre length fractionation trials were only carried out using the bump rotor. Pine pulps were fractionated at an aperture velocity of 0.6 ms^{-1}, a constant volumetric reject ratio R_v, a rotor tip speed of V_{tip} and a range of feed consistencies C_f from very dilute to approximately 2%. If the reject line blocked, the trial finished at the feed consistency prior to blocking.

Samples of accept and reject pulp were collected to determine consistency. Separate 5-L samples were collected and diluted to give a 5 to 15 mg sub-sample that could be analysed using the Kajaani FS200 fibre analyser. Data from the analyzer were used to calculate the fractionation index Φ using the method described in Olson *et al.* [22].

Two fractionation trials were done using the standard screen with 1-mm holes and a third was done using the screen with 2.4-mm holes to investigate the effect of feed consistency on fractionation. Screen settings are given in Table 3.12.

Table 3.12 Screen settings for fractionation trials CFFL1-3.

Aperture (mm)	Screen (mm)	Position	Rotor	Furnish	V_s ($m\ s^{-1}$)	V_{tip} ($m\ s^{-1}$)	R_v	Code
1	220	1-8	Bump	Pine[B]	0.6	22	0.5	CFFL1
1	220	1-8	Bump	Pine[M]	0.6	22	0.5	CFFL2
2.4	220	1-8	Bump	Pine[U]	0.6	15	0.5	CFFL3

[B] bleached pine; [M] bleached pine mixed with bleached eucalypt; [U] unbleached pine

3.4.6 Salt Test

A simple test was devised to investigate the backflow phenomenon using the screen with 1-mm holes and the step or bump rotor. Saline was pumped through a ring distributor manifold attached to the accept side of the screen at 33 L min^{-1} whilst water was simultaneously pumped from the pulp tank to the screen at 840 L min^{-1}. The accept flow rate was set at 640 L min^{-1}, which gave a calculated aperture velocity 0.6 m s^{-1} and a volumetric reject ratio of 0.2. Rotor tip speed was set at 22 m L s^{-1}. Samples of the reject and accept streams, which were flowing into the drain, were collected after the screen had been running for 2 min. Conductivity was measured with a standard conductivity meter.

4. EFFECT OF SCREEN LENGTH ON REJECT THICKENING

4.1 Introduction

Screens vary in length and are considered long when the ratio of screen length L_s to screen diameter D_s approaches unity. An example of a long screen is that of the Hooper PSV 2100 screen [142]. This screen is 450 mm long and 280 mm in diameter, giving a length to diameter ratio of 1.6. Screen cylinders are often lengthened by screen manufacturers to economically increase screen area to augment production. Lengthening a screen can be more economic than increasing the diameter of a screen because gear-boxes are often needed for the larger rotor that also has to increase in diameter with increasing screen diameter. However, longer screens generate more reject thickening [89, 91], which can be uneconomic for the pulp producer because valuable wood fibre is lost to the reject stream, but can also be useful for fractionation.

The underlying mechanisms that cause longer screens to reject more fibre are not well understood. Although Pimely and Ress's [89] pulp dewatering mechanism may be involved, it is postulated that there are at least four other factors that should be considered in explaining the effect of screen length L_s on reject thickening. These four factors include: (1) the flow behaviour of longer screens, (2) the relative speed changes along a longer screen, (3) the changes in local passage ratio P_z and (4) the changes in local volumetric flow Q_s. The investigation of these four factors involved modelling and experiment trials. Results from these investigations are presented in this chapter.

4.2 Flow Configuration and Macro Mixing

4.2.1 Application of Screen Modelling Theory

The two flow models discussed in section 2.5, mixed flow (continuously stirred tank reactor - CSTR), and plug flow (tubular or piston flow reactors - PFR), have direct applicability to studying the effect of screen length on reject thickening. The mixed flow model assumes that contents within the separation device are completely mixed and composition is uniform. The plug flow model assumes negligible axial mixing, so composition varies axially. Mixed flow and plug flow represent extremes; in reality, mixing in real separation devices will be between these extremes.

Plug flow is more likely to occur in a tubular vessel with a long length to diameter ratio (aspect ratio of 100) [173]. Although a pressure screen with an aspect ratio of 1 or more

is considered a long screen, plug flow behaviour can still arise due to the presence of the rotor, which reduces the flow area and extends the apparent aspect ratio especially when a closed rotor is used like in this study. The rotor provides mechanical agitation in the feed annulus so some axial mixing can occur, at least on a scale proportional to macro turbulent eddies generated by the rotor (Figure 4.1). The presence of a macro mixing zone of finite length L_{mix} (Figure 4.1) will cause significant errors when the plug flow model is applied to screens of decreasing length. Therefore, an alternate modelling approach, which considers a pressure screen as a series of well-mixed screen sections (or well-mixed "tanks" to use the analogy with chemical reaction engineering), is developed in this thesis. This "tanks-in-series" model (as it will be called in this research), has the potential to account for a finite axial mixing length in screens of decreasing length.

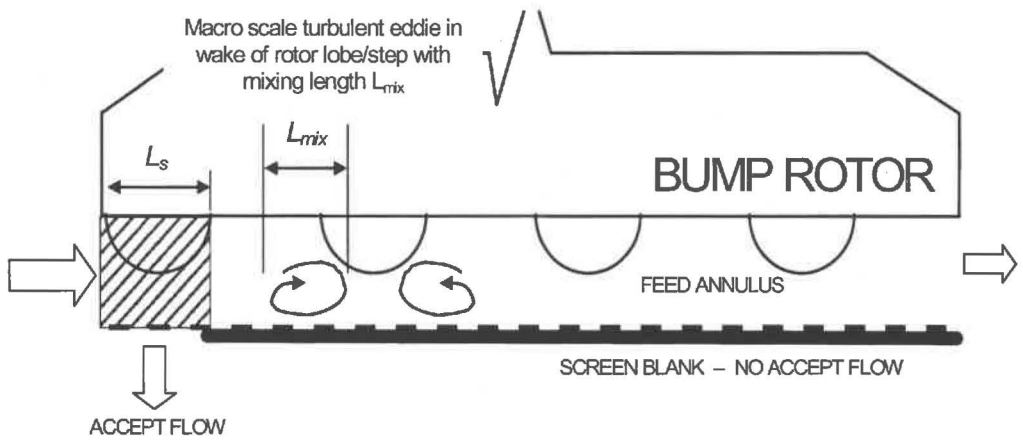

Figure 4.1 Macro turbulent eddies with mixing length L_{mix} in the feed annulus of a pressure screen.

In terms of reject thickening behaviour, most standard screens appear to exhibit plug flow [5, 43, 93, 166]. When a screen is shortened so mixing length of macro scale turbulent eddies (L_{mix}) is proportional to screen length ($L_{mix} \sim L_s$), as shown in Figure 4.1, there will be an appreciable amount of back-mixing, axial mixing and mixing in direction of flow through the screen. At a higher level of axial mixing relative to overall screen length, pulp consistency should become more uniform in the feed annulus and flow behaviour becomes more mixed. Therefore, shortening the screen will decrease thickening simply because the relative scale of axial mixing (L_s/L_{mix}) has changed. Where this ratio is much greater than unity, the screen will exhibit plug flow screening. Where the ratio is near unity, the screen will conform to mixed flow screening.

The plug flow and mixed flow model of reject thickening derived by Gooding and Kerekes [93] demonstrates that reject thickening will decrease as the flow becomes more mixed. Reject thickening was modelled for plug flow (Equation 2.66) and mixed flow (Equation 2.65) using a passage ratio of 0.5 (Figure 4.2). There is a pronounced reduction in reject thickening at volumetric reject ratios less than 0.2. For example, at a relatively low volumetric reject ratio of 0.1, the thickening factor for plug flow is 3.16, whereas the thickening factor for mixed flow is 1.82.

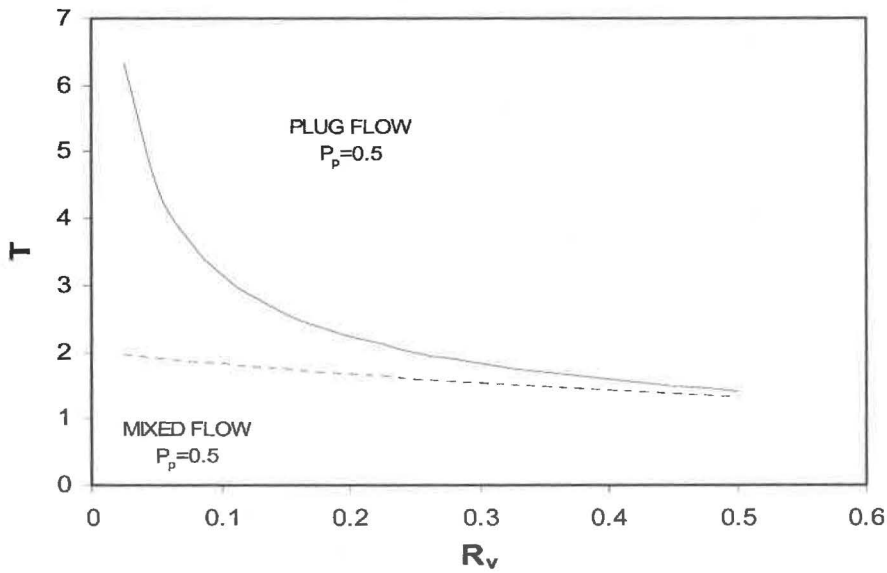

Figure 4.2 Reject thickening factor as a function of volumetric reject ratio. Mixed flow and plug flow compared for passage ratio of 0.5.

4.2.2 Tanks-in-Series Modelling

A tanks-in series model was used to represent a pressure screen and predict the effect of screen length L_s on reject thickening. A long screen was modelled as a relatively high number of well-mixed tanks or screen sections in series (Figure 4.3). Because pulp is completely mixed throughout the section, it was assumed that each tank would exhibit mixed flow behaviour. If the number of tanks is high enough, they collectively exhibit plug flow behaviour [170-172]. As tanks are progressively eliminated (simulating shortening or blanking sections of the screen), a screen will begin to exhibit mixed flow. Eventually the screen is reduced to one tank, which exhibits mixed flow behaviour.

If other factors are equal (i.e. with passage ratio constant), the change in flow behaviour along the screen will cause the reject thickening factor to decrease appreciably when volumetric reject ratio is relatively low (R_v<0.2, Figure 4.2). Although the length of each well-mixed screen section is undefined, it is likely to have mechanistic and physical significance. It is possible that each well mixed section represents the mixing length of

macro-turbulent eddies in the wake of a rotor, lobe or step. An open foil-type rotor, which experiences more axial mixing, is likely to have a longer mixing length than a closed type rotor. Mixing length along the screen may also change as the relative velocity between the fluid and rotor change (Section 4.3).

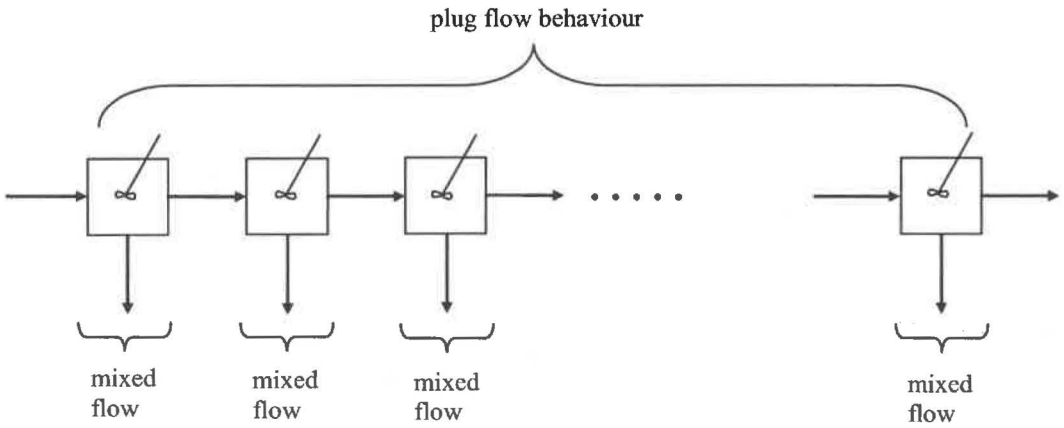

Figure 4.3 Schematic of the tanks-in-series model.

Two tanks-in-series

Reject thickening can be modelled as any number of tanks in series (e.g. 2, 10, 100, 1000, etc). The plug flow model presented by Gooding and Kerekes [93] can be viewed as an infinite number of narrow screen sections in series. Modelling thickening using two tanks in series (Figure 4.4) will be described in detail because the procedure can be applied to any number of screens.

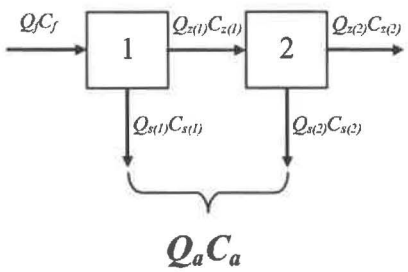

Figure 4.4 Two tanks-in-series model.

Pulp flows into the first tank at a volumetric flow rate of Q_f and consistency C_f. At the first tank, mass flows across the screen to the accept chamber at a volumetric flow rate Q_s and consistency C_s. Mass flows to the second tank (in the direction of the reject) at a volumetric flow rate $Q_{z(1)}$ and consistency $C_{z(1)}$. At the second tank, mass flows to the accept at a volumetric flow rate $Q_{s(2)}$ and consistency $C_{s(2)}$, and mass flows to the reject stream at a flow rate $Q_{z(2)}$ and consistency $C_{z(2)}$.

The local reject thickening T_z of the first and second tank is calculated using Equations 4.1 and 4.2 respectively, where C_f is feed consistency, $C_{z(1)}$ is consistency of pulp exiting the first tank, and C_r is consistency of pulp exiting the second tank. Thus, local thickening is a function of pulp consistency exiting the tank and pulp consistency flowing into the tank.

$$T_{z(1)} = \frac{C_{z(1)}}{C_f} \tag{4.1}$$

$$T_{z(2)} = \frac{C_{z(2)}}{C_{z(1)}} \tag{4.2}$$

The overall reject thickening for the two tanks in series is the product of the local reject thickening factors (Equation 4.3).

$$T = T_{z(1)}T_{z(2)} = \frac{C_{z(1)}C_{z(2)}}{C_f C_{z(1)}} = \frac{C_{z(2)}}{C_f} \tag{4.3}$$

Local volumetric reject ratio R_z of the first and second tank is calculated using Equations 4.4 and 4.5, where Q_f is feed volumetric flow rate, $Q_{z(1)}$ is flow rate of pulp exiting the first tank, and $Q_{z(2)}$ is flow rate of pulp exiting the second tank (reject stream flow rate).

$$R_{z(1)} = \frac{Q_{z(1)}}{Q_f} \tag{4.4}$$

$$R_{z(2)} = \frac{Q_{z(2)}}{Q_{z(1)}} \tag{4.5}$$

Overall reject ratio R_v for the two tanks in series is the product of the local reject ratios (Equation 4.6).

$$R_v = R_{z(1)}R_{z(2)} = \frac{Q_{z(1)}Q_{z(2)}}{Q_f Q_{z(1)}} = \frac{Q_{z(2)}}{Q_f} \tag{4.6}$$

The two tanks operate in unison so the local volumetric accept flow rate of the first tank equals the volumetric accept flow rate of the second tank (Equation 4.7)

$$Q_{s(1)} = Q_{s(2)} \tag{4.7}$$

The overall volumetric accept flow rate is the sum of the two local flow rates (Equation 4.8), and the overall mass accept flow rate is the sum of the two local mass flow rates (Equation 4.9).

$$Q_a = Q_{s(1)} + Q_{s(2)} \tag{4.8}$$

$$Q_a C_a = Q_{s(1)} C_{s(1)} + Q_{s(2)} C_{s(2)} \tag{4.9}$$

The local passage ratios for the first $P_{z(1)}$ and second $P_{z(2)}$ tanks are defined by Equations 4.10 and 4.11.

$$P_{z(1)} = \frac{C_{s(1)}}{C_{z(1)}} \tag{4.10}$$

$$P_{z(1)} = \frac{C_{s(2)}}{C_r} \tag{4.11}$$

Alternatively, the local passage ratios can be expressed in terms of the local volumetric reject ratio and thickening factor (Equations 4.12 and 4.13).

$$P_{z(1)} = \frac{\frac{1}{T_{z(1)}} - R_{z(1)}}{1 - R_{z(1)}} \tag{4.12}$$

$$P_{z(2)} = \frac{\frac{1}{T_{z(2)}} - R_{z(2)}}{1 - R_{z(2)}} \tag{4.13}$$

Similarly, the local volumetric reject ratios for the two tanks can be expressed in terms of the local thickening factors and passage ratios (Equation 4.14 and 4.15).

$$R_{z(1)} = \frac{\frac{1}{T_{z(1)}} - P_{z(1)}}{1 - P_{z(1)}} \tag{4.14}$$

$$R_{z(2)} = \frac{\frac{1}{T_{z(2)}} - P_{z(2)}}{1 - P_{z(2)}} \tag{4.15}$$

The local volumetric accept flow rates can also be expressed in terms of the local volumetric reject ratio (Equations 4.16.and 4.17).

$$Q_{s(1)} = Q_f \left[1 - \left(\frac{\frac{1}{T_{z(1)}} - P_{z(1)}}{1 - P_{z(1)}} \right) \right] \tag{4.16}$$

$$Q_{s(2)} = Q_{z(1)}\left[1-\left(\frac{\frac{1}{T_{z(2)}}-P_{z(2)}}{1-P_{z(2)}}\right)\right] \tag{4.17}$$

The thickening behaviour with volumetric ratio R_v of two tanks in series was computed using the relationship given by Equation 4.3 for a passage ratio of 0.5 in each tank (Figure 4.5). The mixed flow model with a passage ratio of 0.402 fitted the data better than a plug flow model with a passage ratio P_p of 0.687.

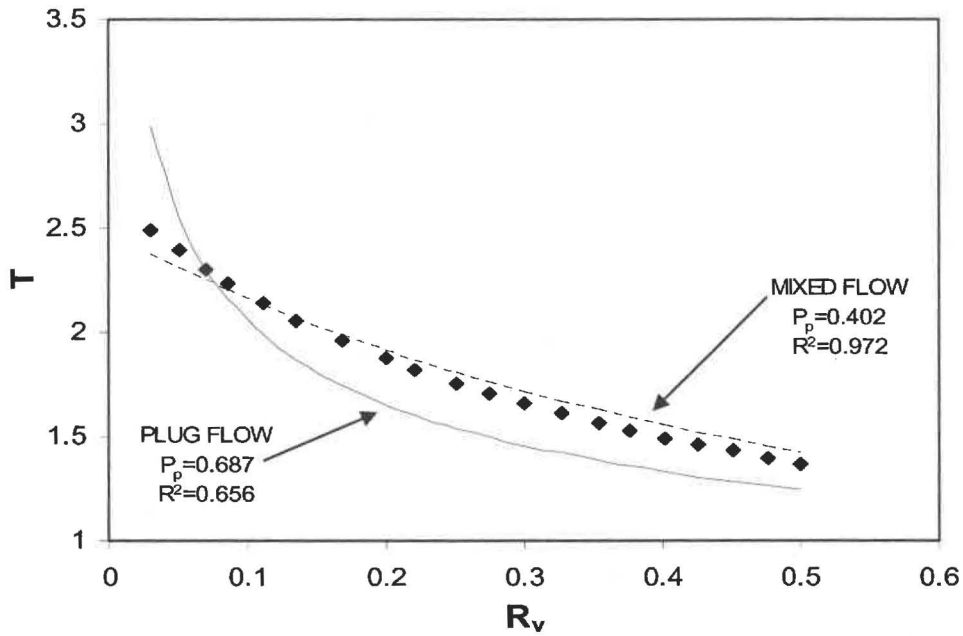

Figure 4.5 The fit for mixed flow and plug flow models to reject thickening for two tanks in series with $P_{z(1)}=P_{z(2)}=0.5$.

Results of modelling reject thickening using two tanks in series (Figure 4.5) were analysed further by calculating passage ratios assuming mixed flow (Equation 4.18), plug flow (Equation 4.19), and non-ideal flow (Equation 4.20).

The non-ideal flow model assumes average fibre concentration in the screening zone is the linear average between the feed and reject streams.

$$P_p = \frac{\frac{1}{T}-R_v}{1-R_v} \tag{4.18}$$

$$P_p = \frac{\log T}{\log R_v}+1 \tag{4.19}$$

$$P_p = \frac{C_a}{\left(\frac{C_f + C_r}{2}\right)} \tag{4.20}$$

For two tanks, passage ratios for plug flow decrease exponentially with volumetric reject ratio and are greater than the 0.5 (Figure 4.6), values for mixed flow increase with volumetric reject ratio and are less than 0.5, whilst passage ratios for non-ideal flow are independent of volumetric reject ratio and about 0.55. Differences between predicted passage ratios for plug and mixed flow models are greatest at low volumetric reject ratios and approach a common value as volumetric reject ratio increases.

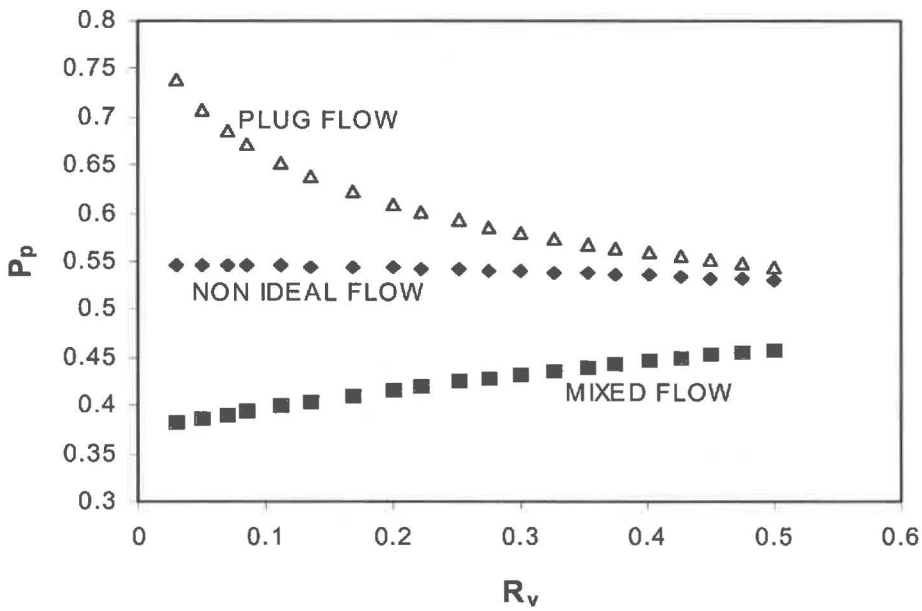

Figure 4.6 Effect of flow model and volumetric reject ratios on passage ratio for two tanks in series with $P_{z(1)}$=$P_{z(2)}$=0.5.

100 tanks-in-series

Consider a mass of pulp at a volumetric flow rate of Q_f and consistency C_f in a series of tanks (Figure 4.5). At the 100th tank, mass flows to the accept at a volumetric flow rate $Q_{s(100)}$ and consistency $C_{s(100)}$, and mass flows to the reject stream at a flow rate $Q_{z(100)}$ and consistency $C_{z(100)}$ (Figure 4.7). Equations for thickening, volumetric reject ratio and passage ratio for each tank have the same form because Equation 2.65 (mixed flow) is still the governing relationship. Thus, local thickening at an arbitrary tank 'i' can be defined by either the local consistencies or local volumetric ratio and passage ratio (Equation 4.21).

$$T_{z(i)} = \frac{C_{z(i)}}{C_{z(i-1)}} = \frac{1}{R_{z(i)} - R_{z(i)}P_{z(i)} + P_{z(i)}} \tag{4.21}$$

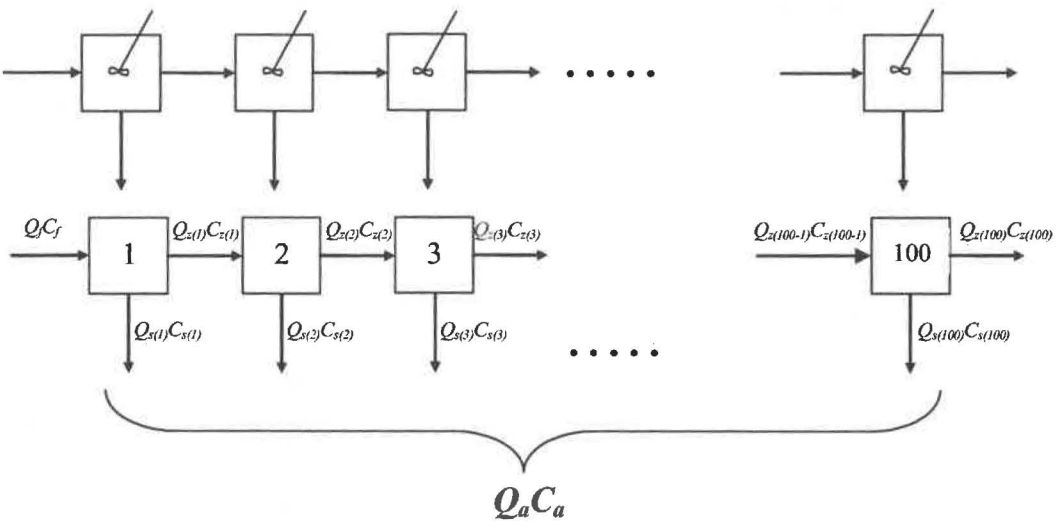

Figure 4.7 Schematic of the 100 tanks-in-series model.

Equations for thickening, volumetric reject ratio and passage ratio for each tank have the same form because Equation 2.65 (mixed flow) is still the governing relationship. Thus, local thickening at an arbitrary tank 'i' can be defined by either the local consistencies or local volumetric ratio and passage ratio (Equation 4.21).

$$T_{z(i)} = \frac{C_{z(i)}}{C_{z(i-1)}} = \frac{1}{R_{z(i)} - R_{z(i)}P_{z(i)} + P_{z(i)}} \tag{4.21}$$

The local volumetric reject ratio can be defined from either the local volumetric flow rate or local thickening and passage ratios (Equation 4.22). This prediction is effectively a rearrangement of the equation for mixed flow (Equation 2.65).

$$R_{z(i)} = \frac{Q_{z(i)}}{Q_{z(i-1)}} = \frac{\frac{1}{T_{z(i)}} - P_{z(i)}}{1 - P_{z(i)}} \tag{4.22}$$

The local passage ratio can also be defined by either local consistencies or by rearranging the equation for mixed flow (Equation 4.23).

$$P_{z(i)} = \frac{C_{s(i)}}{C_{z(i)}} = \frac{\frac{1}{T_{z(i)}} - R_{z(i)}}{1 - R_{z(i)}} \tag{4.23}$$

The cumulative thickening of 100 tanks in series is as follows:

$$T = \frac{C_r}{C_f} = \frac{C_{z(1)}}{C_f}\frac{C_{z(2)}}{C_{z(1)}}\frac{C_{z(3)}}{C_{z(2)}}\cdots\frac{C_{z(100)}}{C_{z(100-1)}} = T_{z(1)}T_{z(2)}T_{z(3)}\cdots T_{z(100)} = \frac{C_{z(100)}}{C_f} \tag{4.24}$$

The global/overall volumetric reject ratio after 100 tanks distributing the flow to accept uniformly is given by:

$$R_v = \frac{Q_r}{Q_f} = \frac{Q_{z(1)}}{Q_f}\frac{Q_{z(2)}}{Q_{z(1)}}\frac{Q_{z(3)}}{Q_{z(2)}}\cdots\frac{Q_{z(100)}}{Q_{z(100-1)}} = R_{z(1)}R_{z(2)}R_{z(3)}\ldots R_{z(100)} = \frac{Q_{z(100)}}{Q_f} \qquad (4.25)$$

Another thickening factor is the internal cumulative thickening factor. After nine tanks, the cumulative thickening is:

$$T_{z(1-9)} = \frac{C_{z(9)}}{C_f} = T_{z(1)}T_{z(2)}T_{z(3)}\ldots T_{z(9)} \qquad (4.26)$$

Reject thickening factor T is plotted against volumetric reject ratio R_v to illustrate reject thickening behaviour of 100 tanks in series (Figure 4.5). The Gooding and Kereks's plug flow model [93] fits these results better than their mixed flow model. Flow configuration changes from mixed flow to plug flow as number of tanks increases from 2 to 100.

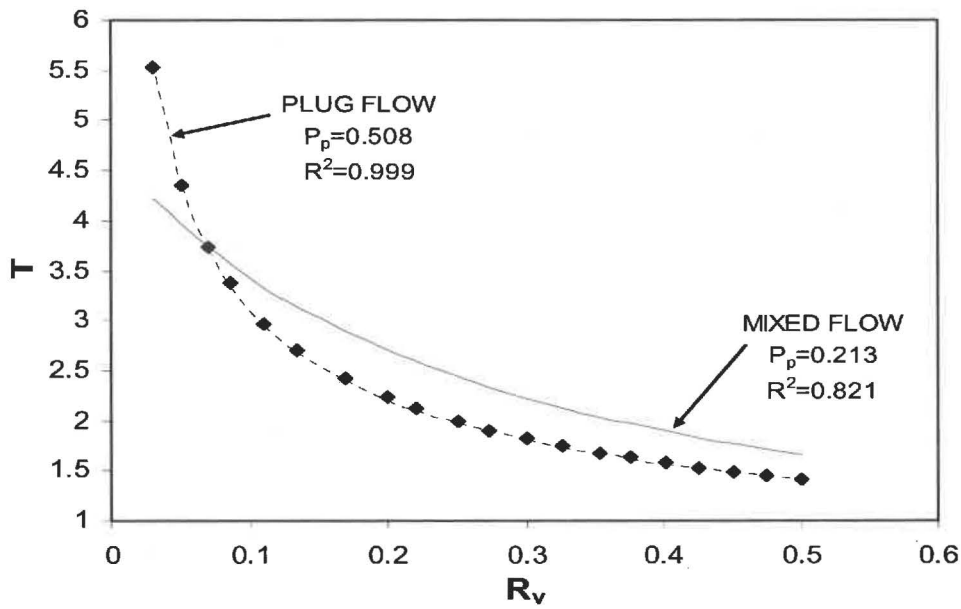

Figure 4.8 Reject thickening factor as a function of volumetric reject ratio, based on 100 tanks in series with $P_{z(i)}$=0.5.

At constant volumetric reject ratio R_v, the number of tanks N_T affects reject thickening factor (Figure 4.9). Up to 100 tanks, there is a semi-logarithmic relationship between reject thickening factor and N_T; reject thickening factor then becomes relatively constant. If plug flow begins at 100 tanks in series, then the equivalent screen length can be regarded as the critical length for plug flow. Above this critical length, plug flow occurs and thickening is constant; below the critical length, there is a shift toward mixed flow and thickening decreases.

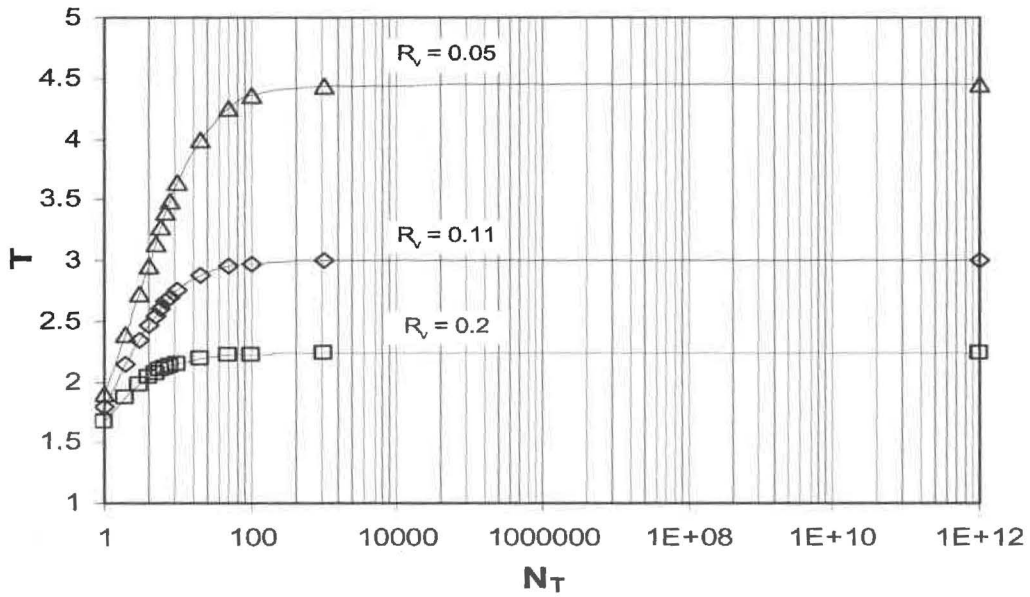

Figure 4.9 Effect of number of tanks (NT) and volumetric reject ratio on reject thickening factor with $P_{z(i)}$=0.5.

Reject thickening curves for screen lengths equivalent to 1 to 100 tanks are presented in Figure 4.10, together with the relationship for plug flow. As number of tanks increase, the curves move up and their shape becomes more like plug flow. Although the 100 tanks-in-series model is similar to that for plug flow, the curve is slightly below that for plug flow, indicating that the model with 100 tanks slightly under predicts thickening.

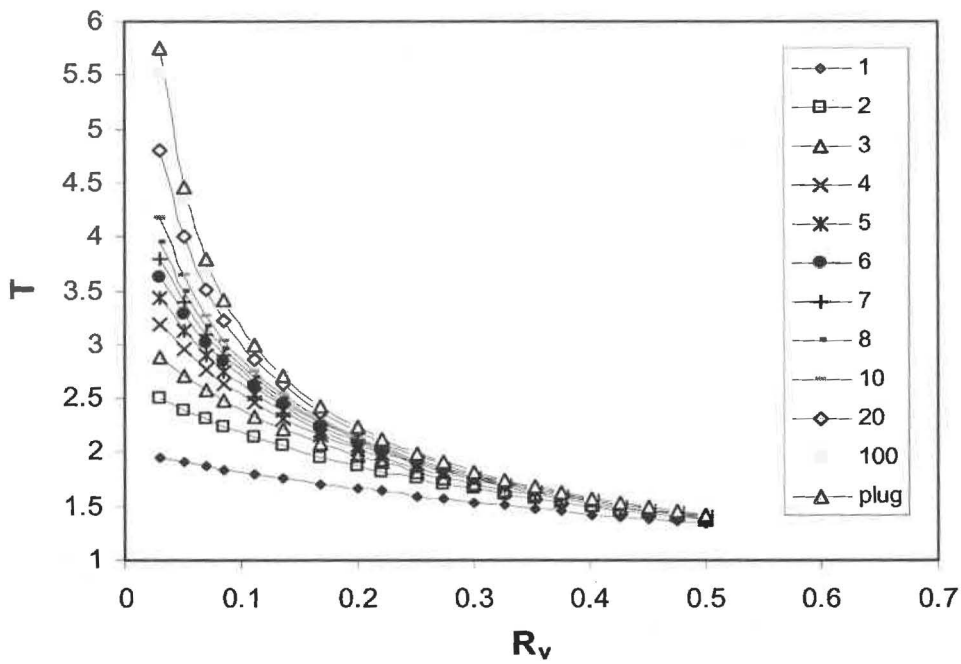

Figure 4.10 Effect of tanks on position and shape of reject thickening curve with $P_{z(i)}$=0.5.

Table 4.1 is for fitting plug flow and mixed flow to reject thickening data in Figure 4.10. For mixed flow, the fit decreases as the number of tanks increases, but with plug flow, the

fit increases. For both mixed flow and plug flow, however, the passage ratios P_p obtained by fitting the models decreased with increasing number of tanks. It is interesting to note that the plug flow model fits data for 6 tanks in series well (R^2=0.931), even though complete plug flow may not develop until the number of tanks N_T is as high as 100.

Table 4.1 Best fit passage ratio P_p for plug flow and mixed flow and corresponding R^2.

Tanks	1	2	4	6	8	10	20	100	Infinity
R^2 (mixed)	1	0.972	0.927	0.902	0.887	0.876	0.849	0.821	0.813
R^2 (plug)	0.058	0.656	0.874	0.931	0.956	0.969	0.991	0.999	1.00
P_p (mixed)	0.5	0.402	0.328	0.296	0.277	0.265	0.238	0.213	0.206
P_p (plug)	0.755	0.656	0.626	0.597	0.578	0.569	0.537	0.508	0.500

Passage ratios for mixed flow (Equation 4.18) were calculated for data originally presented in Figure 4.10. For a single tank, passage ratio equals 0.5 and is independent of the volumetric reject ratio (Figure 4.11). As the number of tanks increases, passage ratio decreases and becomes strongly dependent on the volumetric reject ratio. A flow model is only valid when passage ratio is independent of the volumetric reject ratio.

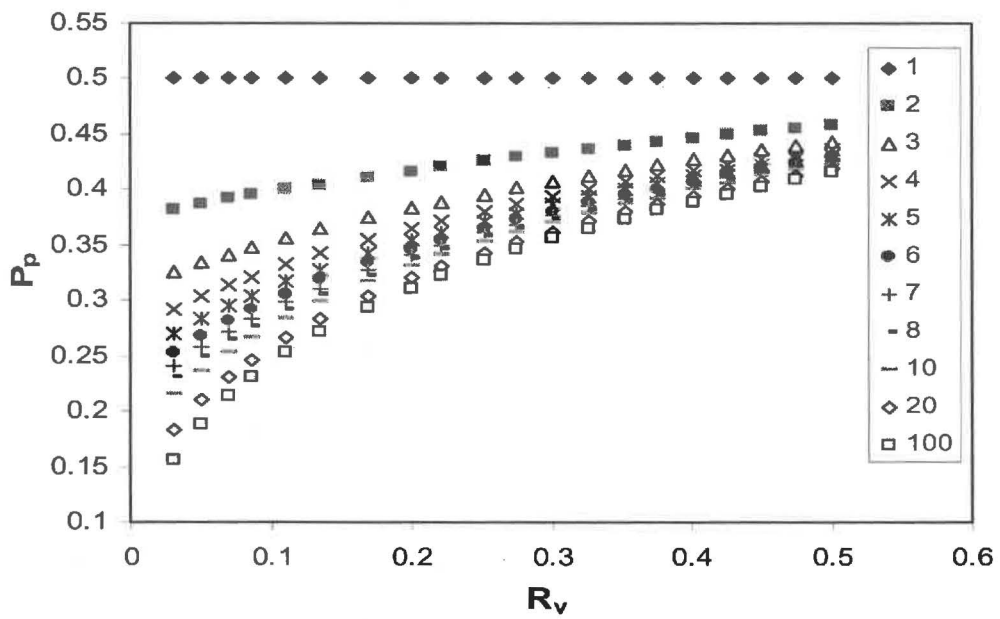

Figure 4.11 Effect of number of tanks on volumetric reject ratio assuming mixed flow.

Passage ratios for plug flow (Equation 4.19) show that as number of tanks increase, passage ratio decreases and is less dependent on the volumetric reject ratio (Figure 4.12). At 100 tanks, passage ratio is relatively independent of volumetric reject ratio.

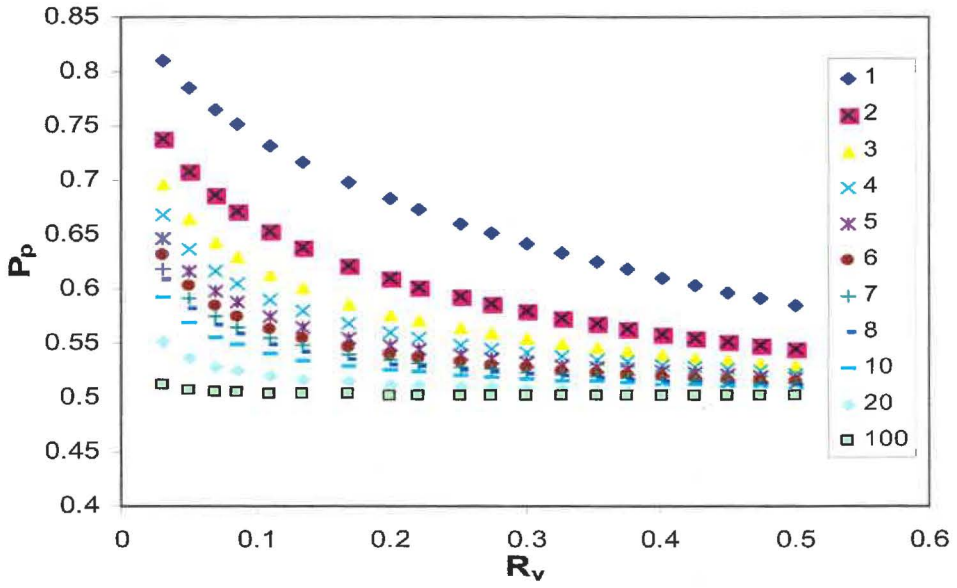

Figure 4.12 Effect of number of tanks on volumetric reject ratio assuming plug flow.

Passage ratios calculated assuming non-ideal flow (Equation 4.20) decrease as number of tanks increase (Figure 4.13). Passage ratio for a single tank is inversely related to reject ratio, relatively independent of reject ratio for two tanks in series but about 10% higher than the 0.5 used to model reject thickening, and non-linear for three or more tanks.

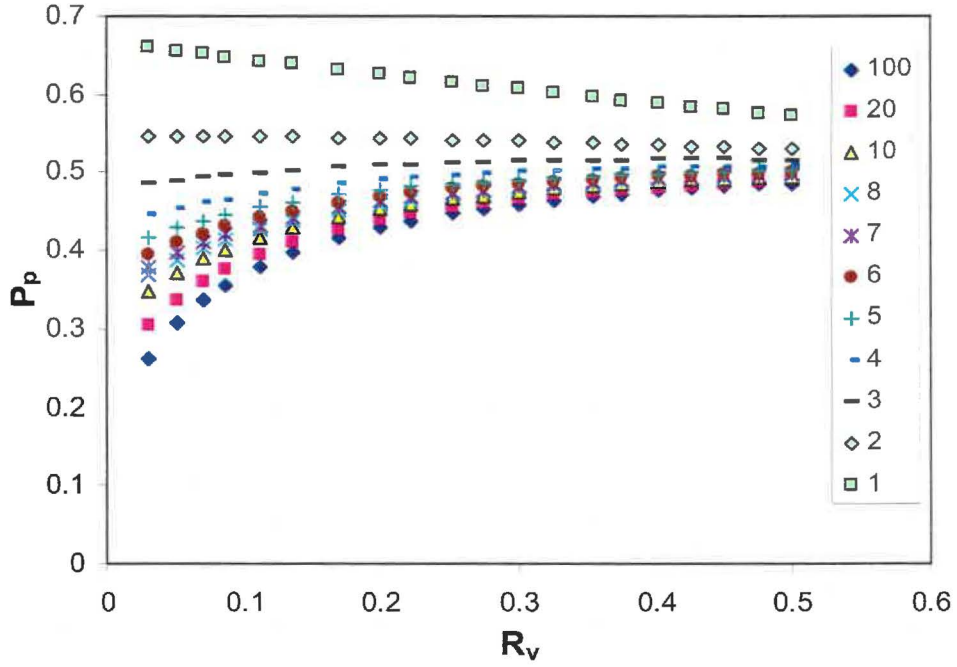

Figure 4.13 Effect of number of tanks on volumetric reject ratio. The passage ratio is calculated assuming non-ideal flow (Equation 4.23).

The internal cumulative thickening factor T_c can be plotted against normalised axial position Z_N (Figure 4.14) to compare the thickening profile of a single tank (equivalent

passage ratio P_z=0.5) with 100 tanks in series. The thickening profile for one tank is a straight line with gradient zero because the tank is well-mixed and consistency C_z is uniform throughout the feed annulus. Pulp instantaneously thickens as it flows into the tank and a large step change from T_c=1 to T_c=1.8 occurs at Z_N=0. In comparison, the thickening profile for 100 tanks is a curve because no mixing occurs between the tanks and pulp thickens incrementally as it flows from tank to tank. Overall, pulp only thickens by a factor of 1.8 with one tank (i.e. at Z_N=1), but by a factor of 2.97 with 100 tanks.

If 100 tanks in series approximate plug flow, then the cumulative thickening profiles (Figure 4.14) can be regarded as comparing mixed with plug flow. With mixed flow, pulp in the feed annulus thickens immediately to 1.8% at a feed consistency of 1%. Pulp remains at this consistency throughout the feed annulus, so mean consistency in the feed annulus is also 1.8%. In comparison, mean consistency in the feed annulus is only 1.51% with plug flow despite pulp thickening to 2.97%. Assuming local passage ratio P_z and aperture flow rate Q_s are the same, a higher mean consistency in the feed annulus results in higher fibre passage across the screen with mixed flow. Greater fibre passage across the screen explains why reject thickening is lower with mixed flow.

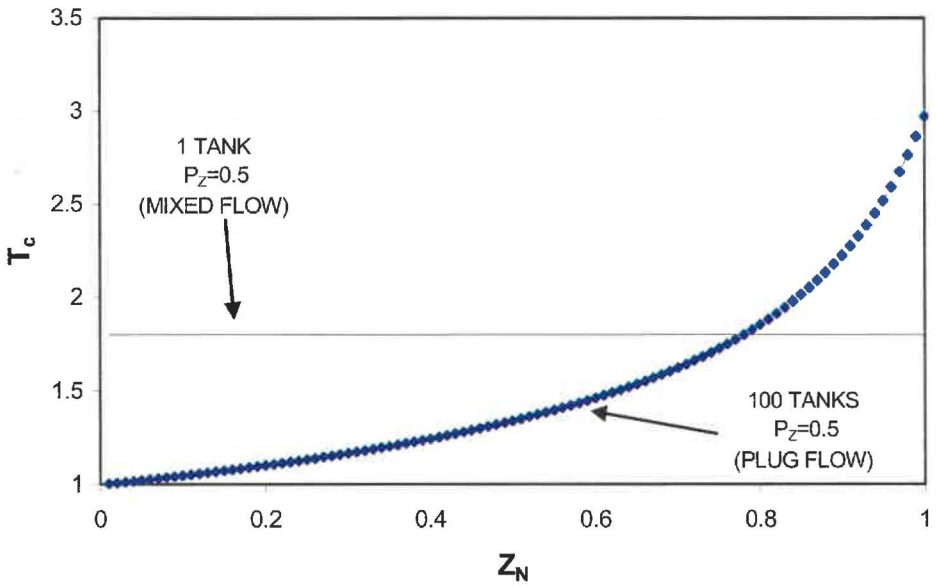

Figure 4.14 Internal reject thickening factor as a function of normalised axial screen position for a single tank and for 100 tanks.

4.2.3 Experimental Results

When screening eucalypt at an aperture velocity of 0.6 ms^{-1}, shortening the standard screen with 1-mm holes to a 27-mm section decreased reject thickening appreciably at low volumetric reject ratios (R_v>0.2) for the bump rotor (Figure 4.15) and the step rotor

(Figure 4.16) but reject thickening was constant at high reject ratios (R_v>0.5). Shortening the screen caused the volumetric accept flow rate to decrease in proportion to the reduction in open area because V_s was held constant.

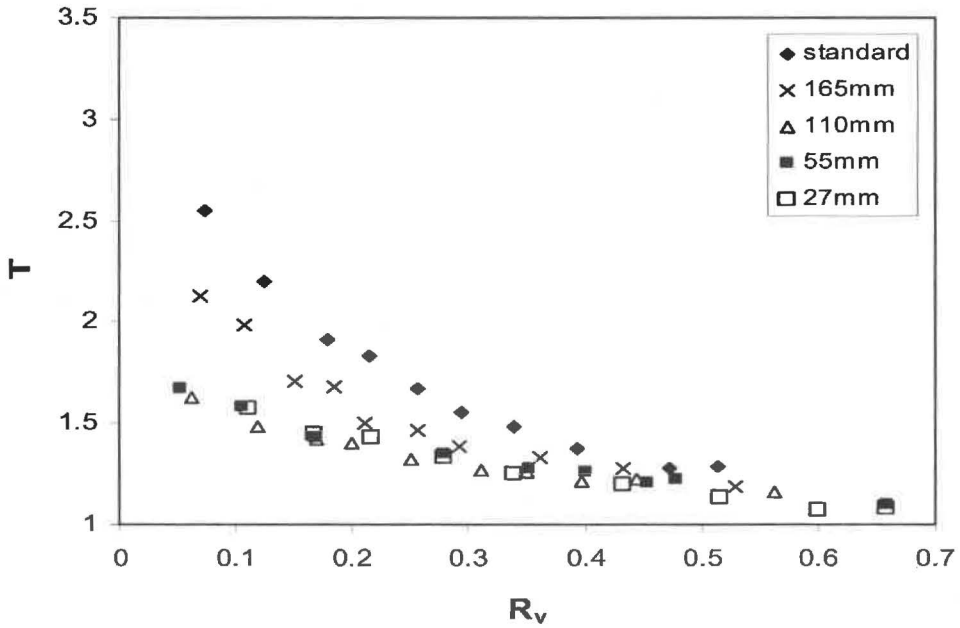

Figure 4.15 Effect of screen length on reject thickening with the bump rotor. 1-mm holes, bleached eucalypt, V_{tip}=22 ms^{-1}, V_s=0.6 ms^{-1}, C_f=0.5%.

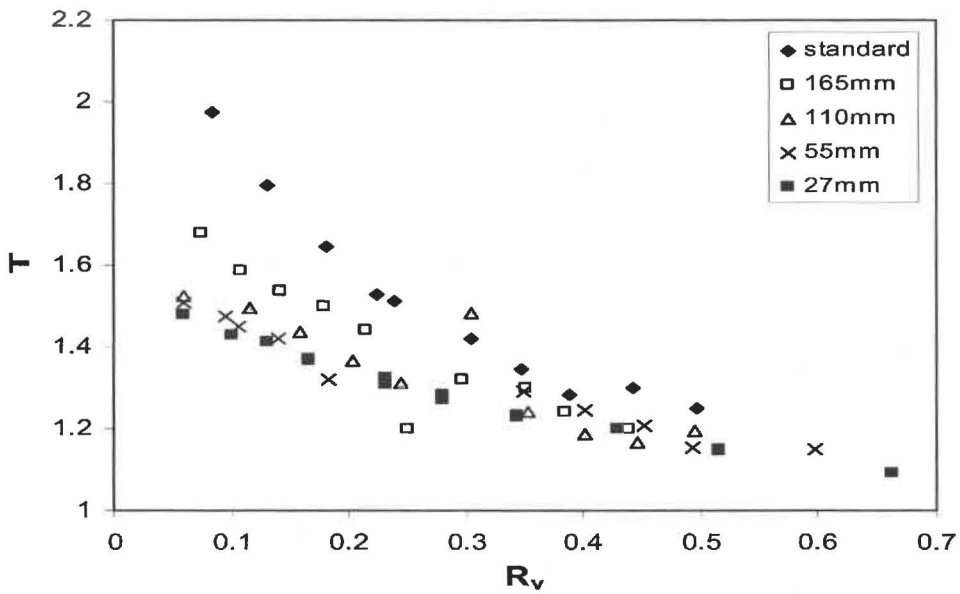

Figure 4.16 Effect of screen length on reject thickening with the step rotor. 1-mm holes, bleached eucalypt, V_{tip}=22 ms^{-1}, V_s=0.6 ms^{-1}, C_f=0.5%.

Plotting reject thickening factor with screen length for a volumetric reject ratio of 0.2 (Figure 4.17) demonstrates the effect of screen length. Halving screen length (i.e. to 110 mm) decreased reject thickening. Further decreases did not affect reject thickening.

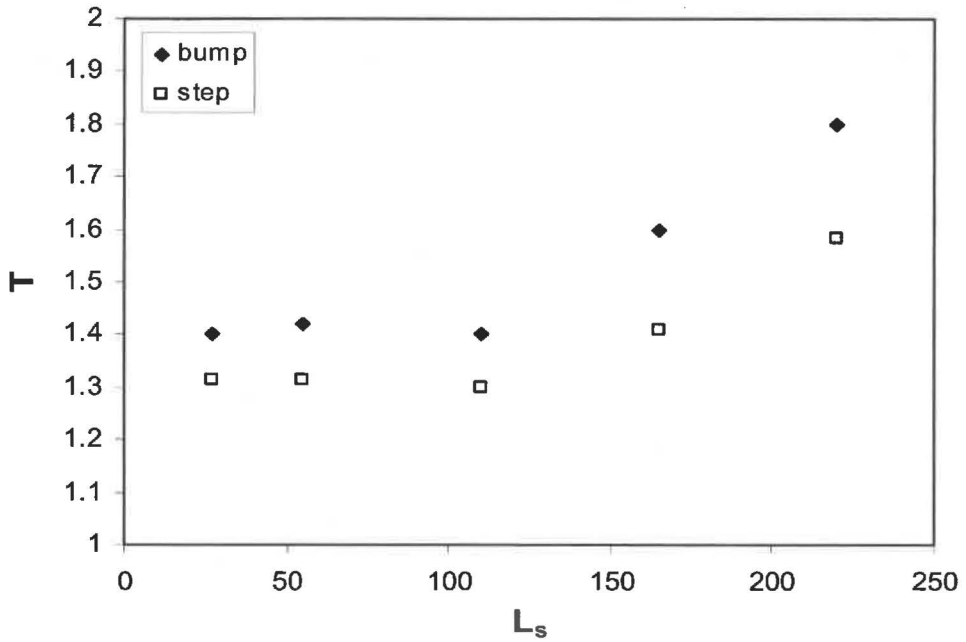

Figure 4.17 Reject thickening factor as a function of screen length for R_v=0.2. 1-mm holes, bleached eucalypt, V_{tip}=22 ms^{-1}, V_s=0.6 ms^{-1}, C_f=0.5%.

The plug flow and mixed flow models for the bump (Figure 4.18) and step (Figure 4.19) rotors were compared with reject thickening factors for the standard length screen using the bump (Figure 4.15) or step (Figure 4.16) rotors. The higher R^2 value indicates that the full-length screen exhibits plug flow but further analysis revealed there was a slight deviation.

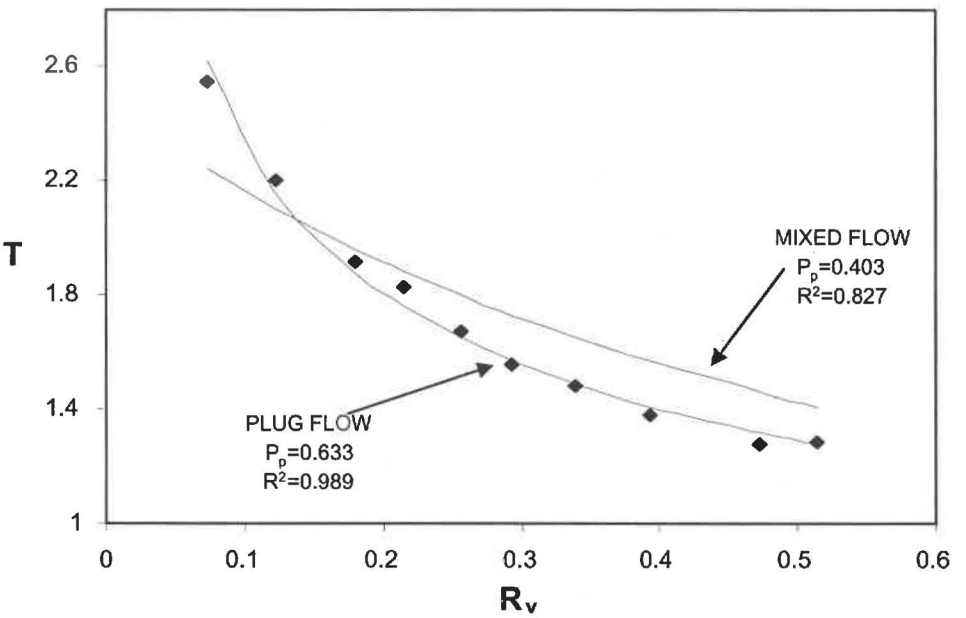

Figure 4.18 Fitting the plug and mixed flow models to reject thickening for screening bleached eucalypt in standard screen with 1-mm holes with a bump rotor. V_{tip}=22 ms^{-1}, V_s=0.6 ms^{-1}, C_f=0.5%.

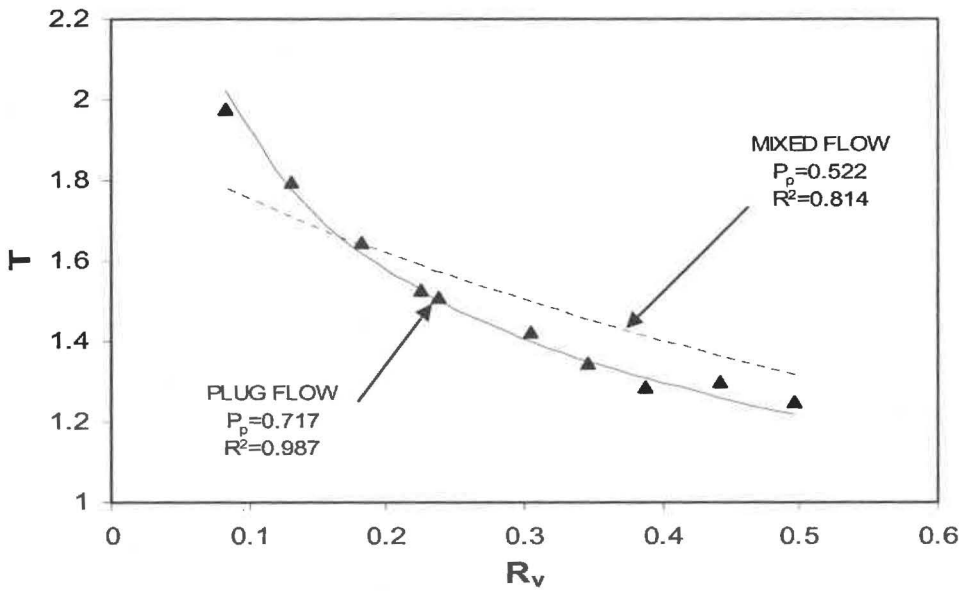

Figure 4.19 Fitting plug and mixed flow models to reject thickening for screening bleached eucalypt in a standard screen with 1-mm holes and step rotor. V_{tip}=22 ms^{-1}, V_s=0.6 ms^{-1}, C_f=0.5%.

There is less variation in passage ratio with volumetric reject ratio when using the plug flow model for the bump rotor (Figure 4.20) and the step rotor (Figure 4.21), further supporting that this is better than the mixed flow model. However, passage ratio for both rotors depend slightly on reject ratio with plug flow (R^2>0), indicating small deviations from plug flow are occurring.

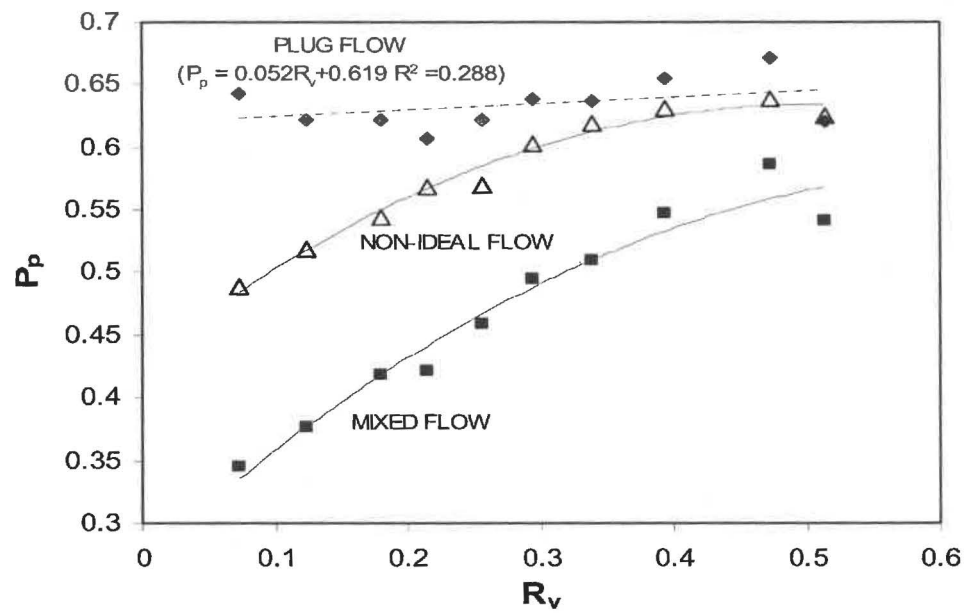

Figure 4.20 Passage ratio as a function of volumetric reject ratio for screening bleached eucalypt in a full-length screen with 1-mm holes and bump rotor. V_{tip}=22 ms^{-1}, V_s=0.6 ms^{-1}, C_f =0.5%.

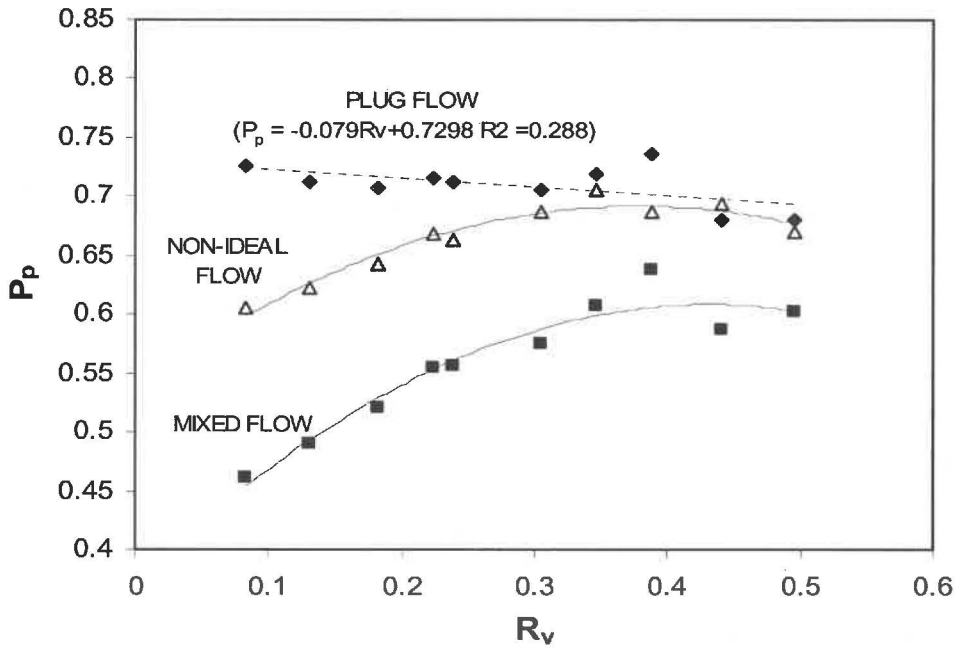

Figure 4.21 Passage ratio as a function of volumetric reject ratio for screening bleached eucalypt using a full-length screen with 1-mm holes and step rotor. V_{tip}=22 ms^{-1}, V_s=0.6 ms^{-1}, C_f=0.5%.

Reject thickening factors for the 27-mm screen (Figures 4.15 and 4.16) are re-presented for the bump (Figure 4.22) and step (Figure 4.23) rotors, and show that the mixed flow model gives a better fit than the plug flow model (higher R^2 value). This indicates a shift from plug to mixed flow as the screen is shortened. The fit is not perfect, indicting a slight divergence from mixed flow behaviour.

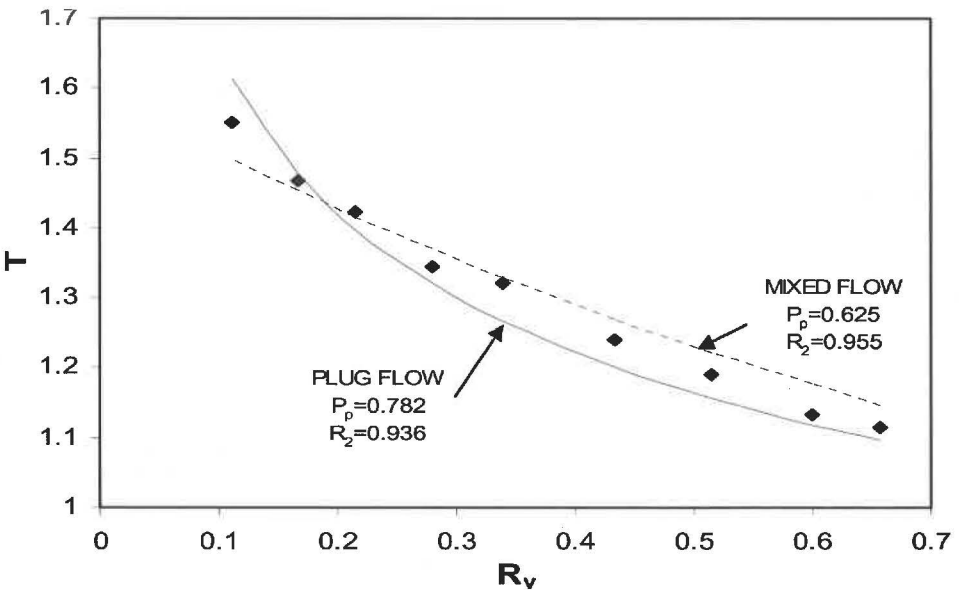

Figure 4.22 Fitting plug flow and mixed flow models to reject thickening for screening bleached eucalypt with a 27-mm screen with a bump rotor. V_{tip}=22 ms^{-1}, V_s=0.6 ms^{-1}, C_f=0.5%.

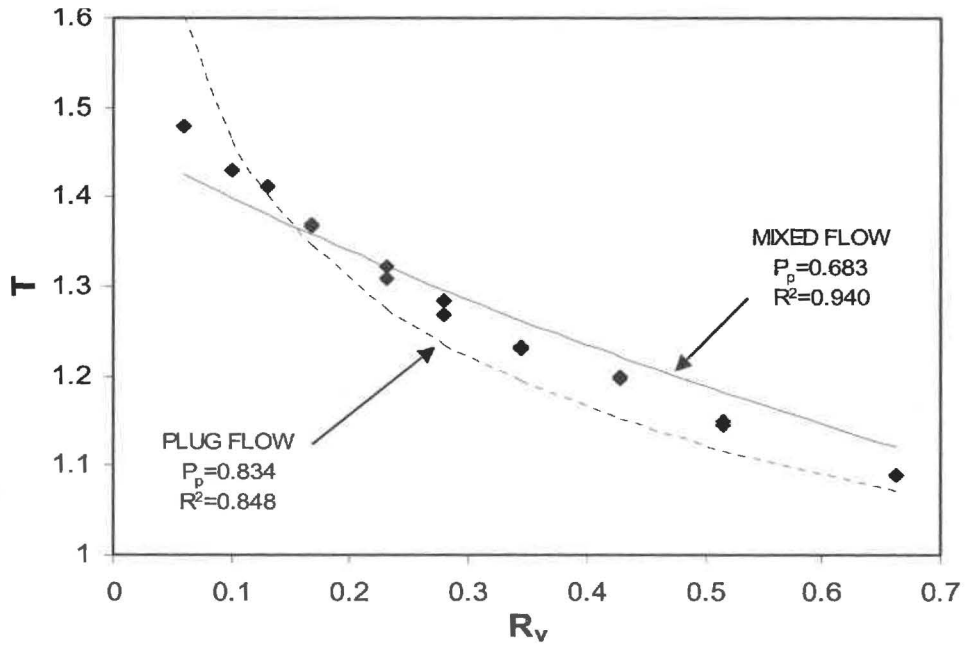

Figure 4.23 Fitting plug flow and mixed flow models to reject thickening for screening bleached eucalypt with a 27-mm screen with a step rotor. V_{tip}=22 ms^{-1}, V_s=0.6 ms^{-1}, C_f=0.5%.

Passage ratios calculated from thickening data in Figures 4.22 and 4.23 are presented in Figure 4.24 (bump) and Figure 4.25 (step). There is a strong relationship between passage ratio and volumetric reject ratio for both the mixed flow and plug flow models and it is concluded that neither the mixed flow nor the plug flow models represents actual flow configuration with a short screen section. However, passage ratio calculated using Equation 4.20 is relatively constant, indicating that flow configuration is non-ideal.

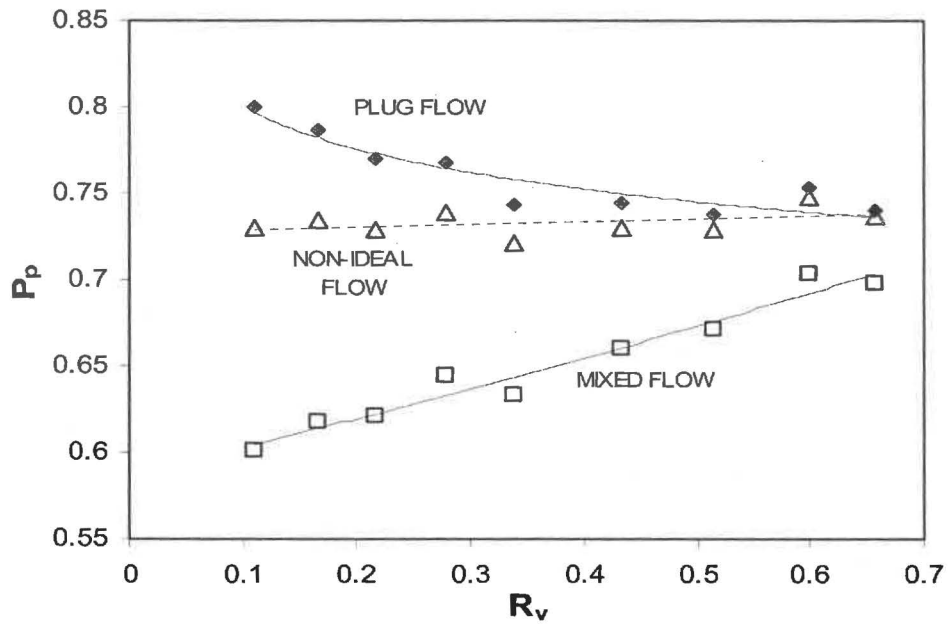

Figure 4.24 Passage ratios for screening bleached eucalypt with a 27-mm screen with a bump rotor. V_{tip}=22 ms^{-1}, V_s=0.6 ms^{-1}, C_f=0.5%.

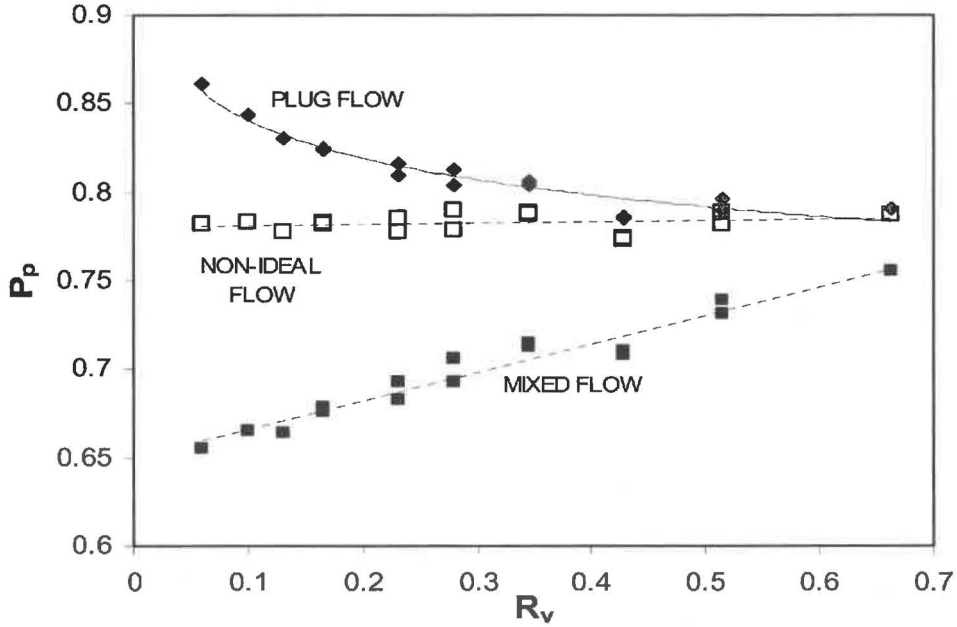

Figure 4.25 Passage ratios for screening eucalypt with a 27-mm screen with a step rotor. Bleached eucalypt, V_{tip} = 22 ms^{-1}, V_s=0.6 ms^{-1}, C_f=0.5%.

Julien Saint Amand and Perrin [128] calculated passage ratios for a shortened screen using Equation 4.20 and also found that passage ratio was independent of the volumetric reject ratio. They did not derive an alternative non-ideal flow model using this passage ratio. Data in Figure 4.6 show that passage ratio is independent of volumetric reject ratio for two tanks in series when passage ratio is calculated using Equation 4.20. Thus, reject thickening behaviour of two tanks in series is consistent with reject thickening behaviour of a 27-mm screen. In both cases, passage ratio is independent of volumetric reject ratio when it is calculated using Equation 4.20

4.2.4 Discussion

Previous studies on the effect of screen length on reject thickening have either not fully described the experimental conditions [89] or not given actual reject thickening data [91]. The current study is the first time that reject thickening factors have been presented, along with a clear description of assumptions and experimental conditions.

Modelling a screen as a series of tanks (or screen sections) predicts that reject thickening will decrease with decreasing length, which is consistent with experimental data from the current study. Reject thickening decreases only slightly when there are many tanks (>1000 tanks) but decreases relatively quickly when there are less than 100 tanks. This decrease in thickening is due entirely to a shift toward mixed flow and greater axial mixing. When consistency in the feed annulus increases, there is a higher overall mass

flow of fibre across the screen to the accept chamber even if passage ratio is the same; less fibre flows to the reject stream, and the reject thickening factor decreases.

Although a tanks-in-series model may better model a pressure screen (because it accounts for partial axial mixing), the model described in section 4.2 still simplifies the screen even though it may not describe the screen realistically. Modelling the screen as a single row of tanks (or screen sections) in series ignores that the real screen is more like two rows of tanks on either side of the screen cylinder with interchange. The model presented in Section 4.2 also ignores any disparities in volumetric flow and passage ratio that may occur along the screen. However, these disparities can be incorporated into the tanks-in-series model more easily than in the plug flow model. This simplicity means that the modified tank-in-series model that does not require the complex integration required in the modified plug flow model.

The experimental data obtained confirmed the model developed, which showed that reject thickening decreases with screen length and there is a shift from plug flow to mixed flow (greater axial mixing). By calculating passage ratio correctly (more accurately), increase in passage ratio was minimal. It can be concluded that a major factor for the decrease in thickening with screen length was due to a change in flow configuration. The result is an increase in overall average fibre concentration on the feed side of the screen. This has not been discussed in previous reports. Furthermore, findings of the current research cannot be compared with previous reports, which tend to lack detail on experimental conditions. Pimely and Rees [89] did report that reject thickening factor decreased from 1.8 to 1.5 when the screen was shortened by 50 percent. Unfortunately, they did not attempt to elucidate the flow configuration and did not calculate passage ratio.

Measurements of consistency changes revealed that standard full-length screens exhibited plug flow behaviour, which is consistent with data from previous reports [43, 93, 127, 147]. The standard screens used in this thesis had an aspect ratio of 1.1 (screen length to diameter ratio), which is a relatively long pressure screen cylinder compared to screens used in other research. Wakelin and co-workers [24,127, 147] reported that their screens exhibited plug flow behaviour, even with an aspect ratio as low as 0.6. They only have a limited analysis of consistency changes. More detailed analysis (e.g. calculating the passage ratio and investigating if there was any relationship with volumetric reject ratio) may have revealed divergence from plug flow.

Even though plug flow more accurately modelled consistency changes in the standard screens, some deviations did occur. It is somewhat surprising that there was only a slight deviation from plug flow with the full length screen, especially when no tubular vessel/reactor or straight pipe can satisfy all the assumptions for plug flow. For example, one assumption is that there is a flat velocity profile, and every particle has the same residence time in the vessel. Laminar or turbulent flow in a straight pipe has a parabolic velocity profile [170]. Particles near the pipe wall have a lower velocity, and consequently have a longer residence time, than a particle in the middle.

Many other assumptions of the plug flow model [93] may not be met in a real pressure screen. Firstly, mechanical agitation of the suspension/slurry provided by the screen rotor as pulp flows through the annulus will create some axial mixing. Secondly, there is likely to be many recirculation/recycle flow loops and back-mixing as pulp flows through the screen (forward flow), and back again (back-flow). Through flow with an external recycle loop may also occur as pulp flows through to the accept chamber and then towards the accept outlet, only to be drawn back to the feed annulus with/in back-flow. Thirdly, axial velocity through the feed annulus will decrease as pulp flows to the accept chamber. If flow is uniformly distributed [93], axial velocity decreases linearly.

4.3 Rotor to Pulp Relative Speed

4.3.1 Application of Related Theory

Relative speed is the velocity difference between the rotor tip V_{tip} (moving relatively fast) and pulp suspension in the feed annulus. Reinecker [148] proposed that relative speed decreases axially, but did not describe how to calculate relative speed. Because layers of the pulp suspension move at different speeds, relative speed depends on where it is measured. It is postulated that the instantaneous point velocity upstream of an aperture V_u will decrease radially from rotor tip (where $V_u=V_{tip}$) to screen (where $V_u=0$), giving velocity profiles similar to those presented in Figure 4.26. If relative speed decreases axially, then velocity profile at the front (feed-end) of the screen will be lower than that at the rear (reject-end) of the screen. Therefore, at any point between the tip of the rotor and screen surface, relative speed at the front (V_{tip}-V_u) will be greater than at the rear.

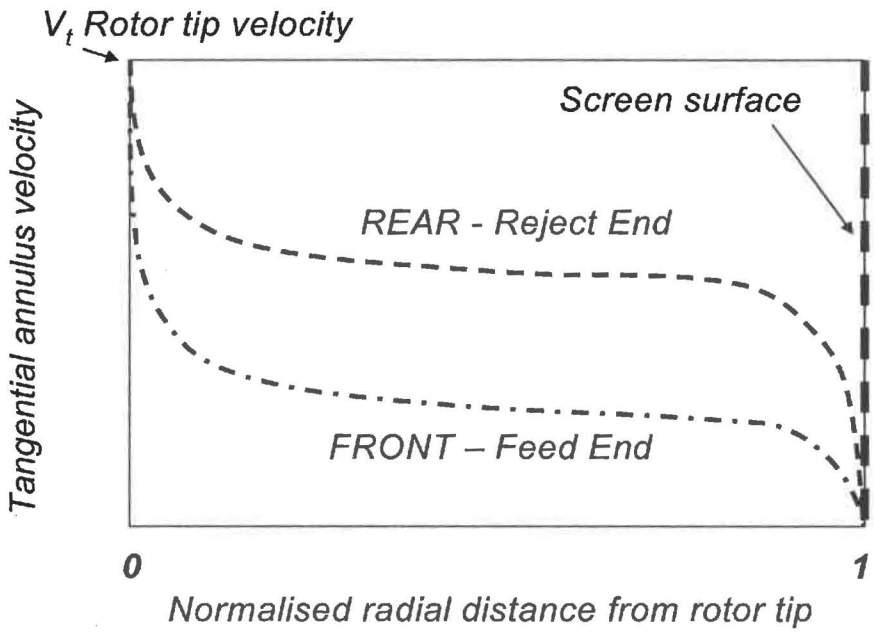

Figure 4.26 Hypothetical velocity profiles for the front and rear of a screen.

The absolute pressure in the feed annulus probably changes along a screen as the relative speed and velocity profile change. Reinecker [148] contends that turbulence intensity and pressure pulsation of the rotor change also. Although he did not measure turbulence intensity or pressure pulsation, he did find that contaminant removal efficiency was higher for a screen section at the feed end of the screen.

Yu [131] measured pressure pulsations along a screen and found that the peak-to-peak pressure difference of a step rotor was higher towards the front of the screen. The difference was minimal and only just discernable when pressure pulses were super-imposed on the same axes. Nevertheless, it is believed that the rotor is more effective at retarding screen plugging at the front of the screen, where relative speed and pressure pulsation is higher.

A screen operating under normal conditions will eventually plug with fibre and fibre flocs if volumetric accept flow rate Q_a is increased to some critical value. This is called plugging or screen blinding. Gooding and Craig [139] deliberately plugged their screens by increasing the volumetric accept flow rate. A sudden drop in the accept flow rate indicated plugging and there was a surge in the reject flow rate. The accept flow rate drops because consolidated fibre and flocs plug the screen apertures, restricting flow of water and fibre through the apertures. Pressure increases in the feed inlet, increasing the pressure drop from feed to reject; consequently reject volumetric flow rate increases.

Incipient plugging of apertures begins when fibre flocs are dragged into the apertures of a screen to form a consolidated floc, which occupies the internal space of the aperture. The floc could originate from several positions in the screen such as in the main flow of the feed annulus or accept chamber, or as a stapled floc on either side of the screen. The floc further consolidates as it filters fibre from flow through the aperture. Actual plugging occurs if the floc is sufficiently consolidated and severely restricts flow of water and fibre through the aperture, or if friction forces (F_F) between floc and aperture surfaces are higher than the suction forces generated by the rotor (F_{NP}) and other hydrodynamic forces (F_H), which would normally remove any consolidated floc.

Incipient blinding and plugging of an aperture occurs when forces acting on the floc balance (Figure 4.27). A condition of static equilibrium exists (Equation 4.27), where F_F is friction force between floc and aperture, F_{PP} is force from positive pressure in the feed annulus, F_H is force from hydrodynamic effects on the floc, and F_{NP} is the force generated by the negative pulse of the rotor.

$$F_F = F_{PP} + F_H - F_{NP} \tag{4.27}$$

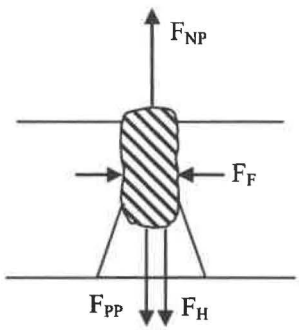

Figure 4.27 Forces acting on a floc within an aperture.

Martinez and Gooding [139] derived an equation (Equation 4.28) that estimates maximum flow rate Q_{max} within 20%, where O_A is open screen area, ρ is fluid or slurry density, K_H is pressure loss coefficient, P_{NP} is magnitude of the negative pulse, μ is static coefficient of friction, T is compressive stress in the floc, and W is aperture width. Q_{max} is a function of an open area term, a hydraulic resistance term, and a force term. If hydraulic resistance at the front and rear of the screen are the same, the first two terms can be ignored. Pressure readings during screening trials (Appendix 1) confirmed this simplification; thus, Q_{max} is proportional to the square root of the negative pulse.

$$Q_{max} = O_A \sqrt{\left(\frac{2}{\rho K_H}\right)} \sqrt{\left[P_{NP} - 2\mu\sigma\left(\frac{T}{W}\right)\right]} \tag{4.28}$$

Rearranging Equation 4.28 gives Equation 4.29, which can be used to estimate magnitude of the negative pulse. Values of f 6 kPa and 0.1 for σ and μ respectively were obtained from [137]; the pressure loss coefficient K_H of 1.5 for a 1-mm screen was from [181].

$$P_{NP} = \frac{Q_{max}^{\ 2}}{O_A^{\ 2}\left(\frac{2}{\rho K_H}\right)} + 2\mu\sigma\frac{T}{W} \qquad (4.29)$$

4.3.2 Experimental Results

Sections of the screen with 1-mm holes were deliberately plugged by increasing the volumetric accept flow rate Q_a to a maximum Q_{max}. The Q_{max} for screening eucalypt pulp at a feed consistency C_f of 0.5% was 700 L min^{-1} for sections at the front of the screen (positions 1&2 and positions 3&4) but only 500 L min^{-1} for a section at the reject-end (Figure 4.28). The lower Q_{max} indicates that the rotor is not as effective in preventing screen plugging at the reject end and infers that the magnitude of the negative pulse P_{NP} is lower and the pressure pulse has a different profile from that at the feed-end of the screen.

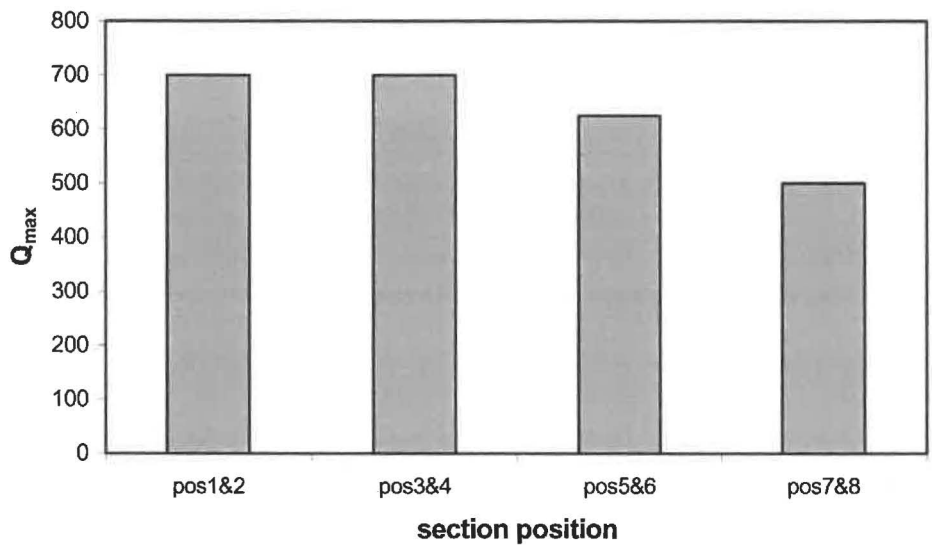

Figure 4.28 Effect of section position on Q_{max}. L_s=55 mm, 1-mm holes, bump rotor, bleached eucalypt, R_v=0.2, V_{tip}=22 ms^{-1}, C_f=0.5%.

Estimations for P_{NP} based on Q_{max} values (Table 4.2) indicate that P_{NP} can be up to 33% lower at the reject-end.

Table 4.2 Estimated magnitude of negative pressure pulse P_{NP} at various screen positions using Equation 4.29.

	POS 1&2	POS 3&4	POS 5&6	POS 7&8
P_{NP} (kPa)	70	70	62	47

Passage ratios P_p for all four sections approached a common value of 0.95 (Figure 4.29) but screen position has a greater effect on fibre passage at low (V_s=0.5 to 1 ms^{-1}) than at higher (V_s>2 ms^{-1}) aperture velocities. The effect of low velocities decreased passage ratio by 0.2 points at the reject-end of the screen. If it is accepted that relative speed and maximum rotor negative pressure P_{NP} are lower at the reject-end, then these data suggest that relative speed and P_{NP} have more impact on fibre passage at relatively low aperture velocities. As velocity increases, however, their impact diminishes.

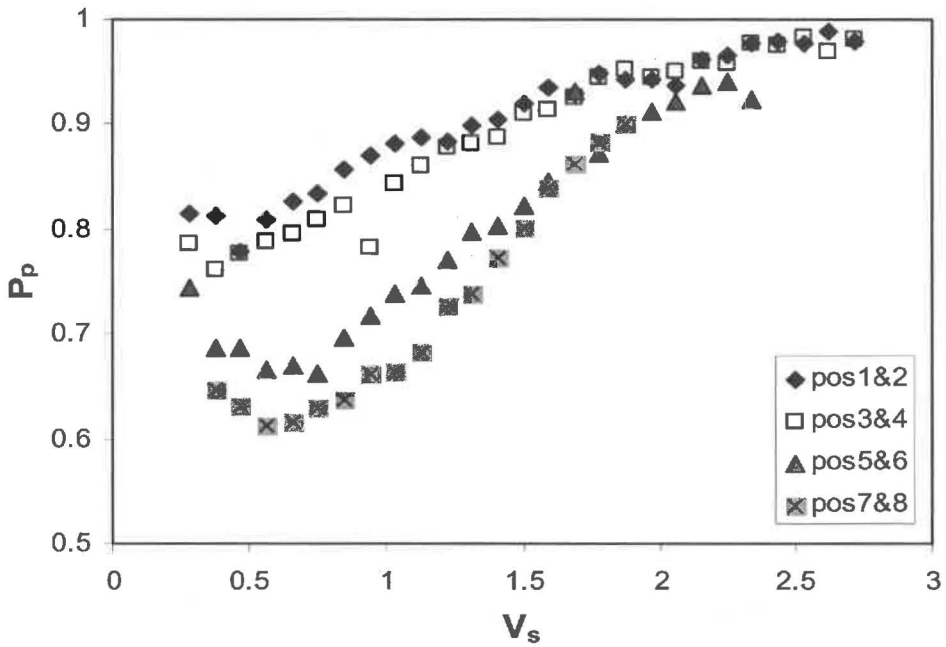

Figure 4.29 Effect of screen section position and aperture velocity V_s on passage ratio P_p. L_s=55 mm, 1-mm holes, bump rotor, bleached eucalypt, R_v=0.2, V_{tip}=22 ms^{-1}, C_f =0.5%.

It was postulated that relative speed and P_{NP} could be lowered by accelerating pulp in a feed chamber upstream of the feed annulus. If fibre passage is lower when relative speed is lower, then a screen should reject more fibre as a result of pulp acceleration (i.e. more reject thickening). Trials showed that accelerating the pulp gave higher reject thickening for a 55-mm screen section at the feed-end (positions 1&2, Figure 4.30) but had no affect when a section was located at the reject-end (positions 7&8 - Figure 4.31). Reject thickening in a standard screen (L_s=220 mm) also increased with pulp acceleration (Appendix 2). The results from these trials suggest that relative speed can only be lower at the feed-end of the screen with pulp acceleration. A minimum relative speed and P_{NP} may arise towards the reject-end because pulp velocity in the feed annulus V_u may be at a maximum. It is possible that pulp velocity V_u cannot continue to increase past a maximum velocity $V_{u(max)}$ due to a maximum in momentum transfer from the rotor tip.

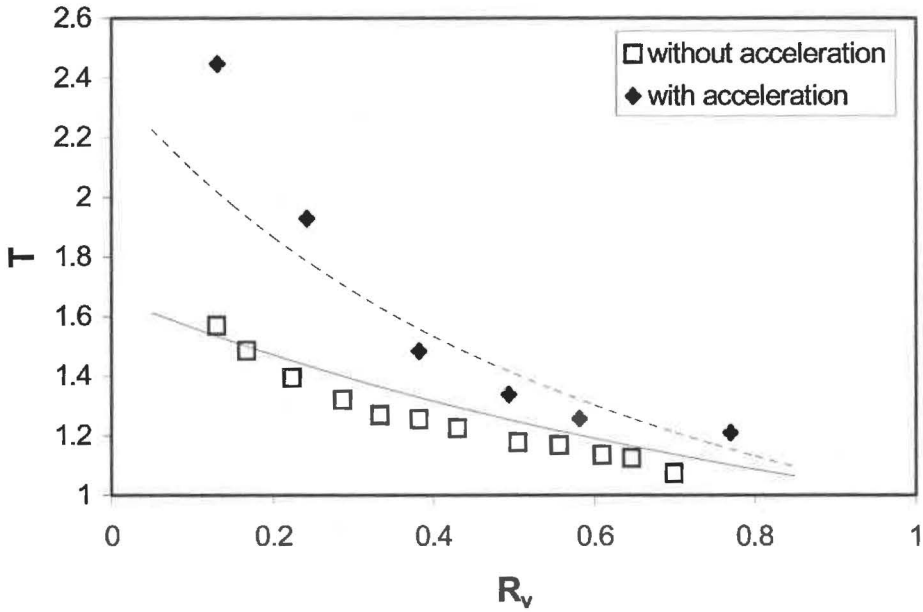

Figure 4.30 Effect of accelerating the pulp on reject thickening behaviour of a 55-mm section at the front (positions 1&2) of the screen. 1-mm holes, bleached eucalypt, V_{tip}=11 ms^{-1}, V_s=0.6 ms^{-1}, C_f=0.5%.

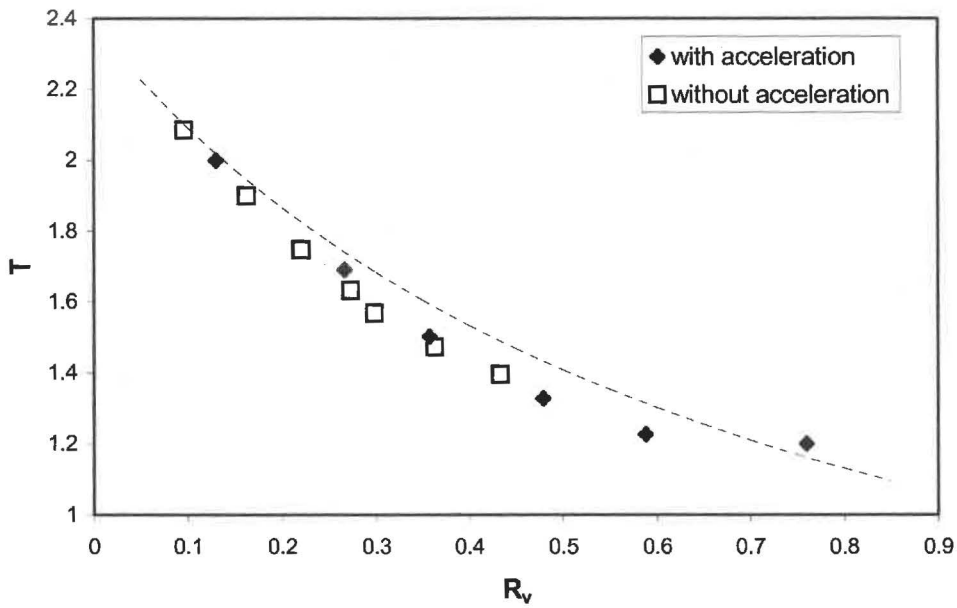

Figure 4.31 Effect of accelerating the pulp on reject thickening behaviour of a 55-mm section at the reject-end (positions 7&8) of the screen. 1-mm holes, bleached eucalypt, V_{tip}=11 ms^{-1}, V_s=0.6 ms^{-1}, C_f=0.5%.

4.3.3 Discussion

There is no published data on Q_{max} values for narrow screen sections or on fibre passage through narrow screen sections located at different axial positions along the screen. Baehr and Rienecker [76] reported that contaminant removal efficiency E was higher for a narrow section at the feed-end of the screen, which suggests contaminant passage is

lower in this region. If fibre passage is lower where contaminant passage is lower, then data from [76] conflict with data presented in the experimental results section above. However, literature indicates that contaminant passage mechanisms are quite different to the mechanisms of fibre passage [128].

Data indicate that local passage ratio P_z could decrease axially by as much as 0.2 due to the decrease in relative speed, which means the assumption that passage ratio is constant along the screen may need to be modified. This has implications for the tanks-in-series model developed in this thesis and Gooding and Kerekes's [93] Plug Flow model. However, it is uncertain if the 0.2 decrease in passage ratio for narrow screen sections will transfer to the standard screen, where upstream events will affect downstream events.

Devices or structures that increase relative speed could improve fibre passage and capacity of relatively long screens. Axially orientated bars (also called turbulence bars) could reduce relative speed and generate extra turbulence in the feed annulus. Increased turbulence (improved fibre mobility) and increased relative speed both favour fibre passage, but it would be difficult to assess their relative contribution. Serres and Rees [91] discuss only increased turbulence from their intermediate de-flocculation device (an axially orientated groove functioning in the same way as an axially orientated turbulence bar), neglecting to mention that the groove could increase relative speed. The latter may be the underlying mechanism that produced the capacity gains reported.

4.4 Local Passage Ratio P_z

Gooding and Kerekes [93] assumed that local passage ratio P_z will not vary axially despite an increase in pulp consistency C_z. However, Pimely and Rees [89] imply that passage ratio reduces to zero at the reject-end of the screen where pulp looses water as it drains against the screen.

It is plausible that local passage will decrease axially as pulp consistency C_z increases. Local fibre passage could also decrease due to other factors including a decrease in relative speed, an increase in long fibre content and a decrease in flow rate Q_s. Olson *et al* [22] showed that passage ratio decreases exponentially with increasing fibre length, and both Gooding [154] and Kumar [157] showed that passage ratio decreases with decreasing flow rate through a single aperture.

4.4.1 Modelling the Effect of Pulp Consistency C_z

The effects of pulp consistency C_z was estimated by modelling the screen as 100 well-mixed tanks in series. Instead of assuming local passage ratio would be independent of consistency, it was assumed that passage ratio would decrease semi-logarithmically. This assumption was based on actual screening data [157].

Local passage ratio $P_{z(i)}$ in the first tank is a function of feed consistency C_f

$$P_{z(1)} = -0.055 LnC_f + \beta \tag{4.30}$$

For all other tanks, local passage ratio is a function of pulp consistency from the upstream tank

$$P_{z(i)} = -0.055 LnC_{z(i-1)} + \beta \tag{4.31}$$

Local passage ratio P_z is plotted against normalised screen length Z_N (Figure 4.32) to illustrate the effect of feed annulus consistency C_z on local passage ratio. Assuming a constant aperture flow rate Q_s, the model predicts that local passage ratio will decrease semi-logarithmically from 0.69 to 0.65 when consistency C_z increases by a factor of 2.05.

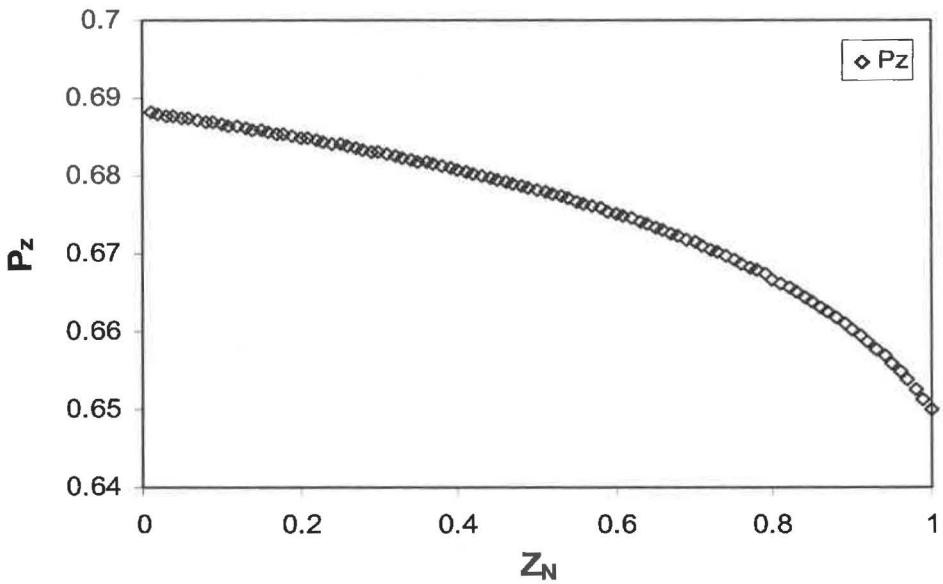

Figure 4.32 Effect of increasing consistency C_z on local passage ratio P_z for R_v=0.1, using a screen model comprised of 100 well-mixed tanks in series.

The internal cumulative reject thickening factor T_c is plotted against normalised axial position Z_N in Figure 4.33. The thickening profile for constant local passage ratio (P_z constant) is similar to the profile where passage ratio decreases with increasing consistency (P_z decreasing). There is only a marginal increase in thickening when

passage ratio decreases. For instance, when passage ratio is constant, pulp thickens by a factor of 1.97; when passage ratio decreases, pulp thickens by a factor of 2.05. Local passage ratio only decreased from 0.69 to 0.65 when consistency C_z thickened by 2.05.

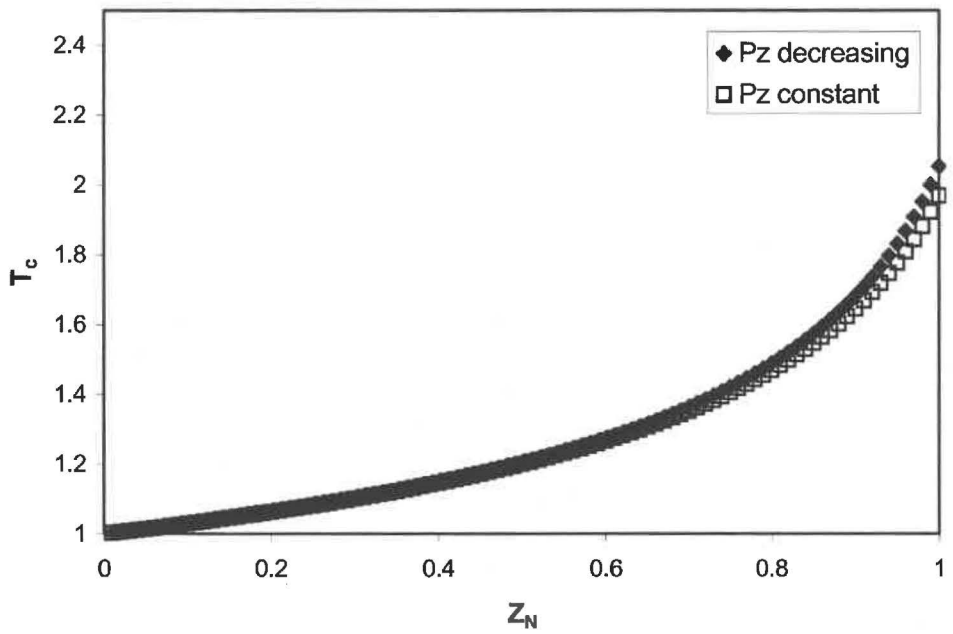

Figure 4.33 Effect of decreasing local passage ratio P_z on internal thickening profile and overall thickening.

4.4.2 Experimental Results

Pulp consistency on the feed side of the screen C_z and accept side (adjacent to the screen) C_s was measured to calculate local passage ratio P_z using Equation 4.32.

$$P_z = \frac{C_s}{C_z} \tag{4.32}$$

Both axial and radial sampling methods (Chapter 3) were used to measure pulp consistency in the feed annulus but consistency on the accept side was measured only by radial sampling. Data normalised for axial position Z_N (Figure 4.34), show that measured consistency in the feed annulus and accept chamber increases with increasing distance from the inlet. In addition, consistency on the accept side of the screen is lower than consistency on the feed side, indicating that passage ratio is less than 1.

Plotting local passage ratios for consistency data in Figure 4.34 with distance show that passage ratio decreases as distance increases from the inlet (Figure 4.35).

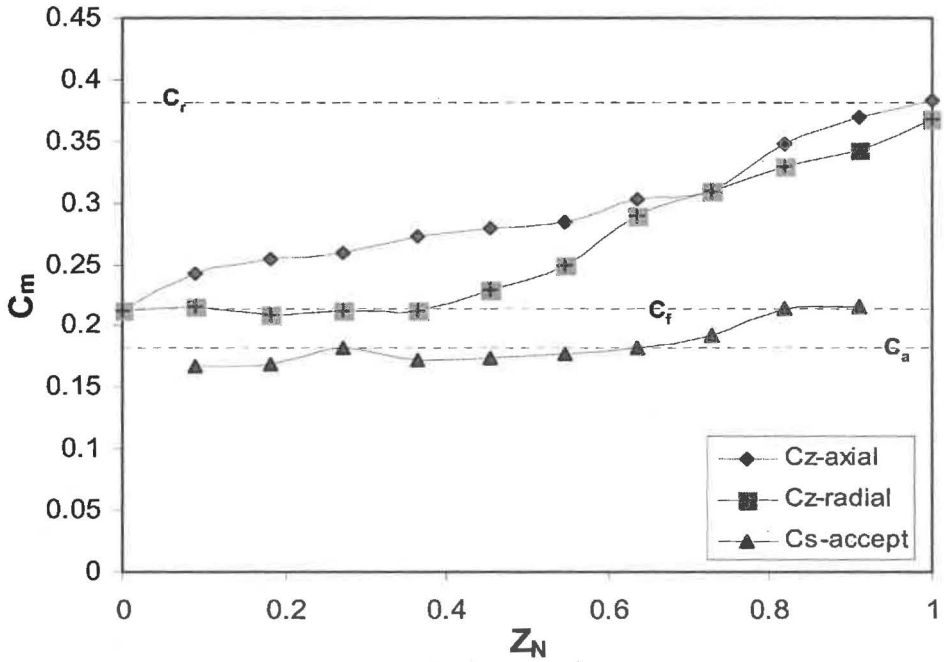

Figure 4.34 Effect of position and internal consistency on local consistency in the feed annulus and accept chamber as a function of normalised axial position.

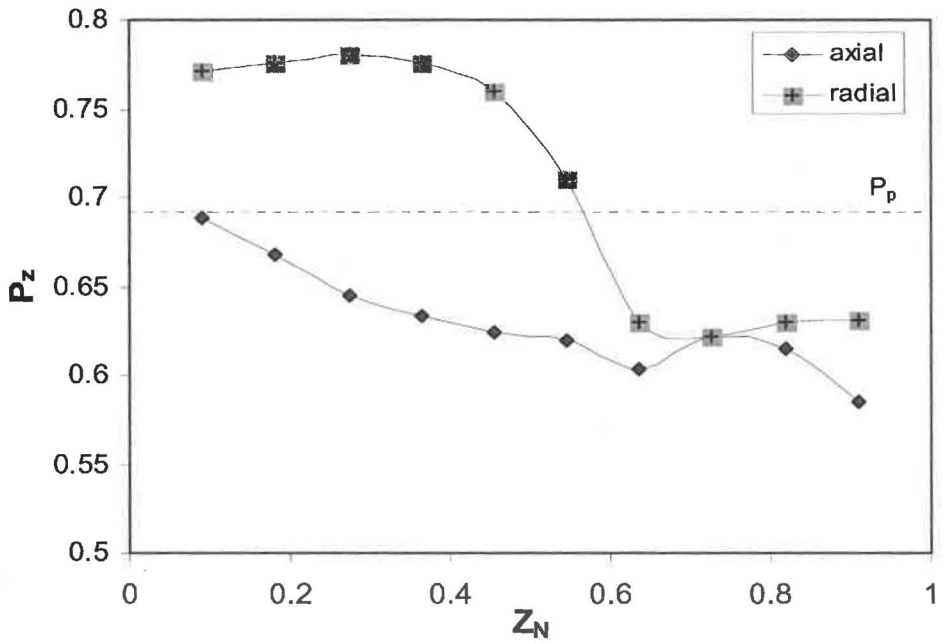

Figure 4.35 Effect of axial position and internal consistency sampling method on local passage ratio along the normalised screen length.

4.4.3 Discussion

The variation in consistency with sampling method means that the internal sampling methods used in this thesis need further investigation. Internal consistency data reported in this thesis used similar methods to data reported previously [86, 186]. Unfortunately,

these papers do not discuss precision of the sampling systems. The methods used in this thesis for sampling pulp from within the screen are unlikely to produce isokinetic sampling; more information on velocities in the feed annulus is needed to obtain isokinetic sampling. Also, both the axial and radial sampling systems could influence normal macro flow patterns through the screen; a larger screen may be needed to minimise this. Other methods of measuring consistency, such as using a custom-built optical sensor, should also be explored.

Local passage ratios have never been presented in the literature so no comparisons are possible. Nevertheless, an axial decrease in passage ratio is consistent with an increase in consistency, long fibre content, and a decrease in relative speed. A decreasing local passage ratio could also be explained by a decreasing local volumetric accept flow rate Q_s. The relative contribution from each of these factors is uncertain, although it appears that the relative contribution from an increase in consistency C_z may be small.

The contribution of other factors such as structure of the fibre suspension and turbulence intensity (pressure pulsation) also needs to be ascertained and represent a challenge to future researchers. An indication of their contribution could be found by re-screening pulp samples collected through narrow sections along the feed annulus. Passage ratio should be lower for pulp collected towards the reject end. If the difference in passage ratio is constant for a range of aperture velocities and rotor tip speeds (parallel curves), then differences in passage ratio will be due to furnish variables such as fibre length, consistency, freeness and flexibility.

4.5 Local Volumetric Aperture Flow

4.5.1 Application of Related Theory

Volumetric flow rates through apertures of a perforated pipe will be equivalent when there is a balance between the kinetic energy and momentum force of the inlet, friction losses along the pipe, and pressure drops across the outlet holes [189]. If inlet stream kinetic energy and momentum force predominate, aperture flow rates are highest towards the closed end; if friction loss along the pipe length predominates, aperture flow rates are highest towards the inlet (feed).

Local volumetric flow rates through the apertures of a pressure screen have been investigated using computational fluid dynamics [183]. Local flow rate appears to be sensitive to screen position (eccentric or concentric), accept outlet position, and shape of

the accept chamber (tapered or parallel walls). For example, the highest local flow rates occurred where the accept outlet was located. When the accept outlet was at the far end of the accept chamber, the highest flow rates occurred at the reject end of the screen and flow rate decreased almost linearly with increasing axial distance from the accept outlet.

4.5.2 Modelling

The effect of a volumetric flow bias on reject thickening was investigated using a model of a screen consisting of 100 tanks in series. Two accept flow biases were investigated:

1. an accept flow bias towards the inlet
2. an accept flow bias towards the reject outlet.

With a flow bias towards the inlet (feed), the highest local flow rate Q_s occurred at the first tank (12.8 L min^{-1}); flow rate decreased linearly and was lowest at the 100th tank at reject end (outlet). The opposite occurred when the flow bias was towards the outlet (reject end), with local flow rate Q_s being highest at the 100th tank.

The effect of the two flow biases were investigated for a linear decrease in local passage ratio P_z from 0.8 at the first tank to 0.6 at the 100th tank. Plotting reject thickening factor T against volumetric reject ratio R_v (Figure 4.36) illustrates that reject thickening was slightly greater when flow was biased towards the inlet than when there was no flow bias. Reject thickening was slightly greater when flow was biased towards the reject outlet due to the greater contribution from screen region towards the reject end, where local passage ratio was lower. Overall, flow biases had a relatively minor effect on reject thickening.

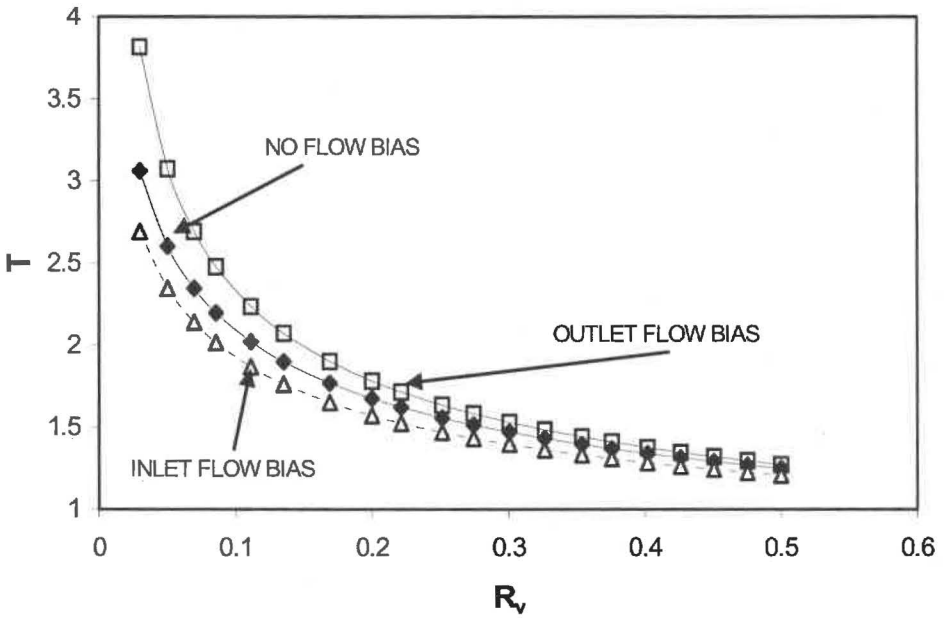

Figure 4.36 Effect of flow bias on reject thickening.

Although the effect of flow biases on overall thickening was only slight, thickening profiles are very different (Figure 4.37). When flow bias is towards the inlet, pulp thickens more quickly at the feed end of the screen but overall thickening is slightly less at Z_N=1. When flow bias is towards the reject outlet, pulp thickens more slowly at the feed (inlet) end but, because the rate of thickening is high in the second half of the screen (Z_N>0.5), there is greater overall thickening at Z_N=1.

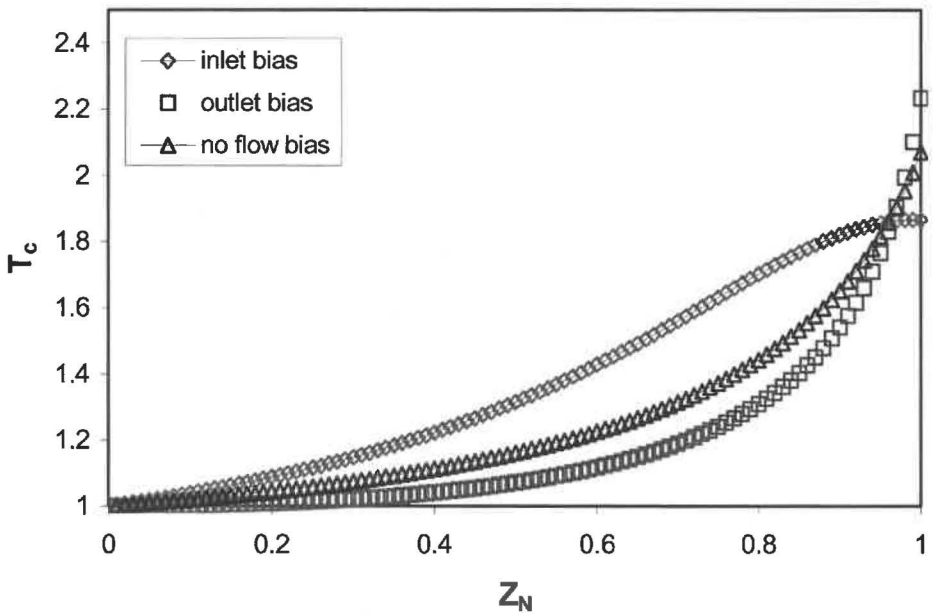

Figure 4.37 Effect of volumetric flow biases on internal cumulative reject thickening factor T_c at R_v=0.1, P_z decreasing from 0.8 to 0.6.

4.5.3 Experimental Results

Consistency data (Figure 4.34) was used to calculate volumetric flow rate Q_s (Equations 4.16 and 4.17). The data were normalized for accept flow rate A_N and axial position Z_N (Figure 4.38). The method used to obtain samples for measuring internal thickening in the feed annulus affected flow profiles. Flow rate is highest in the middle of the screen and there is a net negative flow towards the inlet (Z_N<0.2) for the radial sampling method. Flow rate is highest at the screen inlet for the axial sampling method.

4.5.4 Discussion

The only other published report on local volumetric flow rates [183] showed that peak flow occurred near the accept outlet. Data from radial sampling indicated a peak flow in the middle of the screen (where the accept outlet is located) and are consistent with published flow rates [183]. On this basis, flow rates obtained from radial sampling could represent the true flow rates inside the screen. In contrast, data from axial sampling

predicted peak flow at the front of the screen. Further investigations are needed to determine whether these differences are due to the collection position relative to the accept outlet. Alternatively, either or both sampling methods may not give representative samples.

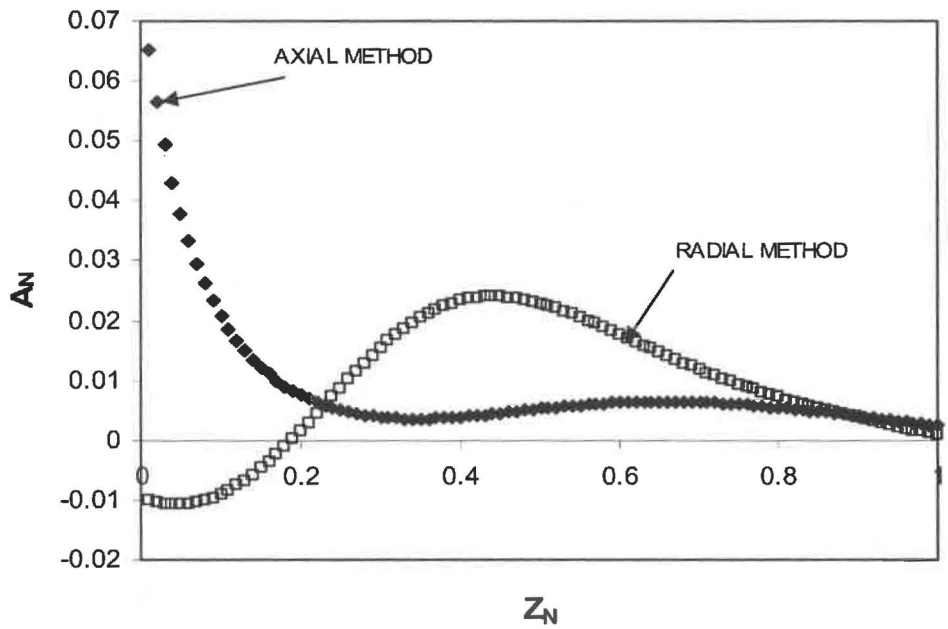

Figure 4.38 Effect of internal consistency measurement method on normalised volumetric accept flow rate as a function of normalised axial position.

4.6 Summary and Minor Conclusions

A tanks-in-series model was developed for a pressure screen, which consisted of a single row of well-mixed tanks in series with two outlets, one for the accept stream and one for the reject stream. Each tank behaved as a continuously stirred tank reactor (CSTR) and the Gooding and Kerekes's Mixed Flow model [93] was applied to predict consistency changes across each tank. The well-mixed tanks exhibited non-ideal flow behaviour when the number of tanks was less than 100 and ideal (plug flow) behaviour when the number of tanks was greater than 100 (N_T>100).

Assuming local passage ratio P_z and local flow Q_s remained constant, reject thickening factor T decreased when the number of tanks N_T decreased from 100 to 1, but T remained relatively constant over the range 100<N_T<100000. Flow behaviour changed when N_T decreased from 100 to 1 but there was no change in flow behaviour for 100<N_T<100000. With constant P_z and Q_s, T could only change at constant volumetric reject ratio R_v if flow behaviour changed due to the way the tanks-in-series model was constructed.

The reject thickening performances of the standard screens (L_s=220mm) fitted well with Gooding and Kerekes's Plug Flow model [93], which was consistent with other workers. A tanks-in-series model consisting of 100 tanks also fitted the performance of the standard screens, but this has not been reported previously. When half the screen was blocked (reject end) to shorten the screen to 110 mm, reject thickening factor T decreased appreciably (e.g. from 1.8 to 1.4 at R_v=0.2). It is concluded the reduction in thickening is mainly attributable to a change in flow behaviour because passage ratio P_p only increased marginally (e.g. from 0.63 to 0.68 when screening with the bump rotor). However, because passage ratio increased marginally, other factors made a minor contribution to the reduction in thickening.

Theory from Martinez and Gooding [137] was used to estimate (from Q_{max} values) that the negative pulse decreased by 33% when a 55-mm screen section was shifted from the feed-end to the reject-end. The hydraulic limit Q_{max} was higher at the feed-end and the passage ratio P_p was appreciably higher for low aperture velocities (V_s of 0.5 to 1 ms^{-1}). When pulp was accelerated in the feed chamber upstream of the feed annulus, there was significantly more reject thickening if the 55-mm section was positioned at the feed-end (P_p decreased by about 0.2) but no reject thickening if the 55-mm section was positioned at the reject end. These results support Reinecker's [148] theory that relative speed decreases along the length of a longer screen and suggest that axial decrease in relative speed is one underlying mechanism causing longer screens to reject more fibre than shorter screens.

Experimental data indicate that local passage ratio P_z could decrease axially by up to 0.2. Modelling showed that local passage ratio P_z decreases from 0.69 to 0.65 when pulp consistency C_z along the feed annulus thicken by a factor of 2. Thus, increasing consistency C_z has only a minor effect on reducing P_z. Most of the reduction in P_z can be attributed to a decrease in relative speed and an increase in long fibre content but the relative contribution of these factors is still unclear. The contribution of the local volumetric accept flow rate Q_s is also uncertain because Q_s was difficult to measure. Modelling showed that variations in Q_s could increase reject thickening in a relatively long screen if there is an axial decrease in local passage ratio P_z (for example, from 0.8 to 0.6). The highest volumetric flow rates occur at the reject end of the screen (outlet bias) where local passage ratio is lowest. However, overall increase in reject thickening is relatively minor.

5. EFFECT OF FEED CONSISTENCY AND ROTOR TYPE ON REJECT THICKENING AND FIBRE PASSAGE

5.1 Introduction

The effects of feed consistency and rotor type on fibre passage through pressure screen apertures are ambiguous. Some researchers report an effect [93, 157] and others report no effect [43, 128, 136]. Insights gained from the investigations carried out are used to explain the underlying mechanisms of fibre passage. Results presented in this chapter begin by discussing the ways a fibre could pass through an aperture and how passage is hindered when fibre accumulates at the apertures. After presenting the main postulates, the effects of rotor flow on overall fibre passage are discussed using a two fibre passage model with forward-flow and back-flow components. Data for reject thickening and passage ratios are then discussed in relation to previous research, screening mechanisms and the two fibre passage ratio models. Fibre and water back-flow are demonstrated.

5.2 Forward and Reverse Fibre Passage through Apertures

5.2.1 Theories of Fibre Passage

Apertures in centrifugal pressure screens can be holes or slots. Holes on the feed side of smooth-holed screens have parallel walls and the open area is typically 10-15%. Holes on the accept side are conical (Figure 5.1). Because $D_a > D_f$, there is more open area and less land distance between holes ($H_a < H_f$) on the accept side has than on the feed side. Apertures have sharp edges on both sides of the screen. Only one edge exists on the feed side of smooth screens (no contouring) but inner and outer edges exist on the accept side.

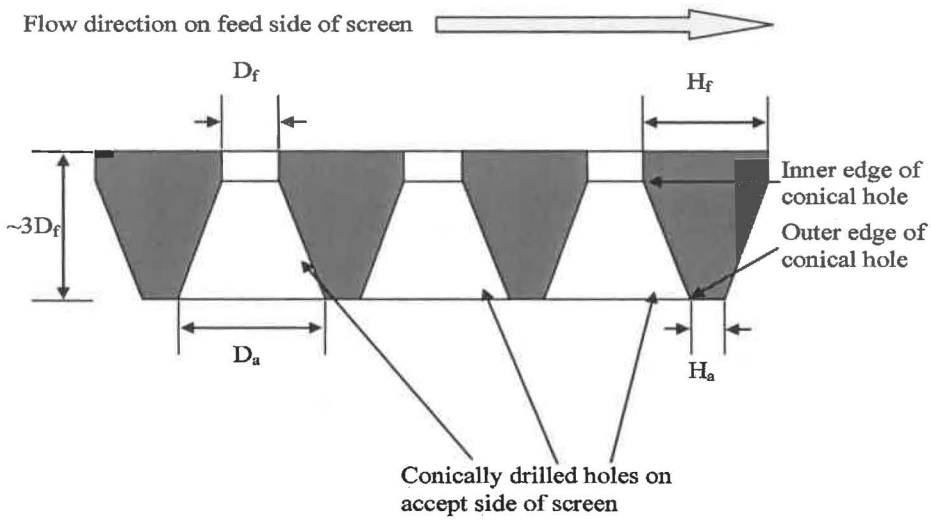

Figure 5.1 Smooth-holed screen with conically drilled holes on the accept side.

Strongly directional flow exits on the feed side of the screen due to the motion of rotor tips and foils relatively close to the inner screen surface. Immediately upstream of a slot (or hole) fibres approach with the velocity of adjacent fluid layers and with approach angles most likely to be affected by neighbouring fibres and fibre flocs, fluid turbulence, and the general flow field present near the screen surface. In a real pressure screen, the approach velocity of fibres is proportional to the rotor tip velocity [154], but fibre approach angles are more random due to action of the rotor, and can either be positive or negative. With a positive approach angle, the leading tip of fibres is further from the aperture (fibre in Figure 2.17 has a positive approach angle), making them less likely to pass through the aperture. Where fibres are close to the screen, surface fibres align in the strong shear field and flow approximately parallel to the screen surface; if this arises upstream of an aperture, there is a strong chance of fibre passage.

According to Yu and DeFoe [156], fibres may pass through screen apertures unhindered by other fibres or by screen apertures in one of three ways: the leading end/tip passes first (Figure 5.2a), the trailing end/tip (T in Figure 2.17) passes first (Figure 5.2b), or the central portion passes first (Figure 5.2c).

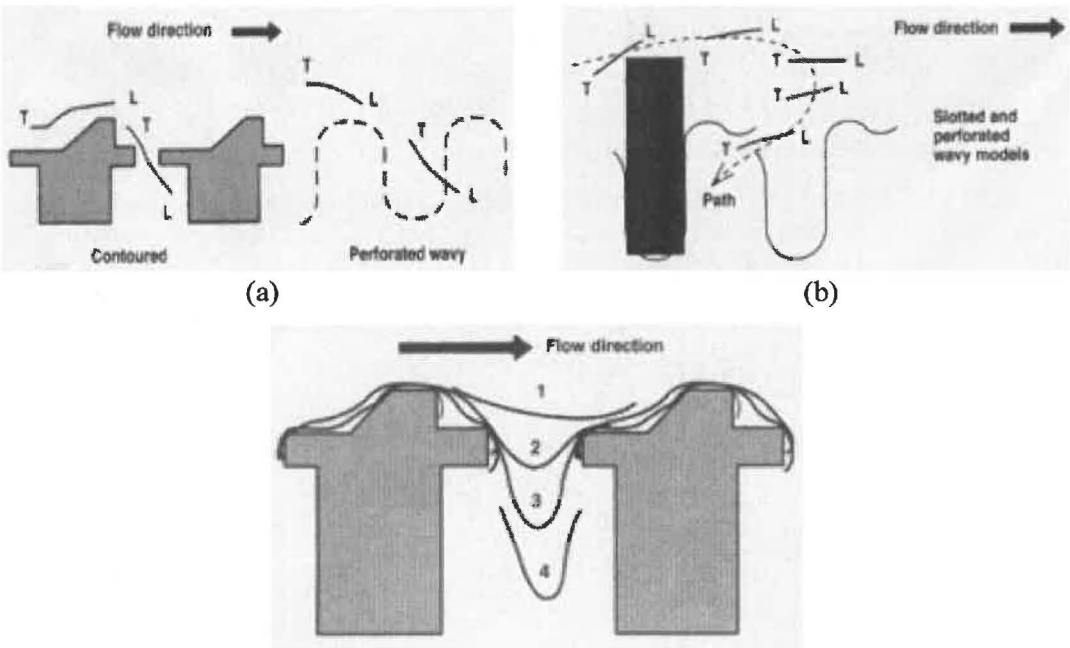

Figure 5.2 Ways fibre can pass through an aperture: by the (a) leading end L; (b) the trailing end T; or (c) the central portion (from [156]).

Alternatively, fibres can impact with the screen aperture and accumulate at openings to form piles/flocs. They can accumulate on the downstream edges of recessed circular

(conically drilled) holes, which Yu and DeFoe [156] termed fibre hanging but Kumar [157] termed fibre stapling on the downstream edge (Figure 5.3a). Fibres can accumulate over the land area two slots with their ends in different slots (Figure 5.3b), which Yu and DeFoe [156] called fibre stapling. Only relatively flexible fibres will conform to the shape of the screen and accumulate by hanging or stapling. A pile of fibres can be viewed as a floc formed by stapling/hanging mechanisms.

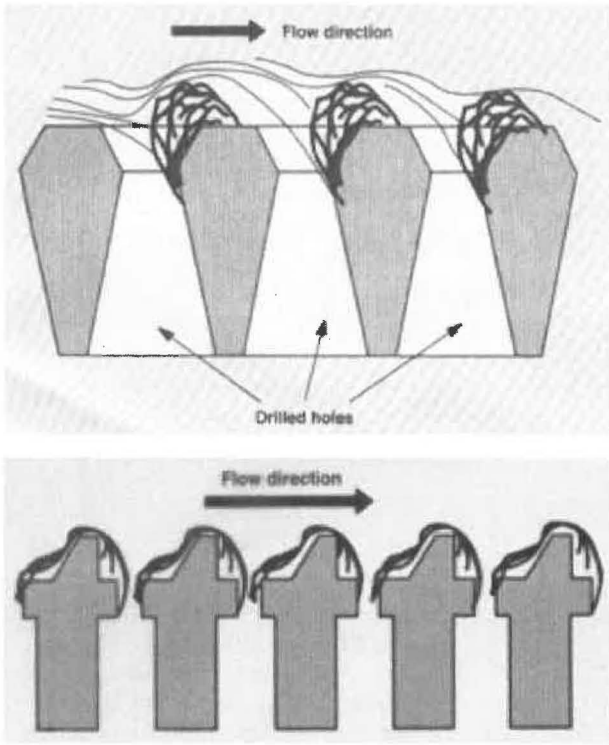

Figure 5.3 Fibre accumulations/piles by (a) hanging or (b) stapling.

Fibre stapling/hanging often occurs where wood fibre flow splits. Kerekes *et al.* [2] observed floc formation on a sharp edge where flow divided and Duffy [113, 114] also observed flexible fibres being depositing on narrow rods positioned perpendicular to flow.

Kumar [157] observed fibre piles forming on the downstream edge of a rectangular slot with a steady (dividing) flow of a dilute nylon fibre suspension. The width of the piles S_w was approximately the fibre length L_f with stiff 1-mm and 3-mm nylon fibres (Figure 5.4). Pile depth S_d depended on flow conditions and consistency. The width of flexible Rayon fibres was longer than fibre length because some fibres in the piles were drawn into the slot and the pile behaved as a stretched floc.

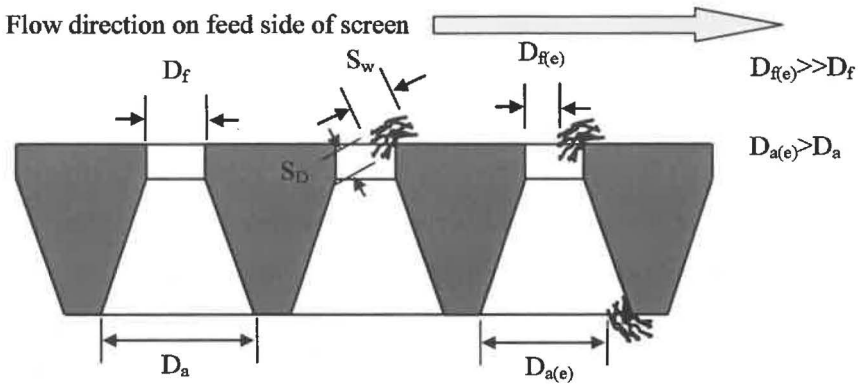

Figure 5.4 Fibres accumulating on the edges of the holes on the feed side and accept side of a smooth-holed screen.

The effective slot width W_e or hole diameter D_e can be less than the actual width W or diameter D due to fibre accumulation and pile/floc growth. On the feed side of a smooth-holed screen, D_f reduces to $D_{f(e)}$ and on the accept side, D_a reduces to $D_{a(e)}$ (Figure 5.4). The ratio of actual width/diameter to effective width/diameter, termed aperture reduction ratio A_r, can be obtained for the feed (Equation 5.1) and accept side (Equation 5.2).

$$A_{r(f)} = 1 - \frac{D_{f(e)}}{D_f} \tag{5.1}$$

$$A_{r(a)} = 1 - \frac{D_{a(e)}}{D_a} \tag{5.2}$$

For equal-sized fibre piles, the aperture reduction ratio of a screen with conically drilled holes is greater on the feed side than on the accept side (Equation 5.3). Thus, a larger pile is needed on the accept side to reduce the open area to the same extent as the feed side.

$$A_{r(f)} > A_{r(a)} \tag{5.3}$$

5.2.2 Mechanisms of Fibre Accumulation at Apertures

Kumar [157] reported that fibres accumulate at an aperture by a rotating mechanism and fibre hanging or stapling. Long stiff fibres were immobilised by a rotating mechanism and were also stapled over the aperture by a horizontal stapling mechanism. Flexible fibres staple/hang over the downstream edge of the slot by a vertical stapling mechanism.

- ***Rotating mechanism***

Near the aperture, where flow splits, flow into the aperture imposes hydrodynamic drag on a fibre approaching a slot (Figure 5.5a) is proportional to V_s and inversely

proportional to y_o. This hydrodynamic drag causes translational and rotational acceleration into the aperture. A fibre accelerating into an aperture in the direction of V_s also moves across the aperture in the direction V_u. The leading tip impacts with the downstream wall of the aperture after penetrating a distance Y (Figure 5.5b). Translational motion then ceases. A proportion of fibre (~L_f-Y) protrudes from the aperture into the main flow. Flow past the aperture imposes moment on the fibre (proportional to the force of the upstream velocity F_{uv}), which causes the fibre to rotate clockwise about the point of contact with the downstream wall. The point of contact shifts along the fibre (in direction of trailing end T) with rotation until the fibre rotates about the downstream edge.

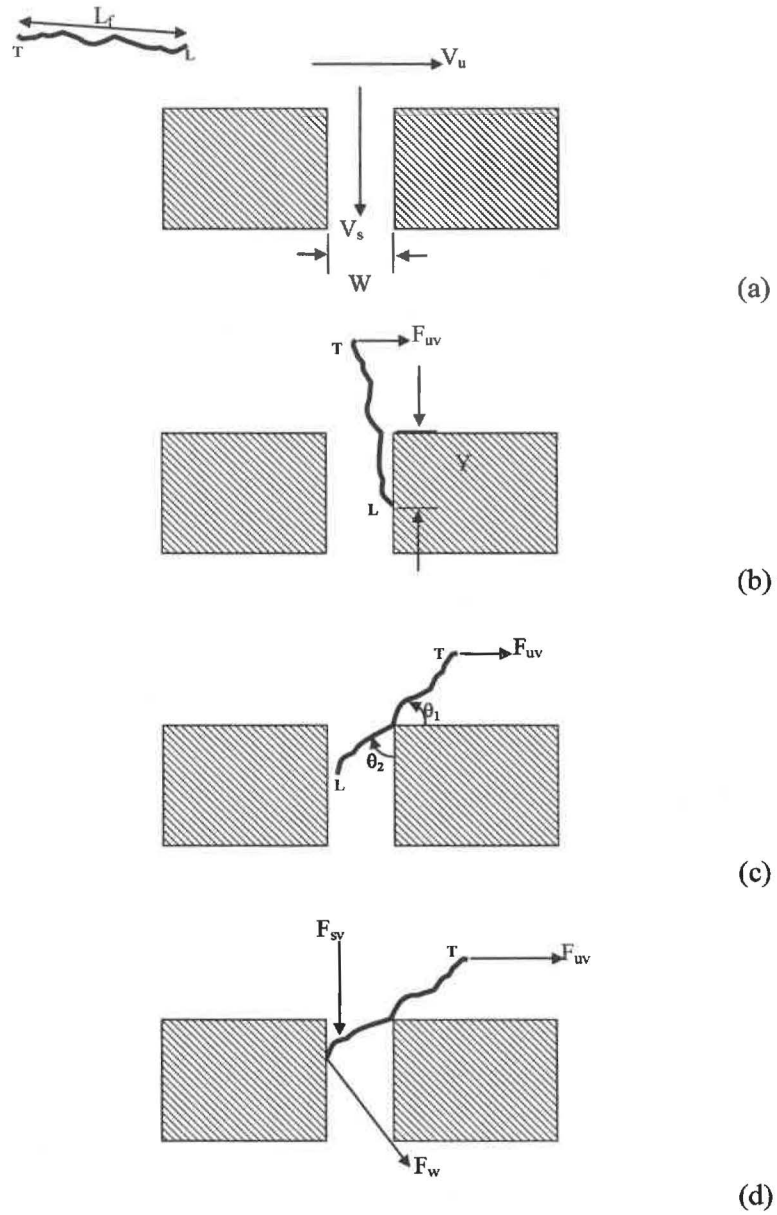

Figure 5.5 Fibre immobilisation at an aperture: (a) fibre approaching, (b) fibre leading end L impacting at penetration distance Y, (c) fibre rotation due to force F_{uv}, and (d) leading end contacting upstream wall of slot.

A point is reached in clockwise rotation when the two angles between fibre and aperture/ screen θ_1 and θ_2 are equal (Figure 5.5c). The moment in the direction of V_u is opposed by a moment in the direction of V_s and the relative velocity difference between fluid and fibre may be as high as V_s and V_s. Kumar [157] estimated the Reynolds number will be between 40-300, which is in the transition range for shear drag and form drag. Assuming form drag and mean drag coefficient are 1, relative drag force is proportional to velocity squared. Relative moment balance on the fibre is given by Equation 5.4 [157].

$$Y^2 V_s^{\,2} = \left(L_f - Y\right)^2 V_u^{\,2} \tag{5.4}$$

When the moment on the right side of Equation 5.4 is greater than that on the left, fibre continues to rotate clockwise until it contacts the upstream wall (Figure 5.5d). A wall force F_w counters the moment causing clockwise fibre rotation, fibre rotational motion ceases and the fibre is immobilised.

- ***Stapling/Fibre Hanging Mechanisms***

Whether vertical or horizontal stapling occurs depends strongly on normalised aperture V_s/V_u [157]. In general, vertical stapling occurs more readily at low normalised aperture velocity and horizontal occurs more often at high normalised velocity.

- ***Vertical Stapling***

The leading tip impacts the downstream wall (Figure 5.5b). Instead of rotating about the downstream edge, the fibre bends and conforms to the shape of the aperture edge (Figure 5.6). The moments diminish but friction forces (F_F) between fibre and screen increase. If friction forces are strong enough, translational motion ceases and the fibre staples/hangs at the edge of the aperture.

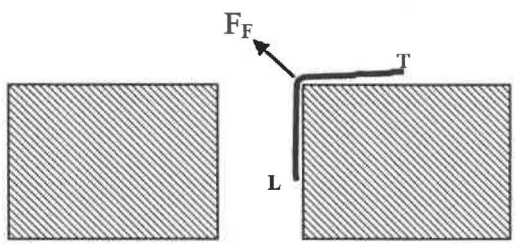

Figure 5.6 Vertically stapled fibre (hanging fibre) on downstream edge of aperture.

- ***Horizontal Stapling***

Kumar [157] observed fibres approaching a slot with a slight positive approach angle θ_o when they became stapled by a horizontal mechanism. Near the slot opening, flow

through the slot drags a fibre into a horizontal position. If the fibre is relatively flexible, it will bend and pass through (Figure 5.2c). If the fibre is relatively stiff, however, the fibre will resist bending and becomes horizontally stapled (Figure 5.7). If the fibre is immobilised, friction forces normal to fibre length will be greater than drag forces generated by flow past the slot.

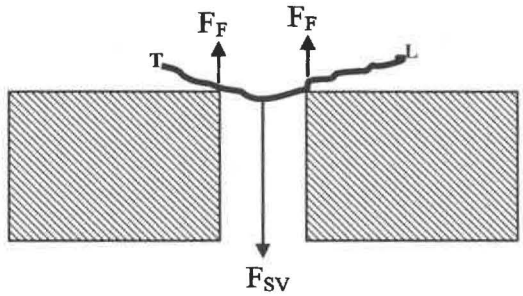

Figure 5.7 Horizontally stapled fibre.

5.2.3 Effects of Fibre Accumulation on Forward and Reverse Passage

Fibre passage is hindered by fibre accumulation and floc formation on the downstream edges of screen apertures. In Kumar's [157] trials with steady flow though a rectangular slot at very low consistencies, the size of a stapled/hanging floc increased with increasing consistency. The effective slot width W_e decreased as passage ratio decreased accordingly. Passage ratio also decreased with increasing consistency in Kumar's other trials on unsteady flow through several slots of a model pressure screen. Although not explicitly stated, it is believed that the effective slot width also decreased with increasing consistency as more fibre accumulated at the slot openings.

It has been proposed that fluid back-flow (and possibly fibre back-flow) from the accept to the reject side, due to the action of the rotor, flushes fibre and stapled fibre flocs from apertures on the feed side of the screen [131, 166, 178]. Normin and Wedin [87] observed this process with high speed cinema-photography. If it is accepted that back-flow occurs, it is reasonable to expect that fibre could build up on the screen's accept side in the same way as on the feed side. Fibre build-up and floc formation by stapling hinders fibre passage from the accept to the feed side, if indeed fibre flows with the back-flow fluid. It can be argued that because fibre flows forward, it is not unreasonable to expect that fibre, and especially very short fibre and fines, to also be present in back-flow (reverse passage). Mechanisms of reverse fibre passage are probably similar even though aperture shape and flow conditions may vary. However, a bigger floc is needed to reduce the slot or hole width to W_e if the aperture is recessed on the accept side.

Applying Kumar's observations to reverse passage suggest that the size of stapled flocs on the accept side should also increase with consistency. Thus, the passage ratio for reverse flow will reduce with increasing consistency as flocs become bigger, in the same way as for forward flow. All other things being equal, a decreasing reverse passage ratio would dilute the feed annulus and reduce reject thickening. In the extreme, the reverse passage ratio could be zero and only water will flow back to the feed, significantly diluting the feed annulus and reducing thickening. Thus, a decreasing reverse passage ratio counters the thickening effect of a decreasing forward passage ratio.

Both passage ratios (forward and reverse) may decrease with increasing pulp consistency as stapled flocs grow on both sides of the screen. Although a decreasing reverse passage ratio could counter a decreasing forward passage ratio, the overall fibre passage ratio will depend on the ratio of volumetric flows in both the forward and reverse directions. A two-passage ratio model is now proposed to quantify these effects.

5.3 Two Passage Ratio Screening Modelling

Pulp passage through screen apertures involves passage in both the forward (feed to accepts) and reverse (accepts to feed) directions in response to the fluctuating rotor pressure pulse. A model for a short screen section (Figure 5.8) shows pulp flowing radially forward from a well-mixed zone or "tank" i_f on the feed-side of the screen at a mass flow rate $M_{F(i)}$. At a well-mixed zone or "tank" i_a on the accept-side of the screen, pulp either flows radially forward at a mass flow rate $M_{s(i)}$ or radially backward (back-flow) at a mass flow rate $M_{B(i)}$. Because the zone on either side of the screen is assumed to be well-mixed, consistency $C_{t(if)}$ is equal to $C_{z(i)}$

$$C_{t(if)} = C_{z(i)} \tag{5.5}$$

At the radial inlet into tank i_a, $C_{F(i)}$ instantaneously changes to $C_{t(ia)}$. This consistency $C_{t(ia)}$ is equal to consistency of pulp flowing radially forward to the accept stream $C_{s(i)}$ via the accept chamber annulus.

$$C_{t(ia)} = C_{s(i)} \tag{5.6}$$

Mass and volumetric flow balances for radial bulk flow are

$$M_{s(i)} = M_{F(i)} - M_{B(i)} \tag{5.7}$$

$$Q_{S(i)} = Q_{F(i)} - Q_{B(i)} \tag{5.8}$$

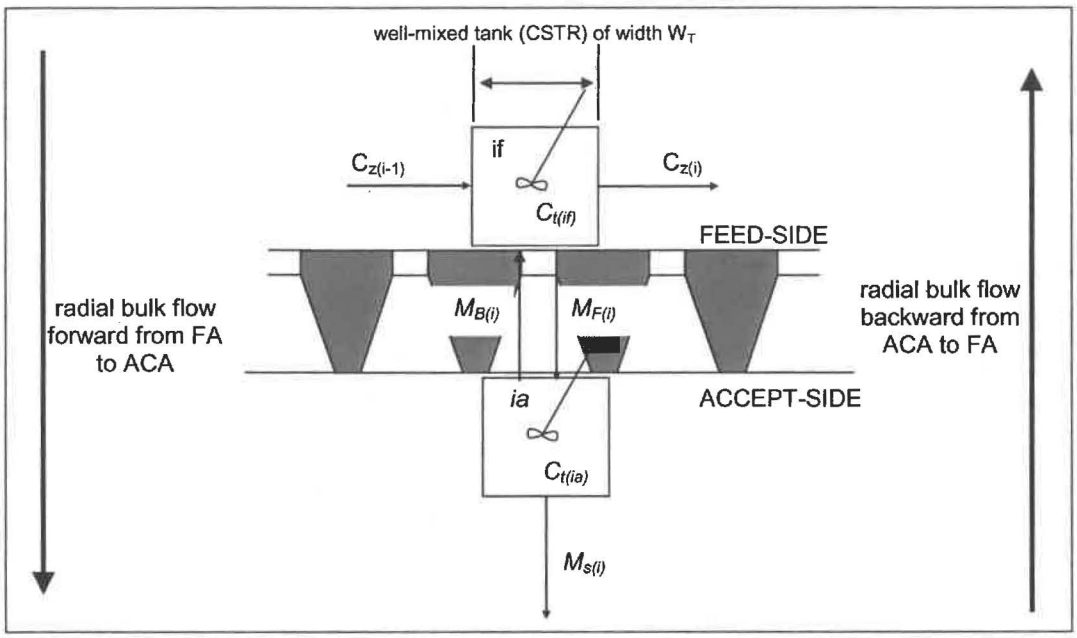

Figure 5.8 Back-flow model for flow in a pressure screen.

The overall local passage ratio of pulp $P_{z(i)}$ is defined by Equation 5.9.

$$P_{z(i)} = \frac{C_{s(i)}}{C_{z(i)}} \tag{5.9}$$

The passage ratio for forward flow $P_{F(if)}$ defined as

$$P_{F(if)} = \frac{C_{F(if)}}{C_{t(if)}} \tag{5.10}$$

or

$$P_{F(if)} = \frac{C_{F(if)}}{C_{z(if)}} \tag{5.11}$$

The passage ratio for back-flow $P_{B(ia)}$ is defined as

$$P_{B(ia)} = \frac{C_{s(i)}}{C_{t(ia)}} \tag{5.12}$$

or

$$P_{B(ia)} = \frac{C_{B(ia)}}{C_{s(i)}} \tag{5.13}$$

Rearranging Equation 5.9 gives an expression for $C_{s(i)}$ in terms of consistency $C_{z(i)}$

$$C_{s(i)} = P_{z(i)} C_{z(i)} \tag{5.14}$$

Consistency of forward flow $C_{F(if)}$ can also be expressed in terms of $C_{z(i)}$ and the passage ratio for forward flow $P_{F(if)}$ by rearranging Equation 5.11.

$$C_{F(if)} = P_{F(if)} C_{z(i)} \tag{5.15}$$

Back-flow consistency $C_{B(ia)}$ is the product of the passage ratio for back-flow $P_{B(ia)}$ and consistency at the end of forward-flow phase $C_{F(if)}$.

$$C_{B(ia)} = P_{B(ia)} C_{s(i)} \tag{5.16}$$

Substituting Equation 5.14 into Equation 5.16 gives $C_{B(ia)}$ in terms of $C_{z(i)}$

$$C_{B(ia)} = P_{B(ia)} C_{z(i)} P_{z(i)} \tag{5.17}$$

Net mass flow rate for forward-flow and back-flow in terms of volumetric flow rate Q and consistency C is

$$M_{s(i)} = Q_{s(i)} C_{s(i)} \tag{5.18}$$

Equations 5.8 and 5.14 can be used to express net mass flow rate $Q_{s(i)}C_{s(i)}$ in terms of $C_{z(i)}$.

$$M_{s(i)} = (Q_F - Q_B) P_{z(i)} C_{z(i)} \tag{5.19}$$

The mass flow rate for forward-flow in terms of Q and C is

$$M_{F(i)} = Q_{F(i)} C_{F(i)} \tag{5.20}$$

Substituting for $C_{F(i)}$ (Equation 5.15) and applying volume balance gives

$$M_{F(i)} = Q_{F(i)} P_{F(i)} C_{z(i)} \tag{5.21}$$

The mass flow rate for back-flow in terms of Q and C

$$M_{B(i)} = Q_{B(i)} C_{B(i)} \tag{5.22}$$

Substituting for $C_{B(i)}$ (Equation 5.17) gives $M_{B(i)}$ in terms of consistency $C_{z(i)}$.

$$M_{B(i)} = Q_{B(i)} P_{B(i)} C_{z(i)} P_{z(i)} \tag{5.23}$$

Substituting Equations 5.19, 5.21 and 5.23 into Equation 5.7 gives a mass balance in terms of the consistency $C_{z(i)}$.

$$(Q_{F(i)} - Q_{B(i)}) P_{z(i)} C_{z(i)} = Q_{F(i)} P_{F(i)} C_{z(i)} - Q_{B(i)} P_{B(i)} C_{z(i)} P_{z(i)} \tag{5.24}$$

Dividing the mass balance by $P_{z(i)}C_{z(i)}Q_{B(ia)}$, applying volume balance and cancelling like terms gives

$$\frac{Q_{F(i)}}{Q_{B(i)}} - 1 = \frac{Q_{F(i)}}{Q_{B(i)}} \frac{P_{F(i)}}{P_{z(i)}} - P_{B(i)} \tag{5.25}$$

Volumetric flow ratio $F_{r(i)}$ is volumetric flow rate for forward-flow $Q_{F(if)}$ divided by volumetric flow rate for reverse flow $Q_{B)ia)}$.

$$F_{r(i)} = \frac{Q_{F(if)}}{Q_{B(ia)}} \tag{5.26}$$

Substituting Equation 5.26 into Equation 5.25 and rearranging gives an expression for $P_{B(ia)}$ based on $F_{r(i)}$, $P_{z(i)}$ and $P_{F(i)}$.

$$P_{B(i)} = F_{r(i)} \frac{P_{F(i)}}{P_{z(i)}} - F_{r(i)} + 1 \tag{5.27}$$

In terms of the overall local passage $P_{z(i)}$.

$$P_{z(i)} = \frac{F_{r(i)} P_{F(i)}}{P_{B(i)} + F_{r(i)} - 1} = \frac{P_{F(i)}}{\frac{P_{B(i)}}{F_{r(i)}} + 1 - \frac{1}{F_{r(i)}}} \tag{5.28}$$

Equation 5.28 predicts the effect of flow ratio F, on overall local passage ratio $P_{z(ia)}$. When reverse flow $Q_{a\text{-}f}$ is small, the flow ratio $F_{r(i)}$ is large because it is dominated by the forward flow $Q_{f\text{-}a}$ ($1/F_{r(i)} = 0$), and overall local passage ratio $P_{z(ia)}$ is approximated by the forward passage ratio $P_{F(ia)}$. Likewise, when back-flow passage ratio $P_{B(ia)} = 1$ (i.e. pulp and water equally passes back through the screen), overall local passage ratio $P_{z(ia)}$ again is approximated by the forward passage ratio $P_{F(ia)}$. If back-flow passage ratio $P_{B(ia)}$ becomes zero (i.e. water only is back-flushing), then overall passage ratio $P_{z(ia)}$ is greater than the forward passage ratio $P_{F(ia)}$ and can become greater than unity. This represents accepts thickening, where accept consistency is above feed consistency and reject consistency is below feed consistency.

Flow ratio is clearly an important parameter of the back-flow model and influences overall fibre passage. It may change with rotor tip speed and rotor type, but if $Q_{S(i)}$ remains constant , then $Q_{F(i)}$ and $Q_{B(i)}$ must decrease when F_r increases. For example, if $Q_{S(i)}$ is 6.4 L min^{-1}, decreasing $Q_{F(i)}$ from 12.8 to 8 L min^{-1} causes F_r to increase from 2 to

5 and $Q_{B(i)}$ to decrease from 6.4 to 1.6 L min^{-1} (Table 5.1). Thus, the total volume of pulp passing through the screen ($Q_{F(i)}$+$Q_{B(i)}$) decreases with increasing F_r.

Table 5.1 Effect of flow ratio, F_r on volumetric flow rates on both sides of the screen.

$Q_{F(i)}$	$Q_{B(i)}$	$Q_{F(i)}$-Q_B	F_r	Q_F+Q_B
12.8	6.4	6.4	2.00	19.2
12.2	5.8	6.4	2.10	18
11.6	5.2	6.4	2.23	16.8
11.0	4.6	6.4	2.39	15.6
10.4	4	6.4	2.60	14.4
9.8	3.4	6.4	2.88	13.2
9.2	2.8	6.4	3.29	12
8.6	2.2	6.4	3.91	10.8
8	1.6	6.4	5.00	9.6

For steady two-dimensional flow through a rectangular slot, Kumar [157] showed that passage ratio P_p decreased logarithmically with C_f. As an approximation, $P_{F(i)}$ also decreases logarithmically with $C_{z(i)}$.

$$P_{F(i)} = -a \ln C_{z(i)} + b \tag{5.29}$$

Substituting Equation 5.28 into Equation 5.27 gives

$$P_{B(i)} = F_{r(i)} \frac{-a \ln C_{z(i)} + b}{P_{z(i)}} - F_{r(i)} + 1 \tag{5.30}$$

By assuming that $C_{z(i)}$ is equal to C_f and $P_{z(i)}$ is equal to P_p, Equation 5.30 can be rewritten for a narrow section of a screen

$$P_B = F_r \frac{-a \ln C_f + b}{P_p} - F_r + 1 \tag{5.31}$$

5.4 Experimental Results and Discussion

Feed consistency C_f was increased progressively from a dilute state (N<1) until a concentrated state (N>60) of approximately 2% was reached. No fibre aggregates (flocs or unstable fibre bundles) were seen in the pulp tank when for dilute eucalypt of pine feed pulp but aggregates could be seen at 2%. Aggregates of the pine furnishes were larger than those of the eucalypt furnish. Screened accepts had smaller aggregates than rejects.

Under recirculating flow conditions, feed pulp properties did not change significantly during an experimental trial.

5.4.1 Reject Thickening Behaviour

A typical plot of reject thickening factor versus feed consistency (Figure 5.9) shows that the bump and step rotors have characteristic reject thickening curves over a range of consistencies from extremely dilute (no flocculation) to concentrated (flocculation). When screening long fibre, the bump rotor gave higher reject thickening than the step rotor over all consistencies. There are three discernable regions where reject thickening factor is either constant or increases with consistency. The two inflection points on curves for both rotors occur at feed consistencies of approximately 0.007% and 0.7%. It is postulated that these inflection points indicate a mechanistic change in reject thickening and fibre passage. Where curves are similar (Regions 1 and 2), both rotors have similar mechanisms for fibre passage

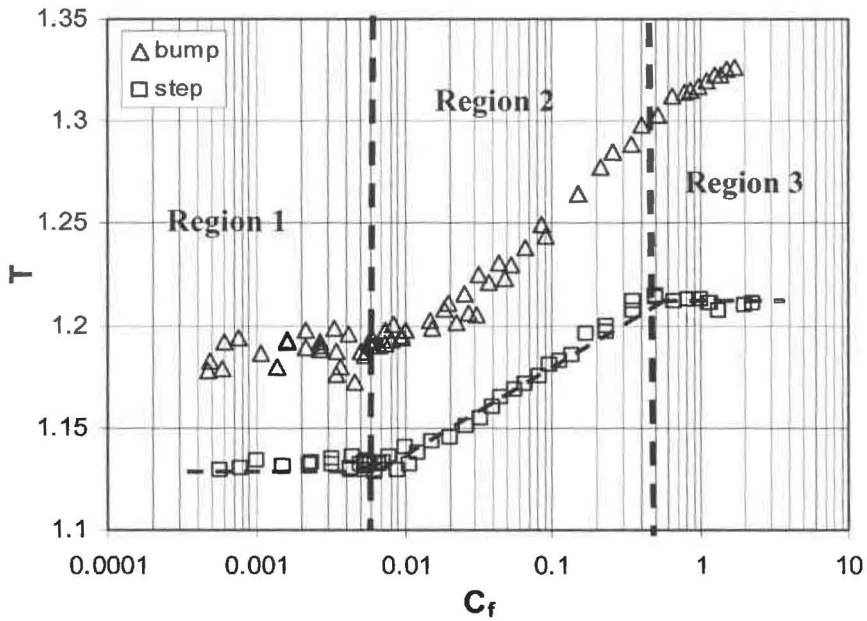

Figure 5.9 Reject thickening curves using a bump or step rotor to screen kraft pulp. 55-mm long screen with smooth 1-mm holes, V_s=0.6 ms^{-1}, V_{tip}=22 ms^{-1}, R_v=0.77 (step) and R_v=0.73 (bump).

Changing furnish from long (radiata pine) to short (eucalyptus) fibre and halving rotor speed did not dramatically alter the shape of the reject thickening curves (Figure 5.10). Again, both the bump and step rotors exhibited thickening behaviour with two inflection points and three distinct regions. At very low feed consistencies, thickening was independent of feed consistency (Region 1). Thickening levels with the bump rotor were

lower than for the step rotor at the same rotor speeds and accept flow rates. At a critical consistency of about 0.012% (compared with 0.007% for long fibre, Figure 5.9), thickening increased linearly with consistency to a second critical consistency at about 0.1% (Region 2). After this, the relationship between thickening and consistency was similar to that for long fibre (Region 3). It is worth noting that at the lower speed, the step rotor exhibited greater thickening than the bump rotor in most regions.

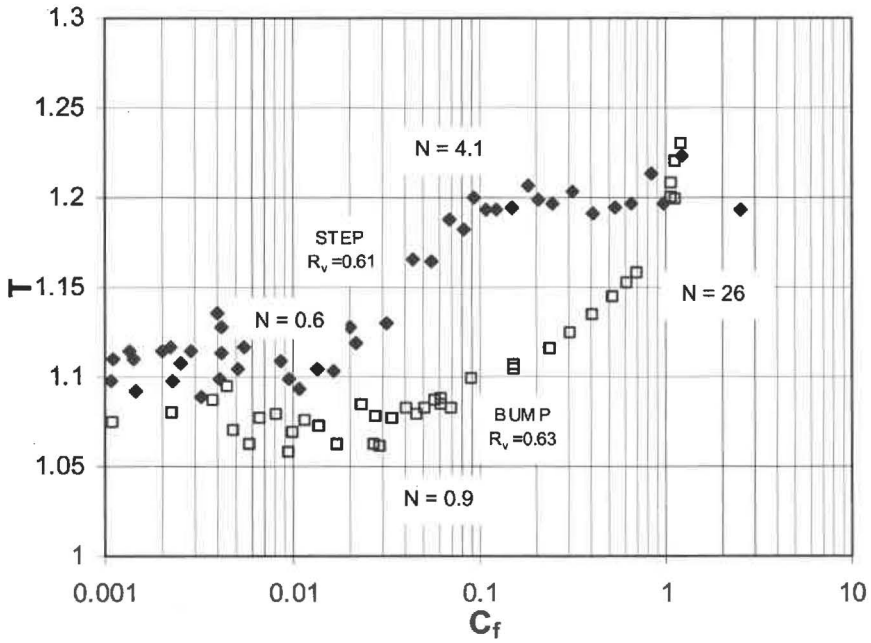

Figure 5.10 Reject thickening curves using a bump and step rotor to screen kraft eucalypt. Screening conditions the same as in Figure 5.9 except V_{tip}=11 ms^{-1}, and R_v=0.63 (bump).

Reject thickening data can also be plotted against crowding number N (Figure 5.11), calculated from feed consistency data using Equation 2.12 (assuming $C_f = C_m$). Kerekes and Schnell [40] report that flocculation begins when the N=1, although the calculation for crowding does not include the flow conditions (turbulence intensity or scale). They also report that it is reasonable to expect onset of network formation at N=60. Data obtained in the trials performed show the first inflection point occurs at N of about one and th`e second inflection occurs at about N=60 (Figure 5.11). Inflection points do not always coincide with these critical crowding numbers. For example, the inflections for short fibre (Figure 5.10) occurred at lower crowding numbers than for the long fibre (Figure 5.11), suggesting changes in reject thickening where not simply fibre interaction and flocculation effects on the feed side of the screen.

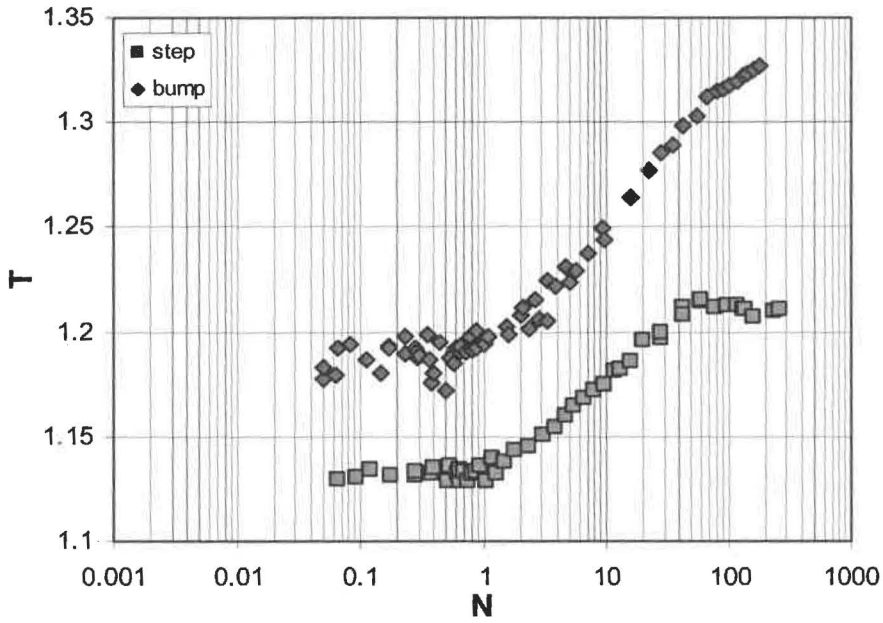

Figure 5.11 Effect of rotor on the relationship between reject thickening factor T and crowding number N in a 55-mm long screen with smooth 1-mm holes. Kraft pine, V_s=0.6 ms^{-1}, V_{tip}=22 ms^{-1}, R_v=0.77 (step) and R_v=0.73 (bump)

5.4.2 Fibre Passage Ratio Behaviour

Inflection points and regions are often more obvious when reject thickening data is presented by plotting passage ratio P_p with feed consistency (Figure 5.12) so data are presented in this way for the rest of this chapter. As with the reject thickening curves, passage ratio curves exhibit two inflection points (critical fibre concentrations) and three distinct regions. Trends in Regions 1 and 2 are independent of rotor type but differ in Region 3. Passage ratio is constant in Region 1, decreases linearly on a semi-log plot in Region 2, and either continues to decrease or plateau in Region 3.

Passage ratios for narrow (27- and 55-mm) screen sections were calculated assuming two tanks in series (Equation 4.20); those for the full screen used the plug flow model (Equation 4.19). The method for calculating passage ratios and the reasoning for modelling short screens as two tanks in series is described in Section 4.2.2.

Data for 27-mm sections at different screen positions show that changes in relative velocity along the screen (Section 4.3) do not change the shape of the passage ratio curves for either rotor but do change where the curves are located. Passage ratios for screening eucalypt furnish with the step rotor continue to have distinct curves with two inflection points and three clear regions (Figure 5.13). Those for the bump rotor (Figure 5.14) are similar to previous data but exhibit only one inflection point, probably because

insufficient data were obtained. For both rotors, consistency for first inflection shifts downward and slightly to the left as screen section changes from the front (position 2) to the back (position 6 or 8) of the screen.

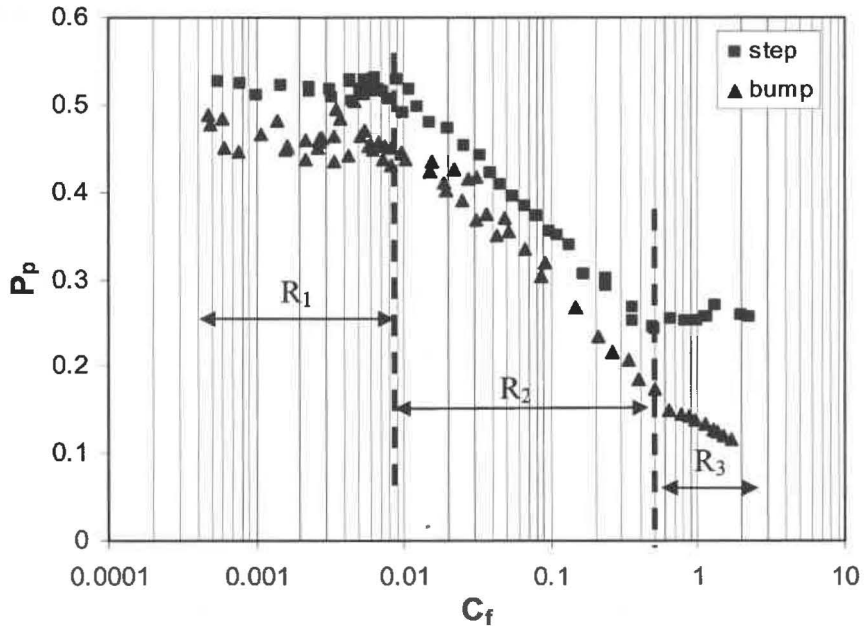

Figure 5.12 Effect of rotor on passage ratio P_p in the 55-mm long screen. Unbleached pine screened at V_s=0.6 ms^{-1}, V_{tip}=22 ms^{-1}, R_v=0.77 (step rotor). Bleached pine screened at V_s=0.6 ms^{-1}, V_{tip}=22 ms^{-1}, R_v=0.73 (bump rotor).

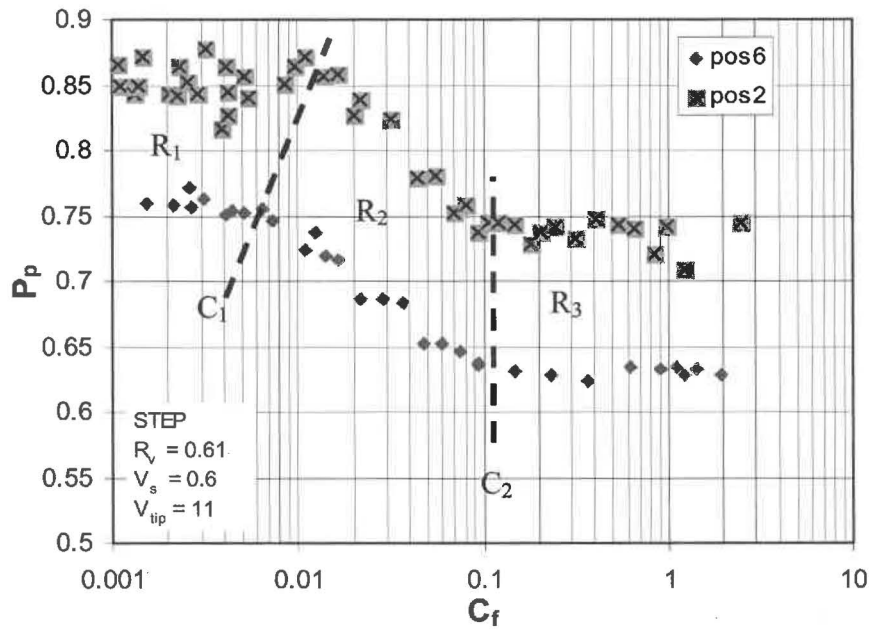

Figure 5.13 Effect of feed consistency and position of 27-mm screen section with 1-mm holes on fibre passage ratio. Eucalypt kraft, step rotor, R_v~0.5, V_s=0.6 ms^{-1}, V_{tip}=22 ms^{-1}.

Furnish (Figure 5.12, Figure 5.13, Figure 5.16) and rotor tip speed (Figure 5.15, Figure 5.17) did not change the shape of passage ratio curves but did affect location of the critical concentrations and magnitude of passage ratio values in each region.

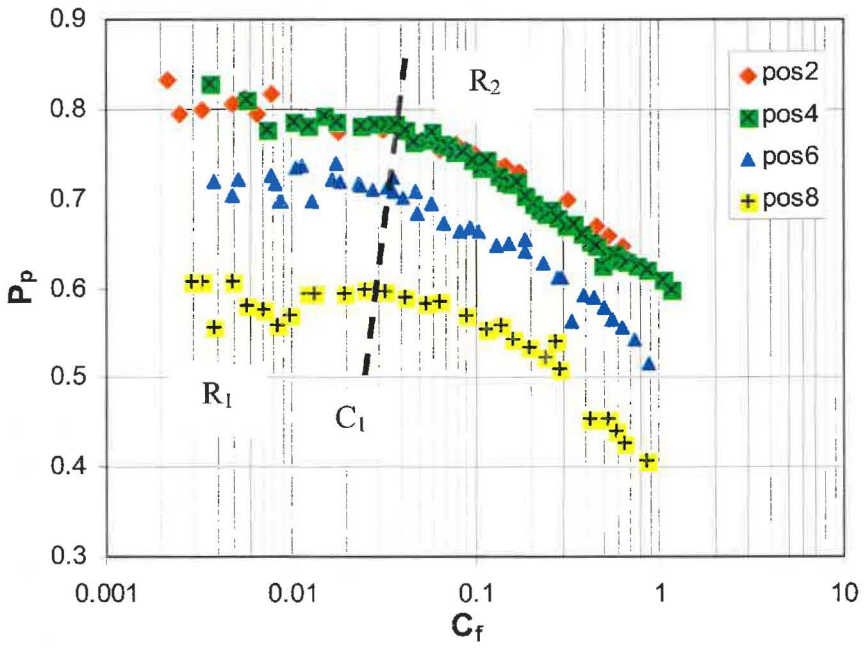

Figure 5.14 Effect of feed consistency and position of 27-mm screen section with 1-mm holes on fibre passage ratio. Eucalypt kraft, bump rotor, R_v~0.5, V_s=0.6 ms^{-1}, V_{tip}=22 ms^{-1}

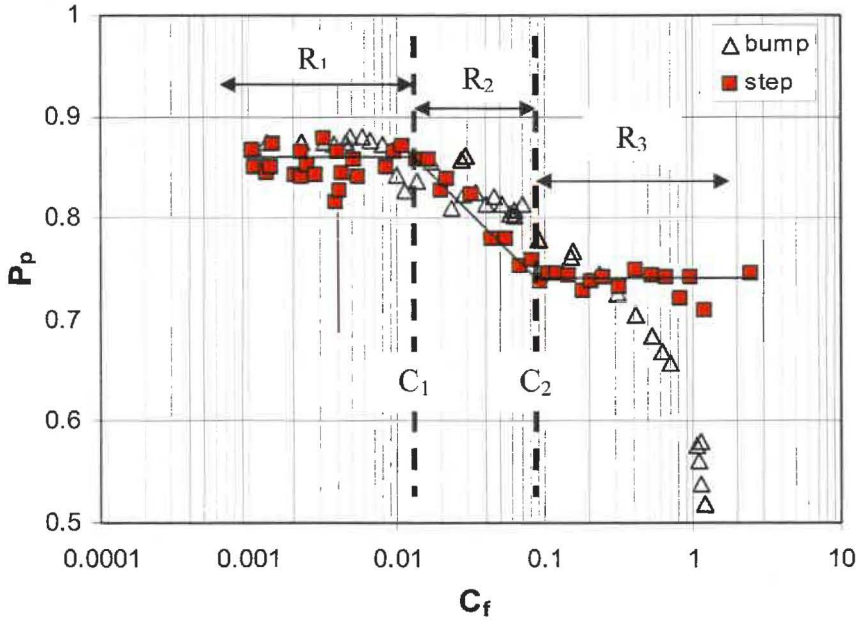

Figure 5.15 Effect of rotor type on passage ratio using a 55-mm screen section with 1-mm holes in position 3&4. Bleached eucalypt, V_s=0.6 ms^{-1}, V_{tip}=11 ms^{-1}, R_v=0.77 (step rotor) or R_v=0.63 (bump rotor).

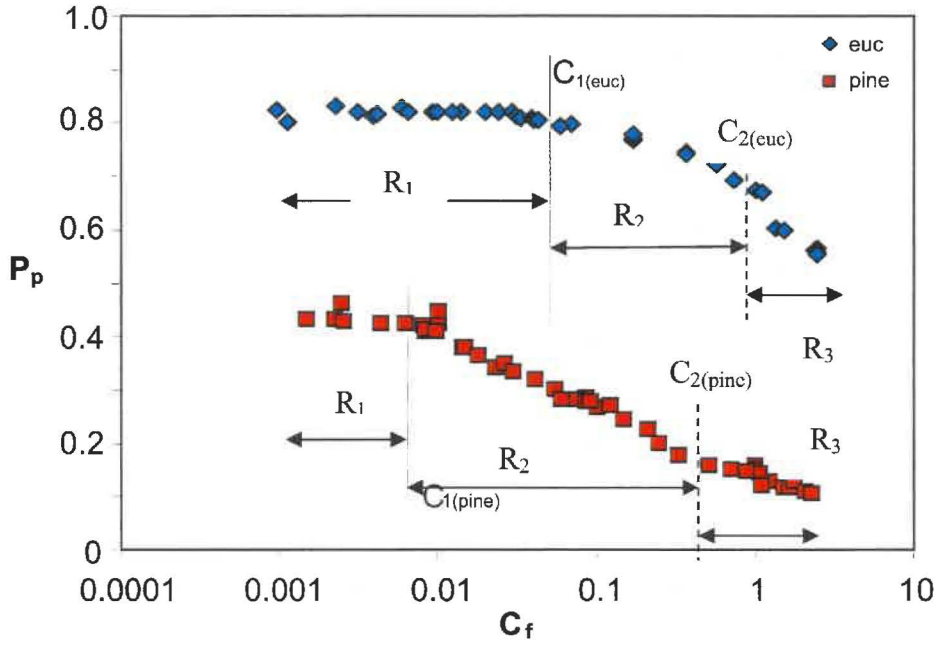

Figure 5.16 Effect of fibre length on critical feed consistency C_1 in screen with 1-mm holes and bump rotor. L_s=220 mm, R_v~0.5, V_s=0.6 ms^{-1}, V_{tip}=22 ms^{-1}.

The value of C_1 (consistency between Regions 1&2) for screening pine furnish with the bump rotor occurred at about 0.009% (N=1.04) but at 0.03% (N=1.11) for eucalypt furnish (Figure 5.16). Although furnish had a smaller effect on C_1 in other trials, usually C_1 for long fibre were less than that for short fibre (see Figure 5.12 and Figure 5.16), and the critical crowding factors were usually about 1 (see Figure 5.11).

In most experiments, C_1 occurred at crowding numbers less than unity regardless of furnish type and screening conditions. Therefore, it is reasonable to conclude that fibre-fibre interaction effects in Region 1 are minimal until onset of Region 2. In Region 1, fibres passage is independent of screen consistency and probably can be described by the fibre alignment theory of screening. Fibre passage in Region 1 is strongly affected by approach velocity (Figure 5.14) and fibre length (Figure 5.16) but less by rotor type (Figure 5.12). Long pine fibres staple over ridges and edges of holes more readily than short eucalypt fibres [113, 114], which contribute to long fibres having lower passage ratios. Both fibre stapling and fibre-fibre interactions restrict fibre mobility in the dynamic flow field near screen apertures, decreasing passage ratio with consistency. Visual evidence of fibre stapling in a real screen (dynamic flow field) is needed to better understand the relative contributions of these two effects.

The second critical concentration C_2 occurs at higher concentrations and crowding numbers (Figure 5.16) than C_1 and is ~0.5% (N=57) for pine and ~0.8% (N=30) for

eucalypt. It is proposed this critical concentration is controlled by fibre interactions and possibly fibre stapling effects on the accept side of the screen rather than flocculation and fibre stapling effects on the feed side.

Critical feed consistency C_1 decreased with rotor rotational speeds (i.e. lower V_{tip}). Passage ratio increased when feed consistency was below C_1 and decreased when feed consistency was above C_1. For example, C_1 is 0.1% for V_{tip}=11 ms^{-1} and 0.04% for V_{tip} is 22 ms^{-1} (Figure 5.17). The passage ratio is 5% higher at low consistencies and 5-10% lower at higher consistencies, indicating that feed consistency influences the screening mechanism. At low feed consistencies (Region 1), the mechanism is likely to be fibre alignment . Low rotor speeds reduce the approach velocity of the fibres in the fluid layer near the screen wall, which enhances fibre passage. Also, fibres do not rotate out of the holes as easily when rotor speed is lower so more fibres will momentarily accumulate and then pass through the aperture, which enhances fibre passage. At higher consistencies, clearing accumulated fibre from the apertures becomes more critical. High rotational speeds enhance aperture clearance, which increases the opportunity for fibre passage, resulting in high passage ratios.

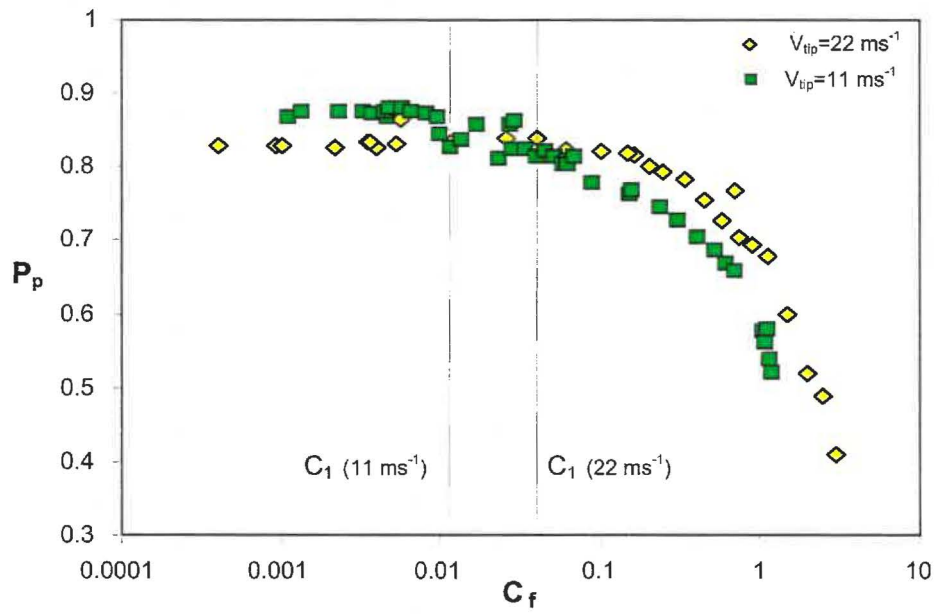

Figure 5.17 Effect of rotor tip speed V_{tip} on critical feed consistency C_1 using screen with 1-mm holes. L_s=220 mm, R_v~0.5, V_s=0.6 ms^{-1}.

When screening pine and eucalypt with the bump rotor, passage ratio increased with hole size (Figure 5.18, Figure 5.19), consistent with previous reports [22,127,151,168]. For pine the passage ratio more than doubled as hole size increased from 1-mm to 2.4-mm.

Under identical conditions eucalypt pulp lay between pine screened through 1.6-mm and 2.4-mm smooth holes. The increase in fibre passage with decreasing average fibre length from 1.44-mm to 0.7-mm is thus consistent with previous reports [22]. Of particular interest is the passage ratio difference between short and long fibres which increases then decreases with increasing feed consistencies. The occurrence of a maximum passage ratio difference at a given feed consistency suggest that fibre length fractionation will be feed consistency dependent and may also be hole size dependent. This is investigated further in Chapter 6.

Passage ratio also increased with hole size when screening with a step rotor but the genral shape of the curve did not change (Figure 5.19). Two inflection points which move upward and to the right with increasing hole size and three regions are clearly visible in curves for 1-mm and 1-6-mm holes. As with other data with the step rotor, passage ratio is constant in Region 1 and Region 3. The constant passage ratio difference in Region 3 indicates that there is unlikely to be an optimum feed consistency for fractionating with a step rotor, unlike the bump rotor.

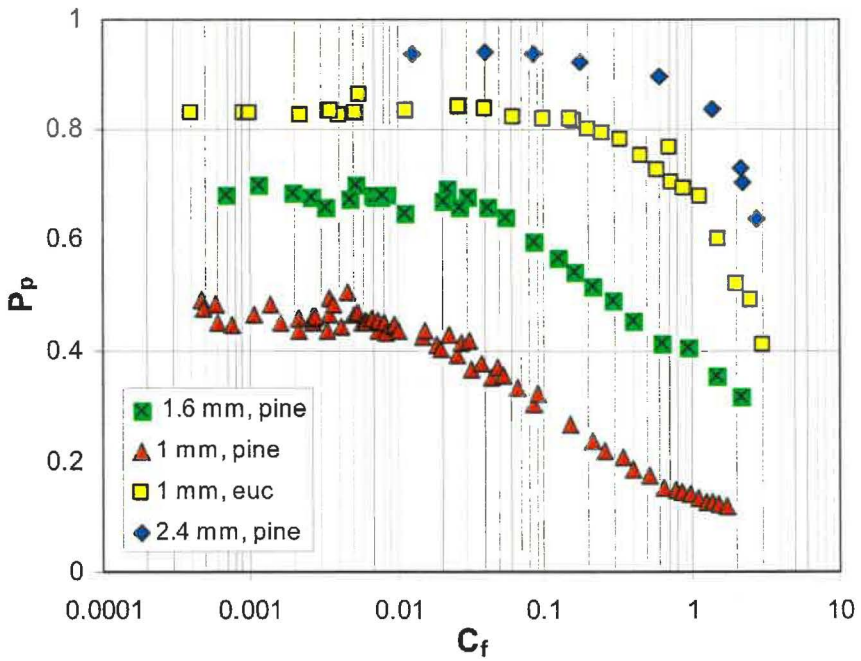

Figure 5.18 Effect of hole size and feed consistency C_f on passage ratio P_p when screening pine and eucalypt pulp with a bump rotor at V_s=0.6 ms^{-1}, V_{tip}=22 ms^{-1}. Pine: for 1-mm holes, R_v=0.73; for 1.6-mm holes, R_v=0.67; for 2.4-mm holes, R_v=0.54. Eucalypt: for 1-mm holes, R_v=0.63.

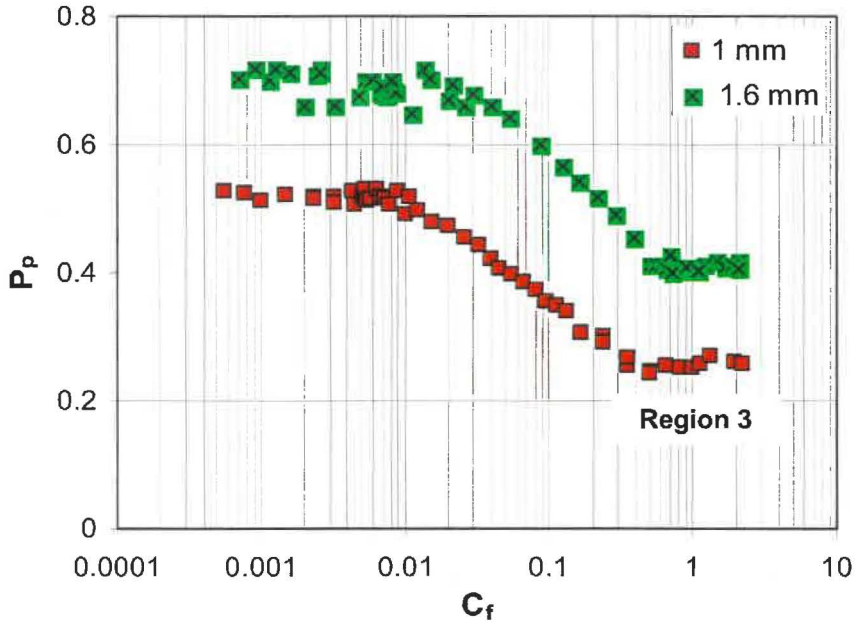

Figure 5.19 Effect of hole size and feed consistency C_f on passage ratio P_p when screening unbleached pine with the step rotor at V_s=0.6 ms^{-1}, V_{tip}=22ms^{-1}. For 1-mm holes, R_v=0.65 and for 1.6-mm holes, R_v=0.71.

Screening characteristics for full length screens had the same characteristic shape for each rotor when screening eucalypt (Figure 5.20) or pine (Figure 5.21) even though there is greater differences in the axial screening conditions with a full length screen.

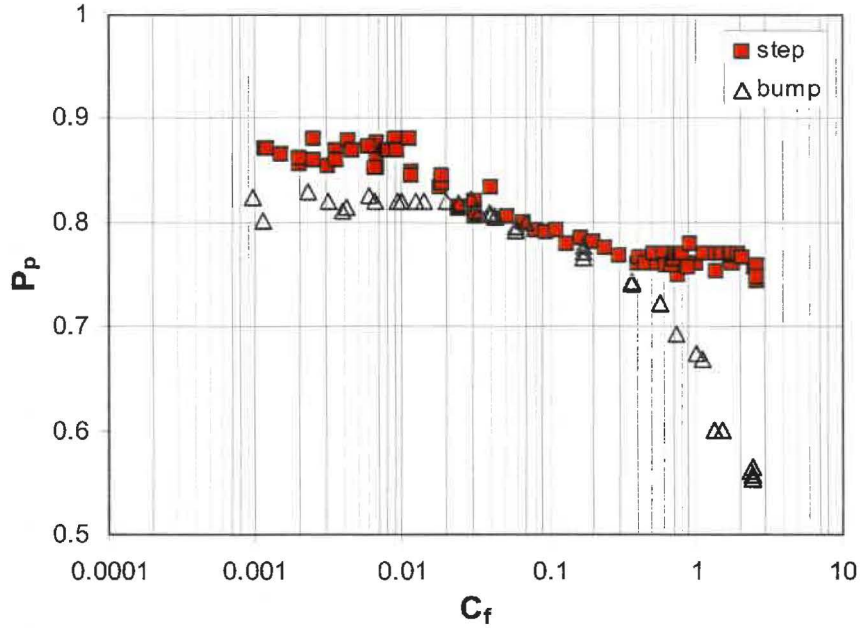

Figure 5.20 Effect of rotor type and feed consistency C_f on passage ratio P_p for bleached eucalypt pulp in a full length screen at V_s=0.6 ms^{-1}, V_{tip}=22 ms^{-1}. R_v=0.41 for the bump rotor and R_v=0.43 for the step rotor.

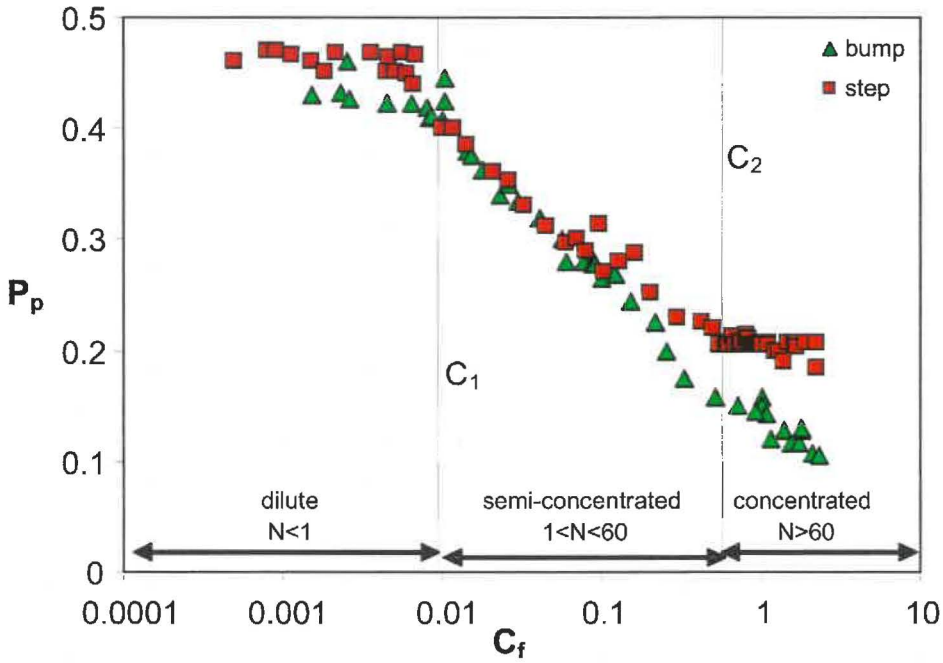

Figure 5.21 Effect of rotor on passage ratio Pp as a function of feed consistency C_f when screening unbleached pine screen with a full-length screen at V_s=0.6 ms^{-1}, V_{tip}=22 ms^{-1}. R_v=0.43 for the step rotor and 0.51 for the bump rotor.

The contoured slot screen also had characteristic curves for the bump (Figure 5.22) and step (Figure 5.23) rotor.

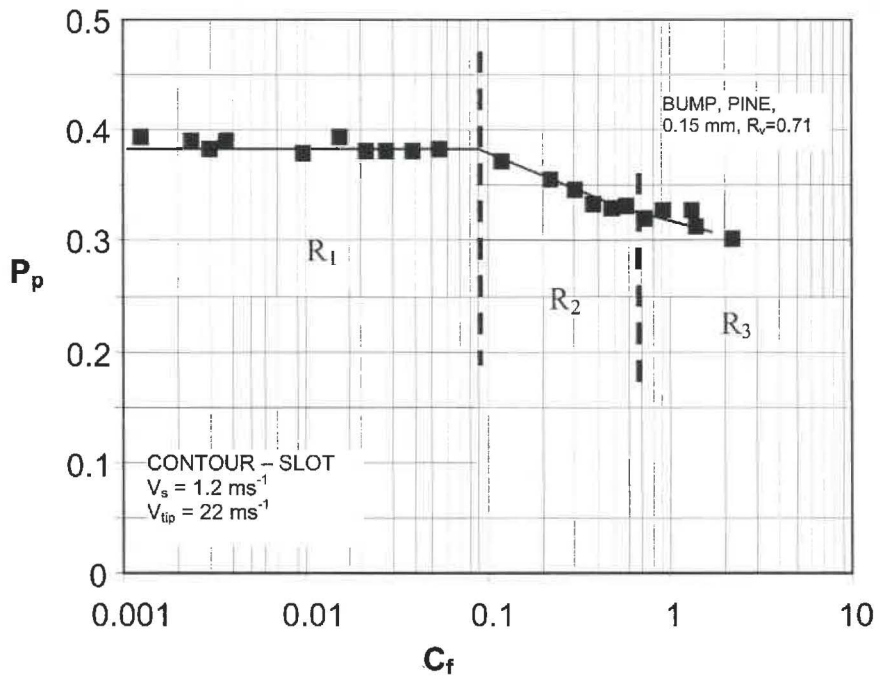

Figure 5.22 Effect of screen aperture profile on fibre passage ratio when screening unbleached radiata pine with a full-length screen with 0.15-mm contoured slots and a bump rotor. V_s=1.2 ms^{-1}, V_{tip}=22 ms^{-1}, R_v=0.71.

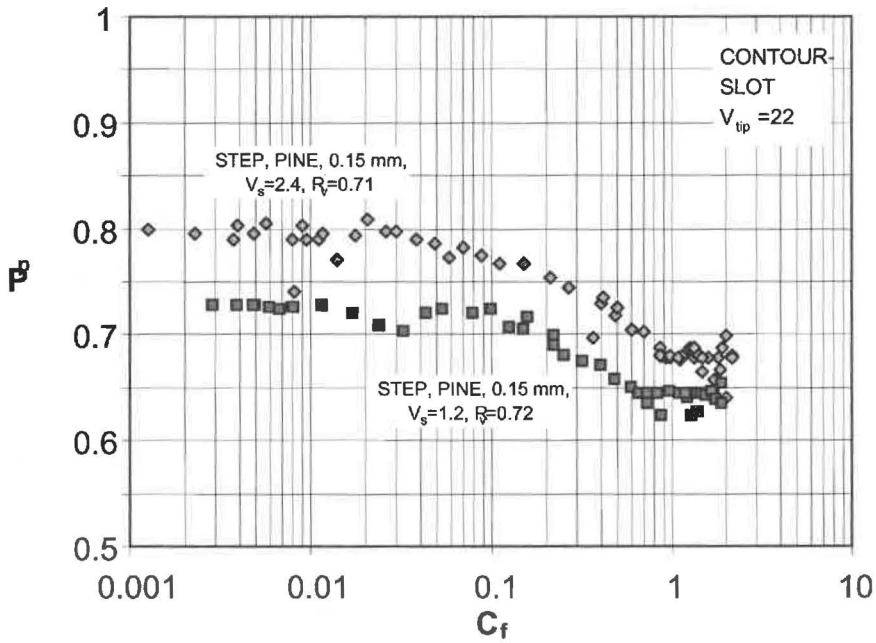

Figure 5.23 Effect of aperture velocity on fibre passage ratio when screening unbleached pine in a full-length screen with 0.15-mm contoured slots and a step rotor. For low velocity, V_s=1.2 ms^{-1}, V_{tip}=22 ms^{-1}, R_v=0.72. For high velocity, V_s=2.4 ms^{-1}, V_{tip}=22 ms^{-1}, R_v=0.71.

Passage ratios for the bump rotor were much lower than for the step rotor at the same speed. The pulse induced by the step rotor gives significantly more turbulence and fibre mobilisation, which enhances fibre passage. Slot velocity also enhances fibre passage and slightly increases the critical concentration. Higher slot velocities aid fibre passage by changing the dynamic balance between fibre accumulation at the aperture and fibre acceptance through the aperture. More work is needed to better understand these affects.

5.4.4 Increasing Rotor Speed

To investigate possible screening mechanisms, bump rotor speed was increased for screening 0.004% eucalypt pulp (Region 1) with the 1-mm smooth hole screen. The screen was successfully operated at steady flow (i.e. V_{tip}=0) with negligible thickening when C_f was less than C_1 (Figure 5.24), confirming that fibre accumulating on the screen by stapling or another mechanism is minimal. Reject thickening factor T increased non-linearly with increasing V_{tip}.

When V_{tip} is zero, pressure drop across the screen (from feed to accept) is the only driving force for flow. This produces a steady flow from the feed- to accept-side with no back-flow. Without back-flow, $1/F_r$ tends to zero, and passage ratio for forward flow P_F equals

overall passage ratio Pp (Equation 5.28). Thus, when reject thickening factors is unity, and passage ratio for forward flow equals unity, $P_F=P_p$.

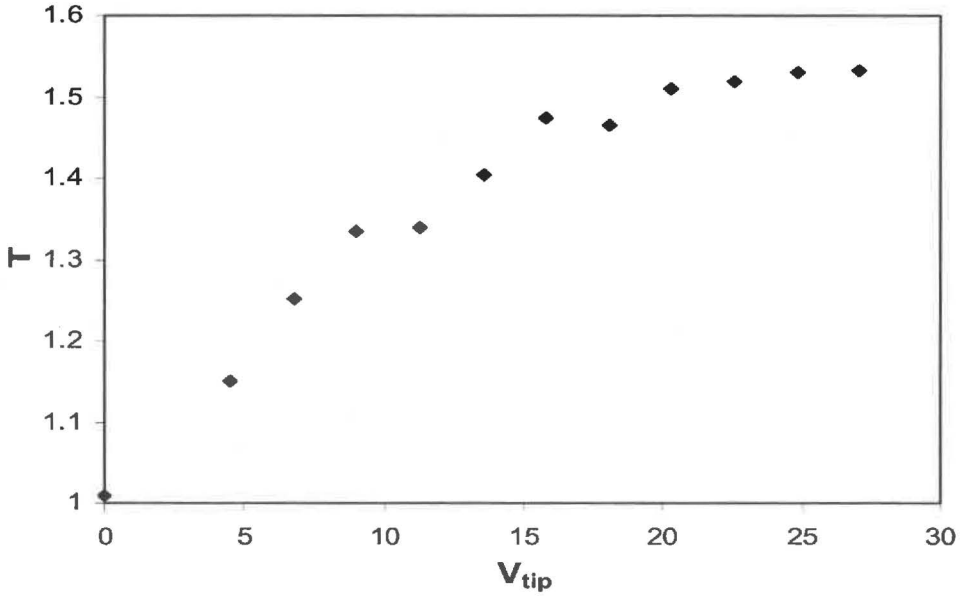

Figure 5.24 Effect of rotor speed on reject thickening. Screening 0.0004% bleached eucalypt with the bump rotor, 1-mm hole screen, V_s=0.6 ms^{-1}, R_v=0.33.

As rotor velocity increases, flow changes from steady to unsteady flow because the rotor pulse begins to induce forward and reverse flow of water, and possibly fibre, through the screen. Because flow velocities across the screen are constantly changing, the process needs to be described in terms of average flows. On average, velocity of fluid upstream of a hole V_u increases with V_{tip}. This is likely to create a recirculation zone of varying size upstream of the hole, which will increase as V_u increases, and reduces the effective average hole diameter $D_{f(e)}$. In addition, fibres usually approach the hole at a higher velocity and spend less time over a hole as V_u increases. Fibre penetration distance Y (Figure 5.6b) thus decreases, so more of a fibre's trailing end is exposed to flow passing the hole. Fluid drag on this trailing end increases in proportion to $V_{u,}$. The moment acting on the trailing end increases, which increases fibre rotation out of the holes. The net effect is a decrease in passage ratio with increasing rotor speed in Region 1 due to the fluid dynamics. Momentary fibre stapling at the edge of holes during unsteady forward passage may also occur but it is not possible to confirm this without visible evidence.

5.5 Explanation of Rotor and Feed Consistency Effects

Bump and step rotors have characteristic passage ratio curves with three regions (Figure 5.25). Overall trends can be explained by rotor-induced forward and reverse flow effects,

and the effects of fibre flocculation and accumulation at screen apertures on both sides of the screen.

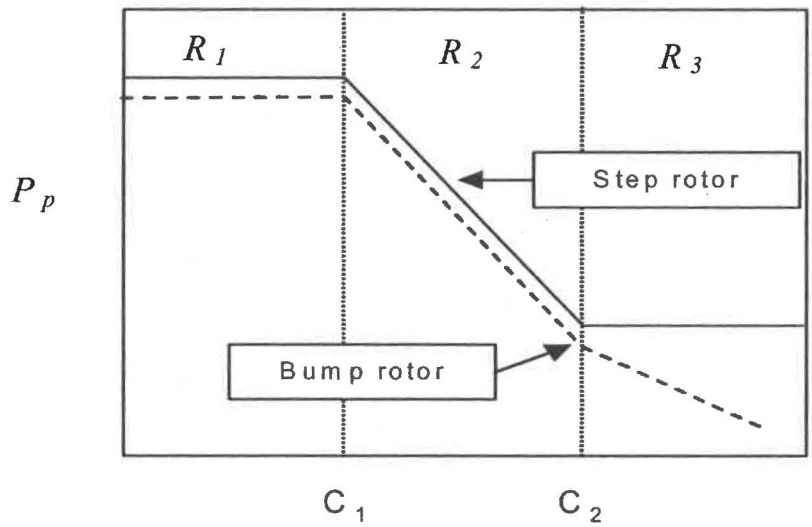

Figure 5.25 Characteristic passage ratio curves for a bump and step rotor.

- **Region 1 ($C_f < C_1$)**

It is proposed that P_p is constant when C_f is less than C_1 because minimal fibre accumulates on the downstream edge of holes and there is insufficient fibre to form a hanging floc that can reduce $C_{f(e)}$ and hinder fibre passage. Fibres pass through the screen holes relatively unhindered by hanging flocs or neighbouring fibres in suspension in both the forward and reverse direction. They can rotate freely and any chance collisions with other fibres do not affect their passage. Fibre passage in the reverse direction occurs with little hindrance. Passage ratios are close to unity because apertures are large, tangential velocities are low, and long-fibre content on the accept side reduce.

- **Region 2 ($C_1 < C_f < C_2$)**

It is proposed that P_p decreases when C_f is greater than C_1 because fibre accumulates on the downstream edge of holes on the feed-side. Effective diameter $D_{f(e)}$ decreases and fibre passage from the feed annulus to the accept chamber annulus is hindered by hanging flocs. These flocs enlarge with increasing consistency because fibres and fibre aggregates deposit on the downstream edge. Subsequently, passage ratio for forward flow P_F decreases with increasing consistency C_f. This proposal agrees with those reported by Kumar's [157] and Normin and Wedin [87] (see Sections 5.2.2 and 5.2.3). Fibre passage ratio in the reverse direction remains high and possibly close to unity in Region 2. Because apertures in the reverse direction are large, tangential velocities are low and average fibre length is smaller.

- **Region 3** ($C_f > C_2$)

It is proposed that C_2 indicates onset of fibre accumulation on the accept-side of the screen. At C_2, sufficient fibre has accumulated on the outer edges of the conically-drilled holes by either single fibre or aggregate deposition forming hanging flocs to reduce effective diameter $D_{a(e)}$ so reverse fibre passage is hindered. Passage ratio for back-flow P_B begins to decrease as hanging flocs grow with increased consistency in the concentrated pulp regime (N>60).

Fibre accumulation on the accept side of the screen is not a new proposal. Other researchers [128, 147] argue that fibre could accumulate on both sides of the screen. However, identifying when fibre begins to build up on the accept side is new knowledge. The C_2 value indicates where sufficient fibre has accumulated to hinder back-flow of fibre and is higher than C_1 because the accepts side hole diameter D_a is larger, consistency C_S lower, and long fibre content of the suspension lower than on the feed side. Also, the zone of intense decaying turbulence in the immediate wake of holes on accepts side is more likely to favour floc destruction than floc creation. Consequently, higher fibre consistency is needed to create a hanging floc large enough to hinder fibre passage.

When a hanging floc of width S_w and depth/height S_d forms on the outer edge of a conically-drilled hole on the accepts side, D_a reduces to $D_{a(e)}$ (Figure 5.4). The same-sized hanging floc on the downstream edge of the parallel-drilled hole on the feed side reduces D_f to $D_{f(e)}$. The normalised aperture reduction A_r is much higher on the feed-side

$$A_r = \frac{A_a - A_e}{A_a} \tag{5.32}$$

where A_a is actual aperture diameter or width and A_e is effective aperture diameter or width. For example, a hanging flocs that reduces D_a by 20% will give a A_r of ~0.5 on the feed-side but only ~0.2 on the accept side. Fibre passage from the feed to the accept side will be hindered by a hanging floc (Figure 5.4) but this sized floc on the other side of the screen is not large enough to hinder fibre passage from the accept side. To hinder reverse flow requires larger size flocs on the accept side or formation of additional hanging flocs.

Passage ratios in the forward and reverse directions can both decline with C_f in Region 3 because fibre is accumulating at holes on both the accept and feed sides. The effect on overall fibre passage P_p depends on the flow ratio F_r (Equation 5.28).

5.5.1 Application of Two-Passage Ratio Model

An iterative approach was used to estimate P_B (measuring P_B or P_F was beyond the scope of this study) by guessing P_F and solving numerically for P_B using Equation 5.30. Because P_p decreases approximately logarithmically with C_f in the semi-concentrated pulp regime (Region 2), the first approximation was P_F decreases at $-0.055\ln C_f$. For P_B to be less than 1, P_F must be lower than or equal to P_P. In the example presented in Figure 5.26 (using data from Figure 5.15), $P_F = P_p$ (but may be less than P_p). For this to happen, P_B has to decrease with consistency at a faster rate than P_F.

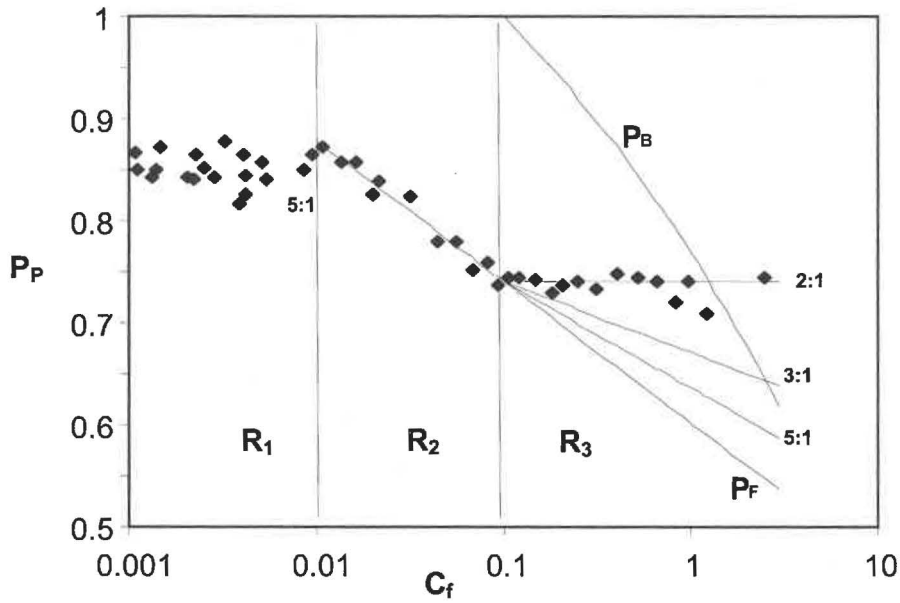

Figure 5.26 Estimating P_B for screening eucalypt using data from Figure 5.15 and Equation 5.30.

Passage ratios for back-flow P_B were calculated from data for screening pine across the same 55-mm section with the step rotor operating at a tip speed of 22 ms^{-1} (Figure 5.9) and using a F_r=2. Passage ratios for back-flow P_B decrease from 1 when C_f=0.06% to 0.1 when C_f=3% (Figure 5.27). The passage ratio for back-flow P_B decreases with increasing consistency at a greater rate than the passage ratio for forward-flow P_F, indicating that the effect of flocculation on the accept-side of the screen are more severe than the effects on the feed side.

Increasing the ratio for forward-flow to back-flow increases the gradient of the overall passage ratio (Figure 5.26). When screening eucalypt, a ratio is 2:1 gives a constant overall passage ratio in Region 3. It is postulated that the passage ratio for back-flow P_B

decreases with increasing consistency at a greater rate than the passage ratio for forward-flow P_F and a constant passage ratio is obtained this ratio is approximately 2:1 for the step rotor and approximately 5:1 for the bump rotor, which is where the gradient of the predicted curves (Figure 5.26) match the gradient obtained in screening trials.

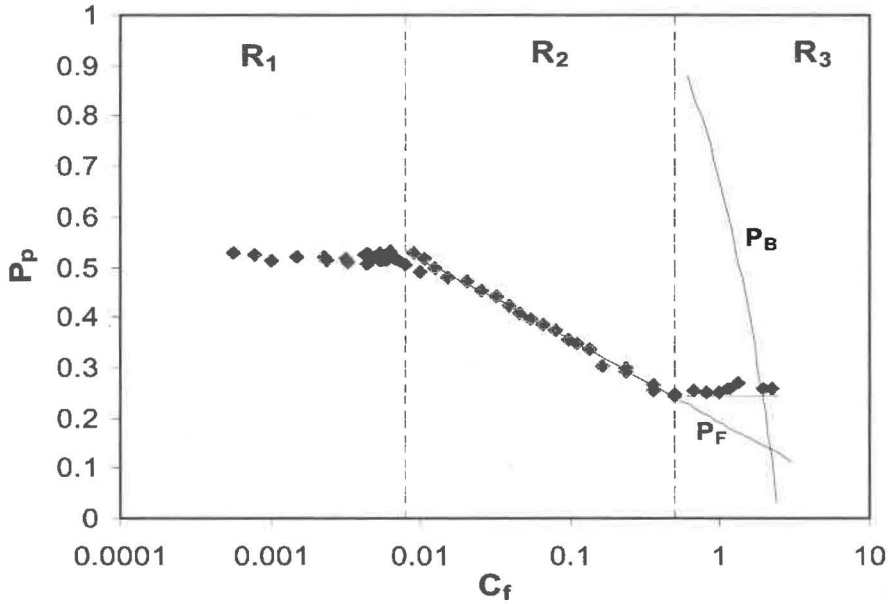

Figure 5.27 Effect of feed consistency on passage ratios for forward- and back-flow.

5.6 Experimental Validation of Water and Fibre Back-Flow

5.6.1 Salt Test

The amount of back-flow induced by the bump and step rotors was tested by measuring salinity of accept and reject streams after introducing saline to the accept side of the screen. Reject stream salinity will increase if back-flow occurs. Control measurements were taken when the bump rotor was stationary. In all tests, salinity of the accept stream was much higher than the reject stream (Figure 5.28) even when the rotor was stationary (i.e. no induced back-flow). Reject stream conductivity did not increase appreciably when the bump rotor was operated at a tip speed of 22 ms^{-1}, indicating that this rotor induces only a small amount back-flow. Reject stream conductivity was much higher when the step rotor was operating at 22 ms^{-1}, indicating that this rotor induces more back-flow. The increase in reject stream conductivity between control and step rotor is about five times that between the control and bump rotor.

5.6.2 Novel Screen Basket

To further support the effect of rotor on back-flow, unbleached radiata pine pulps were screened in a novel screen basket made by fixing six axially-orientated turbulent bars to

the feed side of the screen and aligning the 0.350-mm slots at right angles to the screen axis. (Slots are normally aligned parallel to the axis.) Accept consistency was higher than feed consistency (accept thickening or reject dilution) when screening pine with the step rotor (Figure 5.29), implying that back-flow of either water or dilute pulp must be occurring from the accept chamber to the feed side. Although this back-flow may consist only of water, fines are likely to also be present. Therefore, the passage ratio for back-flow will be greater than zero. If fibre flows forward (as it certainly does), it is reasonable to argue that some fibre other than fines also flows back to the feed side from the accept side. Nevertheless, because reject thickening and not accept thickening was observed with the bump rotor, it is reasonable to conclude that the step rotor induces significantly more back-flow than the bump rotor.

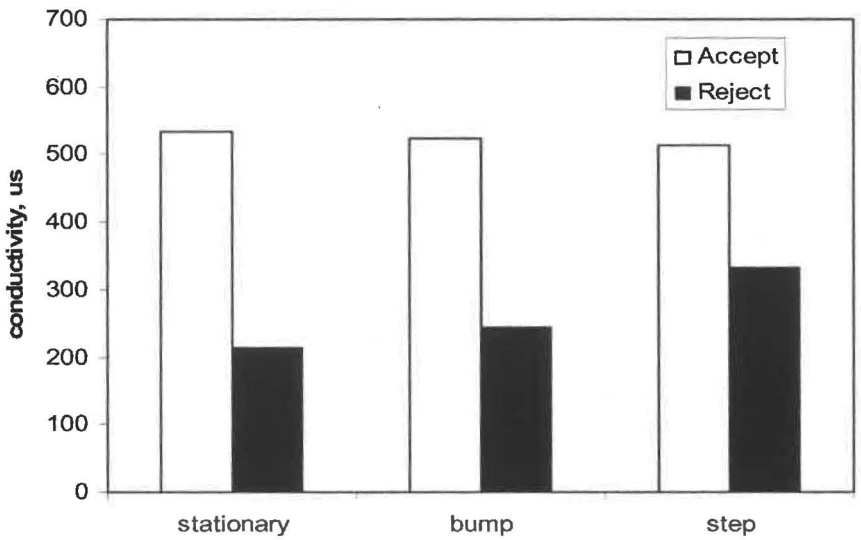

Figure 5.28 Effect of rotor on salinity of accepts and rejects streams.

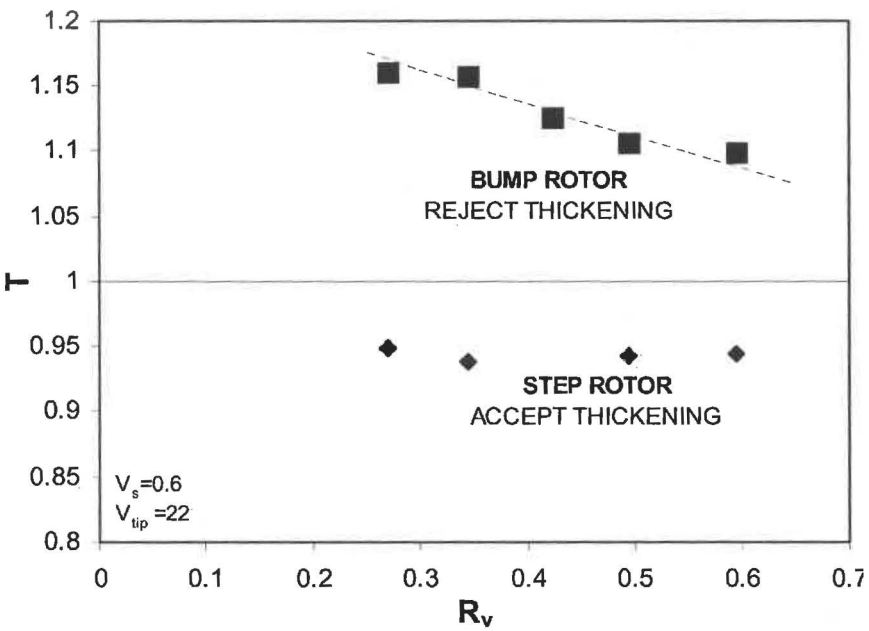

Figure 5.29 Effect of rotor on screening behaviour of a novel screen basket. Unbleached radiata pine, V_s=0.6 ms^{-1}, V_{tip} = 22 ms^{-1}.

5.6.3 Test for Fibre Back-Flow

The possibility of fibre back-flow was investigated by filling the accept chamber with 2% consistency bleached radiata pine, closing the accept valve and pumping water from feed to reject side while running the step or bump rotor at V_{tip} of 11 ms^{-1}. Fibre concentration in the reject stream increased asymptotically to a value equivalent a mass balance on pulp in the accept chamber and original water for both the step and bump rotor. The rate of increase in fibre concentration was greater for the step rotor. The data demonstrated that (a) fibre can back-flush through screen apertures from the accept chamber to the feed side of the screen and (b) that the step rotor does this more quickly than the bump rotor.

5.7 Summary and Conclusions

A back-flow model of fibre passage was derived based on two well-mixed tanks on either side of the screen. Fibre passage is proportional to a forward passage ratio P_F and inversely proportional to a reverse passage ratio P_B. It is also proportional to a volumetric flow ratio F_r, which is the ratio of forward flow Q_F to reverse flow Q_B (back-flow). All other things being equal, overall passage ratio P_p decreases as F_r increases.

Passage ratio P_p was independent of feed consistency when screening dilute pulp (i.e. N<1), but begins to decrease when pulp becomes semi-concentrated. The model developed proposes that fibre begins to accumulate on the feed-side of the screen when pulp becomes semi-concentrated, which will reduce hole diameter. Forward passage ratio P_F decreases, which decreases overall passage ratio. It is also proposed that sufficient fibre to hinder reverse fibre passage does not begin to accumulate on the accept-side of the screen until pulp becomes concentrated because the hole on the accept side is conical. Because of the larger diameter, a larger hanging floc must form before fibre accumulation on the accept side is sufficient to hinder reverse passage. Once fibre accumulation becomes critical on the accept side, passage ratio for back-flow of fibre P_B will begin to decrease as pulp is increasingly concentrated. The effect on overall passage ratio depends on the flow ratio F_r.

Trials using the step rotor showed that overall passage ratio P_p is also independent of feed consistency when screening concentrated pulp (i.e. N>60). The flow ratio F_r is likely to be relatively low (i.e. F_r~2) when screening and overall fibre passage is determined by both forward flow and back-flow. In the concentrated pulp regime, a pulp thickening

effect due to decreasing P_F is counteracted by a pulp thinning effect due to decreasing P_B when F_r is relatively low. As a result, overall passage ratio remains relatively constant in the concentrated pulp regime.

Trials with the bump rotor showed that P_p decreased with increasing consistency when screening concentrated pulp. It is proposed that P_p decreases in the concentrated pulp regime because the flow ratio F_r is relatively high (i.e F_r~5). Forward flow mainly determines fibre passage; the decrease in P_F means that P_p must decrease.

6. EFFECT OF FEED CONSISTENCY ON FIBRE LENGTH FRACTIONATION

6.1 Introduction

Fibre length fractionation efficiency is reported to increase approximately linearly with increasing reject thickening [24, 147]. However, efficiency cannot continue to increase with the highest levels of reject thickening. As the screen begins to reject too much fibre, efficiency begins to decrease and approach zero when the screen rejects all the fibre. This occurs when passage ratio for both long and short fibre fractions is zero and both fibre fractions remain in the reject stream. A unique relationship between feed consistency and fractionation efficiency is likely to exist for different types of screens, apertures sizes and rotor types. Relationships are explored using modelling methods developed by Olsen *et al.* [22] and experimental trials and the results from these investigations are presented in this chapter.

6.2 Fractionation Modelling

Olson *et al.* [22] showed that passage ratio P_p when screening with smooth-holed screens is a function of fibre length L_f and a coefficient λ, and developed the following equation for hole diameters between 0.8-2.1 mm.

$$P_p = e^{\frac{-L_f}{\lambda}} \tag{6.1}$$

For constant λ and constant aperture velocity V_s, P_p decreases as L_f increases (Figure 6.1) and the curves shift downward with as λ decreases. Olson *et al.* [22] reported that λ decreased from 2.5 to 1 when hole diameter was reduced from 1.8 mm to 0.8 mm. Also, the fractionation index Φ and reject thickening factor T increased as hole diameter (and hence λ decreased. Any influence of fibre concentration was ignored by Olsen.

The work reported was extended further using Equations 6.1 to 6.6 previously developed by Olsen [22] to investigate the effect of screen variables such as λ (equivalent to very small aperture size) and R_v on fractionation index at constant V_s. The passage ratios for short and long fibre length fractions were calculated using the data in Figure 6.1. The short fraction comprised the first 40 Kajaani size classes which ranged from 0.05 to 2 mm (Equation 6.2). The long fraction comprised the second 40 Kajaani size classes which ranged from 2.05 to 4 mm (Equation 6.3). Passage ratios for the combined long and short

fraction comprising all 80 size classes (Equation 6.4) indicates reject thickening tendencies (Equation 6.6). With decreasing λ, passage ratios for the short fibre, long fibre and combined mixture decrease towards zero (Figure 6.2). The relative difference between the two passage ratio curves predicts fraction index ϕ (Equation 6.5). Modelled data relating ϕ to λ are presented in Figure 6.3.

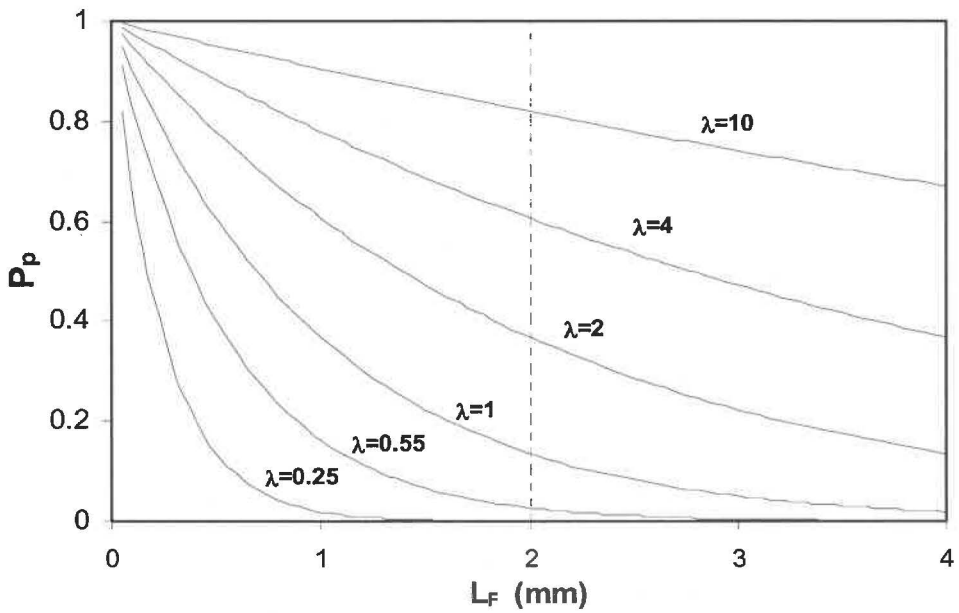

Figure 6.1 Effect of fibre length L_F and the coefficient λ on passage ratio as predicted by Equation 2.76 [22]

$$P_{p(S)} = \frac{\sum_{i=1}^{40} P_{p(i)}}{40} \tag{6.2}$$

$$P_{p(L)} = \frac{\sum_{i=41}^{80} P_{p(i)}}{40} \tag{6.3}$$

$$P_{p(80)} = \frac{\sum_{i=1}^{80} P_{p(i)}}{80} \tag{6.4}$$

$$\phi_m = R_v^{P_L} - R_v^{P_S} \tag{6.5}$$

$$T_m = R_v^{P_{ave}-1} \tag{6.6}$$

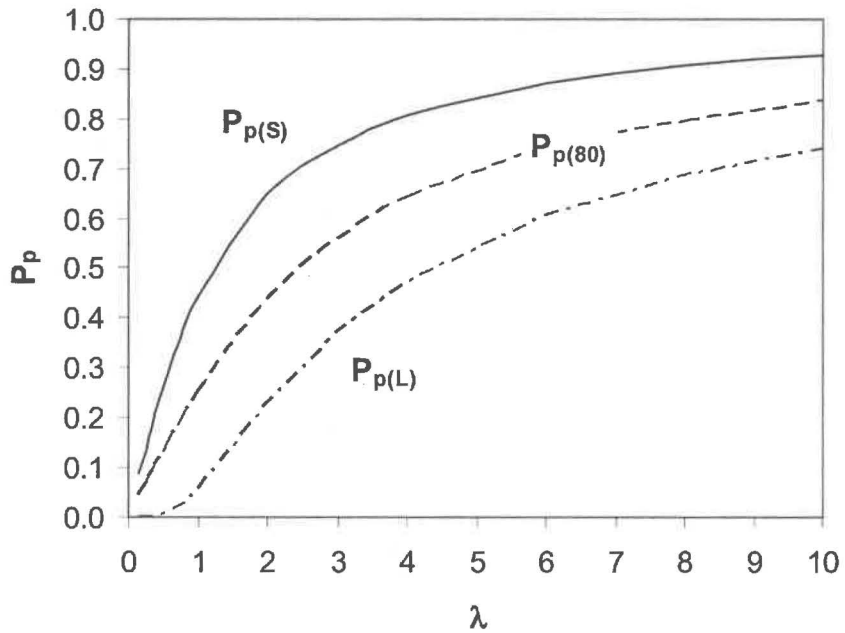

Figure 6.2 Effect of lambda on passage ratio of short, long and combined fractions.

Fractionation index generally increases with R_v, and below a local maximum, decreases with decreasing λ (Figure 6.3). This occurs because efficient long fibre removal is penalised as short fibre also moves to the reject stream when λ is less than 1 and when R_v is low. This effect has not been previously reported and may have significance when designing fractionating screens. Screens are not usually operated at low λ values because high levels of reject thickening often accompany low λ levels causing operation problems with plugging in screens and reject lines.

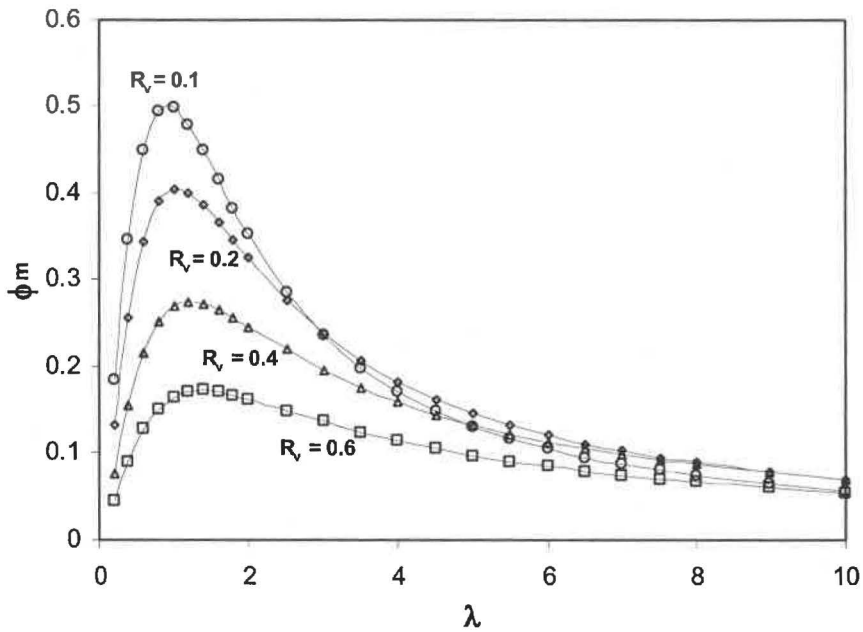

Figure 6.3 Predicted fractionation index Φ_m as a function of coefficient λ at various volumetric rejects rates.

Other relationships exist for predicted reject thickening T_m versus fractionation index ϕ_m at various volumetric reject ratios (Figure 6.4). Initially, fractionation index increasing with reject thickening to a critical level that is unique for each reject rate. The fractionation index then decreases. Lower rejects rates offer the greatest opportunity for high fractionation efficiency, but this advantage is only realised at high levels of thickening (T>4). At modest levels of thickening higher (T<2) rejects rate are predicted to favour fractionation. These predictions have also never been reported previously and experimental validation is needed before firm conclusions can be drawn.

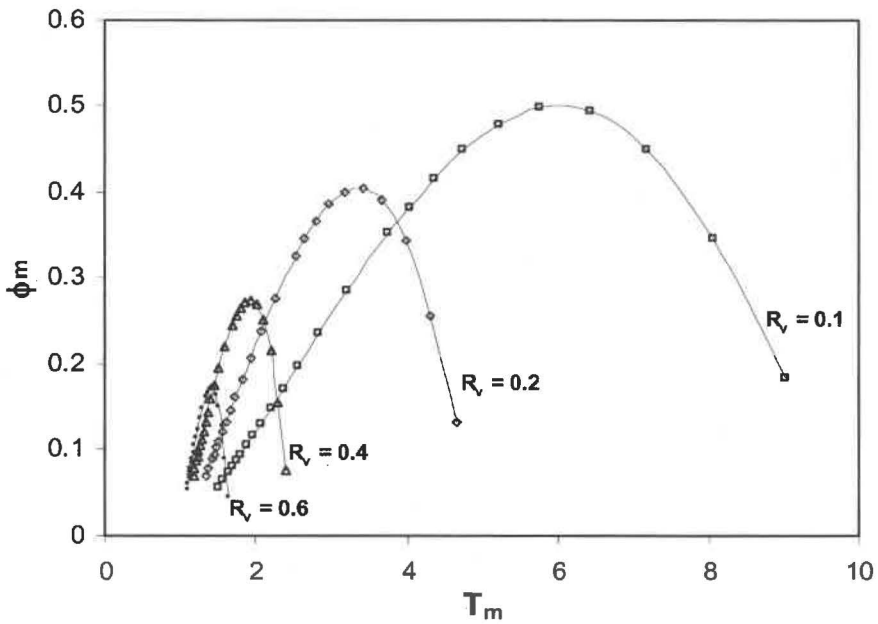

Figure 6.4 Predicted fractionation index ϕ_m as a function of predicted reject thickening factor T_m. The family of curves illustrate the effect of reject thickening and volumetric reject ratio on fibre length fractionation.

The presence of unique maxima at each volumetric reject ratio indicates that at least two competing mechanisms exist. Before the maximum fibre interaction and entanglement effects, long fibres from becoming momentarily mobile and free to migrate to the dilute fluid layer near the screen wall compared to short fibres. Increased thickening enhances this effect so fractionation efficiency increases. The rate of this increase, however, decreases as a second competing mechanism decreasing fibre passage ratios of both long and short fibres begins. As reject thickening increases, increased stapling and blocking of apertures progressively makes fibre acceptance difficult for both short and long fibres. Flow visualisation studies in real screens are needed to confirm these effects.

The maximum difference between long fibre passage ratio and short fibre passage ratio is maximum when λ is unity. The maxima in Figure 6.4 indicate where λ is unity for each

reject rate. Predicting that these maxima increase with increased reject rate may not be realistic. Experimental data are needed before speculating about the cause of this result.

The effect of feed consistency on fractionation efficiency has not been accounted for in previous model. One way to do this is to use passage ratio data from trials reported in Chapter 5. Data for a bump rotor for a feed consistency above 0.1% (Figure 5.18) produce Equation 6.7 for eucalypt (short fibre fraction), Equation 6.8 for pine (long fibre fraction) and Equation 6.9 for an equal mass mixture of eucalypt and pine.

$$P_{p(S)} = P_{p(euc)} = 0.779e^{-0.142C_f} \tag{6.7}$$

$$P_{p(L)} = P_{p(pine)} = 0.141C_f^{-0.269} \tag{6.8}$$

$$P_{p(mix)} = P_{p(pine+euc)} = 0.239C_f^{-0.2265} \tag{6.9}$$

Applying Equations 6.5, 6.7 and 6.8 gives Figure 6.5, which predicts the effect of feed consistency and volumetric rejects rate on fractionation index. Generally, the fractionation index increases with decreasing volumetric reject ratio and increases then decreases with feed consistency. The maximum fractionation index values were obtained at optimum feed consistency values of 0.6% for R_v=0.7 to 1.5% at R_v=0.1%.

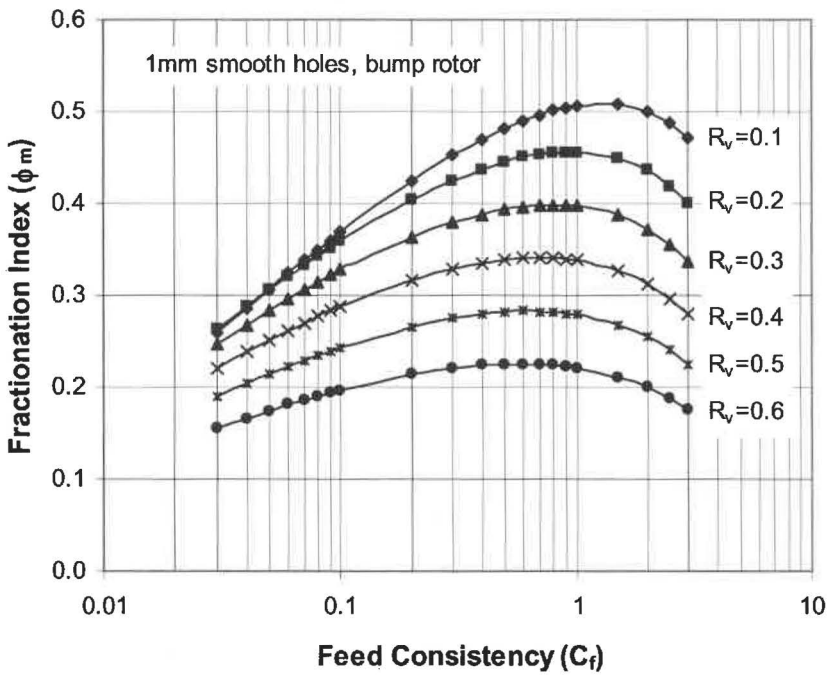

Figure 6.5 Predicted effect of feed consistency on fractionation index Φ_m using passage ratio data for eucalypt (Eq. 6.7) and pine (Eq. 6.8) pulps. Bump rotor, 1-mm smooth holes, V_s=0.6 m_{s-1}, V_{tip}=22 ms^{-1} (from Figure 5.18).

Applying Equations 6.7 and 6.8 to the previous analysis predicts the relationship between reject thickening and fractionation index (Figure 6.6). The individual R_v curves have the same general shape and the optimum fractionation index shifts upward and to the right with reject thickening. From a practical point of view, it is predicted that the fractionation index will be 0.3 when a 1% equal mass mix of eucalypt and pine pulp is screened with a bump rotor operating at R_v=0.3, V_s=0.6 ms^{-1} and V_{tip}=22 ms^{-1}. Rejects are will exit the screen at 2.4%, which corresponds to a reject thickening factor of 2.4.

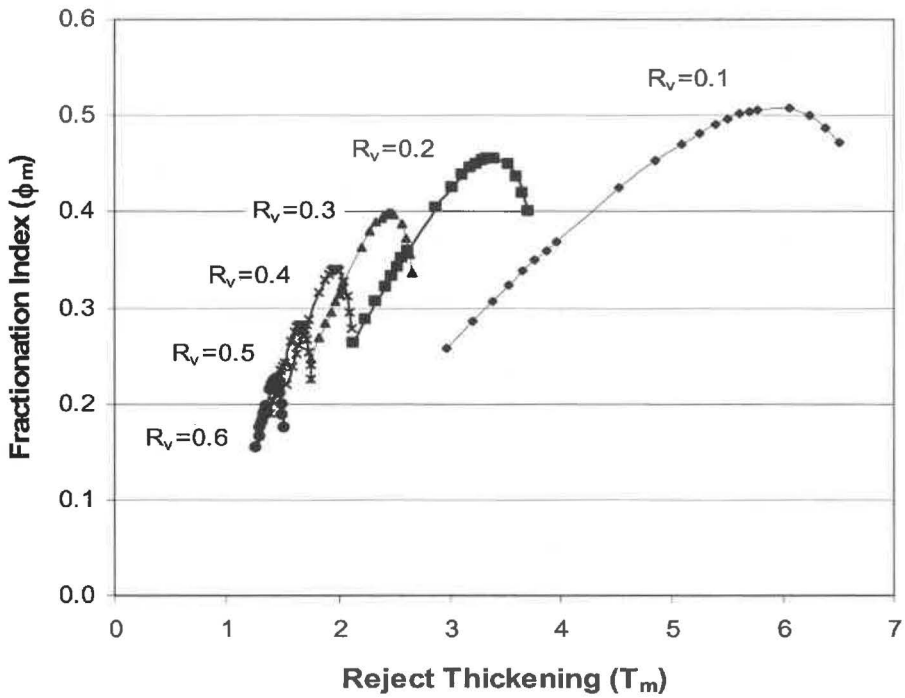

Figure 6.6 Predicted effect of reject thickening on fractionation index Φ_m using passage ratio data for eucalypt (Eq. 6.7) and pine (Eq. 6.8) pulps. Bump rotor, 1-mm smooth holes, V_s=0.6 m^{s-1}, V_{tip}=22 ms^{-1} (from figure 5.18).

Trends shown in Figure 6.5 and Figure 6.6 are only predictive and need to be confirmed by experiments before making any conclusions.

6.3 Experimental Results and Discussion

Fractionation trials were done to test the models. Data from two of the trials show that passage ratio P_p decreases with fibre length L_f and feed consistency C_f (Figure 6.7 and Figure 6.8). The values for λ were obtained by fitting Equation 2.76 and minimising the squared error. Legends in each figure give the coefficients for fitting data for constant C_f. As λ decreases, the dashed curves shift down, indicating greater reject thickening. Coefficients decrease semi-logarithmically from 2.94 to 0.52 with increasing C_f for 1-mm holes (Figure 6.7) and from 7.1 to 1.1 for 2.4-mm holes (Figure 6.8).

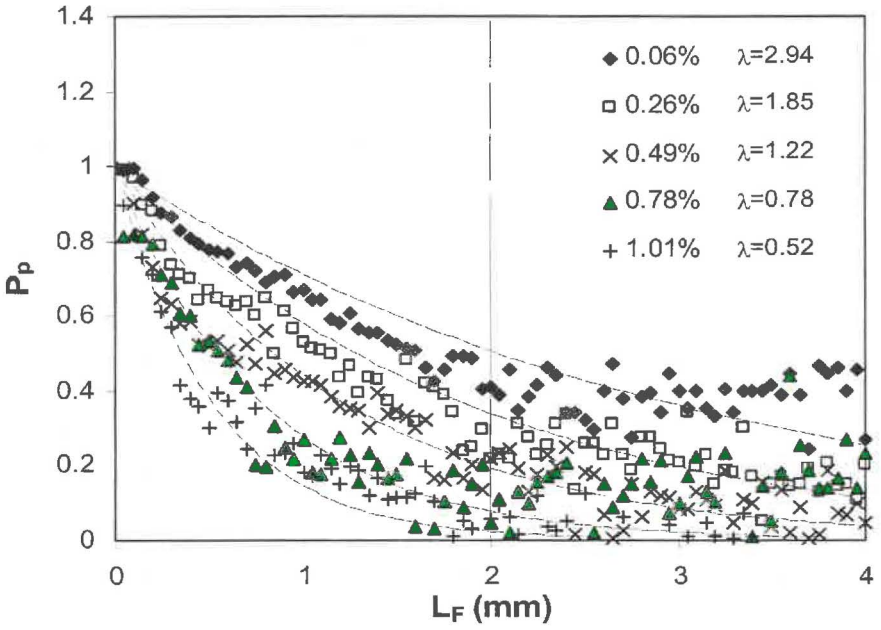

Figure 6.7 Effect of fibre length on passage ratio a full-length screen with 1-mm smooth holes. Pine, bump rotor, R_v=0.2, V_s=0.6 ms^{-1}, V_{tip}=22 ms^{-1}.

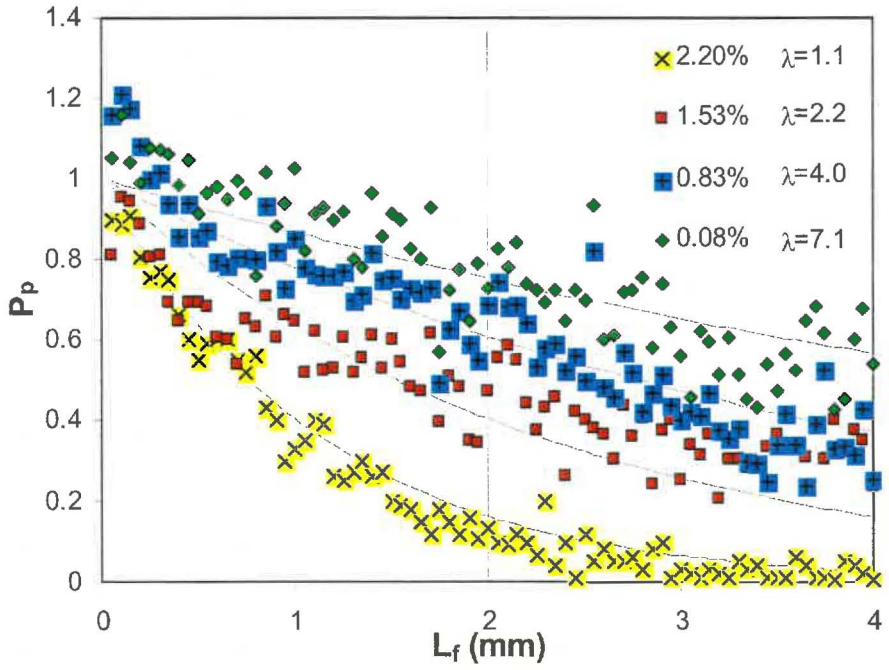

Figure 6.8 Effect of fibre length on passage ratio a full-length screen with 2.4-mm smooth holes. Pine, bump rotor, R_v=0.2, V_s=0.6 ms^{-1}, V_{tip}=15 ms^{-1}.

Feed consistency affects λ (Figures 6.7 and 6.8). Modelling indicates a local maximum exists at λ=1, which corresponds to 0.7% C_f with 1-mm holes and 2% C_f with 2.4-mm holes (Figure 6.9).

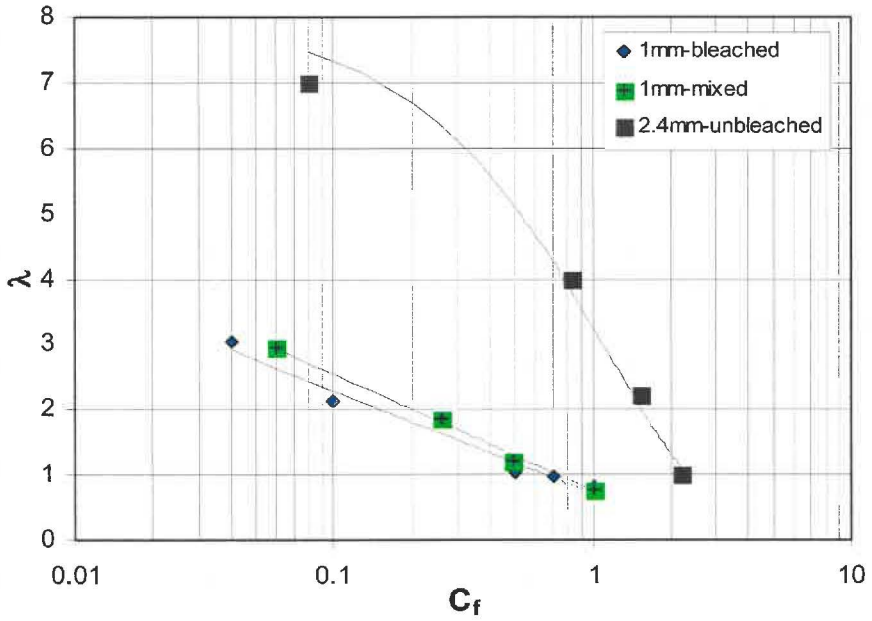

Figure 6.9 Effect of feed consistency C_f on coefficient λ.

Fractionation index increases with feed consistency for screens with 1-mm and 2.4-mm holes (Figure 6.10 and Figure 6.11). After a maximum, the index decreases for the 1-mm hole screen but a maximum was not observed for the screen with 2.4-mm holes because the reject line plugged with thickened pulp when using feed of 2.2% consistency. Trials need to be carried out at feed consistencies above 2.2% to investigate where a maximum fractionation index is reached when using a 2.4-mm hole screen.

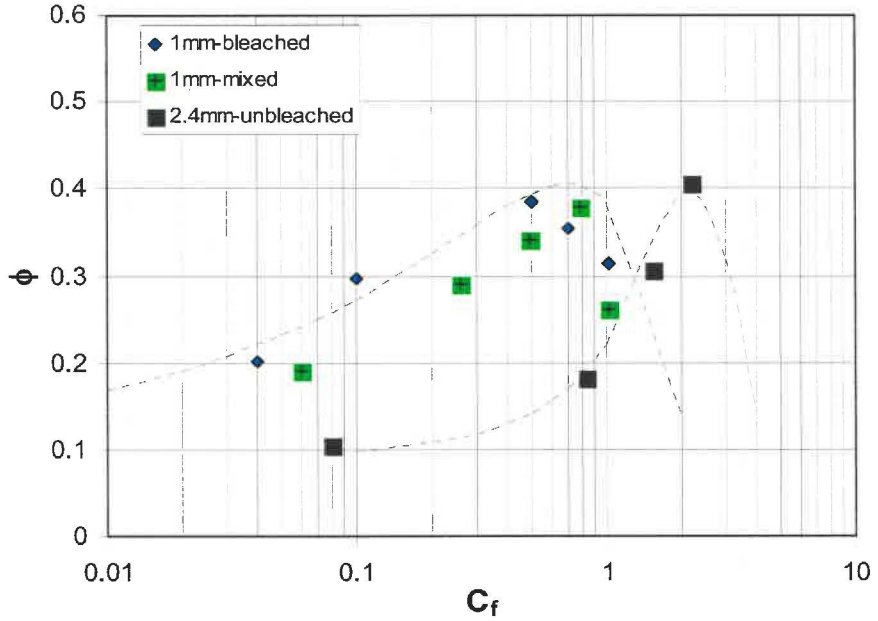

Figure 6.10 Effect of feed consistency Cf on fractionation index Φ for the full-length screen. Bump rotor, R_v=0.2, Vs=0.6 ms-1, V_{tip}=22 ms^{-1} (1-mm holes) or 15 ms^{-1} (2.4-mm holes).

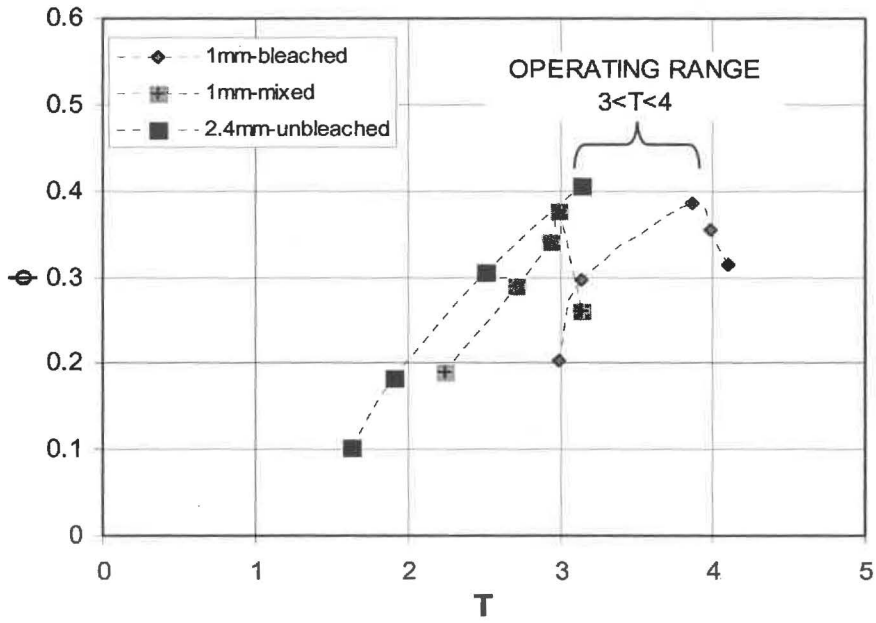

Figure 6.11 Effect of reject thickening T on fractionation index Φ for the full-length screen. Bump rotor, R_v=0.2, V_s=0.6 ms^{-1}, V_{tip}=22 ms^{-1} (1-mm holes) or 15 ms^{-1} (2.4-mm holes).

A maximum fractionation index of 0.4 and a thickening factor approaching 4 was achieved at 0.7% feed consistency for the 1-mm hole screen. The values for the 2.4-mm screen were a maximum fraction index of 0.41, a thickening factor of 3 at 2.2% feed consistency. Significantly, experimental data (Figures 6.7, 6.8) agree with the Olson equations [22], which predict that maximum fractionation when screening with 1-mm smooth holes will occur at thickening factors between 3 and 4 when R_v is 0.2. Experimental fractionation indexes where 15% lower than predicted (0.4 c.f. 0.46).

The modelled relationship (Figure 6.6) between λ_m and T_m did not agree well with Olson's predictions [22], which indicate that λ_m will not increase when reject thickening factor T_m is above 2. It is unclear, however, how these predictions were made. Olson also stated there was little need to operate a screen with thickening factors greater than 2, especially when screens are more likely to plug.

The predicted increase then decrease in λ_m with increasing reject thickening was observed in the experimental data. It is postulated that, at some point, a screen must reject too much fibre when reject thickening increases. Reject thickening increases with feed consistency because the effective diameter of the holes on the feed side ($D_{f(e)}$) decreases. When ϕ is at a maximum, $D_{f(e)}$ is critically small; with further increases in consistency, the decrease in $D_{f(e)}$ produces too much thickening and λ decreases.

The decrease in fractionation index Φ with feed consistency has not been reported previously because other researchers have not operated screens at very high levels of reject thickening. For example, Olson would have had to use unconventionally small holes (D_f<0.8mm). The level of reject thickening would be beyond the normal operating range of commercial screens and workers would be concerned about screen plugging and reject line blocking.

Experimental data from fractionation trials with an industrial screen (Figure 6.10) indicate that the maximum fractionation efficiency for 2.4-mm hole screens is similar to that of 1-mm hole screens but occurs at higher feed consistency. This is a significant finding because fractionating at higher consistencies is potentially more economic [1, 38].

6.4 Summary and Conclusions

Fibre-length fractionation trials show that there is a maximum fractionation with increasing feed consistency; this maximum occurs at a higher consistency as hole size increases. At feed consistencies greater than the maximum, holes become too small due to fibre accumulating at the edges of the holes. Efficient long fibre removal to the reject stream is penalised by short fibre removal to the reject stream, decreasing overall fractionation index. Fractionation using 2.4-mm holes can be as good as fractionation with 1-mm holes, provided it is done at a higher feed consistency.

7. CONCLUSIONS AND RECOMMENDATIONS

7.1 Conclusions

Studies on the behaviour of pressure screens used for wood pulp produced the following conclusions and observations:

- Reject thickening behaviour of narrow screen sections is better characterised by Gooding and Kerekes' mixed-flow model whereas reject thickening behaviour of standard, full-length screens is better characterised by their plug-flow model.
- A tanks-in-series model can be used to predict behaviour of a pressure screen. It shows that reject thickening factor T decreases when a 220-mm screen is shortened to 27-mm, primarily because flow behaviour changes from plug flow to mixed flow.
- A short screen (i.e. L_s<55 mm) at the front (feed-end) of the screen rejects less fibre than the back of the screen because relative speed at the front of the screen is higher than along the rest of the screen.
- Accelerating pulp in the feed chamber reduces relative speed, so the same short screen will reject more fibre.
- The magnitude of the negative pulse decreases axially by about 33% due to the decrease in axial relative speed.
- Reject thickening for the pressure screens when screening pulp of varying consistencies (from 0.0005 to 2.0%) exhibited three distinct regions. The two critical consistencies were shown to be due to fibre accumulation on the feed side (C_1) followed by fibre accumulation on the accept side (C_2).
- The gradient of the reject thickening curves in Region 3 decrease as the volumetric flow ratio of forward to back-flow decreases.
- Step and bump rotors have different reject thickening behaviour in Region 3, primarily because the step rotor induces more back-flow than the bump rotor.
- Fibre passage is independent of C_f when screening dilute pulp (i.e N<1) under normal operating conditions. Sufficient fibre to hinder fibre passage does not accumulate on either feed-side or accept-side of the screen.
- Fibre passage ratio P_p decreases semi-logarithmically with increasing C_f when screening semi-concentrated pulp (i.e 1>N<60). Sufficient fibre to hinder

forward fibre passage accumulates on the feed-side of the screen and P_p decreases in proportion to a decrease in forward passage ratio P_F.

- Fibre begins to accumulate on the accept-side of the screen when pulp is concentrated (i.e. N>60).
- Fibre passage ratio P_p is independent of C_f when screening concentrated pulp (i.e N>60) with a step rotor. Although both passage ratios for forward flow and back-flow decrease, P_p remains relatively constant because volumetric flow ratio F_r is relatively low when screening with this rotor. Fibre passage ratio P_p decreases with C_f when screening concentrated pulp with the bump rotor because F_r is relatively high.
- The fractionation index initially increases with increasing feed consistency C_f when fractionating kraft pulp with smooth-holed screens. This is because the effective diameter of holes in the screen begins to decrease as fibre accumulates at the edges of holes on the feed-side of the screen. At a critical feed consistency, however, fibre accumulation on the feed-side makes the holes to too small and the screen begins to reject too much fibre. At this point, fractionation index decreases rapidly because long fibres and short fibres are efficiently rejected because the hole diameter is decreasing.

6.2 Recommendations

It is recommended that further studies are done to increase the knowledge on pressure screen characteristics.

- Rotor effects

It is still uncertain whether rotor design affects flow behaviour of a screen. Some researchers claim that flow behaviour with open type rotors is different to closed rotors but no evidence has been presented. This is a major gap in the knowledge as flow behaviour can affect overall screen performance. It is recommended that the effect of rotor design on flow behaviour be investigated.

- Volumetric flow ratio

Volumetric flow ratio F_r is an important determinant of fibre passage when screening concentrated pulp. It is likely that rotor design will affect fibre passage. The back-flow model should be further developed so the volumetric flow ratio F_r can be calculated from a residence time distribution.

- Fibre accumulation

Fibre accumulation on the accept side of the screen could be exploited to improve contaminant screening operations based on barrier screening. If fibre accumulation on the accept side is advantageous to contaminant screening, future investigations are needed to investigate to identify the screen designs and/or operating that enhance fibre accumulation on the accept side of the screen.

- Fibre-length fractionation

Future investigations should evaluate whether fibre-length fractionation can be carried out with the medium feed consistency (8-20%). The research in this thesis postulated that unconventionally large holes (i.e 3 to 5 mm) may be required. The effective diameter of these large holes may decrease to a critically small diameter as fibre accumulates on the downstream edge of holes on the feed side of the screen. At this critically small effective diameter, the fractionation efficiency may be as good as with conventional fractionation.

8. REFERENCES

1. Brewer, J.L. and J.A. Bolton, *Fibre fractionation of high-yield Kraft pulp.* Tappi Journal, 1974. **57**(6): 121-129.
2. Kerekes, R.J., R.M. Sozynski, and P.A. Tam Doo, *The flocculation of pulp fibres.* In 4th *Transactions of the Fundamental Research Symposium,* 1985.
3. Fredriksson, B., *High consistency screening proves itself in recycling mills - efficient and economic.* Paper Technology, 1995. **36**(4): 35-40.
4. Gullichsen, J. and E. Harkonen, *Medium consistency technology 1: fundamental data.* Tappi Journal, 1981. **64**(6): 69-72.
5. Olson, J., *The effect of fibre length on passage through narrow apertures*, in *Chemical Engineering*. 1996, University of British Columbia.
6. Kerekes, R. and C.J. Schell, *Effects of fibre length and coarseness on pulp flocculation.* Tappi Journal, 1995. **78**(2): 133-139.
7. Mohlin, U.-B., *Properties of TMP fractions and their importance for the quality of printing papers.* Svensk Papperstidning, 1980. **18**: 513-521.
8. Hentschel, R.A.A., *Structure-property relationships in synthetic fibre papers.* Tappi Journal, 1959. **42**(12): 979-982.
9. Watson, A.J. and H.E. Dadswell, *Influence of fibre morphology on paper properties: Part 1 - fibre length.* Appita Journal, 1961. **14**(5): 168-176.
10. Dinwoodie, J.M., *The relationship between fibre morphology and paper properties: A literature review.* Tappi Journal, 1965. **48**(8): 440-447.
11. Clark, J.d.A., *Pulp Technology and Treatment for Paper.* 1985, San Francisco: Miller Freeman Publications.
12. Sastry, C.B.R., R.M. Kellogg, and R.W. Wellwood, *Measurement and prediction of fibre coarseness in Western Hemlock.* Tappi Journal, 1973. **56**(4): 158-166.
13. Sastry, C.B.R. and R.W. Wellwood, *Coarseness of some coniferous wood pulps: A new approach.* Tappi Journal, 1972. **55**(6): 901-915.
14. Clark, J.d.A., *Weight average fibre lengths - A quick, visual method.* Tappi Journal, 1962. **45**(1): 38-45.
15. Uprichard, J.M. and J.C.F. Walker, *Pulp and paper manufacture*, in *Primary Wood Processing*, J.C.F. Walker, Editor. 1993, Chapman and Hall: London. pp. 481-534.
16. Parham, R.A., *Wood structure - softwoods*, in *Pulp and paper manufacture - Vol 1: Properties of fibrous raw materials and their preparation for pulping*, M.J. Kocurek, Editor. 1983, Joint Textbook Committee of the Paper Industry: Montreal. pp. 22-27.
17. Parham, R.A., *Wood structure - hardwoods*, in *Pulp and paper manufacture - Vol 1: Properties of fibrous raw materials and their preparation for pulping*, M.J. Kocurek, Editor. 1983, Joint Textbook Committee of the Paper Industry: Montreal. pp. 28-34.
18. Smith, I., E. Landis, and M. Gong, *Fracture and Fatigue in Wood.* 2003, New York: John Wiley and Sons.

19. Butterfield, B.G., *The structure of wood: An overview*, in *Primary Wood Processing: Principles and Practice*, J.C.F. Walker, Editor. 1993, Chapman and Hall: London. pp. 1-22.

20. Tam Doo, P.A. and R. Kerekes, *A method to measure wet fibre flexibility.* Tappi Journal, 1981. **64**(3): 113-121.

21. Forgacs, O.L. and S.G. Mason, *The flexibility of wood pulps.* Tappi Journal, 1958. **41**(11): 695-704.

22. Olson, J., B. Allison, and N. Roberts, *Fibre length fractionation caused by pulp screening: smooth-hole screen plates.* Journal of Pulp and Paper Science, 2000. **26**(1): 12-16.

23. Forgacs, O.L., *The characterisation of mechanical pulps.* Pulp and Paper Magazine of Canada, 1963. **64**(Conv. Issue): pp. 89-118.

24. Sloane, M.C., *Kraft pulp processing - pressure screen fractionation.* Appita Journal, 2000. **53**(3): 220-226.

25. Sloane, C.M. *Wastepaper quality development for packaging papers - fractionation or whole stock refining?* In 20th *TAPPI Recycling Symposium,* 1998.

26. Chatterjee, A. and T.T. Dodson, *Formation and distribution of fibre length and flexibility.* Nordic Pulp and Paper Research Journal, 1997. **2**: 120-130.

27. Moller, K. *‚Engineering papers to match market requirements.* In 50th *Appita Annual General Conference,* 1999.

28. Arlov, A.P., *Load-elongation properties of paper sheets made from Bauer-McNett fractions of beaten sulphite pulp.* Norsk Skogindustri, 1959. **13**(10): 342-351.

29. Paavilainen, L., *Conformability - flexibility and collapsibility of sulphate pulp fibres.* Paperi ja Puu, 1993. **75**(9-10): 689-702.

30. Wakelin, R.F., J.K. Jackman, and A. Dell Bawden. *Changes in mechanical pulp fibre cross-sectional dimension distributions caused by screens, hydrocyclones and reject refining.* In 50th *Appita Annual General Conference,* 1999.

31. Claudio-da-Silva, E., *The flexibility of pulp fibres - A structural approach.* In 33rd *International Paper Physics Conference,* 1983.

32. Marton, R. and S.D. Alexander, *Properties of fibre fractions from chemical and mechanical pulps: I softwood pulps.* Tappi Journal, 1963. **46**(2): 65-67.

33. Murray, C.E. and B.B. Thomas, *Papermaking characteristics of cedar fibre.* Tappi Journal, 1961. **44**(9): 625-633.

34. McElwee, R.L., R.C. Tobias, and A.H. Gregory, *Wood characteristics of three southern hardwood species and their relationship to pulping properties.* Tappi Journal, 1970. **53**(10): 1882-1886.

35. Britt, K.W., *Determination of fibre coarseness in wood samples.* Tappi Journal, 1965. **48**(1): 7-17.

36. Ammala, A., *Fractionation of thermomechanical pulp in pressure screening: An experimental study on the classification of fibres with slotted screen plates.* 2001, PhD Thesis, Oulun Yliopisto (Finland).

37. Olson, J., Allison, B. and N. Roberts , *Fibre fractionation for high porosity sack Kraft paper.* Tappi Journal, 2001. **84**(6): 66-80.

38. Mayovsky, J., *Fractionation of OCC - how can it help you?* In 21st *TAPPI Recycling Symposium,* 1998.

39. Kerekes, R.J., *Pulp flocculation in decaying turbulence: A literature review.* Journal of Pulp and Paper Science, 1983. **9**(3): 123-137.

40. Kerekes, R.J. and C.J. Schell, *Characterization of fibre flocculation regimes by a crowding factor.* Journal of Pulp and Paper Science, 1992. **18**(1): 32-38.

41. Meyer, R. and D. Wahren, *On the elastic properties of three-dimensional fibre networks.* Svensk Papperstidning, 1964. **67**(10): 432-447.

42. Mason, S.G., *Fibre motions and flocculation.* Tappi Journal, 1954. **37**(11): 494-501.

43. Paul, S.T., *Fibre suspension processing in viscous media.* 1999, PhD Thesis, The University of Auckland.

44. Jokinen, O. and K. Ebelin, *Flocculation tendency of papermaking fibres.* Paperi ja Puu, 1985. **67**(5): 317-325.

45. Dodson, C.T.J., *Fibre crowding, fibre contacts and fibre flocculation.* Tappi Journal, 1996. **79**(2): 211-216.

46. Duffy, G.G., *Flow of medium consistency wood pulp fibre suspensions.* Appita Journal, 1995. **48**(1): 51-55.

47. Mason, S.G., *The motion of fibres in flowing liquids.* Pulp and Paper Magazine of Canada, 1950. **51**(5): 94-98.

48. Duffy, G.G., *The significance of mechanistic-based models in fibre suspension flow.* Nordic Pulp and Paper Research Journal, 2003. **18**(1): 74-80.

49. Kropholler, H.W. and W.W. Sampson, *The effect of fibre length distribution on suspension crowding.* Journal of Pulp and Paper Science, 2001. **27**(9): 301-305.

50. Thalen, N. and D. Wahren, *Shear modulus and ultimate shear strength of some paper pulp fibre networks.* Svensk Papperstidning, 1964. **67**(7): 259-272.

51. Andersson, O., *Flocculation at sedimentation - Part 5:Factors influencing flocculation tendency.* Svensk Papperstidning, 1961. **64**(11): 417-429.

52. Wahren, D., *MSc Lecture Notes.* In *APPI.* 1990: Melbourne, Australia.

53. Bennington, C.P.J., *Mixing of pulp suspensions.* 1988, PhD Thesis, University of British Columbia.

54. Duffy, G.G. and A.L. Titchener, *Disruptive shear stress of pulp networks.* Svensk Papperstidning, 1975. **75**(13): 474-479.

55. Robertson, A.A. and S.G. Mason, *The flow characteristics of dilute fibre suspensions.* Tappi Journal, 1957. **40**(5): 326-338.

56. Kerekes, R.J., *Pulp floc behaviour in entry flow to constrictions.* Tappi Journal, 1983. **66**(1): 88-91.

57. Andersson, O., *Some observations of fibre suspensions in turbulent motion.* Svensk Papperstidning, 1966. **69**(2): 23-31.

58. Bonano, E.J., *A study of flocculation in flowing concentrated fibre suspensions using coherence functions.* Journal of Pulp and Paper Science, 1984. **10**(4): 102-107.

59. Karema, H., *Transient fluidisation of fibre suspensions in straight channel flow.* In *International Paper Physics Conference,* 1999.

60. Parker, J.D. and R. Hergert, *Simultaneous convergence - A new concept of headbox design.* Tappi Journal, 1968. **51**(10): 425-432.

61. Kerekes, R., *High turbulence for headboxes questioned.* Pulp and Paper Canada, 1979. **80**(9): 31-32.

62. Wagle, D.G. and C.W. Lee. *A visual study of pulp floc dispersion mechanism.* in 13th *TAPPI Engineering Conference,* 1987.

63. Kerekes, R. and R.G. Garner, *Measurements of turbulence in pulp suspensions by laser anemometry.* Transactions Technical Section - CPPA, 1982. **8**(3): TR 53-59.

64. Duffy, G.G. and B. Norman, *Fibre flocculation in conical contractions simulating the paper machine flowbox slice.* In 2nd *International Symposium on Paper Machine Headboxes.* 1979.

65. Duffy, G.G. and L. Abdullah, *Flow of fibre suspensions in small diameter pipes.* In 62nd *Appita Annual General Conference,* 2002.

66. Mason, S.G., *Orthokinetic phenomena in disperse systems.* Journal of Colloid and Interface Science, 1977. **58**(2): 275-285.

67. Wahlstrom, B., *Developments in paper technology in a global perspective.* Svensk Papperstidning, 1981. **18**: 32-39.

68. Kerekes, R.J., *Characterizing fibre suspensions.* In 5th *TAPPI Engineering Conference,* 1996.

69. Duffy, G.G. and P.F.W. Lee, *Drag reduction in the turbulent flow of wood pulp suspensions.* Appita Journal, 1978. **31**(4): 280-296.

70. Duffy, G.G., *The mechanisms of flow of pulp suspensions in pipes.* Appita Journal, 1976. **29**(5): 363-375.

71. Gullichsen, J., *Medium consistency technology: The MC screen.* Tappi Journal, 1985. **68**(11): 54-58.

72. Duffy, G.G. and P.F.W. Lee, *Velocity profiles in the drag reducing regime of pulp suspension flow.* Appita Journal, 1976. **30**(3): 125-137.

73. Julien Saint Amand, F., *Principles and technology of screening.* 1997, Centre Technique du Papier: Grenoble. pp. 1-40.

74. Hourula, I., *Fewer cascade connections, pumping and control loops in screening plants utilising new techniques.* In 11th *TAPPI Recycling Symposium,* 1996.

75. Javid, S.R., *Pressure screen design application is key to headbox pulsation control.* Pulp and Paper, 1983. **57**(3): 182-191.

76. Baehr, T. and R. Rienecker, *New generation of pressure screens for stock preparation systems: spectro screen - D.* In 43rd *TAPPI Pulping Conference,* 1991.

77. Boettcher, P.C., *Results from a new design of contoured screen plate.* In 38th *TAPPI Pulping Conference,* 1986.

78. Borschke, D., D. Bergfeld, and H. Friedrich, *Screening and fractionation - traditional technology now with new perspectives.* In 58th *Appita Annual General Conference,* 1998.

79. Frejborg, F., *Profile screens improve TMP system efficiency and increase pulp quality.* Pulp and Paper, 1987: 99-101.

80. Halonen, L., R. Ljokkoi, and R. Peltonen, *Improvements on screening systems by screen plate design.* In 11th *International Mechanical Pulping Conference,* 1989.

81. Hautala, J., S. Nikula, and B. Nysten, *New technology in PGW screening improves pulp quality and reduces energy consumption.* In 11th *International Mechanical Pulping Conference,* 1989.

82. Henrich, H.O. and K. Schmidt, *Slotted screens for mechanical pulps - the ultimate in screening technology.* In *24th EUCEPA Conference,* 1990. Stockholm.

83. Larsson, H. and K. Stribolt, *Fines screening before washing works well for Sweden's Morrums Bruk.* Pulp and Paper Canada, 1988. **89**(12): 43-45.

84. Locke, R.E., J.C. Kerr, and C.M. Vitorim *Successfully recycling waxed containers.* In 30th *TAPPI Pulping Conference,* 1998.

85. Niinimaki, J., *Effect of feed construction on the efficiency of pressure screening.* Tappi Journal, 1996. **79**(11): 119-127.

86. Niinimaki, J., *Effect of operating parameters and rotor body shape on flow conditions and the performance of a pressure screen.* In 28th *TAPPI Pulping Conference,* 1996.

87. Norman, B. and P.O. Wedin, *Visualisation of flow in a high consistency screen.* In 11th *TAPPI Engineering Conference,* 1986.

88. Phillippe, I.J., *Operating characteristics of non-conventional slotted screen cylinders.* In 22nd *TAPPI Pulping Conference,* 1990.

89. Pimley, J.J. and B. Rees, *Replacing dispersion with screening for the elimination of stickies.* In 58th *APPITA Annual General Conference,* 1998, Brisbane.

90. Sealey, R.J. and G.L. Miller, *Modified screen basket geometry improves pressure screen operation.* Pulp and Paper, 1981. **93**(June): pp. 97-103.

91. Serres, A. and B. Rees, *ID2 brings new leap for the screening process.* Appita Journal, 2002. **55**(4): 267-271.

92. Vitori, C.M. and I.J. Philippe, *Contour surface cylinders boost wastepaper screening efficiency.* Pulp and Paper, 1990. **32**(3): 186-195.

93. Gooding, R.W. and R.J. Kerekes, *Consistency changes caused by pulp screening.* Tappi Journal, 1992. **75**(11): 109-118.

94. Hooper, A.W., *The screening of chemical pulp,* in *Pulp and paper manufacture - Vol 5:Alkaline pulping,* M.J. Kocurek, Editor. 1990, Joint Textbook Committee of the Paper Industry: Montreal. pp.318-366.

95. Bliss, T., *Screening,* in *Pulp and paper manufacture - Vol 6: Stock preparation,* M.J. Kocurek, Editor. 1992, Joint Textbook Committee of the Paper Industry: Montreal. pp. 229-247.

96. Hooper, A.W., *Screening of mechanical pulp - effect of control parameters and screen operation on pulp quality,* in *Pulp and paper manufacture - Vol 2: Mechanical*

pulping, M.J. Kocurek, Editor. 1987, Joint Textbook Committee of the Paper Industry: Montreal. pp. 181-195.

97. Kleinau, J.H., *Contaminants*, in *Pulp and paper manufacture - Vol 3: Secondary fibres and non-wood pulping*, M.J. Kocurek, Editor. 1987, Joint Textbook Committee of the Pulp and Paper Industry: Montreal. pp. 136-142.

98. Doshi, M.R., *Cleaning and screening*, in *Pulp and paper manufacture - Vol 3:Secondary fibers and non-wood pulping*, M.J. Kocurek, Editor. 1987, Joint Textbook Committee of the Paper Industry: Montreal. pp. 221-233.

99. Cornelius, R. and H. Gassmann, *The sticky problem - the economic solution.* In *Appita Annual General Conference,* 2003.

100. Lucas, B.E., R.A. Venditti, and H. Jameel, *Behaviour of pressure sensitive adhesive material in industrial pressure screens and laboratory screens.* Tappi Journal, 2001. **84**(5): 54-61.

101. Laurila, P. *et al.*, *Shives - how they affect paper machine runnability.* Pulp and Paper Magazine of Canada, 1978. **79**(9): T285-T296.

102. Sears, G.R., R.F. Tyler, and C.W. Denzer, *Shives in newsprint: The role of shives in paper web breaks.* Pulp and Paper Canada, 1965. **66**(7): 351-363.

103. Heise, O., *Screening foreign material and stickies.* Tappi Journal, 1992. **75**(2): 78-81.

104. Fredriksson, B., *Evaluation of apparatus and systems for screening mechanical pulp.* Svensk Papperstidning, 1984. **87**(12): 94-98.

105. Nguyen, K.L., A.J. Eagle, and M.E. Van Klaveren, *Analysis and optimization of a pulp screening system.* Appita Journal, 1991. **44**(5): 337-378.

106. Kanazawa, T., *Experience and proposal to improve sticky problems in deinking plant and in recycling paper processing for paper board.* In 24th *Pan Pac Pulp and Paper Technical Conference,* 1992.

107. Hill, J., H. Karlson, and T. Ostman, *Process design and control of screen rooms - Part 1: Characteristics and controllability of screen modules.* Pulp and Paper Canada, 1982. **83**(3): 76-80.

108. Hill, J., H. Karlson, and T. Ostman, *Process design and control of screen rooms - Part 3: Automatic control of screen rooms.* Pulp and Paper Canada, 1982. **83**(5): 125-129.

109. Friesen, T., *Pressure Screen system simulation for optimal fractionation.* In *PAPTAC 88th Annual Meetin,*. 2000.

110. Steenburg, B., *Principles of screen system design.* Svensk Papperstidning, 1953. **56**(20): 171-178.

111. Cornelius, R. and H. Gassmann, *Mechanical filtration of circuit water by pressure filters.* In 63rd *Appita Annual General Conference,* 2003.

112. Wakelin, R.F., G.K. Dahlqvist, and J.E. Isaksen, *Balancing the roles of refiners, screens and hydrocyclones in production of high quality mechanical pulps.* In 59th *Appita Annual General Conference,* 1999.

113. Duffy, G.G., *A new method of fibre fractionation.* In 63rd *Appita Annual General Conference,* 2003.

114. Duffy, G.G., *The development of a new method of fibre separation.* In 63rd *Appita Annual General Conference,* 2003.

115. Sloane, C.M., *Separation techniques for coarse fibre removal to improve pulp and paper quality.* 1993, MPhil Thesis, The University of Auckland.

116. Nan, K., *A new method of fibre separation.* 2001, MSc Thesis, The University of Auckland.

117. Duffy, G.G., *Increasing profit through selective fibre treatment.* In 59th *Appita Annual General Conference,* 1999.

118. Fredriksson, B., *New HC screening technology for recycled fibre pulps.* Paperi ja Puu, 1995. **77**(5): 307-318.

119. Page, R.E. and R.E. Hergert, *Enhancement of paper properties and fibre economics through web stratification.* Appita Journal, 1989. **42**(1): 33-41.

120. Haggblom-Ahnger, U. and D. Eklund, *The role of the middle ply in multi-layered copy paper.* Appita Journal, 1998. **51**(3): 199-204.

121. Collins, N.J. and J. Colley, *Layered paper structures - the influence of furnish geometry on physical properties.* Appita Journal, 1979. **33**(2): 119-123.

122. Stenberg, G., *A new headbox for multilayered printing paper.* Tappi Journal, 1987. **70**(9): 49-55.

123. Lloyd, M.D., *Stratified (multilayer) forming - a technology for the new mellennium?* In 59th *Appita Annual General Conference,* 1999.

124. Guest, D., *Sandwich technology creates a choice of fillings.* Pulp and Paper International, 1996. **38**(2): 39-41.

125. Haggblom-Ahnger, U., *Layering of office paper.* Paperi ja Puu, 1998. **80**(7): 508-513.

126. Drury, R.G., *Process and design evaluation in aproach flow screening.* In 7th *TAPPI Papermakers Conference,* 1991.

127. Wakelin, R.F. and S.R. Corson, *TMP long fibre fractionation with pressure screens.* In 17th *International Mechanical Pulping Conference,* 1995.

128. Julien Saint Amand, F. and B. Perrin, *Fundamentals of screening: effect of rotor design and fibre properties.* In 45th *TAPPI Pulping Conference,* 1999.

129. Niinimaki, J., *Phenomena affecting the efficiency of a pressure screen.* In 45th *TAPPI Pulping Conference,* 1999.

130. Pinon, V., R. Gooding, and J.A. Olson, *Measurements of pressure pulses from a solid core rotor.* Tappi Journal, 2003. **2**(10): 9-12.

131. Yu, C., *Pulsation measurement in a screen Part 1: Pulse signature and magnitude of S-shape rotor.* In 13th *TAPPI Engineering Conference,* 1994.

132. Wikstrom, T. and A. Rasmuson, *Transition modelling of pulp suspensions applied to a pressure screen.* Journal of Pulp and Paper Science, 2002. **28**(11): 374-378.

133. Feng, M., *Numerical simulation of the pressure pulses produced by a pressure screen foil rotor.* Tappi Journal, 2002. **236**(7): 435-448.

134. McCarthy, C., *Various factors affect pressure screen operation and capacity.* Pulp and Paper, 1988. **33**(7): 233-241.

135. Koffinke, R.A., *Secondary fibre trends give impetus to pressure screening.* Pulp and Paper, 1975. **88**(7): 116-121.

136. Wakelin, R.F. and T. Paul, *Effects of some process variables on screen fractionator performance.* Appita Journal, 2001. **54**(4): 357-363.

137. Martinez, A.M. and R.W. Gooding, *A force balance of pulp screen capacity.* Tappi Journal, 1999. **82**(4): 181-189.

138. Shaw, S.F., *"Higher" consistency screening of pulp.* In 12th *TAPPI Engineering Conference,* 1986.

139. Gooding, R.W. and D.F. Craig, *The effect of slot spacing on pulp screen capacity.* Tappi Journal, 1992. **71**(2): 71-75.

140. Yu, C.J., B.R. Crossley, and L. Silveri, *Fundamental study of screening hydraulics - Part 3: Model for calculating effective open area.* Tappi Journal, 1994. **77**(9): 125-134.

141. Anon, *The paper production process - Our challenge.* 2001, VOITH PAPER Technical Publication.

142. Gooding, R.W., *Hydraulic resistance of screen apertures.* I n *Department of Chemical Engineering.* 1996, MSc Thesis, University of British Columbia.

143. Karvinen, R. and L. Halonen, *The effect of various factors on pressure pulsation in a screen.* Paperi ja Puu, 1984. **43**(2): 101-109.

144. Yu, C. and R. De Foe, *Fundamental study of screening hydraulics Part 1: Flow patterns at the feed-side surface of screen baskets; mechanism of fibre-mat formation and mixing.* Tappi Journal, 1994. **77**(8): 123-129.

145. Kumar, A., R.W. Gooding, and R.J. Kerekes, *Factors controlling the passage of fibre through slots.* Tappi Journal, 1998. **81**(5): 247-254.

146. Yu, C.J., R. De Foe, and B.R. Crossley, *Fractionation technology and its applications.* In 15th *TAPPI Pulping Conference,* 1994.

147. Wakelin, R.F., *Objectives and constraints for pressure screen fractionation.* In 11th *International Mechanical Pulping Conference,* 1997.

148. Reinecker, R., *Spectro screen-D: A new concept for effective screening within the stock consistency range of approx. 3%.* 1992, VOITH PAPER Technical Publication.

149. Cowan, A.W., *The screening of groundwood pulp - A reappraisal.* Pulp and Paper Canada, 1969. **Jan**: p. 65-73.

150. Beaulieu, S., *Domtar installs TMP at Donnacona newsprint mill.* Pulp and Paper Canada, 1977. **78**(3): 59-65.

151. Wakelin, R.F., B.G. Blackwell, and S.R. Corson, *The influence of equipment and process variables on mechanical pulp fractionation in pressure screens.* In 54th *Appitta Annual General Conference,* 1994.

152. Julien Saint Amand, F. and B. Perrin., *Basic parameters affecting screening efficiency and fibre loss.* In *PTS-CTP 3rd Deinking Symposium,* 2000.

153. Tangsaghasaksri, W., *Uber die sortierung von Fasersuspensionen mittels geschlitzter Siebe.* 1994, PhD Thesis, Damstad

154. Gooding, R.W., *The passage of fibres through slots in pulp screening*, 1986, MSc Thesis, University of British Columbia.

155. Riese, J. and H. Spiegelberg, *Mechanism of screening: Dilute suspensions of stiff fibres at normal incidence.* Tappi Journal, 1969. **52**(5): 895-903.

156. Yu, C.J. and R. De Foe, *Fundamental study of screening hydraulics - Part 2: Fibre orientation in the feed side of a screen basket.* Tappi Journal, 1994. **77**(9): 119-124.

157. Kumar, A., *Passage of fibres through screen apertures.* In *Department of Chemical Engineering*. 1991, PhD Thesis, University of British Columbia.

158. Lawryshyn, Y.A. and D.C.S. Kuhn, *Simulation of flexible fibre motion through screen apertures.* Journal of Pulp and Paper Science, 1998. **24**(12): 404-411.

159. Tangsaghasaksri, W. and L. Gottsching, *Analytical Assessment of Screening of Fibre Suspensions by Means of Slotted Screens.* Papier, 1995. **49**(5): 213-218.

160. Tangsaghasaksri, W., M. Steuernagel, and L. Gottsching, *Modelling of fibre passage through slotted screens.* Papier, 1994. **48**(10): 635-638.

161. Tangsaghasaksri, W., M. Steuernagel, and L. Gottsching, *Effect of contoured slots on fibre passage - investigations by means of a model screen (Part 1).* Papier, 1994. **48**(5): 172-179.

162. Tangsaghasaksri, W. and L. Gottsching, *Influence of Slot Contours on Fibre Separations - Investigations with the Help of a Model Sorter (Part 2).* Papier, 1994. **48**(5): 235-247.

163. Gooding, R.W. and R.J. Kerekes, *The motion of fibres near a screen slot.* Journal of Pulp and Paper Science, 1989. **15**(2): 59-62.

164. Thomas, A.S.W. and K.C. Cornelius, *Investigation of a laminar boundary-layer suction slot.* AIAA Journal, 1982. **20**(6): 790-796.

165. Olson, J. and G. Wherrett, *A model of fibre fractionation by slotted screen apertures.* Journal of Pulp and Paper Science, 1998. **24**(12): 398-403.

166. Wakelin, R.F. and S.R. Corson, *TMP long fibre fractionation with pressure screens.* In 10th *International Mechanical Pulping Conference,* 1995.

167. Gooding, R.W. and R.J. Kerekes, *Derivation of performance equations for solid-solid screens.* Canadian Journal of Chemical Engineering, 1989. **67**(10): 801-805.

168. Olson, J., *Fibre length fractionation caused by pulp screening, slotted screen plates.* Journal of Pulp and Paper Science, 2001. **27**(8): 255-261.

169. King, C.J., *Separation Processes*. 2nd ed. 1980, New York: McGraw-Hill.

170. Coulson, J.M. and J.F. Richardson, *Chemical Engineering*. 6th ed. Vol. 6. 1999, Oxford: Butterworth-Heinemann.

171. Fogler, H.S., *Elements of Chemical Reaction Engineering*. 2nd ed. 1992, Englewood Cliffs, NJ: Prentice-Hall.

172. Levenspiel, O., *Chemical Reaction Engineering*. 3rd ed. 1999, New York: John Wiley and Sons.

173. Metcalfe, I.S., *Chemical reaction engineering - A first course*. 1997, New York: Oxford University Press.

174. Kubat, J. and B. Steenberg, *Theory of screening. III Screening at low particle concentrations.* Svensk Papperstidning, 1955. **58**(3): 319-324.

175. Nelson, G.L., *The screening quotient: A better index for screening performance.* Tappi Journal, 1981. **64**(5): 133-134.

176. Olson, J. and B.J. Allison, *Optimization of multiple screening stages for fibre length fractionation: two-stage case.* Journal of Pulp and Paper Science, 2000. **26**(3): 113-119.

177. Gooding, R.W., J. Olson, and N. Roberts. *Parameters for assessing fibre fractionation and their application to screen rotor effects.* in 66th *International Pulping Conference,* 2001.

178. Julien Saint Amand, F. and B. Perrin, *Screening: experimental approach and modelling.* In 70th *TAPPI Pulping Conference,* 1998.

179. Walmsley, M. and Z. Weeds, *Flow characteristics of eucalyptus pulp suspensions in a pressure screen with 1-m holes.* In 58th *Appita Annual General Conference,* 1998.

180. Walmsley, M. and Z. Weeds, *Flow characteristics of eucalypt and radiata pine suspensions in a pressure screen with smooth 1-mm holes and 150 micron contoured slot apertures.* In 70th *TAPPI Pulping Conference,* 1998.

181. Weeds, Z., *Flow behaviour of an industrial pressure screen.* 1998, MSc Thesis, The University of Waikato.

182. Ammala, A., *Pressure screening: changes in pulp properties in the screen basket.* Tappi Journal, 1999. **82**(10): 99-104.

183. Schweiss, P., *Application of the finite volume method and design example for a MultiScreen.* 2000, VOITH PAPER Technical Publication.

184. LeBlanc, P.E., *A breakthrough in pressure screening.* In 65th *TAPPI Pulping Conference,* 1986.

185. Martin, A.C. and D.D. McIntosh, *Hot stock screening of Canadian softwood Kraft.* Pulp and Paper Canada, 1989. **90**(5): 38-43.

186. Wakelin, R.F., *Prediction of fractionation efficiency for pressure screens.* In 56th *Appita Annual General Meeting,* 1996.

187. Braaten, K.R. and R.F. Wakelin, *Fibre length fractionation of TMP using pressure screens.* Tappi Journal, 1999. **82**(6): 129-135.

188. Selder, H., *Fractionation - the technology of the future.* Paper Technology, 1992. **33**(3): 13-16.

APPENDIX 1. MISCELLANEOUS DATA

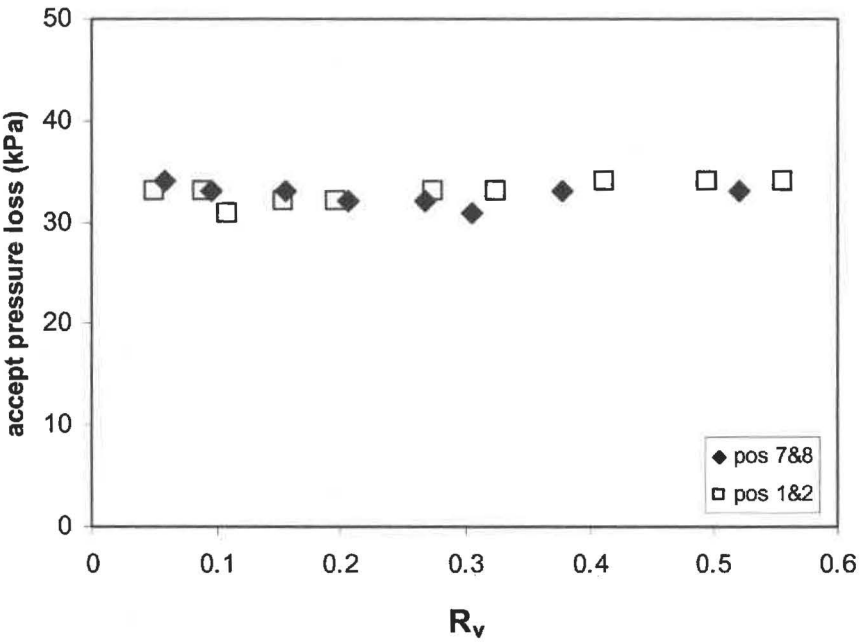

Figure A.1 Accept pressure loss (feed pressure-accept pressure) data for two 55-mm screen sections located at different positions. 1-mm holes, eucalypt, bump rotor, C_f=0.24 %, V_s=0.6 ms^{-1}, V_{tip}=22 ms^{-1}.

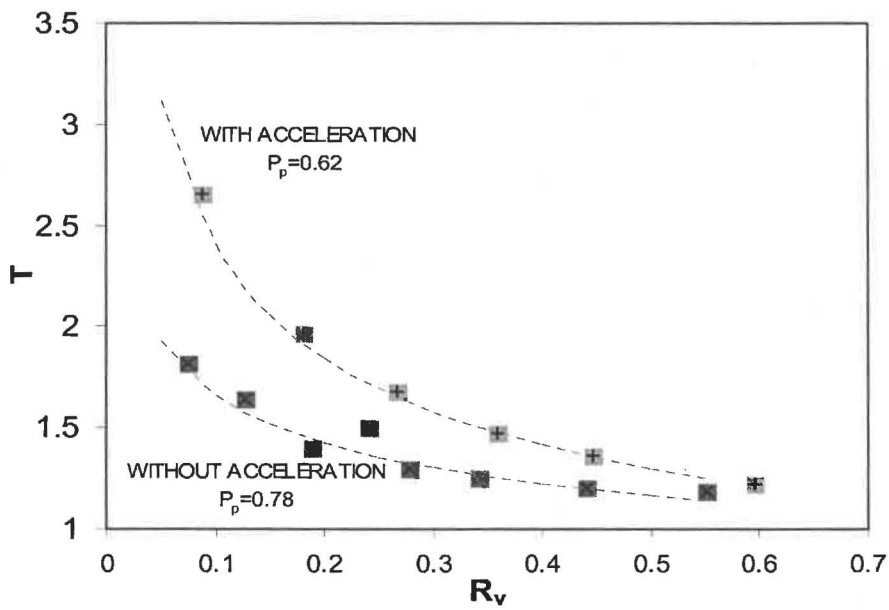

Figure A.2 Effect of pulp acceleration on reject thickening of the standard screen with 1-mm holes. Eucalypt, bump rotor, C_f=0.5%, V_s=0.6 ms^{-1}, V_{tip}=11 ms^{-1}.